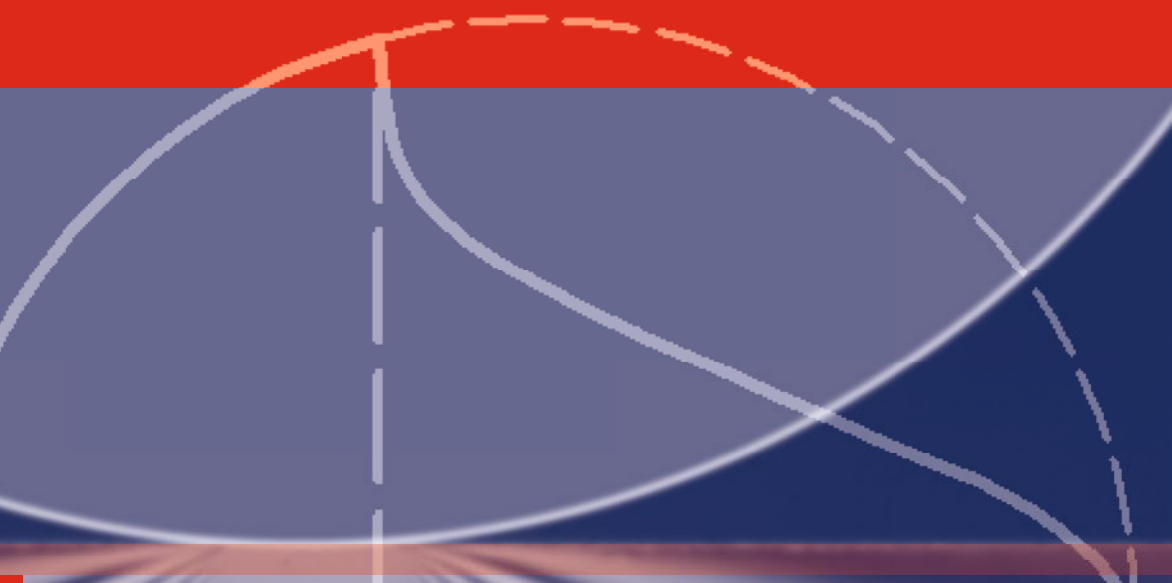

Valentin L. Popov

Contact Mechanics and Friction

Physical Principles and Applications

Second Edition

Springer

Contact Mechanics and Friction

Valentin L. Popov

Contact Mechanics and Friction

Physical Principles and Applications

Second Edition

Springer

Valentin L. Popov
TU Berlin Inst. Mechanik
Berlin, Germany

ISBN 978-3-662-53080-1 ISBN 978-3-662-53081-8 (eBook)
DOI 10.1007/978-3-662-53081-8

Library of Congress Control Number: 2017933487

Printed on acid-free paper

This Springer imprint is published by Springer Nature
The registered company is Springer-Verlag GmbH Germany
The registered company address is: Heidelberger Platz 3, 14197 Berlin, Germany

Dr. Valentin L. Popov
studied physics and obtained his doctorate from the Moscow State Lomonosow University. He worked at the Institute of Strength Physics and Materials Science of the Russian Academy of Sciences. After a guest-professorship in the field of theoretical physics at the University of Paderborn, he has headed the department of System Dynamics and Friction Physics in the Institute of Mechanics at the Berlin University of Technology since 2002. His areas of interest, among others, include tribology, nanotribology, tribology at low temperatures, biotribology, the influence of friction through ultrasound, numerical simulation of frictional processes, research regarding earthquakes, as well as themes relating to materials sciences such as the mechanics of elastoplastic media with microstructure, strength of metals and alloys, and shape memory alloys. He is the joint editor of international journals and regularly organizes international conferences and workshops over diverse tribological themes.

Preface to the Second English Edition

The second English edition of "Contact Mechanics and Friction" was substantially revised compared to the 1st edition. This is especially related to the chapters on "contact mechanics" (normal contact with and without adhesion, tangential contact, and contact with elastomers), which were supplemented with many solutions for axially-symmetric contact problems. The chapter on "wear" now includes a discussion on fretting. The section of elasto-hydrodynamic lubrication was completely rewritten and enriched by several problems. Furthermore, the chapter on numerical simulation methods in contact mechanics has been overhauled and now contains the basic ideas of the application of the boundary element method to adhesive contacts.

I would like to thank M. Hess and R. Pohrt for their help in writing new sections and problems. Also, thanks go to M. Hess and M. Popov for their corrections of this book, Ms. Wallendorf for drawing new figures, and Dr. J. Starcevic for extensive support in the completion of the book.

Berlin, September 2016 V.L. Popov

From the Preface to the First English Edition

The English edition of "Contact Mechanics and Friction" ..... is, for the most part, the text of the 1st German edition (Springer Publishing, 2009). The book was expanded by the addition of a chapter on frictional problems in earthquake research. Additionally, Chapter 15 was supplemented by a section on elasto-hydrodynamics. The problem sections of several chapters were enriched by the addition of new examples.

This book would not have been possible without the active support of J. Gray, who translated it from the German edition. I would like to thank Prof. G. G. Kocharyan and Prof. S. Sobolev for discussions and critical comments on the chapter over earthquake dynamics. Dr. R. Heise made significant contributions to the development and correction of new problems. I would like to convey my affectionate thanks to Dr. J. Starcevic for her complete support during the composition of this book. I want to thank Ms. Ch. Koll for her patience in creating figures and Dr. R. Heise, M. Popov, M. Heß, S. Kürscher, and B. Grzemba for their help in proofreading.

Berlin, November 2009 V.L. Popov

Preface to the First German Edition

He who wishes to better understand the subject of Contact Mechanics and the Physics of Friction would quickly discover that there is almost no other field that is so interdisciplinary, exciting, and fascinating. It combines knowledge from fields such as the theories of elasticity and plasticity, viscoelasticity, materials science, fluid mechanics (including both Newtonian and non-Newtonian fluids), thermodynamics, electrodynamics, system dynamics, and many others. Contact Mechanics and the Physics of Friction have numerous applications ranging from measurement and system technologies on a nanoscale to the understanding of earthquakes and including the sheer overwhelming subject of industrial tribology. One who has studied and understands Contact Mechanics and the Physics of Friction will have acquired a complete overview of the different methods that are used in the engineering sciences.

One goal of this book is to collect and clearly present, in one work, the most important aspects of this subject and how they relate to each other. Included in these aspects is, first, the entirety of traditional Contact Mechanics including adhesion and capillarity, then the theory of friction on a macro scale, lubrication, the foundations of modern nanotribology, system dynamical aspects of machines with friction (friction induced vibrations), friction related to elastomers, and wear. The interplay between these aspects can be very complicated in particular cases. In practical problems, different aspects are always presented in new ways. There is no simple recipe to solve tribological problems. The only universal recipe is that one must first understand the system from a tribological point of view. A goal of this book is to convey this understanding.

It is the solid belief of the author that the essential aspects of mechanical contacts and friction are often much easier than they appear. If one limits oneself to qualitative estimations, it is then possible to achieve an extensive qualitative understanding of the countless facets of mechanical contacts and friction. Therefore, qualitative estimations are highly valued in this book.

In analytical calculations, we limit ourselves to a few classical examples which we can then take as building blocks and apply them to understand and solve a wealth of problems with real applications.

A large number of concrete tribological questions, especially if they deal with meticulous optimization of tribological systems, are not solvable in analytical form. This book also offers an overview of methods of Numerical Simulation for Contact Mechanics and Friction. One such method is then explained in detail, which permits a synthesis of several processes related to contact mechanics from different spatial ranges within a single model.

Even though this book is primarily a textbook, it can also serve as a reference for the foundations of this field. Many special cases are presented alongside the theoretical fundamentals with this goal in mind. These cases are presented as exercises in their respective chapters. The solutions are provided for every exercise along with a short explanation and results.

The basis of this textbook originates and is drafted from lectures that the author has conducted over Contact Mechanics and the Physics of Friction at the Berlin University of Technology, so that the material can be completed in its entirety in one or two semesters depending on the depth in which it is visited.

Thanks

This book would not have been possible without the active support of my colleagues. Several in the department of "System Dynamics and Frictional Physics," from the Institute for Mechanics, have contributed to the development of the practice exercises. For this, I thank Dr. M. Schargott, Dr. T. Geike, Mr. M. Hess, and Dr. J. Starcevic. I would like to express a heartfelt thanks to Dr. J. Starcevic for her complete support during the writing of this book as well as to Mr. M. Hess, who checked all of the equations and corrected the many errors. I thank Ms. Ch. Koll for her patience constructing figures as well as M. Popov and Dr. G. Putzar for their help with proofreading. I thank the Dean of Faculty V, Transportation and Machine Systems, for granting me a research semester, during which this book was completed.

Berlin, October 2008 V.L. Popov

Table of Contents

1 Introduction

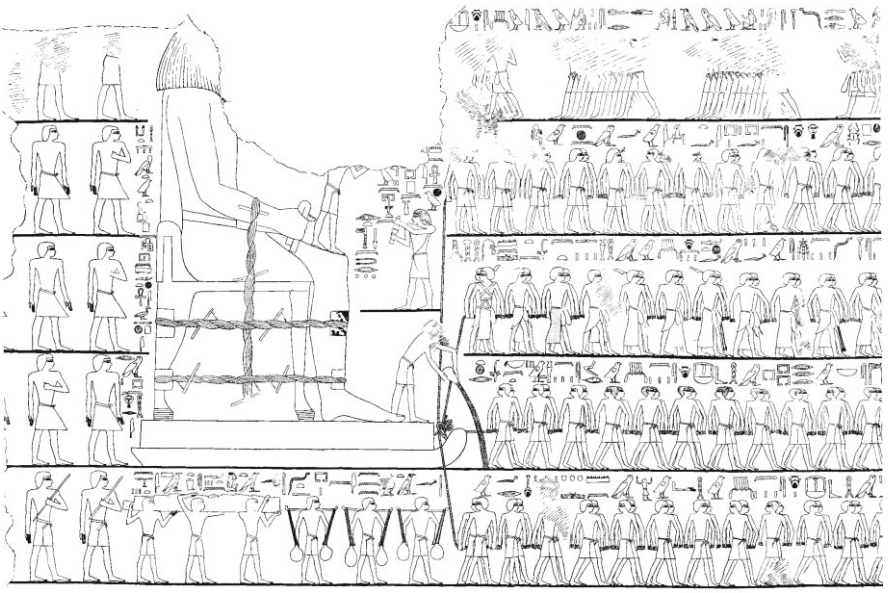

1.1 Contact and Friction Phenomena and their Applications

Contact Mechanics and the Physics of Friction are fundamental disciplines of the engineering sciences, which are indispensable for the construction of safe and energy-saving designs. They are of interest for countless applications, for example clutches, brakes, tires, bush and ball bearings, combustion engines, hinges, gaskets, castings, machining, cold forming, ultrasonic welding, electrical contacts, and many others. These applications have tasks spanning from stress analysis of contact elements and joints, over the influence of lubrication and material design on friction and wear, to applications in micro and nanotechnology. Friction is a phenomenon that people have been interested in for over hundreds and even thousands of years and still today remains in the middle of the development of new products and technologies.

A classical example of contact is a rail-wheel contact, in which we are interested foremost in material strength and force transmission properties. Contacts can transfer mechanical force (screws), conduct electricity or heat, or prevent the flow of material (seals). The contact between the tip of an atomic force microscope and the underlying material or the contact between two tectonic plates are examples of frictional contacts as well. Contact and friction phenomena on different scales, from nanoscale phenomena to those on a mega-scale, have much in common and, thus, can be approached with similar methods. Contact mechanics and the physics

V.L. Popov, *Contact Mechanics and Friction*,
DOI 10.1007/978-3-662-53081-8_1

of friction has proven to be an enormous field in modern research and technology, stretching from the movement of motor proteins and muscular contractions to earthquake dynamics as well as including the enormous field of industrial tribology.

Friction leads to energy dissipation and in micro-contacts, where extreme stress is present, to micro-fractures and surface wear. We often try to minimize friction during design in an attempt to save energy. There are, however, many situations in which friction is necessary. Without friction, we cannot enjoy violin music or even walk or drive. There are countless instances, in which friction should be maximized instead of minimized, for example between tires and the road during braking. Also, wear must not always be minimized. Fast and controllable abrasive techniques can actually form the basis for many technological processes, (e.g., grinding, polishing, and sandblasting.)

Friction and wear are very closely connected with the phenomenon of adhesion. For adhesion it is important to know if a close contact can be created between two bodies. While adhesion does not play a considerable role on a large-scale in the contact between two "hard bodies" such as metal or wood, in instances in which one of the bodies in contact is soft, the role of adhesion becomes very noticeable and can be taken advantage of in many applications. One can also learn much from contact mechanics for the use of adhesives. In micro-technology, adhesion gains even greater importance. Friction and adhesive forces on a micro-scale present a real problem and have been termed "sticktion" (sticking and friction).

Another phenomenon, which is similar to adhesion and will be discussed in this book, is capillary force, which appears in the presence of low quantities of fluid. In very precise mechanisms such as clocks, the moisture contained in the air can cause capillary forces, disturbing the exactness of such mechanisms. Capillary forces can also be used, however, to control the flow of a lubricant to an area of friction.

In a book about contact and friction one cannot silently pass over the closely related sound-phenomena. Brakes, wheel-track contact, and bearings do not only dissipate energy and material. They often squeak and squeal unpleasantly or even with such intensity as to be damaging to one's hearing. Noise caused by technical systems is a central problem today in many engineering solutions. Friction induced vibrations are closely related to the properties of frictional forces and are likewise a subject of this book.

If we had to measure the importance of a tribological field in terms of the amount of money that has been invested in it, lubrication technology would definitely take first place. Unfortunately, it is not possible to grant lubrication a correspondingly large section in this book. The fundamentals of hydrodynamic and elasto-hydrodynamic lubrication, however, are of course included.

The subject of contact mechanics and friction is ultimately about our ability to control friction, adhesion, and wear and to mould them to our wishes. For that, a detailed understanding of the dependency of contact, friction, and wear phenomena on the materials and system properties is necessary.

1.2 History of Contact Mechanics and the Physics of Friction

A first impression of tribological applications and their importance can be conveyed by its history. The term "Tribology" was suggested by Peter Jost in May of 1966 as a name for the research and engineering subject which occupies itself with contact, friction, and wear. Except for the name, tribology itself is ancient. Its beginning is lost in the far reaches of history. The creation of fire through frictional heating, the discovery of the wheel and simple bushings, and the use of fluids to reduce frictional forces and wear were all "tribological inventions" that were already known thousands of years before Christ[1]. In our short overview of the history of tribology, we will jump to the developments that took place during the Renaissance and begin with the contributions of *Leonardo da Vinci*.

In his Codex-Madrid I (1495), da Vinci describes the ball-bearing, which he invented, and the composition of a low-friction alloy as well his experimental examination of friction and wear phenomena. He was the first engineer who persistently and quantitatively formulated the laws of friction. He arrived at the conclusion that can be summarized in today's language as two fundamental Laws of Friction:

1. The frictional force is proportional to the normal force, or load.
2. The frictional force is independent of the contact surface area.

Da Vinci was, de facto, the first to introduce the term coefficient of friction and to experimentally determine its typical value of ¼.

As so often happens in the history of science, these results were forgotten and around 200 years later, rediscovered by the French physicist *Guillaume Amontons* (1699). The proportionality of the frictional force to the normal force is, therefore, known as "Amontons' Law."

Leonard Euler occupied himself with the mathematical point of view of friction as well as the experimental. He introduced the differentiation between static frictional forces and kinetic frictional forces and solved the problem of rope friction, probably the first contact problem to be analytically solved in history (1750). He was the first to lay the foundations of the mathematical way of dealing with the law of dry friction and in this way promoted further development. We have to thank him for the symbol μ as the coefficient of friction. Euler worked with the idea that friction originates from the interlocking between small triangular irregularities and that the frictional coefficient is equal to the gradient of these irregularities. This understanding survived, in different variations, for a hundred years and is also used today as the "Tomlinson Model" [2] in connection with friction on an atomic scale.

---

[1] Detailed information about history of tribology can be found in: D. Dowson. History of Tribology, Longman Group Limited, London, 1979.

[2] The model was proposed in 1928 by Prandtl and and was given the name of Tomlinson by mistake. This model is practically the mathematical translation of the ideas of Leonard Euler.

An outstanding and still relevant contribution to the examination of dry friction was achieved by the French engineer *Charles Augustin Coulomb*. The law of dry friction deservingly carries his name. Coulomb confirmed Amontons' results and established that sliding friction is independent of the sliding speed in a first order approximation. He undertook a very exact quantitative examination of dry friction between solid bodies in relation to the pairing of materials, surface composition, lubrication, sliding speed, resting time for static friction, atmospheric humidity, and temperature. Only since the appearance of his book "Theory of Simple Machines," (1781) could the differentiation between kinetic and static friction be quantitatively substantiated and established. Coulomb used the same idea of the origin of friction as Euler, but added another contribution to friction that we would now call the adhesion contribution. It was likewise Coulomb who established deviations from the known simple law of friction. He found out, for example, that the static force grows with the amount of time the object has remained stationary. For his examinations, Coulomb was well ahead of his time. His book contained practically everything that eventually became the original branches of tribology. Even the name of the measuring instrument, the tribometer, stems from Coulomb[3].

Examinations of rolling friction have not played as a prominent role in history as sliding friction, probably because rolling friction is much smaller in magnitude than sliding friction and, therefore, less annoying. The first ideas of the nature of rolling friction for rolling on plastically deformable bodies, of which the most important elements are still considered correct, come from *Robert Hooke* (1685). A heated discussion between *Morin* and *Dupuit* that took place in 1841-42 over the form of the law of rolling friction showed that the nature of the friction was very dependent on the material and loading parameters. According to Morin the rolling friction should be inversely proportional to the radius of the rolling body, but according to Dupuit it should be inversely proportional to the square root of the radius. From today's point of view both statements are limitedly correct under differing conditions.

Osborne Reynolds was the first to experimentally examine the details of the events happening in the contact area during rolling contact and established that on a driven wheel, there are always areas in which the two bodies are in no-slip contact and areas where slipping takes place. It was the first attempt to put tribological contact underneath a magnifying glass and at the same time the end of the strict differentiation between static friction and kinetic friction. Reynolds accounted for the energy loss during rolling with the existence of partial sliding. A quantitative theory could later be achieved by *Carter* (1926) only after the foundations of contact mechanics were laid by Hertz.

Humans have lubricated mechanical contacts for hundreds of years in order to decrease friction, but it was rising industrial demands that coerced researchers experimentally and theoretically to grapple with lubrication. In 1883 *N. Petrov* per-

[3] A brief summary of tribological work of Coulomb from today's perspective can be found in: Popova E., Popov V.L., The research works of Coulomb and Amontons and generalized laws of friction, Friction, 2015, v. 3, N.2, pp. 183-190.

formed his experimental examinations of journal bearings and formulated the most important laws of hydrodynamic lubrication. In 1886 Reynolds published his theory of hydrodynamic lubrication. The "Reynolds Equation," which he developed, established the basis for calculations in hydrodynamically lubricated systems. According to the hydrodynamic lubrication theory, the coefficient of friction has an the order of magnitude of $\mu \approx h / L$, where h is the thickness of the lubricating film and L is the length of the tribological contact. This holds true so long as the surfaces do not come so close to one another that the thickness of the lubrication film becomes comparable to the roughness of the two surfaces. Such a system would then fall into the realm of mixed friction which was extensively examined by *Stribeck* (1902). The dependence of the frictional force on the sliding speed with a characteristic minimum is named the *Stribeck-Curve*.

Other conditions can come into play with even greater loads or insufficient lubrication in which only a few molecular layers of lubricant remain between the bodies in contact. The properties of this boundary lubrication were investigated by *Hardy* (1919-22). He showed that only molecular layer of grease drastically influenced the frictional forces and wear of the two bodies. Hardy measured the dependence of frictional forces on the molecular weight of the lubricant and the surfaces of the metals and also recognized that the lubricant adheres to the metal surfaces. The decreased friction is owed to the interaction of the polymer-molecules of the lubricant, which is today sometimes called a "grafted liquid."

A further advance in our understanding of contact mechanics, as well as dry friction, in the middle of the twentieth century is bound to two names: *Bowden* and *Tabor*. They were the first to advise the importance of the roughness of the surfaces of the bodies in contact. Because of this roughness, the real contact area between the two bodies is typically orders of magnitude smaller than the apparent contact area. This understanding abruptly changed the direction of many tribological examinations and again brought about Coulomb's old idea of adhesion being a possible mechanism of friction. In 1949, Bowden and Tabor proposed a concept which suggested that the origin of sliding friction between clean, metallic surfaces is explained through the formation and shearing of cold weld junctions. According to this understanding, the coefficient of friction is approximately equal to the ratio of critical shear stress to hardness and must be around 1/6 in isotropic, plastic materials. For many non-lubricated metallic pairings (e.g. steel with steel, steel with bronze, steel with iron, etc.), the coefficient of friction actually does have a value on the order of $\mu \sim 0.16$.

The works of Bowden and Tabor triggered an entirely new line of theory of contact mechanics regarding rough surfaces. As pioneering work in this subject we must mention the works of *Archard* (1957), who concluded that the contact area between rough elastic surfaces is approximately proportional to the normal force. Further important contributions were made by *Greenwood* and *Williamson* (1966), *Bush* (1975), and *Persson* (2002). The main result of these examinations is that the real contact areas of rough surfaces are approximately proportional to the

normal force, while the conditions in individual micro-contacts (pressure, size of micro-contact) depend only weakly on the normal force.

The contact mechanics of rough surfaces has had a significant impact on the understanding of dry friction. Coulomb already knew that the coefficient of static friction increases gradually with time and that the coefficient of sliding friction is dependent on the sliding velocity. Experimental investigations by *Dieterich* (1972) have shown that there is a close relationship between these effects. In particular, the distinction between "static friction" and "sliding friction" has proved to be relative and was replaced by the concept in which the friction depends on the velocity and an internal variable reflecting the state of the ensemble of micro-contacts. It is interesting to note that these studies were initially carried out in the context of earthquake research and has become common knowledge in the field of "classical tribology" just since the middle of the 1990s.

With the development of the automobile industry, along with increasing speeds and power, rubber friction has gained a technical importance. The understanding of the frictional mechanisms of elastomers, and above all, the conclusion that the friction of elastomers is connected with the dissipation of energy through deformation of the material and consequently with its rheology, a fact that is generally accepted today, can be owed to the classical works of *Grosch* (1962).

Contact mechanics definitely forms the foundations for today's understanding of frictional phenomena. In history, frictional phenomena were earlier and more fundamentally examined in comparison to pure contact mechanical aspects. The development of the railroad was most certainly a catalyst for interest in exact calculations of stress values, because in wheel-rail contact the stresses can reach the maximum loading capacity for steel.

Classical contact mechanics is associated with *Heinrich Hertz* above all others. In 1882, Hertz solved the problem of contact between two elastic bodies with curved surfaces. This classical result forms a basis for contact mechanics even today. It took almost a century until *Johnson, Kendall,* and *Roberts* found a similar solution for adhesive contact (JKR-Theory). This may come from the general observation that solid bodies do not adhere to one another. Only after the development of micro-technology, did engineers run into the problem of adhesion. Almost at the same time, *Derjagin, Müller,* and *Toporov* developed another theory of adhesive contact. After an initially fervid discussion, Tabor realized that both theories are correct limiting cases for the general problem.

It is astonishing that wear phenomena, despite their overt significance, were studied seemingly late. The reason for this delay may lie in the fact that the leading cause of wear is through the interactions of micro-contacts, which became an object of tribological research only after the work of Bowden and Tabor. The law of abrasive wear, which states that wear is proportional to load and sliding distance and inversely proportional to hardness of softer contact partners, was discovered by *M. Kruschov* (1956) through experimental examination and later also confirmed by *Archard* (1966). The examinations of the law of adhesive wear, as with abrasive wear, are tied to *Tabor* and *Rabinowicz*. Despite these studies, wear

mechanisms, especially under conditions in which very little wear takes place, are still today some of the least understood tribological phenomena.

Since the last decade of the twentieth century, contact mechanics has experienced a rebirth. The development of experimental methods for investigating frictional processes on the atomic scale (atomic force microscope, friction force microscope, quartz-crystal microbalance, surface force apparatus) and numerical simulation methods have provoked a sudden growth during these years in the number of research activities in the field of friction between solid bodies. Also, the development of micro-technology essentially accounts for the largest pursuit in contact mechanics and the physics of friction. Experimentalists were offered the ability to examine well defined systems with stringently controlled conditions, for instance, the ability to control the thickness of a layer of lubrication or the relative displacement between two fixed surfaces with a resolution on the atomic level. There is, however, a gap between classical tribology and nanotribology that has yet to be closed.

1.3 Structure of the Book

Contact and friction always go hand in hand and are interlaced in many ways in real systems. In our theoretical treatment, we must first separate them. We begin our investigation of contact and frictional phenomena with contact mechanics. This, in turn, begins with a qualitative analysis, which provides us with a simple, but comprehensive understanding of the respective phenomena. Afterwards, we will delve into the rigorous treatment of contact problems and subsequently move on to frictional phenomena, lubrication, and wear.

2 Qualitative Treatment of Contact Problems – Normal Contact without Adhesion

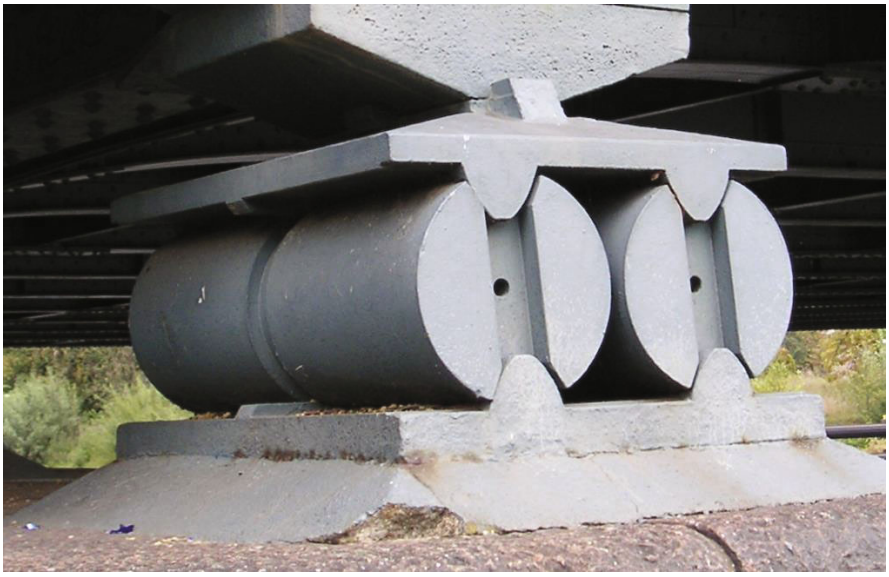

We begin our consideration of contact problems with the *normal contact problem*. A normal contact problem revolves around two bodies which are brought into contact with one another by forces perpendicular to their surfaces. A prominent example is the wheel of a train on a rail. The two most important relationships that the theory of normal contact should deliver are:

(1) The relationship between the contact force and the normal displacement of the body, which determines the stiffness of the contact and therefore the dynamic properties of the system.

(2) The relationships between forces and contact stresses and whether or not they exceed the critical values.

Without actual geometric contact there can be no other contact phenomena, no friction, and no wear. In this sense, one can regard normal contact as a basic prerequisite for all tribological phenomena. It must also be noted that, in general, with normal contact there will still be relative motion in the *tangential* direction, because of the differences in the transverse contraction of the bodies in contact. Thereby, frictional forces in the surface layers come into play. If we consider that frictional forces are essentially due to the contact between micro-asperities of the surface, we see that the normal and tangential loadings and friction are entangled in even the simplest of contact problems. In a first order approximation, we would like to distance ourselves from these complications and investigate the *pure normal contact problem*, in which we assume that there are no frictional forces pre-

V.L. Popov, *Contact Mechanics and Friction*,
DOI 10.1007/978-3-662-53081-8_2

sent in the contact area. Also, the always present attractive force, adhesion, will be neglected for the time being.

An analytical or numerical analysis of contact problems is even in the simplest of cases very complicated. A qualitative understanding of contact problems, on the other hand, is obtainable with very simple resources. Therefore, we begin our discussion with methods of qualitative analysis of contact phenomena, which can also be used in many cases for dependable, quantitative estimations. A rigorous treatment of the most important classical contact problems continues in the following chapters. We will investigate a series of contact problems between bodies of different forms, which can often be used as building blocks for more complicated contact problems.

2.1 Material Properties

This book assumes that the reader is acquainted with the fundamentals of elasticity theory. In this chapter, we will summarize only definitions from the most important material parameters that have bearing on the qualitative investigation of contact mechanical questions. This summary does not replace the general definitions and equations of elasticity theory and plasticity theory.

(a) *Elastic Properties*. In a uniaxial tensile test, a slender beam with a constant cross-sectional area A and an initial length l_0 is stretched by Δl. The ratio of the tensile force to the cross-sectional area is the tensile stress

$$\sigma = \frac{F}{A}. \tag{2.1}$$

The ratio of the change in length to the initial length is the tensile strain or deformation:

$$\varepsilon = \frac{\Delta l}{l_0}. \tag{2.2}$$

A typical stress-strain diagram for many metals and non-metals is presented in Fig. 2.1. For small stresses, the stress is proportional to the deformation

$$\sigma = E\varepsilon. \tag{2.3}$$

The proportionality coefficient E is the *modulus of elasticity* of the material. The elongation is related to the cross-sectional contraction, which is characterized by *Poisson's ratio* (or transverse contraction coefficient) ν. An *incompressible material* has a Poisson's ratio of $\nu = 1/2$.

Similarly, the shear modulus is defined as the proportionality coefficient between the shear stress and the resulting shear deformation. The shear modulus is related to the elasticity coefficient and Poisson's ratio according to

$$G = \frac{E}{2(1+\nu)} . \tag{2.4}$$

The ratio of the stress to the change in volume from hydrostatic pressure is called the compressive modulus:

$$K = \frac{E}{3(1-2\nu)} . \tag{2.5}$$

In elastically deformed bodies, potential energy is stored, whose *energy density* E (energy per unit volume) can be calculated as follows:

$$\mathrm{E} = \frac{1}{2}\varepsilon\sigma = \frac{1}{2}E\varepsilon^2 = \frac{\sigma^2}{2E} . \tag{2.6}$$

The following is valid for shear deformation:

$$\mathrm{E} = \frac{1}{2}G\varepsilon^2 = \frac{\sigma^2}{2G} . \tag{2.7}$$

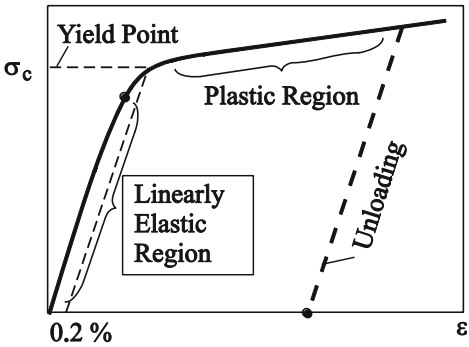

Fig. 2.1 Schematic representation of a stress-strain diagram for many metals and non-metals.

(b) *Plastic Properties*. After reaching the yield point, the stress-strain curve abruptly diverges from its original linear course and continues almost horizontally: the material experiences plastic deformation. Plastic deformation is characterized by the fact that after the material is unloaded some of the deformation remains. As a rule, the transition from elastic to plastic behavior is quick, but continuous, so that no distinct "yield point" can be defined. By convention, the yield point is accepted to be the stress σ_c, at which the plastic deformation averages 0.2%.

The yield point is dependent on the state of deformation of the material. For frictional phenomena the yield stress is taken from an intensively strain hardened state (the ultimate yield stress), which is normally found in the surface after tribological loading. That means that in tribological applications, we use the limiting value of the yield strength of the intensively strain hardened state. According to this, no further essential hardening takes place during deformation and the materi-

al can be considered as if it were elastic perfectly-plastic in a first order approximation.

A simple method for the determination of the yield point of an elastically perfectly-plastic material is the *hardness test*. It consists of the indenting of a rigid pyramid into the examined surface (Fig. 2.2). The ratio of the normal force to the area of the impression is the indentation *hardness*, or simply the hardness of the material[1]:

$$\sigma_0 = \frac{F_N}{\mathrm{A}} . \tag{2.8}$$

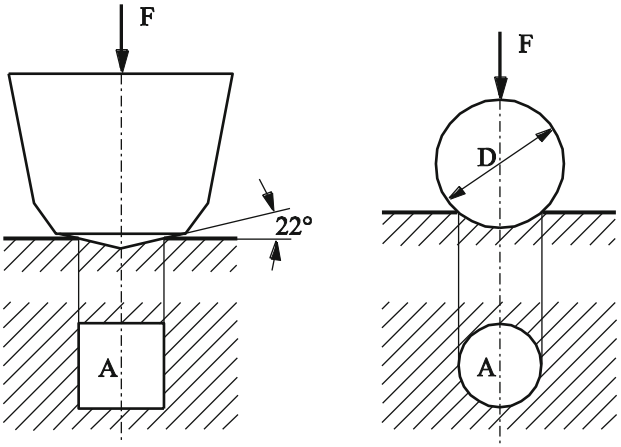

Fig. 2.2 Hardness test according to Vickers and to Brinell.

Tabor showed both theoretically and experimentally that in most cases the hardness is typically around three times the yield stress[2]:

$$\sigma_0 \approx 3\sigma_c . \tag{2.9}$$

The hardness measurement plays a central role in the tribological characterization of materials, because the tribological processes are essentially defined through micro-asperities and such interactions are similar to the hardness test. The indentation hardness is only weakly dependent on the shape of the indenter. In a first order approximation, this dependency can be neglected.

Various material properties, which are of interest for contact mechanics and friction, such as the elasticity modulus, the hardness, the coefficient of thermal expansion, and the surface energy, exhibit strong correlation. Comprehensive ex-

[1] The hardness according to Vickers and Brinell agree with each other from the defined penetration hardness by a scalar coefficient: The hardness according to Vickers is about 0.1 of the defined penetration hardness defined above. We will only use definition (2.8) in this book.

[2] D. Tabor, The Hardness of Metals, Oxford University Press, Oxford, 1951.

perimental data of these correlations can be found in the excellent book by Ernest Rabinowicz "Friction and Wear of Materials[3]."

2.2 Simple Contact Problems

The simplest of contact problems are those in which the deformations are unambiguously determined by the geometry. This is the case in the four following examples.

(1) Parallelepiped

The simplest contact problem is the contact between an orthogonal parallelepiped and a smooth, frictionless, rigid plane (Fig. 2.3). When the body is pressed onto the plane, it is elastically deformed. We define the "*penetration depth"* as the distance that the parallelepiped would penetrate the plane if the plane was not rigid.

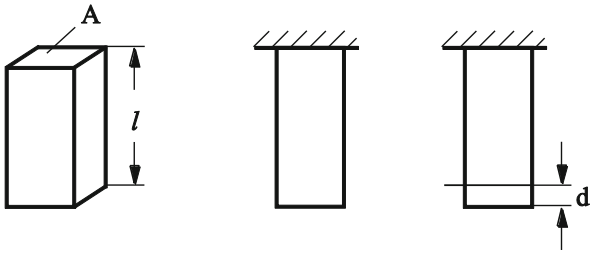

Fig. 2.3 Contact between an elastic parallelepiped and a rigid plane.

In reality, the body cannot penetrate beneath the level of the plane and is deformed a distance of d. If the length of the parallelepiped is much larger than its width, then a *uniaxial stress condition* is presented and the resulting force is

$$F = EA\frac{d}{l}, \tag{2.10}$$

where E is the modulus of elasticity, A is the cross-sectional surface area, and l is the length of the parallelepiped. In this case, the force is proportional to the penetration depth d.

(2) Thin Sheets

If the length of the parallelepiped is much smaller than the width (Fig. 2.4), then the medium cannot deform in the transverse direction and therefore *uniaxial deformation* occurs. In this case, according to the theory of elasticity,

[3] E. Rabinowicz, Friction and wear of materials. Second Edition. John Wiley & Sons, inc., 1995.

$$F = \tilde{E} A \frac{d}{l}, \tag{2.11}$$

with

$$\tilde{E} = \frac{E(1-\nu)}{(1+\nu)(1-2\nu)}. \tag{2.12}$$

for metals $\nu \approx 1/3$, so that $\tilde{E} \approx 1.5E$. For elastomers, which can be viewed as almost incompressible materials, $\nu \approx 1/2$ and the modulus for one-sided compression $\tilde{E} \approx K$ is much larger than E (around 3 orders of magnitude):

$$\tilde{E} \approx K \gg E, \qquad \text{for elastomers}. \tag{2.13}$$

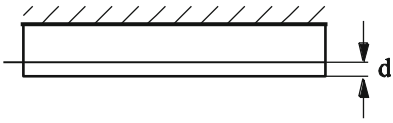

Fig. 2.4 Contact between a thin elastic sheet and a rigid plane.

(3) Spherical Cap

Next, we investigate the contact between a thin, elastic, spherical cap, which is bound to a rigid plane, and a rigid plane (Fig. 2.5).

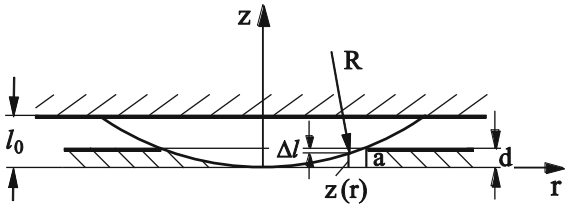

Fig. 2.5 Contact between an elastic**,** spherical protrusion and a rigid plane.

Let the maximum thickness of the spherical cap be l_0 and the radius of curvature R. We will call the radius of the contact a. For the sake of simplicity, we will accept that in the area of interest, the displacement satisfies the following geometric conditions: $d << l_0$, $l_0 << a$**.** In this case, every discrete element of the spherical cap is uniaxially deformed. For uniaxial deformation we use the modulus $\tilde{E}$ (2.12).

The form of a spherical cap with a radius of curvature of *R,* in the region near the minimum, can be presented as

$$z = -\sqrt{R^2 - r^2} + R \simeq \frac{r^2}{2R}. \tag{2.14}$$

It can be easily seen in Fig. 2.5 that the relationship between the radius of the contact area a and penetration depth d is given by the expression $d = a^2 / 2R$. From this, we can solve for the contact radius

$$a = \sqrt{2Rd} \,. \tag{2.15}$$

The vertical displacement of the surface in terms of the coordinate r is $\Delta l = d - r^2 / 2R$. The corresponding elastic deformation can be calculated using

$$\varepsilon(r) = \frac{\Delta l}{l_0} = \frac{d - r^2 / 2R}{l_0} \,. \tag{2.16}$$

The equations of stress and total force in the contact area eventually yield:

$$\sigma(r) = \tilde{E}\varepsilon(r) \,, \; F = \tilde{E}\int_0^a 2\pi r \left(\frac{d - r^2 / 2R}{l_0} \right) \mathrm{d}r = \tilde{E}\frac{\pi}{l_0} R d^2 \,. \tag{2.17}$$

In this case, the contact force is proportional to the square of the penetration depth. The greatest stress (in the center of the contact area) is

$$\sigma(0) = \tilde{E}\frac{d}{l_0} = \left(\frac{\tilde{E}F}{\pi l_0 R} \right)^{1/2} \,. \tag{2.18}$$

(4) Contact between a thin elastic sheet on a rigid, cylindrical base with a rigid plane.

Another system that is interesting in many ways is a rigid cylinder of length L covered with an elastic sheet (thickness l_0) (Fig. 2.6). Assuming that the penetration depth is much smaller and the contact radius is much larger than the sheet thickness, we again have uniaxial deformation. The displacement of the surface points can be calculated using $u_z = d - x^2 / 2R$, which can then be applied to calculate strain:

$$\varepsilon(x) = \frac{u_z}{l_0} = \frac{d - x^2 / 2R}{l_0} \,. \tag{2.19}$$

The total force can then be calculated using

$$F = 2\int_0^{\sqrt{2Rd}} \tilde{E}L \left(\frac{d - x^2 / 2R}{l_0} \right) \mathrm{d}x = \frac{4}{3} 2^{1/2} \frac{\tilde{E}LR^{1/2}}{l_0} d^{3/2} \,. \tag{2.20}$$

The maximum stress (in the middle of the contact area) is

$$\sigma(0) = \left(\frac{9F^2 \tilde{E}}{32L^2 R l_0} \right)^{1/3} . \tag{2.21}$$

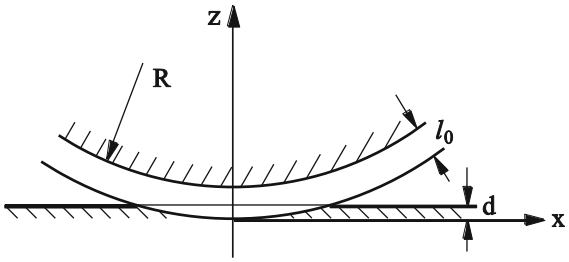

Fig. 2.6 Cylinder with an elastic sheet in contact with a rigid plane.

2.3 Estimation Method for Contacts with a Three-Dimensional, Elastic Continuum

(1) Contact between a rigid, cylindrical indenter and an elastic half-space

Now, we will consider a rigid, cylindrical indenter in contact with an *elastic half-space* (Fig. 2.7 a). With this example, we will explain the most important ideas used for qualitative estimations in contact mechanics.

If the stress distribution acts over a finite area of the surface with a characteristic length D (Fig. 2.7 b), then the deformation of and the stress on the total volume are on the same order of magnitude in a volume with dimension D in all three spatial dimensions. Beyond this "strongly deformed volume" the stress decreases according to $\propto r^{-2}$. That means that this volume $\sim D^3$ gives the largest contribution to energy and force relationships[4].

[4] The fact that the characteristic "penetration depth" of the stress and the deformation must have the same order of magnitude as the characterisitic size of the contact area comes from reasons of dimension. Actually, the equilibrium equation of the theory of elasticity does not contain any factor of the dimension length. The solution of an arbitrary equilibrium problem can, therefore, contain no length parameter other than the length that is given by the boundary conditions.

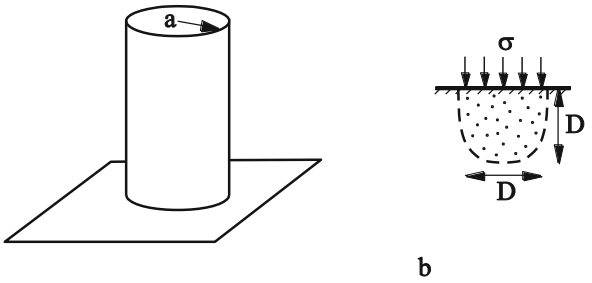

Fig. 2.7 (a) Contact between a rigid cylindrical indenter and an elastic half-space. (b) Strongly deformed area of the elastic half-space.

For a first order qualitative estimation, it is sufficient to suppose that the deformation is constant in the mentioned volume and that only this volume is deformed. Naturally, this is only a very rough estimate of real distributions of deformations and stresses in a continuum. It does, however, give correct results for the qualitative relationships between contact force and the penetration depth as well as the contact radius, except for a scalar factor, which is on the order of 1 and can be determined through analytical or numerical calculation.

We apply this simple estimation rule to our example with a rigid indenter. When the diameter of the cylinder is equal $2a$, then the volume measuring $2a$ in all three directions is strongly deformed. If this volume is indented to a depth of d, we will estimate the deformation as $\varepsilon \approx d/2a$. For the stress, we obtain $\sigma \approx E\varepsilon \approx Ed/2a$ and for the force $F \approx \sigma(2a)^2 \approx 2Eda$: The contact force is proportional to the penetration depth and to the contact radius a. It is interesting to compare this estimation with the exact solution of the problem (Chapter 5). The exact result is

$$F = 2E^* da\,, \tag{2.22}$$

where $E^* = \dfrac{E}{1-\nu^2}$. For metallic materials ($\nu \approx 1/3$), the difference between the exact result and the estimation falls to within only 10%. This example impressively shows that the described estimation method can be used not only for qualitative, but also for good quantitative estimations.

Equation (2.22) indicates that the penetration depth is proportional to the normal force. The coefficient between the force F and the displacement d is called the *stiffness of the contact*:

$$k = 2E^* a\,. \tag{2.23}$$

We emphasize that the stiffness is, in this case, proportional to the *radius* (not the contact area!).

(2) Contact between a rigid sphere and an elastic half-space

Now, we will consider the contact between a rigid sphere with the radius R and an elastic half-space[5]. In this case, we also limit ourselves this time to a qualitative estimation. A rigorous treatment can be found in chapter 5.

If there were no elastic interactions between the sphere and the surface, we would have a penetration depth d, a contact radius $a \approx \sqrt{2Rd}$, and a contact area

$$A = \pi a^2 \approx 2\pi R d . \tag{2.24}$$

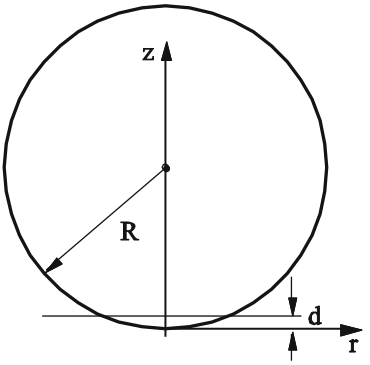

Fig. 2.8 Hertz Contact Problem.

According to the formulated estimation rules, the dimensions of the heavily deformed area are on the same order of magnitude as the contact diameter $2a$. The order of magnitude of the elastic deformation in this area is $\varepsilon \approx d / 2a$. Therefore, the magnitude of the stress is on the order of $\sigma \approx E\frac{d}{2a}$. This yields the force of $F = \sigma A \approx \frac{Ed}{2a}\pi a^2 \approx \frac{Ed}{2}\pi\sqrt{2Rd} = \frac{\pi}{\sqrt{2}}Ed^{3/2}R^{1/2}$. Therefore, the force is proportional to $d^{3/2}$. This is comparable to the exact result of[6]

$$F = \frac{4}{3}E^* R^{1/2} d^{3/2} . \tag{2.25}$$

They differ only by a factor of approximately 1.5.

If the half-space was *plastically* deformed, the ratio between the normal force and the contact area would be

$$\sigma_0 = \frac{F_N}{\mathrm{A}} . \tag{2.26}$$

---

[5] For normal contact, it does not matter if the contact is between an elastic sphere and a rigid plane or if it is between a rigid sphere and an elastic half-space.

[6] See chapter 5.

Using Equation (2.24) results in

$$F_N = 2\pi\sigma_0 Rd\,. \tag{2.27}$$

In the plastic area, the force is proportional to the depth of the indentation. The average stress remains the same and is equal to the hardness of the material.

(3) Contact between a rigid cylinder and an elastic half-space

Next, we will investigate the contact between a rigid cylinder and an elastic half-space (Fig. 2.9). The contact radius is estimated to be $a \approx \sqrt{2Rd}$, as in the case of a sphere. The order of magnitude of the stress is $Ed/2a$ and the contact area $2La$, in which L is the length of the cylinder. This yields a force of $F \approx \frac{Ed}{2a} 2La = ELd$. The exact result is

$$F = \frac{\pi}{4} E^* Ld\,. \tag{2.28}$$

In this case, the discrepancy between the simple estimation and the exact result is also minimal. The force is, in this case, linearly proportional to the indentation depth and is independent from the radius of the cylinder. Also, the contact stiffness can be defined as the coefficient between the force and the vertical displacement d:

$$c = \frac{\pi}{4} E^* L\,. \tag{2.29}$$

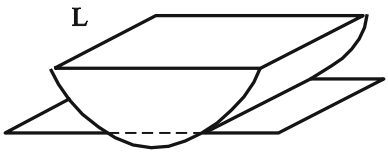

Fig. 2.9 Contact between a rigid cylinder and an elastic half-space.

In the plastic area we obtain

$$F_N \approx \sigma_0 2aL \approx 2^{3/2}\sigma_0 LR^{1/2}d^{1/2}\,. \tag{2.30}$$

(4) Contact between a rigid cone and an elastic body

The contact radius is, in this case, determined by the condition $a\tan\theta = d$ (Fig. 2.10). The deformation is estimated as $\varepsilon \approx d/2a = \frac{1}{2}\tan\theta$. The average stress is on the order of

$$\sigma \approx E\varepsilon \approx \tfrac{1}{2} E \tan\theta \tag{2.31}$$

and is independent of the penetration depth. We obtain the estimation for the normal force using

$$F_N \approx \frac{\pi}{2} E \frac{d^2}{\tan\theta} . \tag{2.32}$$

The force is proportional to the square of the penetration depth. The exact result is[7]

$$F_N = \frac{2}{\pi} E \frac{d^2}{\tan\theta} . \tag{2.33}$$

If the stress (2.31) is smaller than the hardness of the material, it will be elastically deformed. Otherwise, we can assume that the deformation is essentially plastic. In this case, the normal force is provided by the estimation

$$F_N = \pi\sigma_0 \frac{d^2}{\tan^2\theta} . \tag{2.34}$$

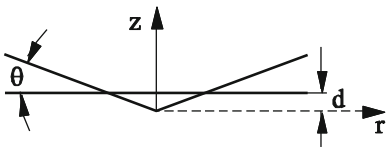

Fig. 2.10 Contact between a cone and a plane.

Problems

Problem 1: Determine the force-displacement dependence, the effective modulus of elasticity, and the shear stress distribution in a contact plane for a thin, round, elastomer sheet with a radius R and a sheet thickness h, assuming that the material is incompressible.

Solution: We will consider two cases:
(a) The sheet sticks to both bodies (Fig. 2.11).

We will solve the problem in two steps: First, we will calculate the elastic potential energy in the sheet as a function of the penetration depth d. The derivative

[7] I.N. Sneddon, The Relation between Load and Penetration in the Axisymmetric Boussinesq Problem for a Punch of Arbitrary Profile. Int. J. Eng. Sci.,1965, v. 3, pp. 47–57.

of this energy with respect to d will then provide the normal force. In order to calculate the potential energy, we use the following equation for the displacement field in the sheet:

$$u_r(r,z) = C\left(\left(\frac{h}{2}\right)^2 - z^2\right)\frac{r}{R}.$$

This equation fulfills the no-slip condition $u_r = 0$ for $z = \pm h/2$. The condition for incompressibility states

$$d \cdot \pi R^2 = 2\pi R \int_{-h/2}^{h/2} u_r(R,z)\mathrm{d}z = \frac{1}{3}\pi RCh^3.$$

This provides $C = \dfrac{3Rd}{h^3}$ and

$$u_r(r,z) = \frac{3rd}{h^3}\left(\left(\frac{h}{2}\right)^2 - z^2\right).$$

The largest part of the potential energy, in this case, is associated with the shearing of the sheet. The shear deformation is

$$\varepsilon_{rz} = \frac{\partial u_r}{\partial z} = -\frac{6d}{h^3}rz,$$

the energy density is

$$\mathrm{E} = \frac{1}{2}G\varepsilon_{rz}^2 = \frac{18Gd^2r^2z^2}{h^6}$$

and the total energy is

$$U = \frac{18Gd^2}{h^6}\int_0^R\int_{-h/2}^{h/2} r^2z^2 2\pi r\mathrm{d}r\mathrm{d}z = \frac{3\pi GR^4}{4h^3}d^2.$$

The force acting on the surface is

$$F_N = \frac{\partial U}{\partial d} = \frac{3\pi GR^4}{2h^3}d.$$

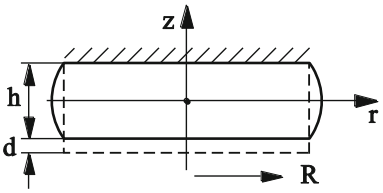

Fig. 2.11 Contact between a thin, round, incompressible, elastomer sheet and two rigid planes, which cling to the elastomer.

A comparison with (2.10) allows us to find the *effective modulus of elasticity*: $\frac{3\pi GR^4}{2h^3} d = E_{eff} \pi R^2 \frac{d}{h}$. This gives us

$$E_{eff} = \frac{3}{2} G \left(\frac{R}{h} \right)^2 = \frac{1}{2} E \left(\frac{R}{h} \right)^2 .$$

This effective modulus is quadratically dependent on the ratio of the radius of the sheet to its thickness and can be much larger than the modulus of elasticity E. For the static stress at the contact surface, we have

$$\sigma_{rz}(r, z = -h/2) = G\varepsilon_{rz}\left(r, z = -h/2\right) = G\frac{3d}{h^2} r = E\frac{d}{h^2} r .$$

It increases linearly from the center and reaches the maximum at the edge of the sheet:

$$\sigma_{rz,\max} = \frac{ERd}{h^2} .$$

In the presence of static friction with a coefficient of friction μ_s, slipping will not occur at any point in the contact area if

$$\frac{\sigma_{rz,\max}}{\sigma_{zz}} = \frac{\sigma_{rz,\max} \pi R^2}{F_N} = \frac{2h}{R} \leq \mu_s .$$

(b) The sheet sticks to the upper surface and slides, without friction, on the lower surface (Fig. 2 12).

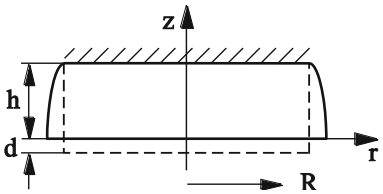

Fig. 2.12 Contact between a thin, round, incompressible, elastomer sheet and a frictionless rigid plane.

In this case, we use the equation

$$u_r(r,z) = C_1\left(h^2 - z^2\right)\frac{r}{R},$$

in which we have the no-slip condition of $u_r(r,h) = 0$ on the upper surface and the free sliding condition of $\left.\frac{\partial u_r(r,z)}{\partial z}\right|_{z=0} = 0$ on the lower surface. The incompressibility requirement is

$$d \cdot \pi R^2 = 2\pi R \int_0^h u_r(R,z)\mathrm{d}z = \frac{4}{3}\pi R h^3 C_1.$$

That means that $C_1 = \frac{3Rd}{4h^3}$ and

$$u_r(r,z) = \frac{3d}{4h^3}\left(h^2 - z^2\right)r.$$

This results in a shear deformation

$$\varepsilon_{rz} = \frac{\partial u_r}{\partial z} = -\frac{3d}{2h^3}zr.$$

The energy density is

$$\mathrm{E} = \frac{1}{2}G\varepsilon_{rz}^2 = G\frac{9d^2}{8h^6}z^2r^2$$

and the total energy is

$$U = G\frac{9d^2}{8h^6}\int_0^R\int_0^h r^2z^2 2\pi r\mathrm{d}r\mathrm{d}z = \frac{3\pi G d^2 R^4}{16h^3}.$$

The force acting on the surface is

$$F_N = \frac{\partial U}{\partial d} = \frac{3\pi G R^4}{8h^3}d.$$

This force is four times smaller than in the case of the stick condition on both surfaces.

Problem 2: For a pneumatic tire contact, determine the size of the contact area, pressure distribution in the contact area, and penetration depth as a function of the normal force.

Solution: The stiffness of a pneumatic tire is mainly determined by the pressure difference between the interior of the tire and the atmosphere outside. In the simplest model, it can be considered as a weakly extensible, flexible membrane in the

form of a torus (Fig. 2.13). Due to the curvature of the membrane, the elastic forces within it maintain the balance with respect to the pressure difference. However, the contact area at the bottom of the membrane is flat (Fig. 2.14). Therefore, in the contact region the elastic forces make no contribution to the equilibrium: in each element of the flattened tire in contact with the floor, the pressure difference caused by the reacting stresses from the floor must be held in equilibrium. *The normal stress in the entire contact area is constant and equal to the pressure difference in the tire*:

$$\sigma_N = \Delta p = p_1 - p_0 .$$

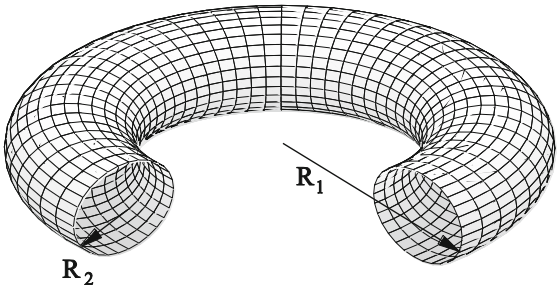

Fig. 2.13 As a first approximation, a pneumatic tire can be considered to be a flexible membrane in the form of a torus with the internal radius R_2 and the outer radius R_1.

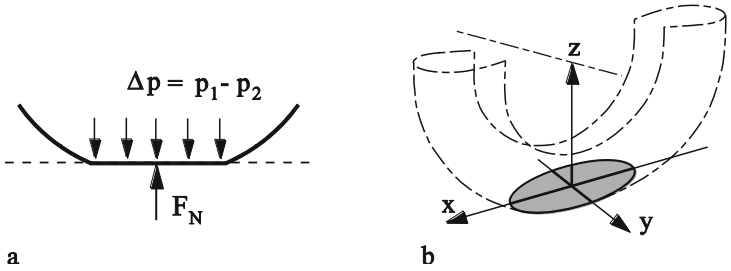

Fig. 2.14 (a) As a first approximation, the normal stress in the contact region may be assumed to be constant and is equal to the pressure difference Δp ; (b) a tire with the flattened bottom using the appropriate coordinate system for this problem.

Outside the contact area, the tire is not deformed. The boundary of the contact area is determined by the equation

$$\frac{x^2}{2R_1} + \frac{y^2}{2R_2} = d ,$$

where d is indentation depth. This equation describes an ellipse with the semi-axes, $a = \sqrt{2R_1 d}$, $b = \sqrt{2R_2 d}$ and the surface area $A = \pi ab = 2\pi d\sqrt{R_1 R_2}$. The total normal force is given by

$$F_N = \Delta p \cdot A = 2\pi \Delta p \sqrt{R_1 R_2} \cdot d \, .$$

This force is proportional to the depth of penetration, as in the case of a simple linear elastic spring.

Problem 3: How does the volume of a pneumatic tire change when you press it into a rigid plane with the force F_N?

Solution: u_p is the displacement of the surface points under the pressure Δp; ΔV_F is the change in the volume of the tire under the influence of the normal force. According to Betti's reciprocity theorem, if a linear elastic body is subjected to two different load systems, the work of the forces in the first system over the displacements of the second system is equal to the work of the forces of the second system over the displacements of the first system. In our case this means:

$$F_N u_p = \Delta p \cdot \Delta V_F \, .$$

As an estimation, we use the equation for the change in the radius R_2 of an elastic cylindrical container due to pressure change Δp:

$$\Delta R_2 \approx R_2 \varepsilon \approx \frac{R_2}{E} \sigma \approx \frac{R_2}{E} \frac{\Delta p R_2}{h} = \frac{\Delta p R_2^2}{Eh} \, ,$$

where E is elastic modulus of the membrane and h is its thickness. The tensile stress $\sigma = \Delta p R_2 / h$ in the membrane is estimated using Barlow's formula. If the inside of the tire is held by a rigid (metallic) rim, then the displacement of the contact point is

$$u_p \approx 2\Delta R_2 \approx \frac{2\Delta p R_2^2}{Eh} \, .$$

From Betti's reciprocity theorem, we obtain the change in volume

$$\Delta V_F = \frac{F_N u_p}{\Delta p} \approx \frac{2F_N R_2^2}{Eh} \, .$$

3 Qualitative Treatment of Adhesive Contacts

In the previous chapter, we examined contact problems with the assumption that the contacting surfaces did not "adhere." In reality, there are relatively weak interactive forces between any two bodies, which decrease very quickly as the distance between the bodies increases. These forces lead, in most cases, to mutual attraction and are known as *adhesive forces*. Adhesive forces play an essential role in many technical applications. It is the adhesive forces that are responsible for the behavior of glue, for instance. Adhesive tape, self-adhesive envelopes, etc. are further examples of adhesive forces.

Adhesive forces play an important role in applications where one of the following conditions is met:

(i) The surface of the body is very smooth, (e.g. that of a magnetic disc of a hard drive).

(ii) One of the contact partners is made of a soft material (e.g. rubber or biological structures) or

(iii) We are dealing with a microscopic system, in which adhesive forces generally have a larger influence than body forces, because the body and surface forces are scaled differently (micro-mechanical devices, atomic force microscope, biological structures, etc.)

Adhesion plays an essential role in rubber friction and is therefore an important phenomenon that must be accounted for in the development of materials for automobile tires.

V.L. Popov, *Contact Mechanics and Friction*,
DOI 10.1007/978-3-662-53081-8_3

In this chapter, we will explain the physical origins of adhesive forces and qualitatively discuss the fundamental ideas for calculations regarding adhesive contacts.

3.1 Physical Background

Electrically neutral atoms or bodies at a distance equal to or greater than the size of the atoms are attracted according to dispersive or van der Waals forces.

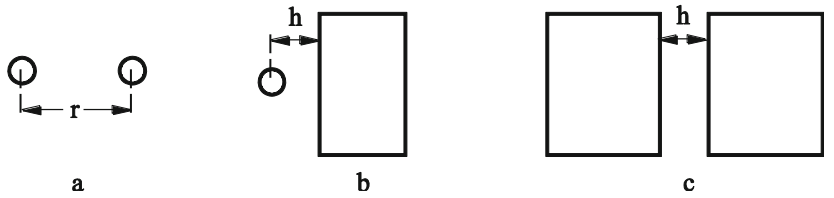

Fig. 3.1 Interaction between two atoms (a), an atom and a half-space (b) and between two half-spaces (c).

The interaction between two neutral atoms at a distance r (Abb. 3.1 a) can be approximately described with the *Lennard-Jones-Potential*: $U = \frac{C_1}{r^{12}} - \frac{C}{r^6}$. The equilibrium distance r_0 calculates to $r_0 = \left(2C_1 / C\right)^{1/6}$. For the sake of simplicity, we will replace this potential in the following estimations with (Fig. 3.2):

$$U_{at-at} = \begin{cases} -\frac{C}{r^6}, & r \geq r_0 \\ \infty, & r < r_0 \end{cases} . \tag{3.1}$$

The simplification has only a slight influence on the most important interaction parameters, the equilibrium distance and the binding energy, but essentially facilitates calculations.

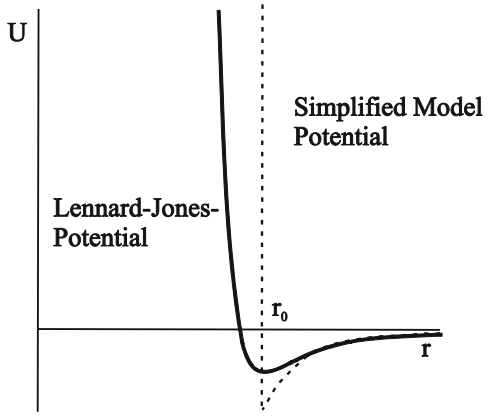

Fig. 3.2 Graph of the Lennard-Jones-potential and the simplified model potential (3.1).

We calculate the interaction between two bodies with atomically smooth surfaces at a distance h in two steps. First, we calculate the interaction energy between an atom at a distance h from a three-dimensional body, which is composed of the same type of atoms with a concentration n (Fig. 3.3 a)[1] :

$$U_{at-sol} = -\int \frac{CndV}{R^6} = -Cn\int_0^\infty dz \int_0^\infty 2\pi r dr \frac{1}{\left((h+z)^2 + r^2\right)^3} = -\frac{\pi Cn}{6h^3}. \qquad (3.2)$$

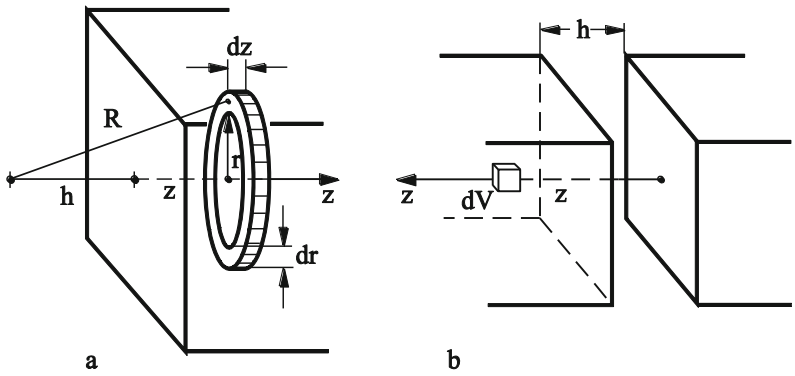

Fig. 3.3 Calculation of the interaction potential between an atom and a three-dimensional body (a) and two three-dimensional bodies at a distance h (b).

In the second step, we calculate the interaction energy between two solid bodies with parallel surfaces and assume thereby that each of bodies is composed of the

[1] In this calculation, we neglect the interactions between the atoms which make up the bodies. The calculation remains, nevertheless, correct up to a linear coefficient. Supplementary information over van der Waals forces can be found in Section 3.6.

same type of atoms (Fig. 3.1 c and Fig. 3.3 b). This interaction energy is found through integration in the first body over the z-coordinate and multiplying it with the surface area A of the body and the atom concentration n. The interaction energy per unit area is

$$\frac{U_{sol-sol}}{A} = -\int_h^\infty \frac{\pi C n^2}{6z^3} dz = -\frac{\pi C n^2}{12h^2} = -\frac{Q}{h^2} \ , \tag{3.3}$$

where $Q = \pi C n^2 / 12$. If two bodies are moved together from a large distance to "direct contact," (meaning to a distance of $\simeq r_0$), the interaction forces perform work per unit area of

$$\frac{W}{A} = \frac{Q}{r_0^2} \ . \tag{3.4}$$

In order to pull the two bodies apart, the same work must be performed by external forces. One can say that in order to create two surfaces, the work (3.4) per unit area is required. Half of this value (i.e. the energy that is required to create one surface) is called the *surface energy density (also surface tension)* γ of the body[2]:

$$\gamma = \frac{Q}{2r_0^2} \ . \tag{3.5}$$

This quantity determines all of the essential contact properties that relate to adhesion. Typical values for the surface energy of various solids and liquids are given in Table 3.1.

Let us estimate the value of the van der Waals forces. We obtain the interaction force per unit area of two atomically smooth bodies at a distance h by differentiating the potential energy per unit area (3.3) with respect to h:

$$\sigma = -\frac{1}{A}\frac{\partial U_{sol-sol}}{\partial h} = -\frac{2Q}{h^3} \ . \tag{3.6}$$

In "direct contact" (i.e. $h \approx r_0$) the van der Waals stress is

$$\sigma = \frac{F}{A} = -\frac{2Q}{r_0^3} = -\frac{2}{r_0}\frac{Q}{r_0^2} = -\frac{4\gamma}{r_0} \ . \tag{3.7}$$

[2] In using the term surface energy in contact mechanics, one must keep in mind that some authors call the energy 2γ necessary to separate the bodies the "surface energy" (e.g. in the book by K. Johnson "Contact Mechanics").

Table 3.1 Surface Energies of Solid and Liquid Materials

Surface Energy of Molecular Crystals and Metals

Material	Surface Energy γ_s (10^{-2} J/m^2)
Nylon	4.64
Polyvinyl chlorid (PVC)	3.9
Polystyrene	3.30
Polyethylene	3.0
Paraffin	2.50
PTFE (Teflon)	1.83
NaCl	16
Al_2O_3	64
Si	128
Al	112
Ag	144
Fe	240
W	450

Surface Energy of Liquids

Liquid	Surface Energy γ_l (10^{-2} J/m^2)
Water	7.31
Benzine	2.88
n-Pentane	1.60
n-Octane	2.16
n-Dodecane $(C_{12}H_{26})$	2.54
n-Hexadecane $(C_{16}H_{34})$	2.76
n-Octadecane ($C_{18}H_{38}$)	2.80

For a value $\gamma \approx 1 \div 2$ J/m^2, which is typical for many metals, and a value $r_0 \approx 4 \cdot 10^{-10}$ m, we obtain a stress $\sigma = 10^{10}$ N/m^2. Thus, a contact surface of 1 cm^2 could hold a weight of 100 tons (much more than as shown in Fig. 3.4 a)!

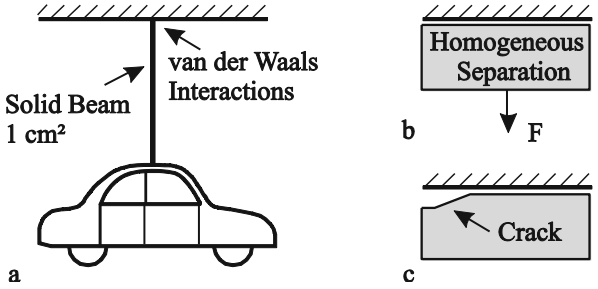

Fig. 3.4 Van der Waals forces between atomically smooth surfaces are much stronger than can be guessed based on our everyday experiences (a); In real systems, they are strongly reduced in part by the roughness of the surfaces and in part by the fact that fractures propagate through existing flaws in the medium.

Such strong adhesive forces are never observed in reality. This estimation explains Kendall's statement in his book *Molecular Adhesion and its Applications (Kluwer Academic, 2001)*:

> "solids are expected to adhere; the question is to explain why they do not, rather than why they do!"

The solution to this adhesion paradox is explained by the fact that molecular bond fractures on a macroscopic scale are never homogeneous (Fig. 3.4 b), rather they are facilitated by propagating through existing flaws (Fig. 3.4 c), which drastically diminish the adhesive force. Also, the roughness of the surface can lead to a drastic reduction of the adhesive force (see the discussion on the influence of roughness on adhesion in 3.4).

3.2 Calculation of the Adhesive Force between Curved Surfaces

The first calculation of the adhesive force between solid bodies with curved surfaces stemmed from Bradley (1932)[3]. We consider a rigid sphere with a radius R at a distance h from a rigid plane of the same material. We calculate the interaction energy between these bodies with an approximation, which we will also use later in most contact problems: *We assume that the contact area is significantly smaller than the radius of the sphere, so that one can approximately assume that the surfaces of the two bodies are parallel, although the separation distance remains dependent on the longitudinal coordinate ("Half-Space Approximation").*

[3] R.S. Bradley, Phil. Mag 1932., v. 13, p. 853.

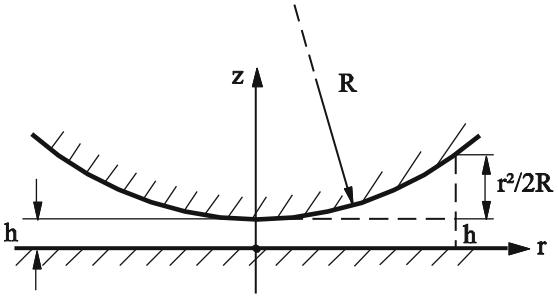

Fig. 3.5 Diagram for calculating the adhesive forces between a rigid sphere with the radius *R,* and a rigid plane.

The interactive potential per unit area at a distance of $z = h + r^2 / 2R$ (see Fig. 3.5) is given by (3.3). By integrating over the entire area, we obtain

$$U_{plane-sphere} = -\int_0^\infty \frac{Q}{\left(h + r^2 / 2R\right)^2} 2\pi r dr = -\frac{2\pi RQ}{h} . \tag{3.8}$$

By differentiating the potential energy with respect to *h,* we obtain the interactive force $F = -\partial U / \partial h$:

$$F = -\frac{2\pi RQ}{h^2} . \tag{3.9}$$

In the case of direct contact ($h \approx r_0$):

$$F_{adh} = -\frac{2\pi RQ}{r_0^2} = -4\pi\gamma R . \tag{3.10}$$

This result differs from the adhesive force between elastic, deformable bodies (see chapter 6) by only a factor of 4/3.

3.3 Qualitative Estimation of the Adhesive Force between Elastic Bodies

We begin with the simplest case of contact between a smooth, rigid plate and a smooth, elastic block (Fig. 3.6). Due to the adhesive forces, the block and the plate adhere to one another and a force must be applied in order to separate the block from the plate. Assume that we try to separate the two by applying a tensile stress σ to the free end of the block. Due to this stress, the block is stretched a length *d*. The density of elastic potential energy of a stretched material is $E\varepsilon^2 / 2 = \sigma^2 / 2E$. The total potential energy is obtained by multiplying the ener-

gy density by the volume of the block: $U_{el} = \frac{\sigma^2}{2E} l_0 A$, where A is the cross-sectional area of the block.

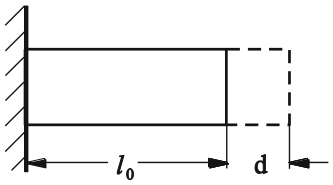

Fig. 3.6 Adhesion of a rectangular block on a smooth wall.

We now want to examine the *conditions, under which the block can spontaneously separate from the rigid surface.* If they were to separate, two new surfaces would be created. In order for this to take place the energy $U_{adh} = 2\gamma A$ is required**.** A process in a closed physical system can only take place if the total potential energy in the system would decrease: $U_{adh} - U_{el} = 2\gamma A - \frac{\sigma^2}{2E} l_0 A < 0$. The critical stress, at which this process can take place, is

$$\sigma_{cr} = \sqrt{\frac{4E\gamma}{l_0}} \,. \tag{3.11}$$

This "failure stress**"** increases with the modulus of elasticity E, and the surface energy γ, and decreases with the thickness of the elastic block. Hence, there is the well known rule for the application of most adhesives: The thinner the layer, the stronger the bond[4]. The application of this rule is, however, limited by the roughness of the surfaces.

As the second example, we consider the contact between a rigid sphere and a flat, *elastic* body. The surfaces of both bodies are assumed to be absolutely smooth. For the penetration depth d the value of the contact area will be $a \approx \sqrt{2Rd}$ (see similar problem without adhesion, chapter 2). If the stress acts on a defined area of the surface of an elastic half-space with a linear $2a$, then the majority of the potential energy is stored in the volume $(2a)^3$. Therefore, one can assume that, in most cases, only the volume highlighted in Fig. 2.7 b is significantly deformed. The magnitude of the elastic deformation is described as $\varepsilon \approx d / 2a$, the energy density as $E\varepsilon^2 / 2$, and the total elastic energy as

[4] It should be noted that most adhesives (after solidifying) are elastic mediums with (relatively) small moduli of elasticity, so that in calculating the elastic energy, only the energy of the adhesive layer must be taken into account.

$U_{el} \sim \frac{E}{2}\varepsilon^2 (2a)^3 = E2^{1/2} R^{1/2} d^{5/2}$. The surface energy is $U_{adh} = -2\gamma\pi a^2 = -4\pi\gamma Rd$. Therefore, the total energy of the system is

$$U_{tot} \approx E2^{1/2} R^{1/2} d^{5/2} - 4\pi\gamma Rd . \tag{3.12}$$

The force acting on the system is $F \approx \frac{\partial U_{tot}}{\partial d} \approx 5E2^{-1/2}\sqrt{R}d^{3/2} - 4\pi\gamma R$. The adhesive force is the maximum negative force that acts on the body. It is found at $d = 0$:

$$F_{adh} \approx -4\pi\gamma R . \tag{3.13}$$

An exact calculation results in $F_{adh} = -3\pi\gamma R$, see chapter 6. Interestingly, the adhesive force between two elastic bodies is of the same order of magnitude as that between two rigid bodies (3.10).

3.4 Influence of Roughness on Adhesion

That adhesive forces in the macroscopic world are very small and can often be neglected is attributed to the fact that practically all surfaces possess roughnesses of various scales. In order to qualitatively discuss the influence of roughness, we consider a smooth, elastic body in contact with a rough, rigid plane.

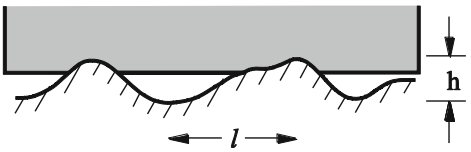

Fig. 3.7 An elastic medium in contact with a rough, rigid surface.

Let the characteristic roughness wavelength be l and the characteristic height h. If the elastic body is deformed so that the "valleys" are completely filled, then the elastic energy $U_{el} \approx \frac{1}{2}G\varepsilon^2 l^3 \approx \frac{1}{2}G\left(\frac{h}{l}\right)^2 l^3 = \frac{1}{2}Glh^2$ is stored[5]. At the same time, the surface energy is reduced by $U_{adh} \approx 2\gamma l^2$. If the adhesive energy is sufficiently large to generate such a deformation, then the body will spontaneously deform and adhere over the entire surface. That happens when $U_{el} < U_{adh}$, or when

[5] A more exact calculation can be found in the first problem of this chapter.

$$h^2 < \frac{4\gamma l}{G}. \tag{3.14}$$

If the roughness is much smaller than the critical roughness, then the surface can be considered absolutely smooth. For larger roughnesses there is only contact at a few points and the adhesive force is significantly decreased. The critical roughness is, in addition to the surface energy γ, dependent on the elastic shear modulus G. Therefore, materials with very small elastic moduli can also adhere to very rough surfaces. An example of this is rubber, which has a typical shear modulus around 1 MPa[6], which is 5 orders of magnitude smaller than those of "stiff" solid bodies, such as metals. For stiff bodies the condition (3.14) is only fulfilled with very smooth, polished surfaces. For typical roughness parameters of $h \approx 1\,\mu\text{m}$, $l \approx 100\,\mu\text{m}$, and $G = 80$ GPa, the relationship is $\frac{Gh^2}{4\gamma l} \approx 10^2 \gg 1$. The adhesive force under these conditions is negligibly small.

3.5 Adhesive Tape

As a further example to the applications of the ideas about the physical nature of adhesion, we will discuss the conditions for the equilibrium of adhesive tape. We consider a flexible membrane of width L, which lays in part on a rigid, planar body (Fig. 3.8 a). The tape is pulled with a force F. We call the energy that is required to separate a unit area of the tape from the rigid body the "effective surface energy" and refer to it as γ^*. We calculate the angle at which the tape must be pulled (with a given force) so that the separation line is in equilibrium. To this aim, let us consider a section of tape of length l_0 between O and A (Fig. 3.8 b).

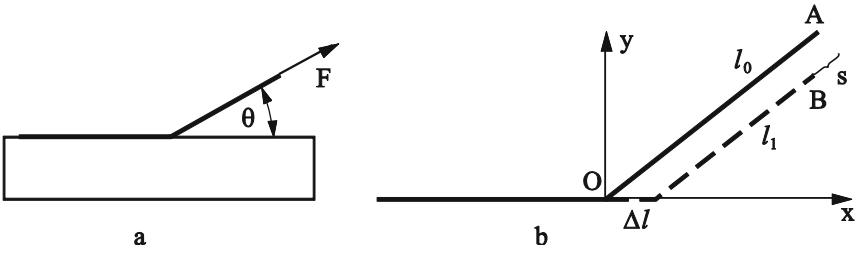

Fig. 3.8 Force diagram of a piece of tape acted on by an external force.

According to the principle of virtual work in equilibrium, the sum of the work of all forces during an arbitrary infinitesimal displacement of the system must be equal to zero. We consider a displacement of the tape that corresponds to a separa-

[6] Pure, unfilled rubber.

tion of the tape from the body of length Δl. With this movement the surface energy is increased by $\gamma^* L\Delta l$; the adhesive forces perform thereby work equal to $-\gamma^* L\Delta l$. At the same time, the end of the tape on which the force acts (point B) is displaced in the direction of the force by a distance s. The work performed by *F* is equal to *Fs*. The equilibrium condition is $Fs = \gamma^* L\Delta l$. It is easy to see that $s = \Delta l(1-\cos\theta)$ and, therefore, $F_0(1-\cos\theta) = \gamma^* L$. For the critical "separation force," F_0 we get

$$F_0 = \frac{\gamma^* L}{1-\cos\theta}. \tag{3.15}$$

The critical separation force (per unit length) perpendicular to the plane is equal to the surface energy. By pulling in the direction π (opposite to the direction of the tape) the critical force is half as large.

3.6 Supplementary Information about van der Waals Forces and Surface Energies

An extensive theory on van der Waals forces was developed by I.E. Dzyaloshinskii, E.M. Lifschitz, and L.P. Pitaevskii (1961)[7]. It says that the van der Waals forces depend significantly on the dielectric constant of the bodies and of the medium between the two bodies. If the dielectric constant of the medium ε_m is smaller as the dielectric constant of both bodies: $\varepsilon_m < \varepsilon_1, \varepsilon_2$, the bodies attract. If it lies between ($\varepsilon_1 < \varepsilon_m < \varepsilon_2$), then the bodies repel! The latter effect is used in atomic force microscopy to prevent the adhesive forces and related instabilities.

According to this theory, a rough first approximation of the van der Waals force between two bodies is proportional to the product $\frac{(\varepsilon_1-\varepsilon_m)(\varepsilon_2-\varepsilon_m)}{(\varepsilon_1+\varepsilon_2)}$. If the medium between the bodies is a vacuum ($\varepsilon_m = 1$), then the force is always positive (the bodies attract) and is proportional to $\frac{(\varepsilon_1-1)(\varepsilon_2-1)}{(\varepsilon_1+\varepsilon_2)}$. One can give a rough empirical rule of calculation for *relative surface energies* in the approximation, in which the equilibrium distance r_0 (3.5), for various bodies is approximately the same and the main difference in the surface energies is caused by the different polarizability and therefore the dielectric constant.

---

[7] I.E. Dzyaloshinskii, E.M. Lifshitz und L.P. Pitaevskii, General Theory of van der Waals' Forces, Sov. Phys. Usp. 1961, v. 4, pp. 153-176.

We define the relative surface energy as the energy (per unit area) that is required to separate the bodies beginning from the equilibrium distance r_0. The relative surface energy for two identical bodies of material 1 is proportional to $\gamma_{11} = 2\gamma_1 \propto \frac{(\varepsilon_1 - 1)^2}{2\varepsilon_1}$. Likewise, the relative surface energy for two identical bodies of material 2 is proportional to $\gamma_{22} = 2\gamma_2 \propto \frac{(\varepsilon_2 - 1)^2}{2\varepsilon_2}$. The relative surface energy for bodies 1 and 2 is $\gamma_{12} \propto \frac{(\varepsilon_1 - 1)(\varepsilon_2 - 1)}{(\varepsilon_1 + \varepsilon_2)}$, from which we obtain[8]

$$\gamma_{12} \approx \sqrt{\gamma_{11}\gamma_{22}} = 2\sqrt{\gamma_1\gamma_2} \,. \tag{3.16}$$

The relative surface energy is roughly equal to the geometric average of the surface energies of the two solids. In the case of two bodies, each composed of different materials, the γ in Equations (3.11) and (3.13) should be replaced with $\gamma_{12}/2$, half of the relative surface energy.

Problems

Problem 1: A smooth, elastic body (rubber) is in contact with a rigid, rough surface which is characterized by a characteristic wave length l and a characteristic height $\hat{h}$. The "width" of the medium L is much larger than l. Under the assumption that the roughness can be modeled as $z = \hat{h}\cos(2\pi x/l)$, calculate the critical relationship $\hat{h}/l$, at which the "valleys" will be completely filled. What is the maximum allowable characteristic roughness with $l = 100\mu$m at which the rubber will still completely adhere to the rigid surface? Pure (unfilled) rubber has a shear modulus G of about 1 MPa; the relative surface energy of a rigid contact partner to rubber is around $\gamma_{12} \approx 3 \cdot 10^{-2}$ J/m^2 (Fig. 3.9).

[8] We have thereby replaced the geometric average $\sqrt{\varepsilon_1\varepsilon_2}$ with the arithmetic average $(\varepsilon_1 + \varepsilon_2)/2$. For the accuracy of the approximation, this assumption is acceptable.

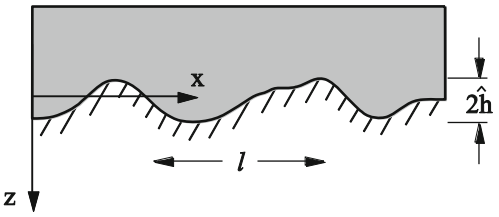

Fig. 3.9 Complete contact between a wavy, rigid surface and an elastic medium (rubber).

Solution: For an isotropic, linearly elastic medium in equilibrium it holds true that

$$\nabla \mathrm{div}\mathbf{u} + (1-2\nu)\Delta\mathbf{u} = 0 \,.$$

The solution of this equation with the boundary conditions $u_z(x, z=0) = \hat{h}\cos kx$ and $\sigma_{zx}(x, z=0) = 0$ (frictionless in the horizontal direction) provides us with

$$u_z = \hat{h}\left(1 - \frac{kz}{2(1-\nu)}\right)\cos kx \cdot e^{kz}$$

and

$$u_x = \hat{h}\left(\frac{1-2\nu}{2(1-\nu)} + \frac{kz}{2(1-\nu)}\right)\sin kx \cdot e^{kz} \,,$$

where $k = 2\pi / l$. From the general equation for the stress tensor

$$\sigma_{ik} = \frac{\nu E}{(1+\nu)(1-2\nu)} \sum_{l=x,y,z} u_{ll}\delta_{ik} + \frac{E}{1+\nu} u_{ik} \,,$$

with $u_{ik} = \frac{1}{2}\left(\partial u_i / \partial x_j + \partial u_j / \partial x_i\right)$, we get the normal stress on the surface:

$$\sigma_{zz}\big|_{z=0} = \frac{E\hat{h}k\cos kx}{2(1-\nu^2)} \,.$$

The elastic energy that is saved in the section of the medium with the length l in the x-direction can be calculated as

$$U_{el} = \frac{1}{2}\int_0^l u_z(x)\sigma_{zz}(x)L dx = \frac{\pi E\hat{h}^2 L}{4(1-\nu^2)} \,.$$

The rubber will adhere to the entire surface if this energy is smaller than the surface energy $\gamma_{12} Ll$:

$$\frac{\pi E\hat{h}^2 L}{4(1-\nu^2)} < \gamma_{12} Ll \,.$$

The critical amplitude of the undulation is then

$$\hat{h}_c^2 = \frac{4\gamma_{12} l(1-\nu^2)}{\pi E} = \frac{2\gamma_{12} l(1-\nu)}{\pi G}.$$

(Compare this result to that of the estimation in (3.14)!). From the given numerical values and $\nu \approx 0.5$ the critical roughness is found to be $h_c \approx 1\mu\text{m}$.

Problem 2: A rigid body with a wavy surface ($h = \hat{h}\cos kx$) is given. Estimate the maximum thickness t_c of a gold foil, which remains attached only because of adhesive forces. Use the following values for your estimation: E = 80GPa, $\gamma_{12} = 2$ Jm^{-2} and $l = 2\pi/k = 100\mu\text{m}$, $\hat{h} = 1\mu\text{m}$. There are two cases to investigate: The case in which the elastic energy is determined (a) exclusively by lengthening or (b) exclusively by bending.

Solution:
(a) Due to the deflection $w(x)$ in the transverse direction, the length of the section of foil changes with the length l by the amount

$$\Delta l \approx \tfrac{1}{2}\int_0^l w'^2(x)dx = \tfrac{1}{2}\int_0^l \hat{h}^2 k^2 \sin^2(kx)dx = \frac{\pi^2 \hat{h}^2}{l}.$$

Thereby, the elastic energy

$$U_{el} = \frac{1}{2}\frac{E}{1-\nu^2}\frac{Lt\pi^4\hat{h}^4}{l^3}$$

is saved. Here, L is the width of the foil and ν is Poisson's Ratio. The foil adheres completely if this energy is smaller than the adhesive energy $\gamma_{12} Ll$:

$$t < \frac{2\gamma_{12} l^4}{\pi^4 \hat{h}^4}\frac{1-\nu^2}{E}.$$

Based on the given values, $t < 46\mu\text{m}$.
(b) The elastic energy of a section of a bent plate with the length *l* is

$$U_{el} = \frac{Et^3}{24(1-\nu^2)} L\int_0^l w''^2 dx = \frac{Et^3}{48(1-\nu^2)} Lk^4 \hat{h}^2 l.$$

The plate adheres completely to the base if this energy is smaller than the adhesive energy $\gamma_{12} Ll$:

$$t^3 < \frac{48\gamma_{12}}{k^4\hat{h}^2}\frac{(1-\nu^2)}{E} = \frac{3\gamma_{12} l^4}{\pi^4 \hat{h}^2}\frac{(1-\nu^2)}{E}.$$

Based on the given values, $t_c \approx 4.1\ \mu\text{m}$.

A comparison of the cases (a) and (b) shows that the criteria for complete adhesion at a given roughness value is mainly determined by the bending stiffness of the plate. The correct critical value of the plate thickness is, therefore, $t_c \approx 4{,}1\mu\text{m}$.

Problem 3: Many insects possess mechanisms that allow them to adhere to smooth surfaces. In Fig. 3.10a, a simplified model is shown which takes the essential relationships of such an insect foot into account. Determine (a) the relationship between the penetration depth and the normal force; (b) the maximum contact radius in the case in which the external normal force approaches zero; (c) and the dependence of the separation force on the original compressive force**.** Given: γ_{12}, A_0, $k = EA_0 / l_0$, l_0

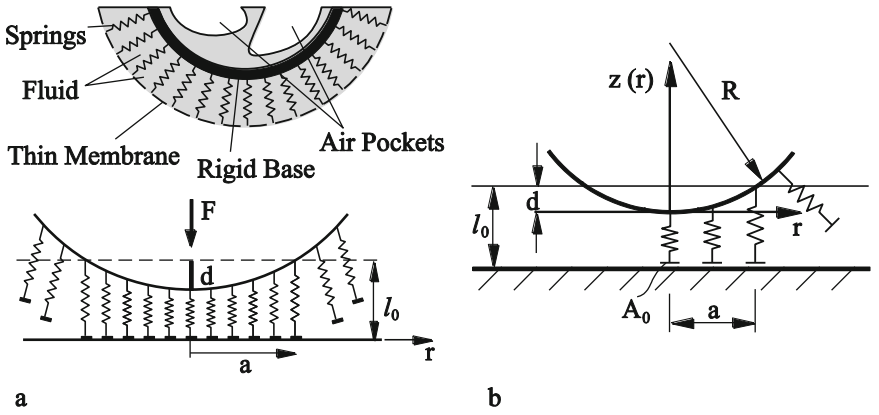

Fig. 3.10 (a) Structure of the "adhesive pad" of a grasshopper; (b) Explanation of notations for calculation of the adhesive forces.

Solution: The length of the springs which are in contact with the rigid surface is calculated as $l(r) = l_0 - d + r^2 / 2R$. *In the phase in which the two surfaces in contact are approaching each other,* the springs at the edge of the contact area have the length l_0: $l_0 - d + a^2 / 2R = l_0$. The radius of the contact area is $a = \sqrt{2dR}$, and the total compressive force is found by

$$F_N = -\frac{k}{A_0}\int_0^a \left(\frac{r^2}{2R} - d\right) 2\pi r \mathrm{d}r = \frac{\pi k R d^2}{A_0} = \frac{\pi E R d^2}{l_0}.$$

If the foot was originally strongly pressed onto the surface and then pulled away with a force F, then the contact area is defined by the condition that the springs at the boundary are in the critical state. The critical lengthening is calculated from

(3.11) as $\Delta l = \sqrt{\frac{2\gamma_{12} l_0}{E}}$ and the contact radius from the constraint $l(a_{\max}) = l_0 - d + \frac{a_{\max}^2}{2R} = l_0 + \sqrt{\frac{2\gamma_{12} l_0}{E}}$ as:

$$a_{\max}^2 = 2R\left(d + \sqrt{\frac{2\gamma_{12} l_0}{E}}\right).$$

Therefore, the force acting on the foot is

$$F_A = -\frac{k}{A_0}\int_0^{a_{\max}}\left(\frac{r^2}{2R} - d\right)2\pi r \mathrm{d}r = -\frac{\pi k}{2A_0}a_{\max}^2\left(\sqrt{\frac{2\gamma_{12} l_0}{E}} - d\right) = -\frac{\pi E}{l_0}R\left(\frac{2\gamma_{12} l_0}{E} - d^2\right).$$

The maximum negative value of this force we call the *adhesive force.*

$$\left|F_{A,\max}\right| = 2\pi\gamma_{12} R\,.$$

A detailed calculation of the arbitrary compressive force F_N provides the following adhesive forces[9]

$$F_A\left(F_N\right) = \begin{cases} F_{A,\max} & , F_N \geq F_{A,\max} \\ 2\sqrt{F_{A,\max} F_N} - F_N & , F_N < F_{A,\max} \end{cases}.$$

[9] M. Schargott, V.L. Popov, S. Gorb, Spring model of biological attachment pads. J. Theor. Biology., 2006, v. 243, pp. 48-53.

4 Capillary Forces

In the interactions between solid surfaces and liquids or between solid bodies in the presence of small amounts of liquids, the so called capillary forces play an important role. Capillary forces are responsible for the wetting of solids by liquids or the "repelling" of liquids. The transportation of water in all organs of plants is caused by capillary forces. They are behind the unwanted "spreading" of lubricating oil and its transportation to friction sites in the for-life lubrication of systems. Capillary forces are among the most important causes of "sticktion" between the small components in micro-technology. They can considerably influence frictional forces, especially that of static friction.

4.1 Surface Tension and Contact Angles

The most important physical parameters that influence capillary forces in various situations are the surface tension and the contact angle. In order to clarify the concept of surface tension of a liquid, we visualize a soap film stretched within a

V.L. Popov, *Contact Mechanics and Friction*,
DOI 10.1007/978-3-662-53081-8_4

square-shaped wire frame. If we pull on a movable side of the frame, the area of the film gets larger. Consequently, the surface energy rises. With a displacement of Δx the energy rises by the amount $\Delta E = 2\gamma l \Delta x$, where γ is the surface energy density of the liquid, often referred to simply as "surface energy"; the factor of 2 accounts for the fact that the film has two sides. According to the principle of virtual work, this change in energy must be equal to the work performed by the external force $W = F\Delta x = 2\gamma l \Delta x$. Thus, $F = 2\gamma l$. That means that a uniform load of $f = F / l = 2\gamma$ acts on the edge of the frame. Due to the fact that the film has two identical sides, both are acted on by a uniform load of γ, which is simply equal to the surface energy. Therefore, every free surface is in "tension", from where the term "surface tension" for surface energy originates.

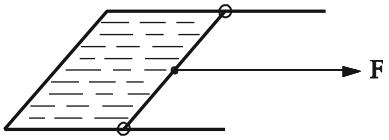

Fig. 4.1 An experiment with a soap film, in order to explain the notion of surface tension.

If a droplet of liquid is at rest on a solid surface, the surface of the liquid forms a specific angle θ (Fig. 4.2), which, in equilibrium, only depends on the thermodynamic properties of the system. This angle is called the *contact angle* and affects most of the important properties dealing with the contact between solid bodies and liquids.

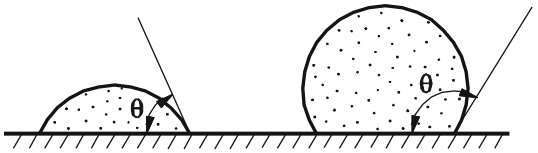

Fig. 4.2 Drop of liquid on a solid surface.

In the boundary line of the droplet, three interfaces meet each other (Fig. 4.3 a). In every interface, a corresponding surface tension acts. In equilibrium,

$$\gamma_{sv} = \gamma_{sl} + \gamma_{lv} \cos\theta \tag{4.1}$$

is valid, in which γ_{sv} is the relative surface energy of the interface between the solid body and the vapor, γ_{sl} is the relative surface energy between the solid body and the liquid, and γ_{lv} is the relative surface energy between the liquid and the vapor. The angle θ can assume any value between 0 and π depending on the relationships of the three relevant surface energies. If the contact angle is smaller than $\pi / 2$, it is said that the liquid *wets* the given surface. At contact angles larger than $\pi / 2$ we then talk about "*repelling*" surfaces. When dealing with water, surfaces with a contact angle smaller than $\pi / 2$ are called *hydrophilic*, while surfaces

with a contact angle larger than $\pi/2$ are called *hydrophobic*. The meaning of the differentiating between contact angles larger and smaller than $\pi/2$ is first clarified through the investigation of capillary bridges. At a contact angle of zero it is said that complete wetting takes place. In this case, the droplet would completely disperse and form an infinitely thin film (as seen macroscopically). Complete wetting exists when the condition

$$\gamma_{sv} - \gamma_{sl} = \gamma_{lv} \tag{4.2}$$

is met. For $\gamma_{lv} < \gamma_{sv} - \gamma_{sl}$, the liquid spreads out until it forms a film with a thickness of a few molecular diameters. The dispersion of thin liquid films is known as "creep." The driving force for this process is given by the difference

$$\gamma_{creep} = \gamma_{sv} - \gamma_{sl} - \gamma_{lv}\,. \tag{4.3}$$

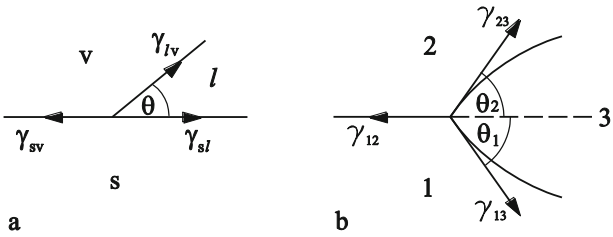

Fig. 4.3 Calculating the equilibrium of the contact line: (a) between a liquid and a solid body, (b) between two liquids.

In the equilibrium equation (4.1) we have accounted for only the force equilibrium in the horizontal direction. The surface tension component in the vertical direction is in equilibrium with the reaction force from the rigid body**.** If we are dealing with the contact between two liquids (or between two solid bodies in thermodynamic equilibrium, for example, after an extended exposure to high temperatures), then both components must be taken into account (Fig 4.3 b). Hence, two characteristic contact angles can be provided from the equations

$$\gamma_{12} = \gamma_{13}\cos\theta_1 + \gamma_{23}\cos\theta_2 \quad \text{and} \quad \gamma_{13}\sin\theta_1 = \gamma_{23}\sin\theta_2\,. \tag{4.4}$$

Whether or not a liquid completely wets a surface, is dependent on the three surface energies of the three interfaces. It has been empirically shown, however, that the wettability is already for the most part defined by the relationship between the surface energies of the solid body and the liquid. If the surfaces can only interact through van der Waals forces, then the surface energies at the interfaces of both substances can be estimated as[1]

[1] F.M. Fowkes, Dispersion Force Contributions to Surface and Interfacial Tensions, Contact Angles and Heats of Immersion. In Contact Angle, Wettability and Adhesion, American Chemical Society, 1964, pp.99-111.

$$\gamma_{sl} \approx \gamma_s + \gamma_l - 2\sqrt{\gamma_s \gamma_l}\,. \tag{4.5}$$

It can be noted that this estimation differs from the estimation of the surface energy of solid bodies (3.16), where the physical origins of the surface energy is different (for solids it is the force that is required to separate the bodies, while for liquids it is the force required to reconstruct them during stretching). The energy (4.5) vanishes in contact between identical liquids.

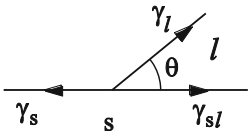

Fig. 4.4 Estimation of contact angles for known surface energies between a liquid and a solid body.

From the force equilibrium of the boundary (see Fig. 4.4) observing (4.5) we get

$$\gamma_s = \gamma_l + \gamma_s - 2\sqrt{\gamma_l \gamma_s} + \gamma_l \cos\theta\,. \tag{4.6}$$

From which we can then calculate the contact angle

$$\cos\theta = 2\sqrt{\frac{\gamma_s}{\gamma_l}} - 1\,. \tag{4.7}$$

The right side of this equation assumes the value 1 (contact angle $\theta = 0$, complete wetting) at $\gamma_s \approx \gamma_l$. The value -1 ($\theta = \pi$, complete repelling) is never reached. The contact angle is equal to $\pi/2$ for $\gamma_l \approx 4\gamma_s$. The driving force for creep (4.3) is given by $\gamma_K = \gamma_s - \gamma_{ls} - \gamma_l = -2\gamma_l + 2\sqrt{\gamma_l \gamma_s} = 2\left(\sqrt{\gamma_l \gamma_s} - \gamma_l\right)$. It reaches a maximum at $\gamma_l \approx \gamma_s / 4$.

Oils with very small surface energies (e.g. silicon oil with $\gamma_l \approx 2{,}1 \cdot 10^{-2}$ J/m^2) wet all solid surfaces (with the exception of Teflon, see Table 3.1). They can inconspicuously contaminate manufacturing plants. The spreading of lubricants can lead to disturbances in parts of machines and loss of function, because they can flow out of friction sites where lubrication is needed. This unwanted spreading can be impeded through the epilamization process. During epilamization, the surface tension of the machine part is reduced by the application of a film which makes the solid surface repellent.

4.2 Hysteresis of Contact Angles

We have so far assumed that no forces other than the surface tension act on the line of contact. If the contact is between a liquid and a solid body, *frictional forces* can also appear in the line of contact. The equilibrium condition (4.1) then changes to

$$\gamma_{sv} = \gamma_{sl} + \gamma_{lv}\cos\theta \pm f_R\,, \tag{4.8}$$

where f_R is the frictional force per unit length of the line of contact. The sign of the frictional force is dependent on the direction of the movement of the droplet. Therefore, the actual contact angle will depend on the direction of motion. This phenomenon is called the *hysteresis of the contact angle.* From the hysteresis, the frictional force can be defined. This force is responsible for droplets sticking on macroscopically smooth, sloped surfaces. It is of interest for many technical applications.

The frictional force in the line of contact can be caused by the roughness of the solid surface, its heterogeneity, or the atomic structure of the solid body. These factors lead to the fact that the energy of a droplet is dependent on its position on the solid surface. Thus, static friction is made possible.

4.3 Pressure and the Radius of Curvature

If the surface of a droplet of liquid is curved, then there is a pressure difference between the "outside" and "inside" of the droplet. For a spherical droplet (Fig. 4.5 a), this pressure difference is easy to calculate. If a definite amount of liquid is "pumped" into the droplet, the radius would grow by an amount dR. Thereby, the surface changes by $dA = 8\pi R dR$. The work $dW = (p_1 - p_2)dV = (p_1 - p_2)4\pi R^2 dR$, which is performed through the difference in pressure, must be equal to the change in the surface energy[2] $\gamma_l dA = \gamma_l 8\pi R dR$. From which:

$$\Delta p = (p_1 - p_2) = \frac{2\gamma_l}{R}\,. \tag{4.9}$$

If the force of gravity is neglected, then the pressure is constant everywhere inside of the droplet. Therefore, the radius of curvature must also be constant: *A droplet takes the form of a sphere.* On flat solid surfaces, it is always a portion of a sphere (Fig. 4.2).

[2] We denote the surface tension of the vapor-liquid interface, which is normally simply referred to as the surface tension of the liquid, as $\gamma_l = \gamma_{lv}$.

For non-spherical surfaces it is generally true that

$$\Delta p = \gamma_l \left(\frac{1}{R_1} + \frac{1}{R_2} \right), \tag{4.10}$$

where R_1 and R_2 are the *principal radii of curvature*. Here, we would like to stress that in Equation (4.10), the radii of curvature can also be negative. The sign of the radius of curvature is defined by whether the center of the curve lies on the positive or negative side of the surface of the liquid. The radii of curvature have different signs for saddle-shaped surfaces (Fig. 4.5 c).

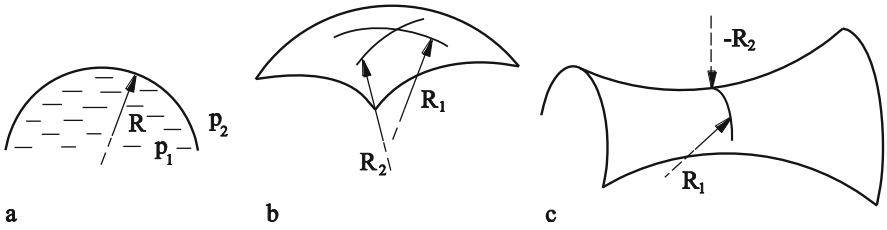

Fig. 4.5 Curved surfaces with different ratios of the principal radii of curvature.

4.4 Capillary Bridges

We observe a rigid cylinder near a solid surface with a small amount of liquid in between. For the sake of simplicity, we assume that both of the "contact partners" are composed of the same material.

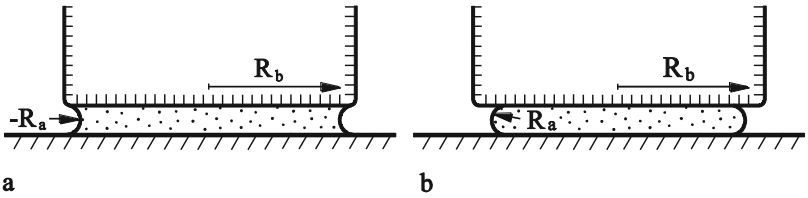

Fig. 4.6 Capillary bridges at a contact angle (a) smaller than $\pi/2$, (b) larger than $\pi/2$.

In equilibrium, the liquid forms a capillary bridge, which has two radii of curvature. The largest radius R_b is always positive. The sign of the smaller radius depends on if the contact angle is larger or smaller than $\pi/2$. For small contact angles, in the case of wetting of the surface, R_a is negative. There is a reduced pressure in the liquid, which leads to a force that we call *capillary force*. In order to keep the system in equilibrium, an opposing reaction force must be applied. The capillary force is calculated by multiplying the pressure difference by the area of the capillary bridge:

$$F_{cap} = A\gamma_l \left(\frac{1}{R_b} - \frac{1}{R_a} \right) \approx -A\gamma_l \frac{1}{R_a}, \tag{4.11}$$

where $|R_a| \ll |R_b|$ is assumed. However, if the surface is not wettable by a given liquid (contact angle larger than $\pi/2$), then the contact partners repel each other. This property explains the origin of the distinction between "wettable" and "repelling" surfaces (or hydrophilic and hydrophobic surfaces in the case of water) depending on if the contact angle is larger or smaller than $\pi/2$.

4.5 Capillary Force between a Rigid Plane and a Rigid Sphere

We consider a capillary bridge between a rigid sphere and a rigid plane of the same material, for which the contact angle is zero (complete wetting), Fig. 4.7. Let the radius of the bridge be *r* and the radius of the sphere *R*. The height of the capillary bridge is $h \approx r^2/2R$ and the surface $A = \pi r^2$. The (small) radius of curvature is clearly $r_0 = h/2$. For $|r_0| << |r|$, the resulting pressure difference in the liquid is

$$\Delta p = -\frac{\gamma_l}{r_0} = -\frac{2\gamma_l}{h} = -\frac{4\gamma_l R}{r^2}. \tag{4.12}$$

The capillary force is, therefore,

$$F_{cap} = A\Delta p = -\pi r^2 \frac{4\gamma_l R}{r^2} = -4\pi\gamma_l R. \tag{4.13}$$

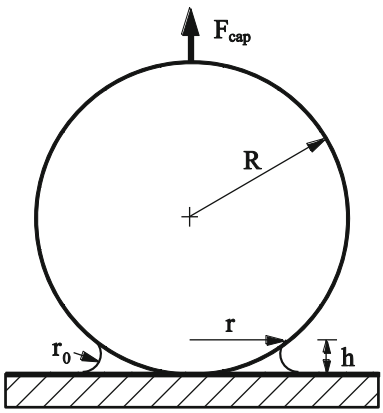

Fig. 4.7 A capillary bridge between a rigid plane and a rigid sphere.

It is proportional to the radius of curvature of the sphere and independent from the amount of liquid. The force, F_{cap}, which is required to pull the sphere from the surface has the same magnitude.

4.6 Liquids on Rough Surfaces

Up to now, we have assumed that the solid surface is ideally smooth and even. That is almost never the case in reality. Roughness leads to a macroscopically observable change in the contact angle. Depending on the type of roughness, a variety of situations can occur. If the level of roughness is small, then the liquid will remain in complete contact with the solid body over the entire area (in Fig. 4.8, to the right of the boundary of the droplet). If there is no pressure difference between the atmosphere and the liquid, then the sum of the radii of curvature for every point of the surface must be zero.

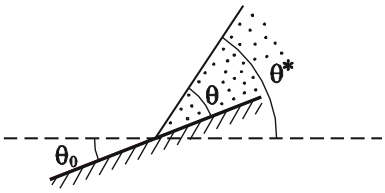

Fig. 4.8 Surface of a liquid in contact with an inclined solid surface.

Because of this, the surface on average, is flat and at a small distance from the contact line inclined at an angle θ^* from the horizontal (Fig. 4.8). The horizontal component of the uniform load in the contact is

$$\gamma_{sv}\cos\theta_0 - \gamma_{sl}\cos\theta_0 - \gamma_{lv}\cos\theta^* . \tag{4.14}$$

In order for the boundary line to remain in equilibrium, the average linear force must be zero:

$$\left(\gamma_{sv} - \gamma_{sl}\right)\left\langle\cos\theta_0\right\rangle - \gamma_{lv}\cos\theta^* = 0 . \tag{4.15}$$

Observing equation (4.1) it follows that

$$\cos\theta^* = \left\langle\cos\theta_0\right\rangle \cdot \cos\theta \tag{4.16}$$

(R.N. Wenzel, 1936). Because $\left\langle\cos\theta_0\right\rangle$ is always smaller than 1, the visible contact angle for hydrophilic surfaces is always larger than the "real" contact angle, while for hydrophobic, it is always smaller. This equation can also be derived purely from thermodynamic reasoning.

If the gradient of the roughness profile is large, then the liquid can remain on the peaks of the roughness (Fig. 4.9). If the surface has a form as is shown in

Fig. 4.9 a, then the liquid remains atop the peaks only if the contact angle is larger than $\pi - \theta_{max}$, where θ_{max} is the maximum angle of elevation of the surface. If the liquid were then to be acted on by some additional pressure, its surface would curve and it would press deeper into the recesses of the roughness until it reaches an instability point and the entire surface is wet. This can, however, be hindered by air trapped in the recesses. If the surface roughness has the form as in Fig. 4.9 c, then fluids with a contact angle of less than $\pi/2$ can remain hanging without coming into complete contact with the surface.

Fig. 4.9 Sheet of fluid on a rough surface.

4.7 Capillary Forces and Tribology

There are several situations in which the capillary forces promote the movement of liquids. If a droplet is at rest on a curved surface, then its energy grows with the curvature. Therefore, the droplet is repelled by areas of high curvature, especially at edges or sharp points (Fig. 4.10, see also Problem 2 in this chapter). If a liquid is in a capillary or crevice of varying width, then capillary forces cause it to move in the direction of the smaller crevice width or capillary diameter.

Fig. 4.10 Droplet is repelled from a sharp point.

This effect can be used to keep lubricants in place. In narrow joints, these forces are so large that they allow for life-long lubrication without reapplication. Such examples can be found in clockwork, measurement instruments, electricity meters, etc. If oil is wanted to reach such an area, the described effect can be used in the design of the joint so that the oil moves in the direction of the narrowest point.

Problems

Problem 1: Determine the total surface energy of a drop of liquid resting on a solid surface.

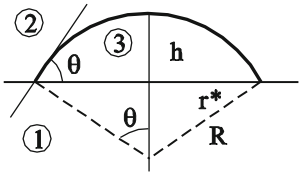

Fig. 4.11 Droplet of liquid on a flat, solid surface.

Solution: Using the notation defined in (Fig. 4.11), we obtain the following equations for A as the surface area of the droplet, V as its volume, θ as the contact angle, and r^* as the "contact radius":

$$A = 2\pi Rh, \quad V = \frac{\pi h^2 (3R - h)}{3}, \quad \cos\theta = \frac{R - h}{R}, \quad r^{*2} = 2Rh - h^2 .$$

The surface energies are related through the equation

$$\cos\theta = \frac{\gamma_{sv} - \gamma_{sl}}{\gamma_{lv}} .$$

For both geometric values R and h, which are completely determined by the configuration of the droplet, we have

$$R^3 = \frac{3V}{\pi (1 - \cos\theta)^2 (2 + \cos\theta)}, \quad h = R(1 - \cos\theta) .$$

Therefore, we obtain the following expression for the sum of all of the surface energies:

$$E = (\gamma_{sl} - \gamma_{sv})\pi r^{*2} + \gamma_{lv} A = \frac{3\gamma_{lv} V}{R} = \gamma_{lv} \left(9V^2 \pi (1 - \cos\theta)^2 (2 + \cos\theta)\right)^{1/3} .$$

For a constant surface tension γ_{lv} of the liquid, it is a monotonically increasing function of the contact angle. For a heterogeneous surface, the droplet would be *repelled from areas with larger contact angles*.

Problem 2: Determine the total surface energy of a drop of liquid resting on a slightly curved surface (radius of curvature R_0). Let the contact angle be $\pi/2$ (Fig. 4.12).

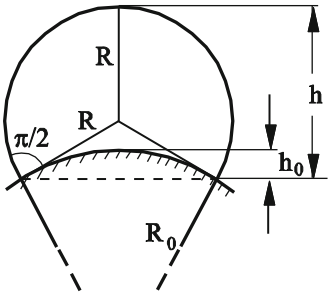

Fig. 4.12 Droplet of liquid on a curved surface. The contact angle is equal to $\pi/2$.

Solution: The contact angle is $\pi/2$ when $\gamma_{sv} = \gamma_{sl}$. In this special case, the surface energy is reduced to $E = \gamma_{lv} A$. Through geometric reasoning we obtain

$$h = R + \frac{R^2}{\sqrt{R_0^2 + R^2}}, \qquad h_0 = \frac{R^2}{\sqrt{R_0^2 + R^2}} + R_0 - \sqrt{R_0^2 + R^2}\,.$$

The volume, $V_T = \frac{\pi}{3}\left(h^2\left(3R - h\right) - h_0^2\left(3R_0 - h_0\right)\right)$, and surface area of the droplet, $A = 2\pi Rh$, are calculated using the terms up to the first-order of the curvature $\kappa = 1/R_0$:

$$V_T = \frac{2\pi R^3}{3} + \frac{3\pi R^4}{4}\kappa, \qquad A = 2\pi R^2 + 2\pi R^3 \kappa\,.$$

For a small change in the radius R and the curvature κ (from the value $\kappa = 0$), the volume and surface change as follows:

$$dV_T = 2\pi R^2 dR + \frac{3\pi R^4}{4} d\kappa, \qquad dA = 4\pi R dR + 2\pi R^3 d\kappa\,.$$

If we maintain a constant volume, then $dR = -\frac{3}{8} R^2 d\kappa$. The change in the surface is then $dA = \frac{1}{2}\pi R^3 d\kappa$. The "extra energy," which is related to the curvature, is therefore,

$$\Delta E \approx \frac{\pi \gamma_{lv} R^3}{2R_0} = \frac{3V_T \gamma_{lv}}{4R_0}.$$

The surface energy increases with the curvature of the base surface. Hence, the droplet is *repelled from areas with a larger curvature*.

Problem 3: Determine the capillary force between a curved surface with the Gaussian radii of curvature R_1 and R_2 and a plane. The surfaces of both bodies are assumed to be completely wettable.

Solution: Because the pressure in the liquid is overall constant, the radius of curvature and the height $h = 2r_0$ must also remain constant. The form of the contact area is determined by the constraint

$$\frac{x^2}{2R_1} + \frac{y^2}{2R_2} = h.$$

The semi-axes of this ellipse are equal to $\sqrt{2R_1 h}$ and $\sqrt{2R_2 h}$, and its area is $A = 2\pi h\sqrt{R_1 R_2}$. Thus, the capillary force is calculated as

$$|F| = \frac{\gamma}{r_0} A = 4\pi\gamma\sqrt{R_1 R_2}.$$

Problem 4: Determine the capillary force between a sphere and a plane. The contact angles are θ_1 and θ_2.

Solution: $F = 2\pi R\gamma\left(\cos\theta_1 + \cos\theta_2\right)$.

Problem 5: Determine the overhead pressure that is necessary to force a liquid through a lattice of round, parallel rods (Fig. 4.13). Let the distance between the rods be L.

Solution: If the overhead pressure on the liquid is Δp, then it forms a uniformly curved surface with a radius of curvature of R (Fig. 4.13):

$$\frac{1}{R} = \frac{\Delta p}{\gamma_{lv}}.$$

At the same time, the angle between the surfaces of the rod and the liquid must equal to the contact angle θ. If the pressure rises, then the liquid is pressed even farther between the rods, until a critical condition is met. For contact angles of $\theta \le \pi/2$, this critical condition is met when the contact points of the liquid come together from both sides of the rod (Fig. 4.14 a, b). For contact angles $\theta > \pi/2$ it

is met sooner. In the case of a completely repellant surface, contact angle $\theta = \pi$, the critical condition is shown in Fig. 4.14 c.

Fig. 4.13 Liquid on a lattice of straight rods.

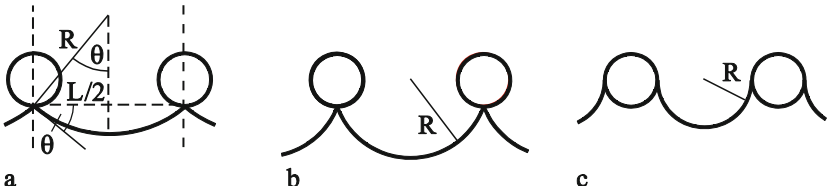

Fig. 4.14 Critical configurations for (a) $\theta < \pi/2$, (b) $\theta \approx \pi/2$, (c) $\theta \approx \pi$.

For wettable surfaces ($\theta < \pi/2$) it follows, from Fig. 4.14 a, that in the critical condition $\frac{1}{R} = \frac{2}{L}\sin\theta$. For the maximum possible overhead pressure, we obtain

$$\Delta p = \frac{2}{L}\gamma_{lv}\sin\theta\,.$$

It reaches a maximum for rods with $\theta = \pi/2$ and is equal to

$$\Delta p_{\max} = \frac{2}{L}\gamma_{lv}\,.$$

Problem 6: A cylindrical pin (mass m, length L) lays on the surface of water (Fig. 4.15). Determine the displacement of the pin beneath the undisturbed surface of the water and the maximum weight that the surface can hold, under the assumption that inclination of the surface of the water is small at every point.

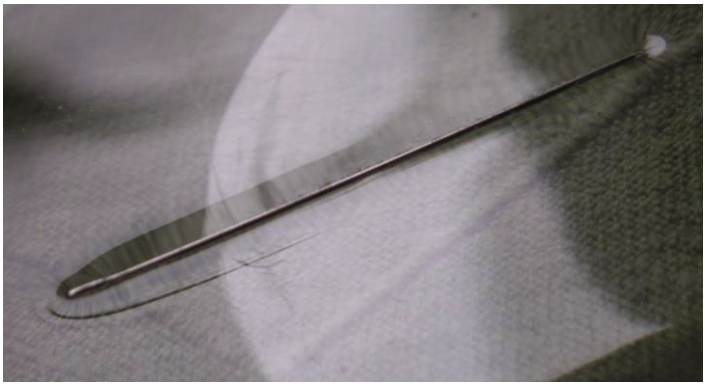

Fig. 4.15 A pin floating on the surface of the water.

Solution: In the solution, we will use the diagram in Fig. 4.16. The pressure difference at point (x,z) on the surface can be calculated either by using (4.10), or by calculating the hydrostatic pressure difference at a depth of z:

$$\Delta p = \gamma_{lv} / R = \gamma_{lv} z'' = \rho g z \,.$$

The solution of the differential equation with respect to $z(x)$ with the boundary condition of $z \to 0$ for $x \to \infty$ yields:

$$z = A \exp\left(-\left(\frac{\rho g}{\gamma_{lv}} \right)^{1/2} x \right).$$

The displaced water volume is equal to

$$V = 2L \int_0^\infty z(x) dx = 2AL \left(\frac{\gamma_{lv}}{\rho g} \right)^{1/2} .$$

In equilibrium, the weight is equal to the buoyancy force, according to Archimedes' buoyancy principle, thus, $\rho V = m$. For the depth that the pin has sunk, it follows that

$$z(0) = A = \frac{m}{2L} \left(\frac{g}{\rho \gamma_{lv}} \right)^{1/2} .$$

The angle of inclination of the surface at $x = 0$ is determined using

$$\tan \varphi = \frac{mg}{2L\gamma_{lv}} .$$

It is easy to see, geometrically, that the contact angle θ cannot be smaller than φ. The maximum weight that the surface can hold is, therefore, calculated as

$$mg = 2L\gamma_{lv} \tan \theta \,.$$

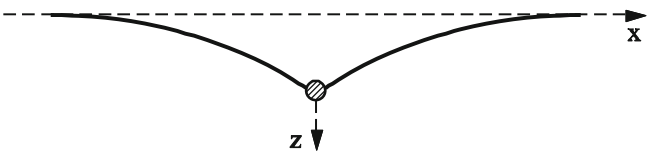

Fig. 4.16 A cylindrical pin supported by the surface of the water.

5 Rigorous Treatment of Contact Problems – Hertzian Contact

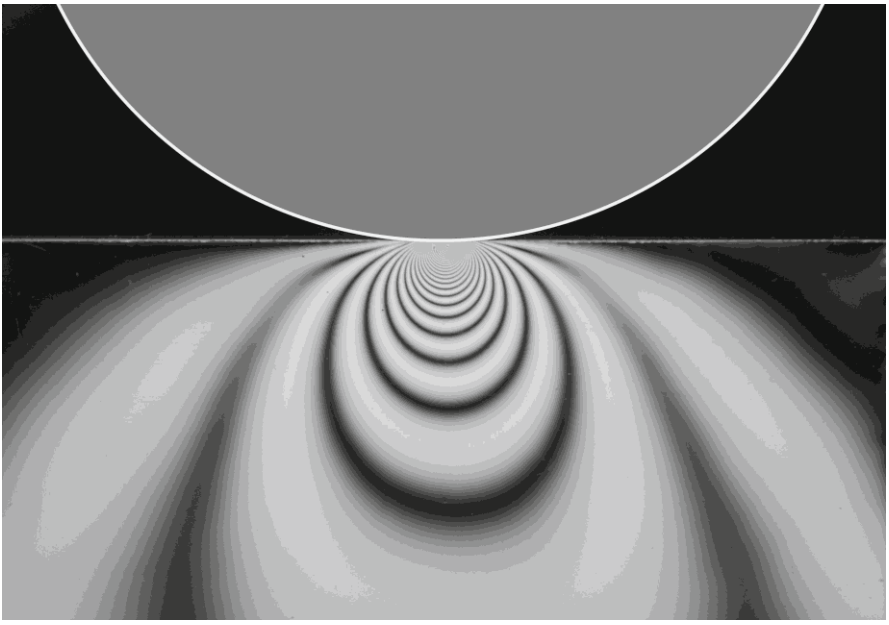

In this chapter, a method is illustrated to find the exact solutions of contact problems in the framework of the "half-space approximation." We examine, in detail, the classical contact problem of normal contact between a rigid sphere and an elastic half-space, which is often used to analyze more complex models.

As a preparatory step, we will summarize a few results of the theory of elasticity that have a direct application to contact mechanics. We consider the deformations in an elastic half-space, which are caused by a given stress acting upon its surface. The calculation of the deformation of an elastic body whose surface is being acted upon by a force ("direct problem of the theory of elasticity") is much easier than the solution of contact problems, because in the latter, neither the stress distribution, nor the contact area are known to begin with. The classic solutions from Hertz (non-adhesive contact) and Johnson, Kendall, and Roberts (adhesive contact) use the known solutions for "direct problems" as building blocks to the construction of a solution for a contact problem.

V.L. Popov, *Contact Mechanics and Friction*,
DOI 10.1007/978-3-662-53081-8_5

5.1 Deformation of an Elastic Half-Space being Acted upon by Surface Forces

We consider an elastic medium that fills an infinitely large half-space (i.e. its only boundary is an infinite plane). Under the influence of the forces that act on the free surface, the medium is deformed. We place the xy-plane on the free surface of the medium; the filled area corresponds to the positive z-direction. The deformations in the complete half-space can be defined in analytical form and found in textbooks over the theory of elasticity[1]. Here, we will only mention the formula for the displacement from a force acting at the origin in the positive z-direction.

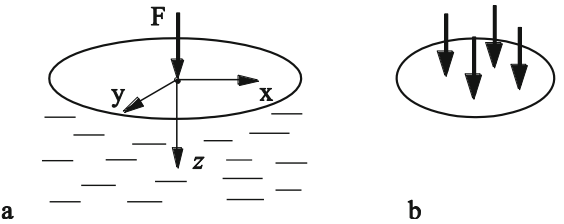

Fig. 5.1 (a) A force acting on an elastic half-space; (b) a system of forces acting on a surface.

The displacement caused by this force is calculated using the following equations:

$$u_x = \frac{1+\nu}{2\pi E}\left[\frac{xz}{r^3} - \frac{(1-2\nu)x}{r(r+z)}\right]F_z, \tag{5.1}$$

$$u_y = \frac{1+\nu}{2\pi E}\left[\frac{yz}{r^3} - \frac{(1-2\nu)y}{r(r+z)}\right]F_z, \tag{5.2}$$

$$u_z = \frac{1+\nu}{2\pi E}\left[\frac{2(1-\nu)}{r} + \frac{z^2}{r^3}\right]F_z, \tag{5.3}$$

with $r = \sqrt{x^2+y^2+z^2}$.

In particular, one obtains the following displacements of the free surface, which we have defined as $z = 0$:

$$u_x = -\frac{(1+\nu)(1-2\nu)}{2\pi E}\frac{x}{r^2}F_z, \tag{5.4}$$

[1] L.D. Landau, E.M. Lifschitz, Theory of elasticity. (Theoretical Physics, Vol. 7), 3rd edition, 1999, Butterworth-Heinemann, Oxford, §§ 8,9.

$$u_y = -\frac{(1+\nu)(1-2\nu)}{2\pi E}\frac{y}{r^2}F_z, \tag{5.5}$$

$$u_z = \frac{(1-\nu^2)}{\pi E}\frac{1}{r}F_z, \tag{5.6}$$

with $r = \sqrt{x^2 + y^2}$.

If several forces act simultaneously (Fig. 5.1 b), we will get a displacement as the sum of the respective solutions that result from every individual force.

We will continue to work in approximation of the half-space, in which it is assumed that the gradient of the surfaces in the area of contact and within relative proximity is much smaller than one, so that in a first order approximation, the surfaces are "even." Although the contact constraints for the two surfaces must continue to be met, the relation between the surface forces and the displacements can be seen, however, exactly as they appear with an elastic half-space.

For contact problems *without friction,* only the z-component of the displacement (5.6) is of interest within the framework of the half-space approximation. Especially in the case of a continuous distribution of the normal pressure $p(x, y)$, the displacement of the surface is calculated using

$$u_z = \frac{1}{\pi E^*}\iint p(x', y')\frac{dx'dy'}{r}, \qquad r = \sqrt{(x-x')^2 + (y-y')^2} \tag{5.7}$$

with

$$E^* = \frac{E}{(1-\nu^2)}. \tag{5.8}$$

Before we move on to actual contact problems, we want to solve two preparatory problems. We assume that a pressure with a distribution of $p = p_0\left(1 - r^2/a^2\right)^n$ is exerted on a circle-shaped area with the radius a and search for the vertical displacement of the surface points within the area being acted upon by the pressure.

a. Homogeneous Normal Displacement ($n = -1/2$).
The coordinate system used is shown in Fig. 5.1. The normal stress is distributed according to the equation

$$p = p_0\left(1 - \frac{r^2}{a^2}\right)^{-1/2}. \tag{5.9}$$

The resulting vertical displacement is[2]:

$$u_z = \frac{\pi p_0 a}{E^*},\ r \le a\,. \tag{5.10}$$

The vertical displacement is the same for all points in the contact area. From this result, it directly follows how we can produce the assumed pressure distribution: it is produced by the indentation of a rigid cylindrical rod into an elastic half-space. The total force acting on the area under pressure is equal to

$$F = \int_0^a p(r) 2\pi r \mathrm{d}r = 2\pi p_0 a^2\,. \tag{5.11}$$

The stiffness of the contact is defined as the relationship between the force F and the displacement u_z:

$$k = 2aE^*\,. \tag{5.12}$$

If written in the form[3]

$$k = 2E^* \beta \sqrt{\frac{A}{\pi}}\,, \tag{5.13}$$

where A is the contact area of the rigid indenter, Equation (5.12) is also valid for cross-sections that are not round. The constant β always has an order of magnitude of 1:

Round cross-section:	β=1.000
Triangular cross-section:	β=1.061
Rectangular cross-section:	β=1.021

(5.14)

b. Hertzian Pressure Distribution ($n = 1/2$).
For the pressure distribution of the form

$$p = p_0 \left(1 - \frac{r^2}{a^2}\right)^{1/2}\,, \tag{5.15}$$

the resulting vertical displacement (Appendix A) is

$$u_z = \frac{\pi p_0}{4E^* a}\left(2a^2 - r^2\right),\ r \le a\,. \tag{5.16}$$

The total force follows as

---

[2] A detailed derivation can be found in Appendix A.

[3] Q. Li, V.L. Popov, Indentation of flat-ended and tapered indenters with polygonal geometries, Facta Universitatis, series: Mechanical Engineering, 2016, v. 14, N. 3, pp. 241-249.

$$F = \int_0^a p(r) 2\pi r dr = \frac{2}{3} p_0 \pi a^2 \ . \tag{5.17}$$

The displacement of the surface inside and outside of the area under pressure is shown in Fig. 5.2.

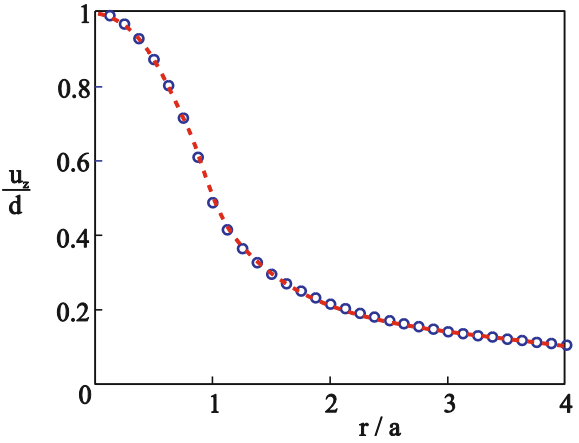

Fig. 5.2 Surface displacement u_z resulting from a pressure distribution (5.15); $d = u_z(0)$ is the indentation depth.

5.2 Hertzian Contact Theory

In Fig. 5.3, a contact between a rigid sphere and an elastic half-space is shown schematically. The displacement of the points on the surface in the contact area between an originally even surface and a rigid sphere of radius R is equal to

$$u_z = d - \frac{r^2}{2R} \ . \tag{5.18}$$

We have seen in (5.16) that a quadratic distribution of the vertical displacement results from a pressure distribution of the form in (5.15).

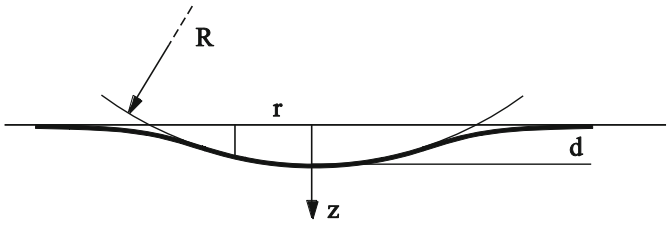

Fig. 5.3 A rigid sphere in contact with an elastic half-space.

We will try to find the parameters a and p_0 that cause exactly the displacement in (5.18):

$$\frac{1}{E^*}\frac{\pi p_0}{4a}\left(2a^2 - r^2\right) = d - \frac{r^2}{2R}. \tag{5.19}$$

The variables a and d must, therefore, fulfill the following requirements:

$$a = \frac{\pi p_0 R}{2E^*}, \qquad d = \frac{\pi a p_0}{2E^*}. \tag{5.20}$$

It follows for the contact radius

$$a^2 = Rd \tag{5.21}$$

and for the maximum pressure

$$p_0 = \frac{2}{\pi}E^*\left(\frac{d}{R}\right)^{1/2}. \tag{5.22}$$

Substituting from (5.21) and (5.22) into (5.17) we obtain a normal force of

$$F = \frac{4}{3}E^* R^{1/2} d^{3/2}. \tag{5.23}$$

With (5.22) and (5.23), the pressure in the center of the contact area can be calculated as well as the contact radius as a function of the normal force:

$$p_0 = \left(\frac{6FE^{*2}}{\pi^3 R^2}\right)^{1/3}, \quad a = \left(\frac{3FR}{4E^*}\right)^{1/3}. \tag{5.24}$$

We can also determine the expression for the potential energy of the elastic deformation U. Since $-F = -\partial U / \partial d$, we obtain the following expression for U:

$$U = \frac{8}{15}E^* R^{1/2} d^{5/2}. \tag{5.25}$$

5.3 Contact between Two Elastic Bodies with Curved Surfaces

The results from Hertzian theory (5.21), (5.22), and (5.23) can also be used with few modifications in the following cases.

(A) If both bodies are elastic, then the following expression for E^* must be used:

$$\frac{1}{E^*} = \frac{1-\nu_1^2}{E_1} + \frac{1-\nu_2^2}{E_2} . \tag{5.26}$$

Here, E_1 and E_2 are the moduli of elasticity and ν_1 and ν_2 the Poisson's ratios of both bodies.

(B) If two spheres with the radii R_1 and R_2 are in contact (Fig. 5.4 a), then the equations (5.21), (5.22), and (5.23) are valid using the equivalent radius R :

$$\frac{1}{R} = \frac{1}{R_1} + \frac{1}{R_2} . \tag{5.27}$$

This is also valid if one of the radii is negative (Fig. 5.4 b). The radius of curvature is negative if the center of curvature lies outside of the medium.

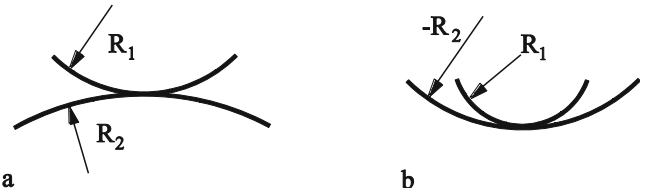

Fig. 5.4 Contact between two bodies with curved surfaces.

(C) In a contact between an elastic half-space and a rigid body with the principal radii of curvature of R_1 and R_2 (Fig. 5.5 a), an elliptical contact area results. The semi-axes are

$$a = \sqrt{R_1 d} , \quad b = \sqrt{R_2 d} . \tag{5.28}$$

Consequently, the contact area is calculated as[4]

$$A = \pi ab = \pi \tilde{R} d , \tag{5.29}$$

where the effective *Gaussian radius of curvature* of the surface is

$$\tilde{R} = \sqrt{R_1 R_2} . \tag{5.30}$$

This radius can also be used in place of R in other Hertzian relationships[5].

[4] Equations (5.28) represent only a rough estimation. On the other hand, equations (5.29) and (5.30) are valid with high accuracy as long as the ratio a / b is close to "1".

The pressure distribution is given by

$$p(x,y) = p_0\sqrt{1-\frac{x^2}{a^2}-\frac{y^2}{b^2}}\,. \tag{5.31}$$

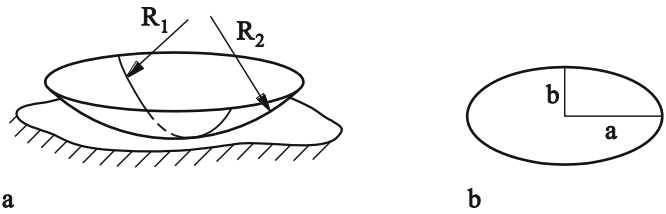

Fig. 5.5 A body with a curved surface (principal radii of curvature R_1 and R_2) in contact with an elastic half-space.

(D) If two elastic cylinders are in contact and lie on perpendicular axes with radii R_1 and R_2 (Fig. 5.6 a), then the distance between the surfaces of both bodies at the moment of the first contact (still without deformation) is given by

$$h(x,y) = \frac{x^2}{2R_1}+\frac{y^2}{2R_2}\,. \tag{5.32}$$

This is exactly in accordance with case (C) for ellipsoids with radii of curvature R_1 and R_2. Therefore, Hertzian relations are valid, if the effective radius

$$\tilde{R} = \sqrt{R_1 R_2} \tag{5.33}$$

is used. If both cylinders have the same radii, $R = R_1 = R_2$, then the contact problem is equivalent to the contact problem between a sphere of radius R and an elastic half-space with an even surface.

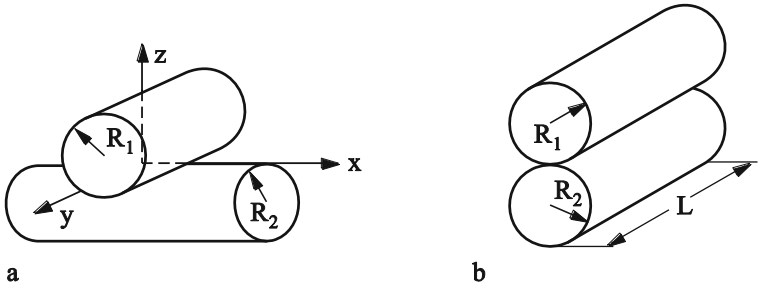

Fig. 5.6 (a) Two crossed cylinders in contact; (b) Two cylinders in contact with parallel axes.

[5] This statement is not exact. The closer the ratio R_1 / R_2 is to 1, the more precise the Hertzian relationships hold. Even with a ratio of $R_1 / R_2 = 10$, however, Equation (5.23) can be applied to elliptical contacts with a precision of 2.5%.

(E) In the case of the contact between two cylinders with parallel axes (Fig. 5.6 b), the force is linearly proportional to the penetration depth (which we already saw in Chapter 2):

$$F \approx \frac{\pi}{4} E^* L d \,. \tag{5.34}$$

It should be noted here that the indentation depth in this so-called line contact is not unambiguously defined because of the logarithmic divergence of the displacement field at infinity. The exact definition of the indentation depth and the relation between the normal force and the indentation depth depends on the size and shape of the whole body. However, this dependence is weak (logarithmic) so that equation (5.34) can be used as a rough approximation. What is interesting is that the radius of curvature does not appear at all in the relationship (5.34). Half of the contact width is given through the equation

$$a \approx \sqrt{Rd} \,, \quad \frac{1}{R} = \frac{1}{R_1} + \frac{1}{R_2} \,, \tag{5.35}$$

as in the contact between two spheres and the pressure distribution is

$$p(x) = p_0 \sqrt{1 - \left(\frac{x}{a}\right)^2} \,. \tag{5.36}$$

The maximum pressure is equal to

$$p_0 = \frac{E^*}{2}\frac{d}{a} = \frac{E^*}{2}\left(\frac{d}{R}\right)^{1/2} = \left(\frac{E^* F}{LR}\right)^{1/2} \,. \tag{5.37}$$

5.4 Contact between a Rigid Cone-Shaped Indenter and an Elastic Half-Space

When indenting an elastic half-space with a rigid cone-shaped indenter (Fig. 5.7 a), the penetration depth and the contact radius are given through the relationship[6]

$$d = \frac{\pi}{2} a \tan\theta \,. \tag{5.38}$$

The pressure distribution has the form

[6] Detailed derivation is seen in Problem 7 of this chapter.

$$p(r) = -\frac{Ed}{\pi a\left(1-\nu^2\right)} \ln\left(\frac{a}{r} + \sqrt{\left(\frac{a}{r}\right)^2 - 1}\right). \tag{5.39}$$

The stress has a logarithmic singularity (Fig. 5.7 b) at the point of the cone (at the center of the contact area). The total force is calculated as

$$F_N = \frac{2}{\pi} E^* \frac{d^2}{\tan\theta}. \tag{5.40}$$

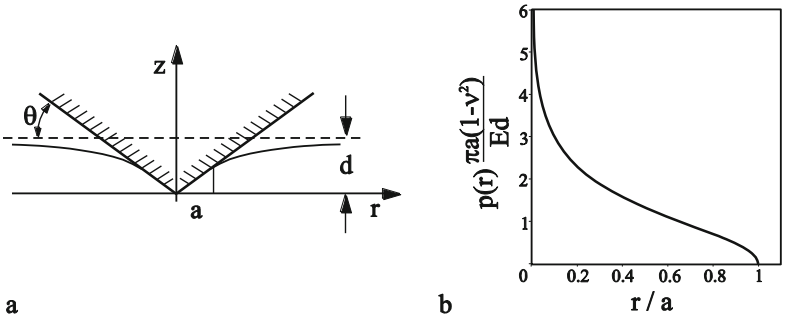

Fig. 5.7 (a) Contact between a rigid cone-shaped indenter and an elastic half-space; (b) Pressure distribution in the normal contact between a rigid cone-shaped indenter and an elastic half-space.

5.5 Internal Stresses in Hertzian Contacts

The stresses under the influence of a single, vertical force, F, acting at the origin, are defined by[7]

$$\sigma_{xx} = \frac{F}{2\pi}\left[-3\frac{x^2 z}{r^5} + (1-2\nu)\left(\frac{x^2(2r+z)}{r^3(r+z)^2} - \frac{r^2 - rz - z^2}{r^3(r+z)}\right)\right], \tag{5.41}$$

$$\sigma_{yy} = \frac{F}{2\pi}\left[-3\frac{y^2 z}{r^5} + (1-2\nu)\left(\frac{y^2(2r+z)}{r^3(r+z)^2} - \frac{r^2 - rz - z^2}{r^3(r+z)}\right)\right], \tag{5.42}$$

$$\sigma_{zz} = -\frac{3F}{2\pi}\frac{z^3}{r^5}, \tag{5.43}$$

[7] H.G. Hahn, Elastizitätstheorie. Teubner, 1985.

$$\tau_{xy} = \frac{F}{2\pi}\left[-3\frac{xyz}{r^5} + (1-2\nu)\frac{xy(2r+z)}{r^3(r+z)^2}\right], \tag{5.44}$$

$$\tau_{yz} = \frac{3F}{2\pi}\frac{yz^2}{r^5}, \tag{5.45}$$

$$\tau_{xz} = \frac{3F}{2\pi}\frac{xz^2}{r^5}. \tag{5.46}$$

The calculation of the stresses by an arbitrary normal pressure distribution p on the surface is made possible through superposition. The normal stress in the z-direction, σ_{zz}, is exemplary

$$\sigma_{zz}(x,y,z) = -\frac{3z^3}{2\pi}\iint_{(A)}\frac{p(x',y')}{\left((x-x')^2+(y-y')^2+z^2\right)^{5/2}}dx'dy', \tag{5.47}$$

where $\iint_{(A)}$ means the integral over the area being acted upon by the pressure.

For the Hertzian pressure distribution in (5.15), various results are discussed in the following. Fig. 5.8 shows the stresses at the z-axis for $\nu = 0.33$. All of the shear stresses are 0; for all points along the z-axis, the principal axes coincide with the coordinate axes. The analytical solution for the components of the stress tensors provides us with[8]

$$\sigma_{zz} = -p_0\left(1+\frac{z^2}{a^2}\right)^{-1}, \tag{5.48}$$

$$\sigma_{xx} = \sigma_{yy} = -p_0\left[(1+\nu)\left(1-\frac{z}{a}\arctan\frac{a}{z}\right) - \frac{1}{2}\left(1+\frac{z^2}{a^2}\right)^{-1}\right]. \tag{5.49}$$

Furthermore, the maximum shear stress, $\tau_1 = \frac{1}{2}|\sigma_{zz} - \sigma_{xx}|$, is depicted in Fig. 5.8. One comes to the conclusion that the maximum shear stress lies in the interior, for $\nu = 0.33$ at $z \approx 0.49a$. Fig. 5.9 shows the equivalent stress according to the von Mises criterion in the x-y plane:

$$\sigma_V = \frac{1}{\sqrt{2}}\left[(\sigma_{xx}-\sigma_{yy})^2 + (\sigma_{xx}-\sigma_{zz})^2 + (\sigma_{zz}-\sigma_{yy})^2 + 6(\tau_{xy}^2+\tau_{xz}^2+\tau_{yz}^2)\right]^{1/2}. \tag{5.50}$$

[8] K.L. Johnson, Contact mechanics. Cambridge University Press, Ninth printing 2003.

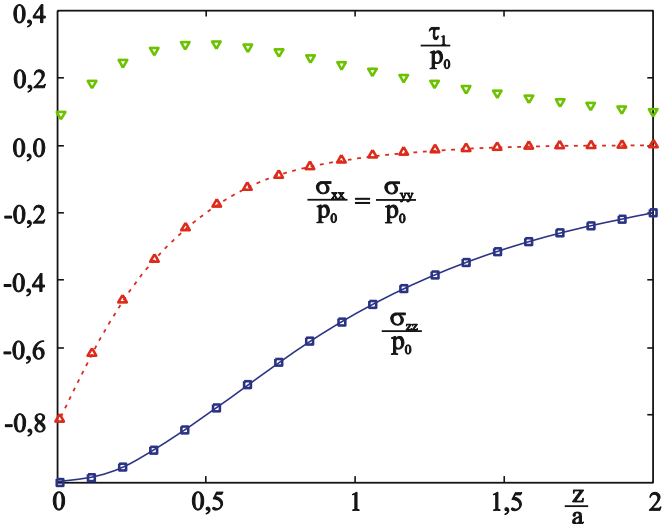

Fig. 5.8 Stresses along the z-axis ($x = y = 0$) for Hertzian pressure distribution.

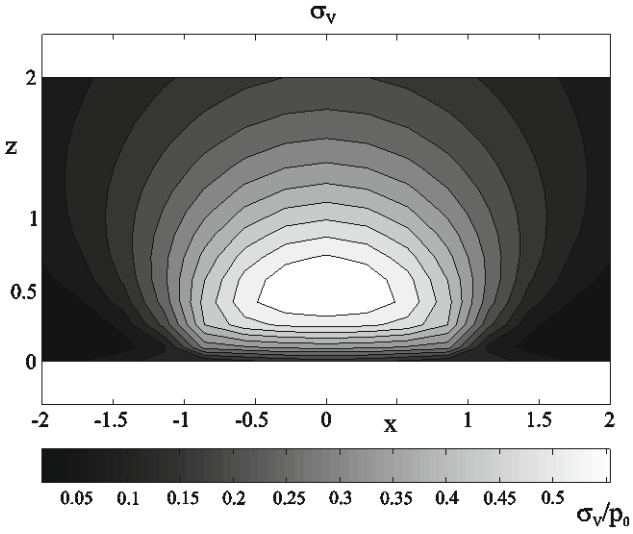

Fig. 5.9 Equivalent stress σ_V according to (5.50) for Hertzian pressure distribution (x-z plane).

5.6 Method of Dimensionality Reduction (MDR)

The contact of axial symmetric bodies with any shape can be easily and elegantly solved by the so-called Method of Dimensionality Reduction (MDR)[9]. The MDR maps a three-dimensional contact onto a contact with a one-dimensional array of independent springs (Winkler foundation), and it therefore simplifies both the analytical and the numerical treatment of the contact problem. Despite its simplicity, all results for axial-symmetric contacts are exact. With the MDR, non-adhesive and adhesive contacts, tangential contacts with friction, and contacts of viscoelastic media can be studied. In this section, we describe the application of the MDR for the treatment of normal contact problems. Generalizations for other problems will be discussed at appropriate sections in subsequent chapters. The proof of the correctness of the fundamental equations of the MDR is given in Appendix B.

The MDR basically consists of two simple steps: (a) replacement of the three-dimensional continuum by a strictly defined one-dimensional Winkler bedding and (b) transformation of the three-dimensional shape into a two-dimensional shape using the MDR-transformation. If these two steps are completed, the contact problem can be considered to be solved.

Two preliminary basic steps of the MDR

We consider a contact between two elastic bodies with moduli of elasticity of E_1 and E_2 and Poison's numbers of ν_1 and ν_2. We denote the difference between the profiles of the bodies as $z = f(r)$. In the framework of the MDR, two independent steps are conducted:

I. First, the three-dimensional elastic (or viscoelastic) bodies are replaced by a one-dimensional Winkler foundation. This is considered to be a linear array of elements having independent degrees of freedom and a sufficiently small separation distance Δx.

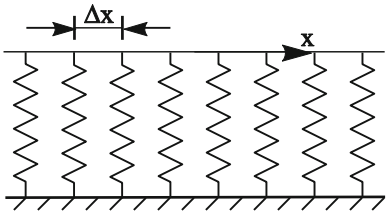

Fig. 5.10 One-dimesnional elastic foundation.

[9] V.L. Popov, M. Heß, Method of Dimensionality Reduction in Contact Mechanics and Friction, Springer, 2015.

In the simplest case of the elastic contact, the foundation consists of linearly elastic spring elements that have a normal stiffness Δk_z (Fig. 5.10):

$$\Delta k_z = E^* \Delta x \,, \tag{5.51}$$

where E^* is given by (5.26).

II. In the second step, the three-dimensional profile $z = f(r)$ (Fig. 5.11, left) is transformed into a one-dimensional profile (Fig. 5.11, right) according to

$$g(x) = |x| \int_0^{|x|} \frac{f'(r)}{\sqrt{x^2 - r^2}} \mathrm{d}r \tag{5.52}$$

The reverse transformation is

$$f(r) = \frac{2}{\pi} \int_0^r \frac{g(x)}{\sqrt{r^2 - x^2}} \mathrm{d}x \,. \tag{5.53}$$

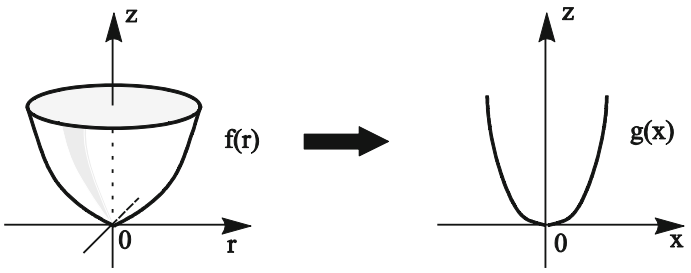

Fig. 5.11 The three-dimensional profile is transformed into a one-dimensional profile using the MDR

Calculation steps of the MDR

The one-dimensional profile according to (5.52) is now pressed into an elastic foundation corresponding to (5.51) with the normal force F_N (see Fig. 5.12).

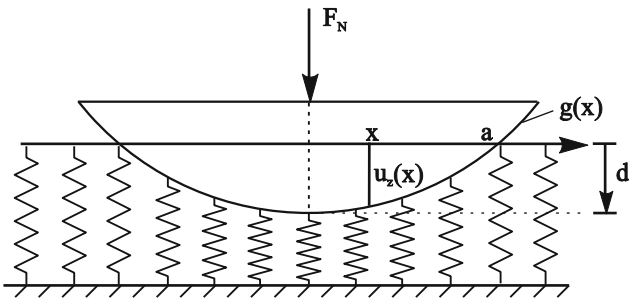

Fig. 5.12 Equivalent MDR model of normal contact.

The normal surface displacement at the point x within the contact area results from the difference between the indentation depth d and the profile form g:

$$u_z(x) = d - g(x). \tag{5.54}$$

At the edge of the non-adhesive contact $x = \pm a$, the surface displacement must be zero:

$$u_z(\pm a) = 0 \quad \Rightarrow \quad d = g(a). \tag{5.55}$$

This equation determines the relationship between the indentation depth and the contact radius a. It should be noted that this relationship is independent of the rheology of the medium. The force of a spring at the point x is proportional to the displacement at this point:

$$\Delta F_z(x) = \Delta k_z u_z(x) = E^* u_z(x) \Delta x. \tag{5.56}$$

The sum of all spring forces must correspond to the normal force in equilibrium. In the limiting case of very small spring separation distances $\Delta x \to \mathrm{d}x$, the summation becomes the integral

$$F_N = E^* \int_{-a}^{a} u_z(x)\,\mathrm{d}x = 2E^* \int_{0}^{a} \left(d - g(x)\right)\mathrm{d}x. \tag{5.57}$$

Equation (5.57) provides the normal force with respect to the contact radius and the indentation depth if (5.55) is taken into account.

We now define the linear force density $q_z(x)$:

$$q_z(x) = \frac{\Delta F_z(x)}{\Delta x} = E^* u_z(x) = \begin{cases} E^*\left(d - g(x)\right), & |x| < a \\ 0, & |x| > a \end{cases}. \tag{5.58}$$

As shown in Appendix B, the stress distribution in the original three-dimensional system can be determined with the help of the one-dimensional force dencity using the integral transformation

$$p(r) = -\frac{1}{\pi} \int_{r}^{\infty} \frac{q_z'(x)}{\sqrt{x^2 - r^2}}\,\mathrm{d}x. \tag{5.59}$$

The normal surface displacement $u_{3D,z}(r)$ (both inside and outside of the contact area) is given by the transformation:

$$u_{3D,z}(r) = \frac{2}{\pi} \int_{0}^{r} \frac{u_z(x)}{\sqrt{r^2 - x^2}}\,\mathrm{d}x. \tag{5.60}$$

For the sake of completeness, we still give the reverse transformation to (5.59):

$$q(x) = 2\int_x^\infty \frac{rp(r)}{\sqrt{r^2 - x^2}}\,\mathrm{d}r\,. \tag{5.61}$$

Equations (5.52), (5.55), (5.57), (5.59), (5.60) solve the normal contact problem completely. In the problems of this chapter, several examples are discussed.

Problems

Problem 1: Estimate the maximum pressure and the size of the contact area in a rail-wheel contact. The maximum load per wheel is around $F \approx 10^5$ N for cargo trains, the wheel radius is ca. $R = 0.5$ m.

Solution: The rail-wheel contact can be regarded, in a first-order approximation, as the contact between two cylinders lying on axes perpendicular to each other with roughly the same radius R. Therefore, it is equivalent to the contact between an elastic sphere with the radius R and an elastic half-space. The effective modulus of elasticity is $E^* \approx E/2(1-\nu^2) \approx 1.2 \cdot 10^{11}$ Pa. The pressure in the center of the contact area is found to be $p_0 \approx 1.0$ GPa according to (5.24). The contact radius is $a \approx 6.8\,mm$.

Problem 2: Two cylinders of the same material and with the same R are brought into contact so that their axes form an angle of $\pi/4$ (Fig. 5.13). Determine the relationship between force and penetration depth.

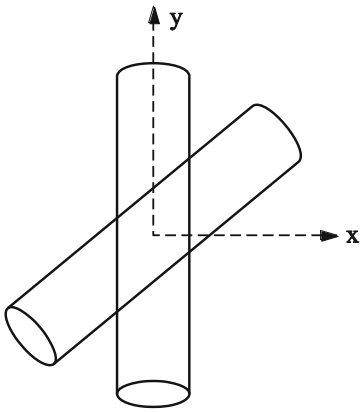

Fig. 5.13 Contact between two identical cylinders which form an angle of $\pi/4$ (when seen from above).

Solution: We assume that the contact plane is horizontal. The distance between the surface of the first cylinder and this plane (at the first moment of contact) is equal to $z_1 = \frac{x^2}{2R}$, and the distance for the second cylinder is equal to $z_2 = -\frac{(x-y)^2}{4R}$. The distance between both surfaces is then

$$h = \frac{x^2}{2R} + \frac{(x-y)^2}{4R} = \frac{1}{R}\left(\frac{3}{4}x^2 - \frac{1}{2}xy + \frac{1}{4}y^2\right).$$

The principal curvatures are calculated as the eigenvalues of this quadratic form, using the equation,

$$\begin{vmatrix} \frac{3}{4R} - \kappa & -\frac{1}{4R} \\ -\frac{1}{4R} & \frac{1}{4R} - \kappa \end{vmatrix} = \kappa^2 - \frac{\kappa}{R} + \frac{1}{8R^2} = 0 .$$

to $\kappa_{1,2} = \frac{1 \pm 1/\sqrt{2}}{2R}$. The principal radii of curvature are accordingly $R_{1,2} = \frac{2R}{1 \pm 1/\sqrt{2}}$. The resulting Gaussian radius of curvature is $\tilde{R} = \sqrt{R_1 R_2} = 2\sqrt{2}R$. Because both cylinders are made from the same material, then according to (5.26) $E^* = \frac{E}{2(1-\nu^2)}$. In this case, the relationship between the force and the penetration depth from (5.23) is

$$F = \frac{2^{7/4}}{3}\frac{E}{(1-\nu^2)} R^{1/2} d^{3/2} .$$

Problem 3: Determine the contact time during an impact of an elastic sphere (Radius R) with a flat wall (Hertz, 1882).

Solution: The displacement of the center of the sphere from the moment of initial contact we will call x. The potential energy of the system is given by (5.25) with $d = x$ and E^* according to (5.26). During the contact time, the energy is conserved:

$$\frac{m}{2}\left(\frac{dx}{dt}\right)^2 + \frac{8}{15}E^* R^{1/2} x^{5/2} = \frac{m v_0^2}{2} .$$

The maximum displacement x_0 corresponds to the point in time at which the velocity, dx/dt, is zero and is

$$x_0 = \left(\frac{15}{16} \frac{m v_0^2}{E^* R^{1/2}} \right)^{2/5} .$$

The contact time τ (during which x varies from 0 to x_0 and again back to 0) is

$$\tau = \frac{2}{v_0} \int_0^{x_0} \frac{dx}{\sqrt{1-(x/x_0)^{5/2}}} = \frac{2x_0}{v_0} \int_0^1 \frac{d\xi}{\sqrt{1-\xi^{5/2}}} = \frac{2{,}94 x_0}{v_0} .$$

Problem 4: Determine the maximum contact pressure during an impact between a sphere and a wall.

Solution: We calculated the maximum indentation depth x_0 in Problem 3. The maximum pressure p_0 is given by (5.22) and is equal to

$$p_0 = \frac{2}{\pi} E^* \left(\frac{x_0}{R} \right)^{1/2} = \frac{2}{\pi} \left(\frac{15}{16} \frac{E^{*4} m v_0^2}{R^3} \right)^{1/5} = \frac{2}{\pi} \left(\frac{5}{4} \pi E^{*4} \rho v_0^2 \right)^{1/5} ,$$

where ρ is the density of the material.

For example, by the impact of a steel sphere on a steel wall at $v_0 = 1$ m/s, we have (assuming a purely elastic collision)

$$p_0 \approx \frac{2}{\pi} \left(\frac{5}{4} \pi \left(10^{11}\right)^4 \left(7.8 \cdot 10^3\right) \cdot 1 \right)^{1/5} = 3.2 \cdot 10^9 \text{ Pa} .$$

Problem 5: Determine the differential contact stiffness $\delta F_N / \delta d$ for a contact between an elastic axially symmetric body and a rigid plane with a contact area A (Fig. 5.14).

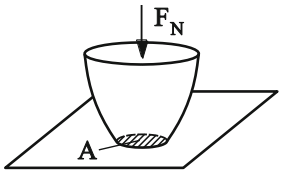

Fig. 5.14 Contact between an elastic, axially-symmetric body and a rigid plane.

Solution: We consider a round contact area with a radius a. The change in the area of the contact due to the infinitesimally small increase of the penetration depth δd can be thought of as taking place in two steps:

First, the existing contact area is rigidly displaced by δd (Fig. 5.15 b). Thereby, the normal force changes according to (5.12) by $\delta F_N = 2 a E^* \delta d$. In the second step, the remaining raised boundary area must then be displaced the same distance (Fig. 5.15 c). The increase in the given normal force is thereby proportional to the

area $2\pi a\delta a$ and to the height of the remaining raised boundary area. Therefore, the infinitesimally small change in force for the second step is of a higher order and can be neglected. The differential stiffness,

$$k_z = \frac{\delta F_N}{\delta d} = 2aE^* ,$$

is, therefore, only dependent on the contact radius and not on the exact form of the axially-symmetric body. For non-axially symmetric bodies, equation (5.13) is valid for the differential stiffness.

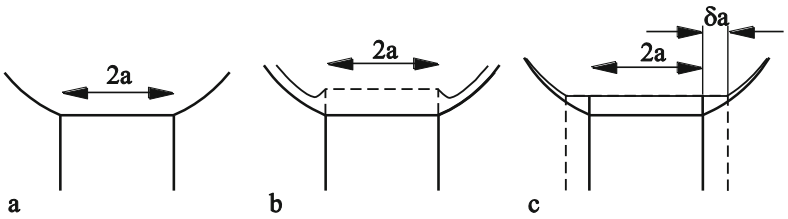

Fig. 5.15 Calculating the differential stiffness.

Problem 6: A constant distributed stress, p_0, acts on a circular contact area with a radius a. Determine the displacement at the center and the boundary of the circular area.

Solution: With help from (5.7) we obtain the following for the displacement in the center of the circle:

$$u_z(0) = \frac{1}{\pi E^*}\int_0^a p_0 \frac{2\pi r}{r}\mathrm{d}r = \frac{2p_0 a}{E^*} .$$

The displacement at the boundary is

$$u_z(a) = \frac{1}{\pi E^*}\int_0^{2a} p_0 \frac{2\varphi(r)\cdot r}{r}\mathrm{d}r = \frac{p_0}{\pi E^*}\int_0^{2a} 2\varphi(r)\mathrm{d}r .$$

(See Fig. 5.16 for the definition of the integration variable r in this case). The angle φ is calculated as $2\varphi = \pi - 2\arcsin\left(\frac{r}{2a}\right)$. Therefore, we obtain

$$u_z(a) = \frac{p_0}{\pi E^*}\int_0^{2a}\left(\pi - 2\arcsin\left(\frac{r}{2a}\right)\right)\mathrm{d}r = \frac{2ap_0}{\pi E^*}\int_0^1\left(\pi - 2\arcsin\left(\xi\right)\right)\mathrm{d}\xi = \frac{4ap_0}{\pi E^*} .$$

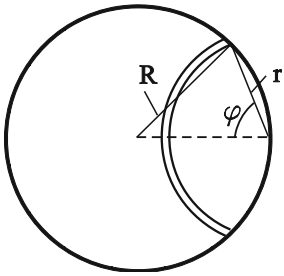

Fig. 5.16 Calculation of the integral in Problem 6.

Problem 7: Use the Method of Dimensionality Reduction to solve the normal contact problems between an elastic half-space and a rigid indenter with the following profiles:

(a) flat cylindrical indenter with radius a: $f(r)=\begin{cases}0, & r<a\\ \infty, & r\geq a\end{cases}$,

(b) parabolic profile $f(r)=r^2/(2R)$,

(c) conical profile $f(r)=r\cdot\tan\theta$,

(d) power function profile $f(r)=c_n r^n$ with arbitrary power n.

Solution: In order to use the MDR, the equivalent profile must first be calculated by means of the transformation (5.52). A simple calculation for the profiles listed above follows:

(a) $g(x)=\begin{cases}0, & |x|<a\\ \infty, & |x|\geq a\end{cases}$,

(b) $g(x)=x^2/R$,

(c) $g(x)=\dfrac{\pi}{2}|x|\tan\theta$,

(d) $g(x)=\kappa_n c_n|x|^n$

with $\kappa_n=\dfrac{\sqrt{\pi}}{2}\dfrac{n\Gamma(\frac{n}{2})}{\Gamma(\frac{n}{2}+\frac{1}{2})}$, where $\Gamma(n)=\int_0^\infty t^{n-1}e^{-t}\mathrm{d}t$ is the Gamma-function.

The contact radius is given by $g(a)=d$, (5.55):

(a) contact radius is constant and equal to a,

(b) $a=\sqrt{Rd}$,

(c) $a=\dfrac{2}{\pi}\dfrac{d}{\tan\theta}$,

(d) $a=\left(\dfrac{d}{\kappa_n c_n}\right)^{1/n}$.

The normal force for the given indentation depth is calculated according to (5.57):

(a) $F_N = 2E^* ad$,

(b) $F_N = \frac{4}{3} E^* R^{1/2} d^{3/2}$,

(c) $F_N = \frac{2}{\pi} E^* \frac{d^2}{\tan\theta}$,

(d) $F_N = \frac{2nE^*}{n+1} \left(\kappa_n c_n\right)^{-\frac{1}{n}} d^{\frac{n+1}{n}}$.

In order to calculate the pressure distribution in the three-dimensional original problem, the linear load should first be calculated according to the definition (5.58) in the MDR:

(a) $q_z(x) = \begin{cases} E^* d, & |x| < a \\ 0, & |x| > a \end{cases}$,

(b) $q_z(x) = \begin{cases} E^* \left(d - x^2 / R\right), & |x| < a \\ 0, & |x| > a \end{cases}$,

(c) $q_z(x) = \begin{cases} E^* \left(d - \frac{\pi}{2} |x| \tan\theta\right), & |x| < a \\ 0, & |x| > a \end{cases}$,

(d) $q_z(x) = \begin{cases} E^* \left(d - \kappa_n c_n |x|^n\right), & |x| < a \\ 0, & |x| > a \end{cases}$.

The derivation of the linear load at x (for a positive x) is calculated as

(a) $q_z'(x) = -E^* d \cdot \delta(x-a)$, where $\delta(x)$ is the Dirac delta function,

(b) $q_z'(x) = \begin{cases} -2E^* x / R, & x < a \\ 0, & x > a \end{cases}$,

(c) $q_z'(x) = \begin{cases} -\frac{\pi}{2} E^* \tan\theta, & x < a \\ 0, & x > a \end{cases}$,

(d) $q_z'(x) = \begin{cases} -E^* \kappa_n c_n n x^{n-1}, & x < a \\ 0, & x > a \end{cases}$.

Substituting the derivative into (5.59) the pressure distribution in the contact area is obtained:

(a) $p(r) = \frac{E^* d}{\pi} \int_r^\infty \frac{\delta(x-a)}{\sqrt{x^2 - r^2}} \mathrm{d}x = \begin{cases} \frac{E^* d}{\pi} \frac{1}{\sqrt{a^2 - r^2}}, & r < a \\ 0, & r > a \end{cases}$,

(b)

$$p(r)=\frac{2E^*}{\pi R}\int_r^{\infty}\frac{x}{\sqrt{x^2-r^2}}\,\mathrm{d}x=\begin{cases}\dfrac{2E^*}{\pi R}\displaystyle\int_r^a\frac{x}{\sqrt{x^2-r^2}}\,\mathrm{d}x=\frac{2E^*}{\pi R}\sqrt{a^2-r^2}, & r<a\\ 0, & r>a\end{cases},$$

(c)

$$p(r)=\frac{E^*}{2}\tan\theta\int_r^{\infty}\frac{\mathrm{d}x}{\sqrt{x^2-r^2}}=\frac{E^*}{2}\tan\theta\int_r^{a}\frac{\mathrm{d}x}{\sqrt{x^2-r^2}}=\frac{E^*}{2}\tan\theta\cdot\ln\left(\frac{a}{r}+\sqrt{\left(\frac{a}{r}\right)^2-1}\right)$$

for $r<a$ and $p(r)=0$ outside the contact area,

(d) $$p(r)=\kappa_n c_n n\frac{E^*}{\pi}\int_r^{\infty}\frac{x^{n-1}}{\sqrt{x^2-r^2}}\,\mathrm{d}x=\begin{cases}\kappa_n c_n n\dfrac{E^*}{\pi}\displaystyle\int_r^a\frac{x^{n-1}}{\sqrt{x^2-r^2}}\,\mathrm{d}x, & r<a\\ 0, & r>a\end{cases}.$$

If we normalize the pressure with the mean pressure in the contact region $\bar{p}=F_N/\left(\pi a^2\right)$ and the polar radius with the contact radius $\tilde{r}=r/a$, we can write the pressure in the contact area in the form

$$\frac{p(r)}{\bar{p}}=\frac{n+1}{2}\int_{\tilde{r}}^1\frac{\xi^{n-1}}{\sqrt{\xi^2-\tilde{r}^2}}\,\mathrm{d}\xi\,.$$

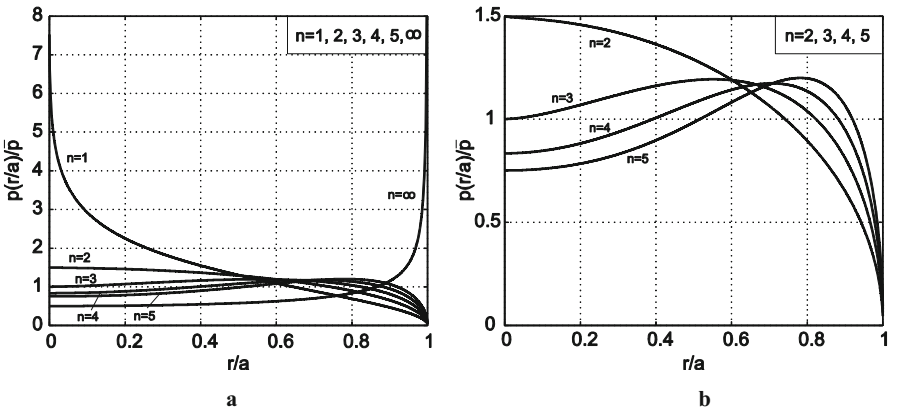

Fig. 5.17 Pressure distribution for simple power function profile (a) for $n=1,2,3,4,5,\infty$, (b) a detail with higher resolution for $n=2,3,4,5$.

Although this integral can be represented for all integers n via elementary functions, it is easier to calculate it numerically. The pressure distributions for $n=1$ (cone), $n=2$ (Hertzian contact), $n=3$, $n=4$, $n=5$ and $n=\infty$ (flat cylindrical punch) are shown in Fig. 5.17 for comparison. For the cone, the pressure has a logarithmic singularity at the tip of the cone. The pressure distribution for all cases with $n>1$ is not singular, but the maximum pressure for $n=2$ appears in the cen-

ter of the contact. Then, for larger n it begins to move towards the edge of the contact area. In the limiting case $n=\infty$, which corresponds to a flat cylindrical punch, the pressure distribution is singular at the edge of the contact area.

Normal displacements outside the contact area ($r>a$) are given by (5.60). The explicit form is

$$u_{3D,z}(r)=\frac{2}{\pi}\int_0^a \frac{u_z(x)}{\sqrt{r^2-x^2}}\,\mathrm{d}x=\frac{2}{\pi}\int_0^a \frac{d-g(x)}{\sqrt{r^2-x^2}}\,\mathrm{d}x,\qquad \text{for}\quad r>a\,.$$

For these special cases (a)-(d) we have:

(a) $$u_{3D,z}(r)=\frac{2d}{\pi}\arcsin\left(\frac{a}{r}\right),$$

(b) $$u_{3D,z}(r)=\frac{d}{\pi}\left[\left(2-\left(\frac{r}{a}\right)^2\right)\cdot\arcsin\left(\frac{a}{r}\right)+\sqrt{\left(\frac{r}{a}\right)^2-1}\right],$$

(c) $$u_{3D,z}(r)=\frac{2d}{\pi}\left[\arcsin\left(\frac{a}{r}\right)-\left(\frac{r}{a}-\sqrt{\left(\frac{r}{a}\right)^2-1}\right)\right],$$

(d) $$u_{3D,z}(r)=\kappa_n c_n\frac{2}{\pi}\int_0^a \frac{a^n-x^n}{\sqrt{r^2-x^2}}\,\mathrm{d}x\,.$$

In case (d), we did not carry out an explicit integration.

Problem 8: With the method of dimensionality reduction, determine the relations between normal force, indentation depth, and contact radius of a flattened parabolic profile (Fig. 5.18):

$$f(r)=\begin{cases}0 & \text{for}\quad 0\le r<b\\ \dfrac{r^2-b^2}{2R} & \text{for}\quad b\le r\le a\end{cases}$$

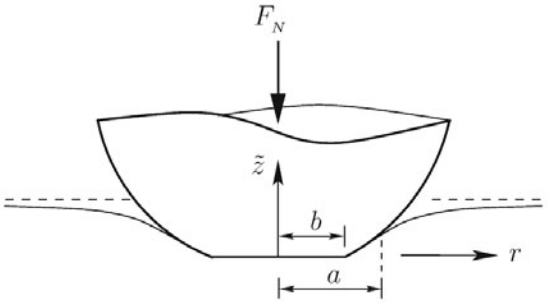

Fig. 5.18 Qualitative illustration of a flattened parabolic profile pressed into an elastic half-space.

Solution: To calculate the MDR-transformed profile according to (5.52), we first calculate the derivative of the original profile:

$$f'(r)=\begin{cases}0 & \text{for} \quad 0\le r<b\\ \dfrac{r}{R} & \text{for} \quad b\le r\le a\end{cases}.$$

Substituting it into (5.52) and subsequently integrating it gives

$$g(x)=\begin{cases}0 & \text{for} \quad 0\le |x|<b\\ \dfrac{|x|}{R}\sqrt{x^2-b^2} & \text{for} \quad b\le |x|\le a\end{cases}.$$

This profile is shown in Fig. 5.19 as compared to the original.

The indentation depth as a function of the contact radius is obtained from (5.55)

$$d=g(a)=\frac{a}{R}\sqrt{a^2-b^2}\ .$$

The normal force is obtained as the sum of all spring forces

$$F_N=E^*\int_{-a}^{a}\left[d-g(x)\right]\mathrm{d}x=2E^*\int_0^a d\,\mathrm{d}x-\frac{2E^*}{R}\int_b^a x\sqrt{x^2-b^2}\,\mathrm{d}x\ ,$$

which provides the following result after integration and appropriate transformations:

$$F_N(a)=\frac{2E^*}{3R}\left(2a^2+b^2\right)\cdot\sqrt{a^2-b^2}\ .$$

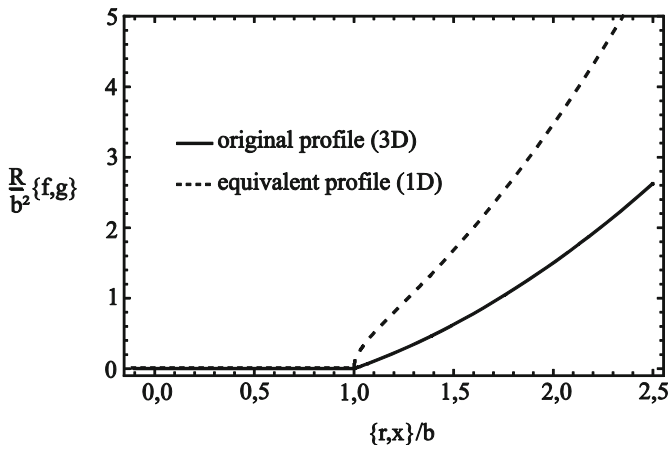

Fig. 5.19 Parabolic indenter with a worn tip: its original and equivalent profile.

For the sake of completeness, the relationship between normal force and indentation depth is given here:

$$F_N(d) = \frac{\sqrt{2}E^* b^3}{3R}\left(2+\sqrt{1+\left(\frac{2R}{b^2}d\right)^2}\right)\cdot\sqrt{-1+\sqrt{1+\left(\frac{2R}{b^2}d\right)^2}}\quad .$$

6 Rigorous Treatment of Contact Problems – Adhesive Contact

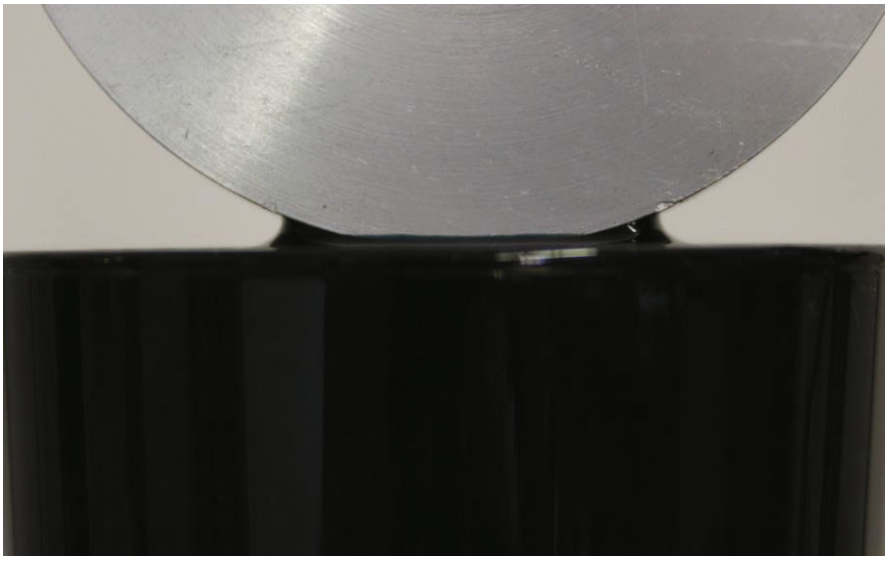

The problem of normal contact (without adhesion) between elastic bodies with slightly curved surfaces was solved in 1882 by Hertz. Bradley presented the solution 50 years later for adhesive normal contact between a rigid sphere and a rigid plane. The resulting adhesive force was found to be $F_A = 4\pi\gamma R$, where γ is the surface energy. The solution for the adhesive contact between elastic bodies was presented in 1971 by Johnson, Kendall, and Roberts (JKR-Theory). They obtained $F_A = 3\pi\gamma R$ for the adhesive force. Derjaguin, Müller, and Toporov published an alternative adhesive theory in 1975, which is known as the DMT-Theory. After an intense discussion in 1976 Tabor came to the realization that the JKR-Theory and the DMT-Theory are both correct and are special cases of the general problem. For absolutely rigid bodies the theory from Bradley is valid; for small, rigid spheres DMT-Theory is valid; and for large, flexible spheres JKR-Theory. The difference between all of these cases, however, is very minor and the JKR-Theory describes adhesion relatively well, even in the scope of the DMT-Theory. Perhaps this is why JKR-Theory is used so prevalently to describe adhesive contacts. For this reason, we will also limit ourselves in this chapter to the presentation of the theory from Johnson, Kendall, and Roberts.

V.L. Popov, *Contact Mechanics and Friction*,
DOI 10.1007/978-3-662-53081-8_6

6.1 JKR-Theory

The classical theory of adhesive contact was accomplished in 1971 by Johnson, Kendall, and Roberts and carries the name JKR-Theory. We consider an elastic sphere with the radius R in contact with a rigid, planar surface. The always present attractive force between two solid bodies (van der Waals forces) leads to the fact that an elastic sphere in contact with a smooth plane forms a characteristic "neck" (Fig. 6.1).

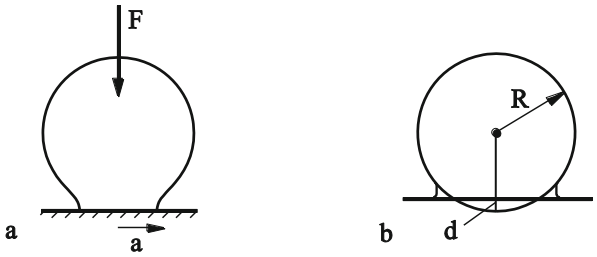

Fig. 6.1. During adhesive contact a "neck" is formed between the two contacting bodies.

We define the radius of the contact area as a and assume that $d, a << R$, where $R-d$ is the distance between the center of the sphere and the rigid surface.

In order for the sphere to take the form shown in Fig. 6.1 b, the points on the surface of the sphere must be displaced so that they lie on the rigid plane after deformation.

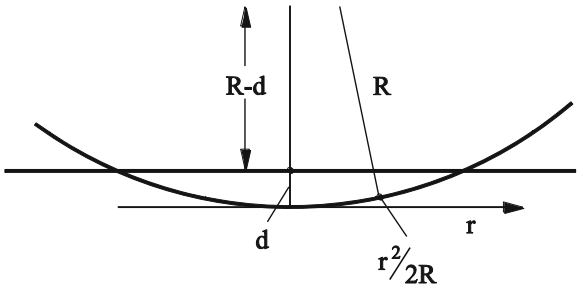

Fig. 6.2 The contact geometry between an elastic sphere and a rigid, planar surface.

It is apparent from Fig. 6.2, that the following equation is valid for the vertical displacement:

$$u_z = d - \frac{r^2}{2R}. \tag{6.1}$$

From the results of the previous chapters, we know that a pressure distribution of the form

$$p = p_0 \left(1 - r^2 / a^2\right)^{-1/2} \tag{6.2}$$

leads to a vertical displacement of

$$u_z = \frac{\pi}{E^*} p_0 a \,, \tag{6.3}$$

while a pressure distribution of the form

$$p = p_0 \left(1 - r^2 / a^2\right)^{1/2} \tag{6.4}$$

causes a displacement of

$$u_z = \frac{\pi}{4E^* a} p_0 \left(2a^2 - r^2\right). \tag{6.5}$$

The application of both pressure distributions at the same time obviously leads to a quadratic distribution of the displacement in the contact area, which stands in accordance with the geometric specification in (6.1).

Because of the reasons mentioned, we will use the following pressure distribution:

$$p = p_0 \left(1 - r^2 / a^2\right)^{-1/2} + p_1 \left(1 - r^2 / a^2\right)^{1/2}. \tag{6.6}$$

The corresponding displacement, obtained from the principle of superposition, is

$$u_z = \frac{\pi a}{E*} \left[p_0 + \frac{1}{2} p_1 \left(1 - \frac{r^2}{2a^2} \right) \right]. \tag{6.7}$$

Equating (6.1) and (6.7) yields

$$\frac{\pi a}{E*} \left(p_0 + \frac{p_1}{2} \right) = d \,, \qquad \frac{\pi p_1}{4E* a} = \frac{1}{2R} \,. \tag{6.8}$$

From this, it follows that

$$p_1 = \frac{E*}{\pi} \frac{2a}{R} \,, \qquad p_0 = \frac{E*}{\pi} \left(\frac{d}{a} - \frac{a}{R} \right). \tag{6.9}$$

The two equations (6.9) contain three unknown quantities: p_1, p_0 and a (for a given penetration depth d). In order to be able to unambiguously determine the state of deformation and stress for a given penetration depth d, a further constraint is necessary. For this purpose, we use the requirement that the total energy of the system assumes a minimum at a constant d.

The energy of the sphere is composed of an elastic contribution and an adhesive contribution. The potential energy for the elastic deformation of the sphere can be calculated with the equation

$$U_{el} = \frac{1}{2} \int\limits_{\substack{contact \\ area}} p(\mathbf{x}) u_z(\mathbf{x})\, dxdy\,, \tag{6.10}$$

which is valid for arbitrary linearly elastic systems. Substituting (6.6) and (6.1) into (6.10) provides us with

$$U_{el} = \pi d \int_0^a r \left[p_0 \left(1 - r^2 / a^2\right)^{-1/2} + p_1 \left(1 - r^2 / a^2\right)^{1/2} \right] \left(1 - \frac{r^2}{2dR}\right) dr\,. \tag{6.11}$$

After the substitution of $\xi = 1 - r^2 / a^2$, $d\xi = -2rdr / a^2$, we obtain

$$U_{el} = \frac{\pi d a^2}{2} \left[p_0 \left(2 - \frac{2}{3}\frac{a^2}{dR}\right) + p_1 \left(\frac{2}{3} - \frac{2}{15}\frac{a^2}{dR}\right) \right] \tag{6.12}$$

and considering (6.9),

$$U_{el} = E^* \left[d^2 a - \frac{2}{3}\frac{da^3}{R} + \frac{a^5}{5R^2} \right]. \tag{6.13}$$

The total energy is[1]

$$U_{tot} = E^* \left[d^2 a - \frac{2}{3}\frac{da^3}{R} + \frac{a^5}{5R^2} \right] - \gamma_{12} \pi a^2\,. \tag{6.14}$$

We obtain the radius at equilibrium a by requiring that the energy of the system assumes the minimum value:

$$\frac{\partial U_{tot}}{\partial a} = E^* \left[d^2 - 2\frac{da^2}{R} + \frac{a^4}{R^2} \right] - 2\gamma_{12}\pi a = E^* \left(d - \frac{a^2}{R} \right)^2 - 2\gamma_{12}\pi a = 0\,. \tag{6.15}$$

It follows that

$$d = \frac{a^2}{R} \pm \sqrt{\frac{2\gamma_{12}\pi a}{E^*}}\,. \tag{6.16}$$

Inserting this relationship into (6.14) provides the total energy as a function of the contact radius

$$U_{tot} = E^* \left[\frac{8}{15}\frac{a^5}{R^2} + \frac{\gamma_{12}\pi a^2}{E^*} \pm \frac{4}{3}\frac{a^3}{R}\sqrt{\frac{2\gamma_{12}\pi a}{E^*}} \right]. \tag{6.17}$$

[1] Here is γ_{12} the relative surface energy.

The equation with the minus sign corresponds to the state of lowest energy. We obtain the total force acting on the sphere in this state from the derivative of the energy with respect to the displacement d of the center of the sphere:

$$F = -\frac{dU_{tot}}{d(d)} = -\frac{\partial U_{tot}}{\partial(d)} - \frac{\partial U_{tot}}{\partial a}\frac{da}{d(d)}. \tag{6.18}$$

We must bear in mind that the value of a corresponds to the minimum of U_{tot} for a given d and, therefore, $\frac{\partial U_{tot}}{\partial a} = 0$. So, instead of (6.18) we come to a more simplified equation:

$$F = -\frac{\partial U_{tot}}{\partial(d)} = E^*\left[2da - \frac{2}{3}\frac{a^3}{R}\right]. \tag{6.19}$$

We insert (6.16) into this equation and obtain the force as a function of the contact radius

$$F = E^*\left[2\left(\frac{a^2}{R} - \sqrt{\frac{2\gamma_{12}\pi a}{E^*}}\right)a - \frac{2}{3}\frac{a^3}{R}\right] = E^*\left[\frac{4}{3}\frac{a^3}{R} - \left(\frac{8\gamma_{12}\pi a^3}{E^*}\right)^{1/2}\right]. \tag{6.20}$$

The maximum negative value of this force is reached when

$$a = a_{crit} = \left(\frac{9}{8}\frac{\gamma_{12}\pi R^2}{E^*}\right)^{1/3} \tag{6.21}$$

and is equal to

$$F_A = -\frac{3}{2}\gamma_{12}\pi R. \tag{6.22}$$

The absolute value of this force is called the *adhesive force*.

For the dimensionless variables: $\tilde{F} = F/|F_A|$, $\tilde{a} = a/a_{crit}$, (6.20) takes the form

$$\tilde{F} = \tilde{a}^3 - 2\tilde{a}^{3/2}. \tag{6.23}$$

This is graphically depicted in Fig. 6.3 a.

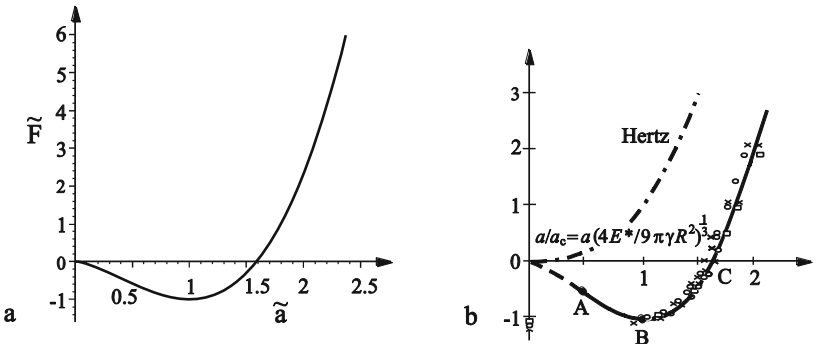

Fig. 6.3 (a) Dependence of the normalized force on the normalized contact radius; (b) Experimental data from Johnson for gelatin spheres with various radii: 24.5 mm, 79 mm and 255 mm (K.L. Johnson, Contact mechanics. Cambridge University Press, Ninth printing 2003.).

The penetration depth (Equation (6.16) with a minus sign) in the critical state (6.21) is equal to

$$d_{crit} = -\left(\frac{3\pi^2\gamma_{12}^2 R}{64E^{*2}}\right)^{1/3}. \tag{6.24}$$

If we insert the dimensionless penetration depth $\tilde{d} = d/|d_{crit}|$, we can rewrite equation (6.16) in the dimensionless form,

$$\tilde{d} = 3\tilde{a}^2 - 4\tilde{a}^{1/2}. \tag{6.25}$$

Together with (6.23), it defines the parametric form of the dependence of the dimensionless normal force on the dimensionless penetration depth (Fig.6.4).

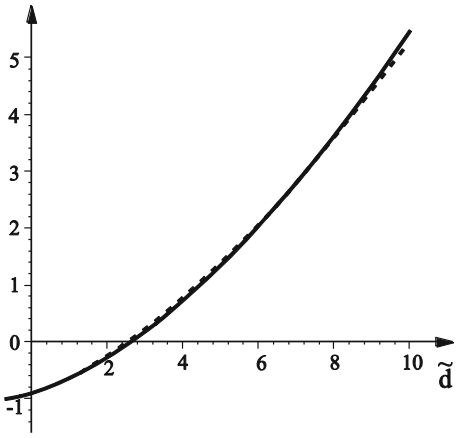

Fig. 6.4 Dependence of the dimensionless normal force on the dimensionless penetration depth.

This dependence is presented in Fig. 6.4 (solid line). In the area of interest for many adhesion problems, if the penetration depth is of the same order of magnitude as d_{crit}, it can be approximated very well using the following relationship (dashed line in Fig. 6.4):

$$\tilde{F} \approx -1 + 0{,}12 \cdot (\tilde{d} + 1)^{5/3} . \tag{6.26}$$

Lastly, we would like to quickly discuss the pressure distribution in the adhesive contact. This distribution is given by equations (6.6) and (6.9). It can be noted that p_1 is always positive and $p_0 = \frac{E^*}{\pi}\left(\frac{d}{a} - \frac{a}{R}\right) = -\sqrt{\frac{2\gamma_{12}E^*}{\pi a}}$ is always negative. The resulting pressure distribution is shown in Fig. 6.5. The significant difference between this and non-adhesive contact is the fact that at the edges of the contact area, the stress is not zero, rather it assumes an infinitely large negative value.

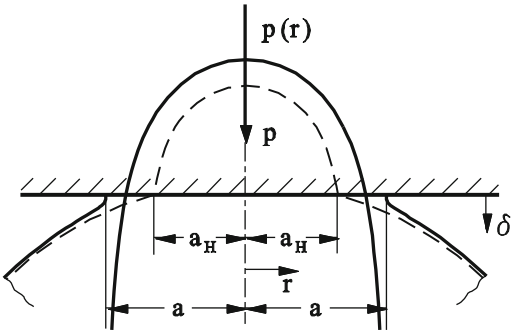

Fig. 6.5 Form of the body in contact and the pressure distribution in an adhesive contact.

Allowing the adhesive forces to act over a finite range removes this singularity. Nevertheless, the stresses at the edges of an adhesive contact area reach very large values (from the order of magnitude of the "theoretical strength" of the van der Waals contact), which can lead to increased wear (compare a similar situation for "tangential contact," see chapter 8).

6.2 Adhesive Contact of Rotationally Symmetrical Bodies

In Section 5.6, a simple method has been described with which normal contact problems for *any axially-symmetric bodies* can be solved (method of dimensionality reduction, MDR). Adhesive contacts of axisymmetric indenters can also be described exactly by the MDR.

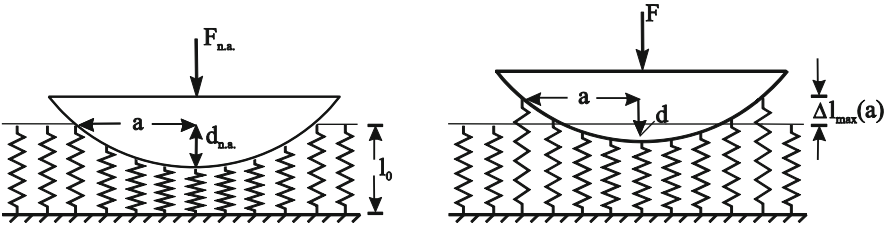

Fig. 6.6 Qualitative illustration of the indentation and retraction process of a spherical 1D-indenter in contact with an elastic foundation, which exactly reflects the characteristics of the adhesive contact between a rigid spherical indenter and the elastic half-space.

Below, we describe the calculation procedure for an adhesive contact using the MDR. The proof of the correctness of the method is given in Appendix C. The calculation procedure is comprised of the following steps:

- In the first step, the given three-dimensional profile $z = f(r)$ is transformed into an equivalent one-dimensional profile $g(x)$ by (5.52).
- The profile $g(x)$ is now pressed into the one-dimensional elastic foundation defined in (5.51), and a contact radius a is generated. In this process the adhesion is still not considered. This process is shown in Fig. 6.6 left.
- In the third step, the indenter is pulled upward, and it is assumed that all springs in contact adhere to the indenter - the contact radius remains constant. During the progressive pulling movement springs at the edge are increasingly loaded in tension. If the elongation of the outer springs reaches the maximum value:

$$\Delta l_{\max}(a) = \sqrt{\frac{2\pi a \gamma_{12}}{E^*}}\,, \tag{6.27}$$

they break away. The detachment criterion (6.27) was found by M. Hess[2] and is known as the rule of Hess. A derivation of this criterion is given in Appendix C (A.39). It can be shown that with this relation, the state of equilibrium described by the three parameters (F, d, a) is exactly the same as that of the three-dimensional adhesive contact.

The difference from the algorithm for the non-adhesive contact described in section 5.6 is only the formula for calculating the indentation depth: the displacement of the springs at the edge is not zero but negative and equal to the critical value $u_z(a) = -\Delta l_{\max}(a)$. It follows that

$$d = g(a) - \Delta l_{\max}(a)\,. \tag{6.28}$$

The normal force is still given by (5.57):

[2] M. Heß, Über die exakte Abbildung ausgewählter dreidimensionaler Kontakte auf Systeme mit niedrigerer räumlicher Dimension, Cuvillier Verlag Göttingen, 2011.

$$F_N = 2E^* \int_0^a \left(d - g(x)\right) \mathrm{d}x = 2E^* \left[ad - \int_0^a g(x)\,\mathrm{d}x \right]$$
$$= 2E^* \left[ag(a) - \int_0^a g(x)\,\mathrm{d}x - a\Delta l_{\max}(a) \right] \tag{6.29}$$

or

$$F_N = 2E^* \left[\int_0^a x g'(x)\,\mathrm{d}x - a\Delta l_{\max}(a) \right]. \tag{6.30}$$

If the force is controlled during pull-off, then the critical value of the contact radius a_c at the moment of stability loss is determined by the condition $\mathrm{d}F_N / \mathrm{d}a = 0$:

$$\left. \frac{\mathrm{d}g(a)}{\mathrm{d}a} \right|_{a_c} = \sqrt{\frac{9\pi\gamma_{12}}{2a_c E^*}}. \tag{6.31}$$

Substituting this critical radius into (6.30) we obtain the adhesive force:

$$F_A = -2E^* \left[\int_0^{a_c} x g'(x)\,\mathrm{d}x - a_c \Delta l_{\max}(a_c) \right]. \tag{6.32}$$

The transformation rules of the MDR, e.g. (5.59), for the pressure distribution and Equation (5.60) for the displacements are still valid in the case of an adhesive contact.

To illustrate the application of this method, we consider the adhesive contact between a flat cylindrical punch with a radius a and an elastic half-space. The MDR-transformed image of the system is shown in Fig. 6.7.

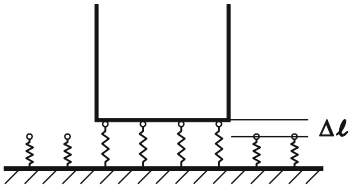

Fig. 6.7 Equivalent one-dimensional system for the adhesive contact of a flat cylindrical punch with an elastic half-space.

In this case, the critical radius is trivially equal to the radius of the cylinder $a_c = a$. Because $g'(x) = 0$ for a flat cylinder, the first term in (6.32) vanishes and the adhesive force is

$$F_A = 2E^* a \Delta l_{\max}(a) = \sqrt{8\pi a^3 E^* \gamma_{12}}, \tag{6.33}$$

which exactly coincides with the three-dimensional result[3].

Further examples will be discussed in the solutions of this chapter.

Problems

Problem 1: What is the longest length that the slender beam shown in Fig. 6.8 can have with which adhesive contact (as seen in the sketch) can be prevented? Let the relative surface energy between the beam and base be γ^*. Let the width of the beam (perpendicular to the plane of the figure) be a and the thickness t.

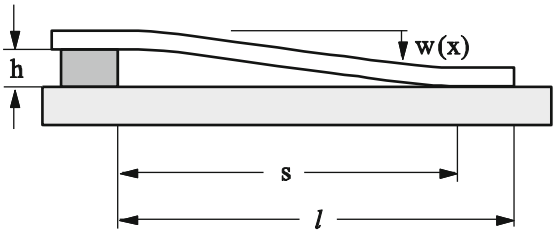

Fig. 6.8 The adhesive contact for a micromechanical model consisting of a slender, elastic beam and a base.

Solution: The differential equation of a beam, in this case, is: $d^4w/dx^4 = 0$. Its solution, which fulfills the boundary conditions $w(0) = 0$, $w(s) = h$, $w'(0) = 0$, and $w'(s) = 0$, yields

$$w(x) = \frac{h}{s^3}\left(3x^2 s - 2x^3\right).$$

The elastic energy of a bent beam is calculated using

$$U_{el} = \int_0^s \tfrac{1}{2} EIw''(x)^2 dx = \frac{6EIh^2}{s^3},$$

where the geometrical moment of inertia is

$$\mathrm{I} = \frac{at^3}{12}.$$

The total energy is equal to

$$U = \frac{6EIh^2}{s^3} - \gamma^*\left(l - s\right)a.$$

[3] K. Kendall, The adhesion and surface energy of elastic solids. Journal of Physics D: Applied Physics, 1971, v. 4, pp. 1186-1195.

It assumes a minimum at

$$s = \left(\frac{3Eh^2 t^3}{2\gamma^*} \right)^{1/4} .$$

If the length of the beam is smaller than s, then it cannot "remain stuck" to the base.

Problem 2: A sheet with a thickness t is separated from a body by external forces overcoming the surface tension (Fig. 6.9). Find the relationship between the surface tension and the form of the separating sheet[4].

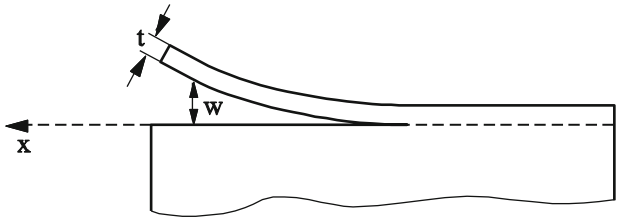

Fig. 6.9 A sheet is separated from an elastic body.

Solution: We consider the separating sheet as a plate with width a (perpendicular to the plane of the figure), which one edge (the separation line) is horizontally clamped. The solution of the differential equation of a plate, $d^4 w / dx^4 = 0$, which satisfies the boundary conditions $w(0) = h$, $w(s) = 0$, $w''(0) = 0$, and $w'(s) = 0$, yields

$$w(x) = \frac{h\left(x^3 - 3xs^2 + 2s^3\right)}{2s^3} .$$

The elastic energy is equal to

$$U_{el} = \int_0^s \tfrac{1}{2} Daw''(x)^2 \, dx = \frac{3Dah^2}{2s^3} ,$$

with $D = \dfrac{Et^3}{12(1-\nu^2)}$. The total energy is

$$U = \frac{3Dah^2}{2s^3} + 2\gamma sa .$$

[4] J.W. Obreimoff (1930) examined this problem in conjunction with the method he developed for measuring the surface energy of mica; these measurements were the first to directly measure the surface energy of solids. See: J.W. Obreimoff, The splitting strength of mica. Proc. Ro. Soc. of London, 1930, v. 125, pp. 290-297.

It assumes a minimum at

$$s = \frac{\sqrt{6}}{2} D^{1/4} h^{1/2} \gamma^{-1/4} .$$

Taking into account the equation $w''(x) = \frac{3hx}{s^3}$, it follows that

$$\gamma = \frac{D}{4} w''(s)^2 .$$

Problem 3: Consider the adhesive contact between a rigid conical profile, $f(r) = \tan\theta \cdot r$, and an elastic half-space. Determine the dependence of indentation depth and normal force on the contact radius and the adhesive force under fixed-load conditions.

Solution: In the first step, we calculate the equivalent one-dimensional profile by the integral transformation (5.52): $g(x) = (\pi/2)\tan\theta \cdot |x|$. The relation between the indentation depth and the contact radius is given by (6.28):

$$d = \frac{\pi}{2}\tan\theta \cdot a - \sqrt{\frac{2\pi a \gamma_{12}}{E^*}} .$$

Equation (6.30) for the normal force takes the form

$$F_N = 2E^* \left[\frac{\pi \tan\theta\, a^2}{4} - a\sqrt{\frac{2\pi a \gamma_{12}}{E^*}} \right].$$

The maximum negative force is reached at $a_c = \frac{18\gamma_{12}}{\pi \tan^2\theta \cdot E^*}$ and it is equal to

$$F_c = -\frac{54 {\gamma_{12}}^2}{\pi \tan^3\theta \cdot E^*} .$$

The indentation depth in this critical state is $d_c = \frac{3\gamma_{12}}{\tan\theta \cdot E^*}$. By introducing the normalized variables $\tilde{F}_N := F_N / |F_c|$, $\tilde{d} := d / |d_c|$, and $\tilde{a} := a / a_c$, the indentation depth and normal force have the following dimensionless form:

$$\tilde{F}_N(\tilde{a}) = 3\tilde{a}^2 - 4\tilde{a}^{3/2} \quad \text{and} \quad \tilde{d}(\tilde{a}) = 3\tilde{a} - 2\tilde{a}^{1/2} .$$

Problem 4: Investigate the adhesive contact between a rigid, axially-symmetric indenter with the form $f(r) = c_n \cdot r^n$ and an elastic half-space.

Solution: This problem can be particularly elegantly solved using the MDR. The equivalent one-dimensional profile has already been calculated in Problem 7 of Chapter 5:

$$g(x) = \kappa_n c_n |x|^n \quad \text{with} \quad \kappa_n = \frac{\sqrt{\pi}}{2} \frac{n\Gamma(\frac{n}{2})}{\Gamma(\frac{n}{2}+\frac{1}{2})} .$$

The relation between the indentation depth and contact radius is given by (6.28):

$$d = g(a) - \Delta\ell_{\max}(a) = \kappa_n c_n a^n - \sqrt{\frac{2\pi a \gamma_{12}}{E^*}} .$$

Equation (6.30) for the normal force is

$$F_N(a) = 2E^* \frac{n}{n+1} \kappa_n c_n a^{n+1} - \sqrt{8\pi a^3 E^* \gamma_{12}} .$$

The force reaches its minimum value

$$F_c = \frac{1-2n}{n+1} \left[\left(\frac{3}{2n\kappa_n c_n} \right)^3 (2\pi\gamma_{12})^{n+1} E^{*n-2} \right]^{\frac{1}{2n-1}}$$

at

$$a_c = \left(\frac{9\pi\gamma_{12}}{2n^2 \kappa_n^2 c_n^{\,2} E^*} \right)^{\frac{1}{2n-1}} .$$

The indentation depth at the moment of stability loss equals

$$d_c = \left(1 - \frac{2}{3}n\right) \left[\frac{9\pi\gamma_{12}}{2n^2 E^*} \left(\frac{1}{\kappa_n c_n} \right)^{1/n} \right]^{\frac{n}{2n-1}} .$$

Normalizing by the critical values, $\tilde{F}_N = F_N / |F_c|$, $\tilde{d} = d / |d_c|$ and $\tilde{a} = a / a_c$, the equilibrium relations can be written in a particularly simple form:

$$\tilde{F}_N(\tilde{a}) = \frac{1}{|1-2n|} \left[3\tilde{a}^{n+1} - 2(n+1)\tilde{a}^{3/2} \right] \quad \text{and} \quad \tilde{d}(\tilde{a}) = \frac{1}{|3-2n|} \left(3\tilde{a}^n - 2n\tilde{a}^{1/2} \right) .$$

The results for $n = 1$ coincide with those of Problem 3, while the classic JKR theory for a parabolic profile is found for $n = 2$.

7 Contact between Rough Surfaces

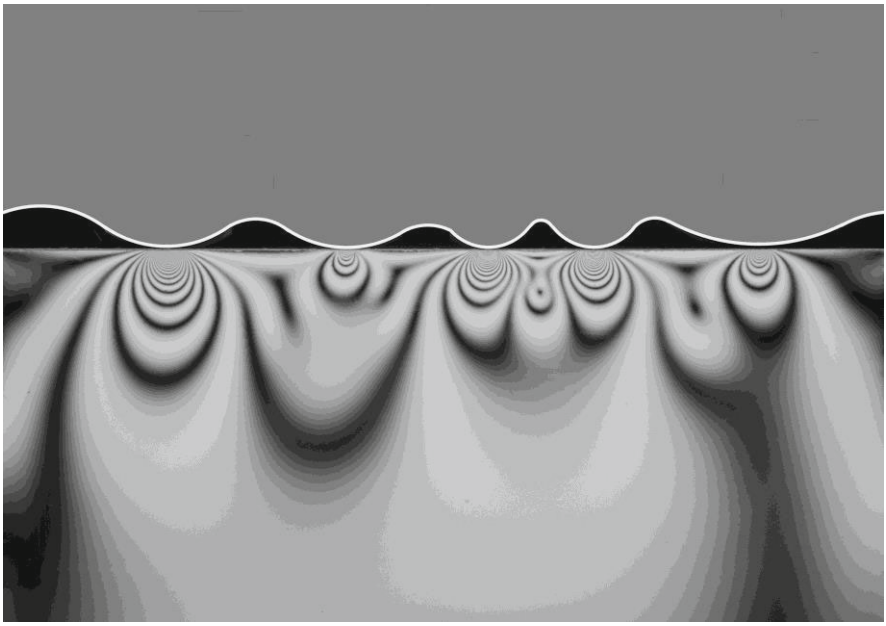

The surface roughness has a large influence on many physical phenomena such as friction, wear, sealing, adhesion, and electrical as well as thermal contacts. Initially, if two bodies with rough surfaces are pressed together, the "real" contact area is much smaller than the "apparent" contact area. The size of the "real" contact area determines, for example, the electrical and thermal resistance between the bodies. The size of the contact area and the maximum stress ultimately determines the size of the wear particles and therefore the rate of wear. The size of the real contact area is also a crucial factor in frictional processes. The cause of frictional forces can be visualized as the fracturing of microscopic bonds between the contacting bodies. The fracture strength, and therefore the frictional force, should be, according to this viewpoint, approximately proportionally to the "real" contact area. In this chapter, we will investigate the dependence of the contact area, length, and overall configuration on the normal force.

V.L. Popov, *Contact Mechanics and Friction*,
DOI 10.1007/978-3-662-53081-8_7

7.1 Model from Greenwood and Williamson

We begin with a discussion of rough surfaces in *elastic* contacts. For a simple model of a rough surface, one can visualize a regular series of roughnesses of the same form, having the same radius of curvature and the same height[1] (Fig. 7.1).

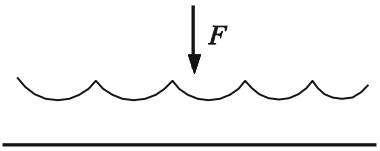

Fig. 7.1 Simple model of a rough surface.

The treatment of a contact problem between such surfaces is simple: The total force is the sum of all of the equal "summit" forces, which can be calculated using Hertzian contact theory. The individual "micro" contact areas, and therefore, the total contact area, are in this case $\Delta A \sim F^{2/3}$. This contradicts not only direct experiments, but also Amontons' law of friction, according to which the frictional force is approximately proportional to the normal force. Therefore, we expect a somewhat linear increase in the contact area with respect to normal force.

The situation changes if we take into account that a real surface is, as a rule, stochastically rough. The simplest method of modeling an irregular surface was proposed in 1966 by J.A. Greenwood and J.B.P. Williamson. We refer to this model as the GW-Model after its authors. Greenwood and Williamson assumed that all roughness peaks ("asperities") have the same radius of curvature and that the height of the peaks is stochastically distributed around an average value (Fig. 7.2).

If the contacting peaks are far enough away from each other, then their deformations can be considered independent of each other. Thus, the position of the peaks, and therefore the exact configuration of the surface, matters little in the contact problem (under the given assumptions). Only the height distribution of the peaks is of importance. We describe the probability density of an asperity to have the maximum height z as $\Phi(z)$. That means that the probability that an asperity has the maximum height in the interval $[z, z+\mathrm{d}z]$ is equal to $\Phi(z)\mathrm{d}z$. If the total number of asperities is N_0, then the number of asperities in the interval $[z, z+\mathrm{d}z]$ is equal to $N_0\Phi(z)\mathrm{d}z$.

[1] Such regular surfaces are not actually defined as "rough", rather as "profiled" or "textured".

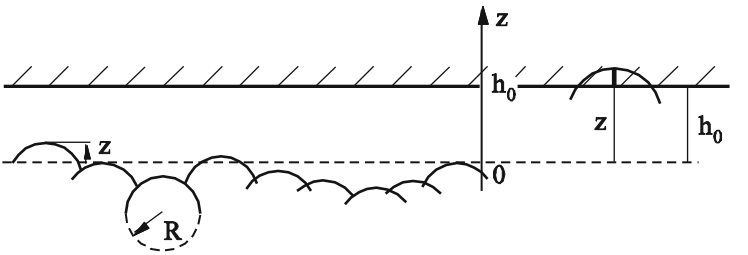

Fig. 7.2 Model of a stochastic surface according to Greenwood and Williamson.

For many technical and natural surfaces, it can be assumed that the height of the peaks is normally distributed:

$$\Phi(z) = \left(\frac{1}{2\pi l^2}\right)^{1/2} e^{-\frac{z^2}{2l^2}}. \tag{7.1}$$

Here, the value l is the root mean square of the height distribution:

$$l = \sqrt{\langle z^2 \rangle}, \tag{7.2}$$

which we call *roughness*.

We consider a contact between an elastic body with the described statistical roughness and a rigid plane at a distance h_0 from the middle level, at which the value of zero for the z-axis is assumed (Fig. 7.2). Under the assumption that one can neglect the elastic interactions between the asperities, all of the asperities with a height $z > h_0$ are in contact with the rigid plane. The "penetration depth" of an asperity with the height z is $d = z - h_0$. For a single contact, we obtain $a^2 = d \cdot R$, according to Hertzian theory (Equation (5.21)). Therefore, the contact area of a single asperity is

$$\Delta A = \pi a^2 = \pi d \cdot R = \pi \left(z - h_0\right) R \tag{7.3}$$

and the single force,

$$\Delta F = \frac{4}{3} E^* R^{1/2} d^{3/2} = \frac{4}{3} E^* R^{1/2} \left(z - h_0\right)^{3/2}. \tag{7.4}$$

The total number of contacts, the total contact area, and the total normal force F_N are found through integration over all of the asperities in contact. This means that the integration must be performed over all heights from $z = h_0$ to infinity:

$$N = \int_{h_0}^{\infty} N_0 \Phi(z) dz, \tag{7.5}$$

$$A = \int_{h_0}^{\infty} N_0 \Phi(z) \pi R (z - h_0) dz \,, \tag{7.6}$$

$$F_N = \int_{h_0}^{\infty} N_0 \Phi(z) \frac{4}{3} E^* R^{1/2} (z - h_0)^{3/2} dz \,. \tag{7.7}$$

The total area, total force, and the number of contacts increase exponentially as the bodies are pressed closer together (decrease in h_0), while the relationships between these values remain relatively unchanged. For the *average contact area of an asperity*, for example, we get

$$\langle \Delta A \rangle = \frac{A}{N} = \frac{\int_{h_0}^{\infty} dz N_0 \Phi(z) \pi R \cdot (z - h_0)}{\int_{h_0}^{\infty} dz N_0 \Phi(z)} \,. \tag{7.8}$$

By inserting the dimensionless variable $\xi = z / l$ and defining $\xi_0 = h_0 / l$ we obtain

$$\langle \Delta A \rangle = \pi R l \left[\frac{\int_{\xi_0}^{\infty} d\xi \exp\left(-\xi^2 / 2\right) \cdot (\xi - \xi_0)}{\int_{\xi_0}^{\infty} d\xi \exp\left(-\xi^2 / 2\right)} \right] . \tag{7.9}$$

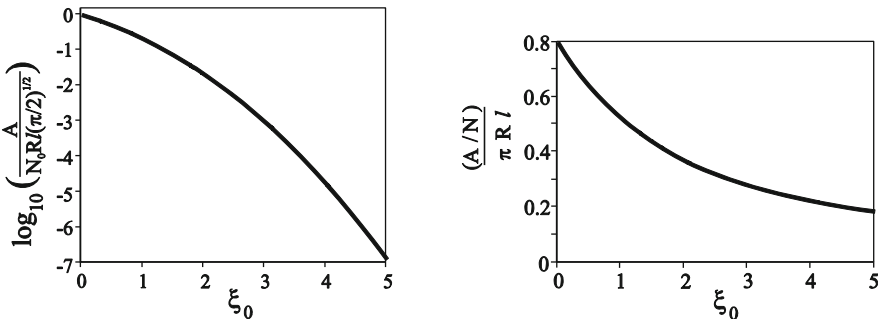

Fig. 7.3 Dependence of the contact area and the average contact area of a single micro-contact on the separation variable ξ_0.

In Fig. 7.3, one can see that the contact area (7.6) changes by 7 orders of magnitude as the relative distance between two surfaces changes from $\xi_0 = 0$ to 5, while the average contact area $\langle \Delta A \rangle$ is less than tripled. The value $\xi_0 = 0$ corresponds

to a very strong compressive force at which the contact surface is about half of the apparent contact surface. The values of $\xi_0 > 4$ are not realistic, because with such contacts only very few contact points can exist at most. The "typical" range of average normal forces which correspond to a real contact area of between 10^{-2} and 10^{-4} of the apparent contact area is achieved for $\xi_0 = 2.5$ to 3.5. The ratio $\langle \Delta A / \pi R l \rangle$ changes in this range only marginally around the value 0.3. A good approximation for the average area of an asperity is, therefore,

$$\langle \Delta A \rangle \approx R l \,. \tag{7.10}$$

The average value of a microscopic contact area remains practically constant (or changes very slowly) as the force changes by several orders of magnitude.

Similarly, the ratio of the total contact area to the force changes slowly:

$$\frac{A}{F_N} = \frac{\int_{h_0}^{\infty} N_0 \Phi(z) \pi R (z - h_0) dz}{\int_{h_0}^{\infty} N_0 \Phi(z) \frac{4}{3} E^* R^{1/2} (z - h_0)^{3/2} dz} = \left(\frac{R}{l}\right)^{1/2} \frac{3\pi}{4E^*} \frac{\int_{\xi_0}^{\infty} d\xi \exp\left(-\xi^2/2\right) \cdot (\xi - \xi_0)}{\int_{\xi_0}^{\infty} d\xi \exp\left(-\xi^2/2\right) \cdot (\xi - \xi_0)^{3/2}} \,. \tag{7.11}$$

In Fig. 7.4, it can be seen that in the domain relevant to macroscopic frictional problems, namely from $\xi_0 = 2.5$ to 3.5, the ratio $\frac{A}{F_N} \Big/ \left(\frac{R}{l}\right)^{1/2} \frac{3\pi}{4E^*}$ changes only marginally around the value 1.4.

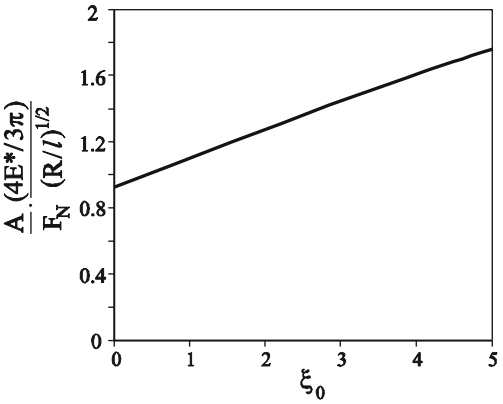

Fig. 7.4 Dependence of the ratio of contact area and compressive force on the separation variable ξ_0.

A good approximation for the ratio of the real contact area to the compressive force is

$$\frac{A}{F_N} \approx \left(\frac{R}{l}\right)^{1/2} \frac{3.3}{E^*}. \tag{7.12}$$

The contact area is proportional to the normal force by a factor that weakly depends on F_N.

The average pressure is found from the same equation through inversion:

$$\langle \sigma \rangle \approx \frac{F_N}{A} \approx 0.3 \cdot E^* \left(\frac{l}{R}\right)^{1/2}. \tag{7.13}$$

In modern literature over contact mechanics, one can often find another form of the ratio F_N / A for rough surfaces. One can qualitatively "deduce" this form as follows. The ratio F_N / A can be estimated as the average of the individual microcontacts $\langle \Delta F / \Delta A \rangle$ (with a coefficient of order unity) and this, in turn, as $\sqrt{\langle (\Delta F / \Delta A)^2 \rangle}$ (again with a coefficient of order unity). Because the ratio F_N / A is only weakly dependent on the compressive force (i.e. the convergence of the surfaces), we can estimate: $\frac{F_N}{A} \sim \sqrt{\langle (\Delta F / \Delta A)^2 \rangle} \sim \sqrt{\left\langle \left(\frac{4E^*}{3\pi}\right)^2 \frac{z}{R} \right\rangle}$ at $h_0 = 0$. The radius of curvature for an asperity is calculated using $1/R = -z''$. Therefore, for the ratio F_N / A, we get

$$\frac{F_N}{A} \sim \frac{4E^*}{3\pi} \sqrt{\langle -z \cdot z'' \rangle} = \frac{4E^*}{3\pi} \sqrt{\langle z'^2 \rangle}. \tag{7.14}$$

For the last equation, we have taken into account that the average $\langle -z \cdot z'' \rangle$ is defined as the integral $-\frac{1}{L}\int_0^L z(x) \cdot z''(x) dx$ over a sufficiently large distance L. Partial integration yields $\frac{1}{L}\int_0^L z'(x) \cdot z'(x) dx$ and, thus, $\langle z'^2 \rangle$.

This is obviously a very rough estimate. The result (7.14), however, has been verified through precise numerical calculations. One can summarize Equation (7.14) by using the symbol $\nabla z = \sqrt{\langle z'^2 \rangle}$ for the root mean square of the gradient of the surface profile:

$$\frac{F_N}{A} = \kappa^{-1} E^* \nabla z, \tag{7.15}$$

where κ is a coefficient that depends only slightly on the statistical properties of the surface and, as a rule, has an order of magnitude of 2. This equation was proven for various rough, and even fractal, surfaces through exact numerical solutions[2].

According to this, the average pressure in the real contact area is approximated rather well by multiplying half of the effective modulus E^* with the average gradient of the surface profile ∇z:

$$\langle \sigma \rangle = \frac{F_N}{A} \approx \frac{1}{2} E^* \nabla z \,. \tag{7.16}$$

One can arrive at a similar conclusion through the following simple qualitative estimation: if we consider a body with the surface profile $z = \hat{h} \cdot \cos kx \cdot \cos ky$, then the maximum of the surface has a radius of curvature of $1/R = \hat{h}k^2$, the root mean square of z is equal to $l = \hat{h}/2$, and the root mean square of the height gradient is $\nabla z = \hat{h}k/\sqrt{2}$. Consequently,

$$\left(\frac{l}{R} \right)^{1/2} = \nabla z \,. \tag{7.17}$$

Insertion into (7.13) again leads to an equation of the form in (7.16).

Lastly, we estimate the force F_0 at which the real contact area A reaches a value half as large as the apparent contact area A_0:

$$F_0 \approx \frac{A_0}{4} E^* \nabla z \,. \tag{7.18}$$

The average pressure $\hat{\sigma}$ that is necessary for such a state is equal to

$$\hat{\sigma} \approx \frac{1}{4} E^* \nabla z \,. \tag{7.19}$$

7.2 Plastic Deformation of Asperities

If the pressure (7.16) is larger than the hardness of the material σ_0 and hence,

[2] It is interesting to note that the same equation (7.15) with $\kappa \approx 2$ is also valid for sharp abrasive surfaces (see Problem 7 to this chapter).

$$\Psi = \frac{E^* \nabla z}{\sigma_0} > 2\,, \tag{7.20}$$

then the micro-roughnesses are in a completely plastic state of deformation. The quantity Ψ was introduced by Greenwood and Williamson and is called the *plasticity index*. For $\Psi < 2/3$, the surface behaves *elastically* during contact. The fact of the matter is that whether the system behaves elastically or plastically is independent of the normal force!

As an example, we estimate the characteristic value of the critical gradient for a contact between two steel probes: with $E^* \approx 10^{11}\ Pa$ and $\sigma_0 \approx 10^9\ Pa$, we find that two steel probes in contact deform purely elastically if $\nabla z < 2 \cdot 10^{-2}$. For ground surfaces, the profile gradient is normally larger and almost every area of the real contact is in a plastic state of deformation. Conversely, highly polished surfaces with $\nabla z \ll 2 \cdot 10^{-2}$ deform purely elastically.

The gradient ∇z is generally dependent on the resolution with which the surface is measured – it is *scale dependent!* If the gradient is different on different scales, then the surface plastically deforms only on the scales at which the condition $\nabla z > 2\sigma_0 / E^*$ is met.

As soon as the stress in the contact area becomes larger than the critical value, the theory is no longer valid. In a plastic state, we can estimate the size of the contact area by noting that the material deforms until the compressive stress reaches the hardness of the material. For the purpose of estimation, we assume that the material has elastic-perfectly plastic characteristics with the indentation hardness σ_0 and that the pressure in every asperity is approximately equal to the hardness.

According to this, the contact area is proportional to the normal force in the plastic region as well:

$$A \approx F_N / \sigma_0\,. \tag{7.21}$$

As a numerical example, we consider a ground steel cube, with an edge-length of 10 cm, lying on a steel plate. For the parameters $\sigma_0 \approx 10^9$ Pa and $F_N \approx 10^2$ N, we obtain $A = 10^2 / 10^9\ \mathrm{m}^2 = 0.1\ \mathrm{mm}^2$ and $A / A_0 = 10^{-5}$. For a typical diameter of a contact, 10 μm, the number of contacts is $N \approx 10^{-7} / \left(10^{-5}\right)^2 \approx 1000$.

7.3 Electrical Contacts

Until now, we have been interested in the *area* of the real contact between two rough surfaces. There are, however, other types of contact problems for which the

total *length* of a contact is more important rather than the area. Electric and thermal contacts belong to these.

In an electrical contact, an electric current is carried from one conducting body to another which is in very close contact - as a rule, “atomically close” contact. At first glance, it would seem that the quality of a contact depends very strongly on the topography of the bodies in contact and, moreover, exhibits strong fluctuations. In this section, we discuss why an electrical contact actually functions quite reliably in most cases and how one calculates the necessary contact force for producing a desired contact.

A passive conducting element can be characterized by its electrical resistance R. The quantity $\Lambda = 1/R$ is called the electrical conductivity. The electrical resistance of a rod with the cross-sectional area A and the length L is calculated as $R = \rho L / A$, where ρ is the specific resistance of the material. In electrical engineering, it is known that in a series, the resistances are additive, and in parallel, the conductivities.

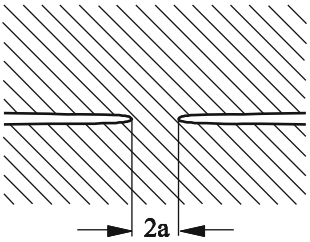

Fig. 7.5 Contact between two conductive half-spaces.

If two extensive bodies with a specific resistance ρ are in ideal contact at a constriction spot of radius a (Fig. 7.5), then the resistance is predominately determined by the size of the contact area. This quantity is called constriction resistance R_C and is calculated using[3]:

$$\frac{1}{R_C} = \Lambda = \frac{2a}{\rho}. \tag{7.22}$$

If there are many micro-contacts that are separated by a distance much greater than their diameters $2a_i$, then the conductivity of all of contact areas are summed. So, the total conductivity is calculated from the sum of the contact diameters of all of the micro-contacts:

$$\Lambda_{tot} = \frac{\sum 2a_i}{\rho} = \frac{L}{\rho}. \tag{7.23}$$

[3] This result was already derived by J.C. Maxwell. J.C. Maxwell, A Treatise on Electricity and Magnetism. Oxford Press, 1891.

The sum of the diameters we denote as L:

$$L := \sum 2a_i \,. \tag{7.24}$$

For the sake of brevity, we call this quantity the *contact length*. In order to calculate the contact length, we use the explanations at the beginning of this chapter and again consider the system shown in Fig. 7.2. The contact radius of a microcontact is calculated as

$$a = \sqrt{\frac{\Delta A}{\pi}} = \sqrt{R\left(z - h_0\right)} \,. \tag{7.25}$$

Similarly to the contact area (7.6), we can calculate the contact length:

$$L = \sum 2a_i = \int_{h_0}^{\infty} 2N_0 \Phi(z) \sqrt{R(z - h_0)} dz \,. \tag{7.26}$$

The ratio of the contact length to the normal force is equal to

$$\frac{L}{F_N} = \frac{3}{2E^*} \frac{\int_{h_0}^{\infty} \Phi(z)(z - h_0)^{1/2} dz}{\int_{h_0}^{\infty} \Phi(z)(z - h_0)^{3/2} dz} = \frac{3}{2E^* l} \left[\frac{\int_{\xi_0}^{\infty} d\xi \exp\left(-\xi^2 / 2\right) \cdot (\xi - \xi_0)^{1/2}}{\int_{\xi_0}^{\infty} d\xi \exp\left(-\xi^2 / 2\right) \cdot (\xi - \xi_0)^{3/2}} \right]. \tag{7.27}$$

The value $\frac{L}{F_N} \cdot \frac{2E^* l}{3}$ is shown in Fig. 7.6 as a function of the variable ξ_0.

In the relevant domain of "typical contact conditions," $\xi_0 = 2.5$ to 3.5, this relationship varies only slightly around the value 2.5.

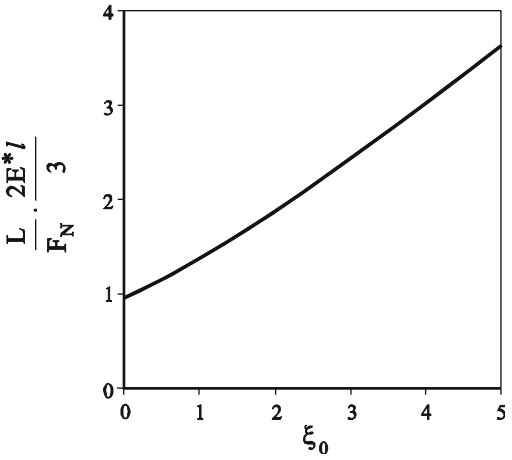

Fig. 7.6 Dependence of the quotient of the contact length and the normal force on the separation variable ξ_0.

Therefore, a good approximation for the contact length is

$$\frac{L}{F_N} \approx \frac{3.7}{E^* l}. \tag{7.28}$$

The contact length is proportional to the normal force by a weak logarithmic factor.

According to (7.23), the electrical conductivity is

$$\Lambda_{tot} \approx \frac{3.7}{E^* \rho l} F_N. \tag{7.29}$$

As with frictional force, conductivity is proportional to the normal force and is independent of the (apparent) contact area. Neither the radius of curvature of the summits nor the profile gradient of the surface appears in this equation. Therefore, the conductivity is only dependent on the height distribution of the rough surface, not on the detailed surface topography.

Until now, we have assumed that individual contacts are small and far enough away from each other so that they can be considered independent of each other. As soon as the contact length L reaches the diameter D of the bodies in contact, the conductivity no longer increases. It reaches its saturation value when the contact length reaches the same order of magnitude as the linear dimension of the bodies:

$$L \approx \frac{3.7}{E^* l} F_N \approx D. \tag{7.30}$$

The necessary force for this is equal to

$$F_{N,c} \approx \frac{DE^* l}{3.7} . \tag{7.31}$$

One can compare this to the force in (7.18), which "squeezes" the surface roughnesses to half of the roughness height: $F_0 \approx \frac{D^2}{4} E^* \nabla z$. Their ratio is

$$\frac{F_{N,c}}{F_0} \approx \frac{4E^* l}{3.7DE^* \nabla z} \approx \frac{l}{D\nabla z} . \tag{7.32}$$

For conductors with linear dimensions, $D > l/\nabla z$, an ideal electrical contact is reached more quickly than an ideal "material contact." This is the case for most contacts with dimensions larger than $0.1\,\text{mm}$.

7.4 Thermal Contacts

The thermal conductivity of a round contact and its mechanical stiffness are also proportional to the radius of the contact. The theory of electrical contacts outlined above can be directly transferred to both of these quantities.

The thermal resistance is the most important characteristic for the sizing of heat sinks for semiconductors or other elements in electrical circuits. It is defined as $R_T = \Delta T / \dot{Q}$, where ΔT is the temperature difference between the ends of the element and $\dot{Q}$ is the amount of heat flowing through the element per second. The thermal conductivity is defined as $\Lambda_T = 1/R_T$. The thermal resistance of a rod of length L and cross-sectional area A is equal to $R_T = L/A\lambda$, where λ is the specific thermal conductivity. It is directly analogous to electrical contacts, meaning only the specific resistance ρ must be replaced with $1/\lambda$. Similarly to (7.29), we can immediately write

$$\Lambda_T \approx \frac{3.7\lambda}{E^* l} F_N . \tag{7.33}$$

The thermal conductivity of a rough contact is directly proportional to the compressive force.

7.5 Mechanical Stiffness of Contacts

If a round contact exists between an elastic and a rigid body with the radius a, then the stiffness for movements perpendicular to the surface is $c_\perp = 2aE^*$ and for movements parallel to the surface, $c_\parallel = \dfrac{8Ga}{2-\nu}$, where G is the shear modulus (see next chapter). Both stiffnesses are proportional to the contact diameter. For several independent contact areas, the stiffnesses are additive:

$$c_{\perp,\,\mathrm{tot}} = E^* \sum 2a_i = E^* L\,, \tag{7.34}$$

$$c_{\parallel,\,\mathrm{tot}} = \frac{4G}{2-\nu} \sum 2a_i = \frac{4GL}{2-\nu}\,. \tag{7.35}$$

Using (7.28) we obtain for normal and transverse stiffnesses of a round contact

$$c_{\perp,\,\mathrm{tot}} = 3.7 \frac{F_N}{l}\,, \tag{7.36}$$

$$c_{\parallel,\,\mathrm{tot}} = \frac{2(1-\nu)}{(2-\nu)} \frac{3.7}{l} F_N \approx 3 \frac{F_N}{l}\,. \tag{7.37}$$

7.6 Seals

In engineering, a seal is an element or structure that has the task of minimizing or preventing unintentional mass transfer from one space into another. The largest group of seals is represented by contact seals, with which the sealing elements are pressed together (Fig. 7.7).

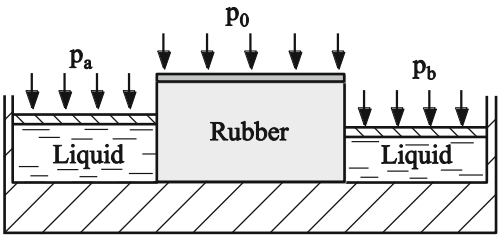

Fig. 7.7 Schematic presentation of how a seal works.

Due to the ever present roughness of the contacting surfaces, they must always be pressed together with a certain minimal pressure so that the contact "seals." This is

illustrated in Fig. 7.8. For small compressive forces, the surfaces are only in real contact over small areas. Liquids or gases can leak around these areas.

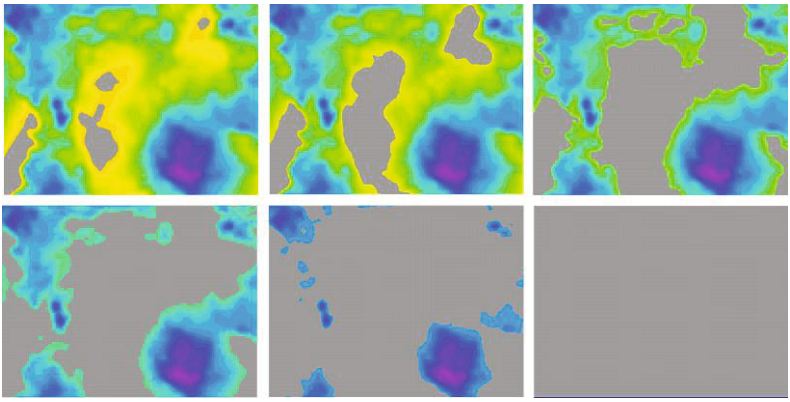

Fig. 7.8 Contact area at various compressive forces. The contact is sealed if the contact areas form a continuous cluster.

By increasing the compressive force, the contacts areas become larger until, at a certain critical force, they form a continuous cluster. Thus, every possible path through the entire contact area is interrupted.

As a rule, this *percolation limit* is reached when the surface roughnesses are approximately half "squeezed." Therefore, a stress on the order of magnitude of (7.19) is necessary:

$$\sigma_{sealed} \approx \frac{1}{4} E^* \nabla z \,. \tag{7.38}$$

It should be noted that ∇z, and therefore the stress, is scale dependent. That means that a contact whose roughness is measured with low resolution can seem sealed, while by closer examination (with higher resolution), leakage paths can still exist. A more exact analysis of this situation leads to the realization that the speed of the leakage of a material through a seal does not vanish after reaching the "macroscopic" critical compressive force (7.38), rather it decreases exponentially with the compressive force (roughly a few orders of magnitude for the increase of one order of magnitude of the compressive force).

7.7 Roughness and Adhesion

Roughness can drastically lower adhesion. In the previous chapter, we introduced the "negative critical penetration depth" $d_{crit} = -\left(\frac{3\pi^2\gamma^2 R}{16E^{*2}}\right)^{1/3}$. It is intuitively

clear that the adhesive behavior of rough surfaces is described by the relationship $|d_{crit}|/l$. If $|d_{crit}| \gg l$:

$$\left(\frac{3\pi^2\gamma^2 R}{16E^{*2}}\right)^{1/3} \gg l, \tag{7.39}$$

then the roughness no longer plays a role. By taking the approximation (7.17) into account, one can also present this equation in the form

$$\frac{3^{1/2}\pi\gamma}{4E^*} \gg l\cdot\nabla z. \tag{7.40}$$

In the opposite case, the adhesive force practically vanishes completely. Numerical simulations show that there is a critical value of the product $l\cdot\nabla z$ at which the macroscopic adhesive force approaches zero:

$$\left[l\cdot\nabla z\right]_{crit} = \Upsilon\frac{\gamma}{E^*}, \tag{7.41}$$

where Υ is a constant on the order of magnitude of 1.

Problems

Problem 1: Determine the compressive force that is needed to create an electrical contact with an electrical resistance of $R = 0.1\ m\Omega$ between two flat copper plates with the roughness $l = 1\ \mu m$.

Solution: The modulus of elasticity of copper is around $E \approx 10^{11}\ Pa$, Poisson's ratio $\nu \approx 0{,}33$, and the specific resistance $\rho \approx 1.8\cdot 10^{-8}\ \Omega\cdot m$. The effective elastic modulus E^* is calculated as

$E^* = \frac{E}{2\left(1-\nu^2\right)} \approx \frac{10^{11}}{2\left(1-0.1\right)}$ Pa $\approx 0.56\cdot 10^{11}\ Pa$. From equation (7.29), which we can rewrite in the form $\frac{1}{R} = \frac{3.7}{E^*\rho l}F_N$, it follows that

$$F_N = \frac{E^*\rho l}{3.7R} \approx \frac{0.56\cdot 10^{11}\,Pa\cdot 1.8\cdot 10^{-8}\,\Omega\cdot m\cdot 10^{-6}\,m}{3.7\cdot 0.1\cdot 10^{-3}\,\Omega} \approx 2.7\ N.$$

Problem 2: Determine the compressive force that is necessary to create an ideal contact between an elastic body with a corrugated surface of the form $z = \hat{h}\cos(kx)$ and a rigid plane.

Solution: If the surfaces were stuck together without any external stress, then the normal stress on the surface would be equal to

$$\sigma_{zz} = \tfrac{1}{2} E^* \hat{h} k \cos kx$$

(see Problem 1 in Chapter 3). The application of a homogeneous normal stress $-\sigma_0$ leads to the following normal stress in the interface due to linearity:

$$\sigma_{zz} = \tfrac{1}{2} E^* \hat{h} k \cos kx - \sigma_0 .$$

It can also be realized by pure compression without glue if everywhere $\sigma_{zz} < 0$, meaning

$$\sigma_0 > \tfrac{1}{2} E^* \hat{h} k .$$

We note that in this case, $\nabla z = \hat{h} k / \sqrt{2}$. So, one can also write this equation in the form $\sigma_0 > \frac{1}{\sqrt{2}} E^* \nabla z$ (compare this stress to the stress in (7.38), which is necessary to create a sealed contact).

Problem 3: Determine the compression force that is necessary to create an ideal contact between an elastic body with a corrugated surface of the form $z = \hat{h}\cos(kx)\cos(ky)$ (Fig. 7.9) and a rigid plane.

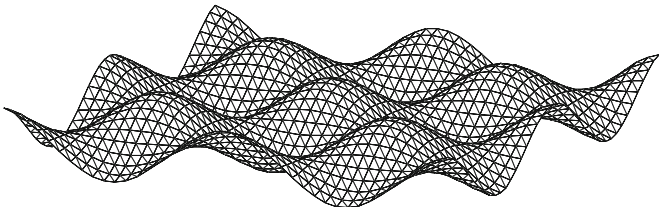

Fig. 7.9 Two-dimensional corrugated surface of an elastic body.

Solution: In Problem 1 in Chapter 3, we found that a surface displacement of $u_z = \hat{h}\cos kx$ led to a normal stress distribution of $\sigma_{zz} = \tfrac{1}{2} E^* \hat{h} k \cos kx$. This conclusion can also be presented in a coordinate-independent form: A cosine-shaped surface deformation $u_z(\vec{r})$ (where $\vec{r}$ is a two-dimensional vector) leads to a stress distribution of $\sigma_{zz} = \tfrac{1}{2} E^* \left|\vec{k}\right| u_z(\vec{r})$. The wave form given in the problem statement can be presented as the sum of two cosine functions:

$$z = \hat{h}\cos(kx)\cos(ky) = \tfrac{1}{2}\hat{h}\left(\cos k(x+y) + \cos k(x-y)\right).$$

This deformation causes the normal stress

$$\sigma_{zz} = \tfrac{\sqrt{2}}{2} E^* k u_z(\vec{r}) = \tfrac{\sqrt{2}}{2} E^* k\hat{h}\cos(kx)\cos(ky).$$

Therefore, the stress necessary in order to create a complete contact is equal to

$$\hat{\sigma} = \tfrac{1}{\sqrt{2}} E^* \hat{h}k .$$

The root mean square of the gradient is equal to $\nabla z = \hat{h}k/\sqrt{2}$. Thus, $\hat{\sigma} = E^* \nabla z$.

Problem 4: Determine the compressive force that is necessary to create an ideal contact between a rigid plane and an elastic body with a corrugated surface of the form $z = \hat{h}\cos(kx) + \hat{h}_1 \cos(k_1 x)$, with $k_1 \gg k$ and $\hat{h}_1 \ll \hat{h}$ (Fig. 7.10).

Fig. 7.10 A surface with corrugations on two scales.

Solution: The corrugations of the short wavelength are completely "squeezed" if the pressure in the deepest areas of the larger corrugations is $\sigma_{0,1} > \tfrac{1}{2} E^* \hat{h}_1 k_1$ (see previous problem). By using the expression for pressure from Problem 2, we obtain the critical pressure through superposition:

$$\sigma_c = \tfrac{1}{2} E^* \left(\hat{h}k + \hat{h}_1 k_1\right).$$

Problem 5: The system sketched in Fig. 7.11 is composed of springs (total number N_0) with the stiffness c, which can adhere if brought into contact. Their adhesive properties are characterized by the length Δd_{crit}, by which a spring can expand before it separates from the surface. Let the height distribution of the springs be $\Phi(z) = \dfrac{1}{l} e^{-\frac{z}{l}}$.

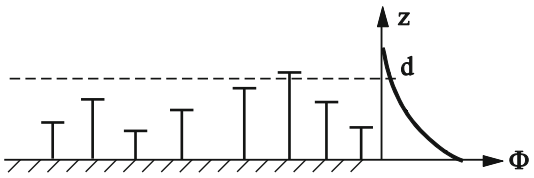

Fig. 7.11 Spring model of a stochastic elastic surface.

A rigid plane is initially pressed onto the system with a force F_N and then pulled away to a distance of d. Determine the adhesive force as a function of the initial compressive force.

Solution: For compression with the force F_N, only those springs with a height of $z > \tilde{d}$ come in contact with the plane, where $\tilde{d}$ is found in the following equation:

$$F_N = \int_{\tilde{d}}^{\infty} \frac{N_0}{l} e^{-\frac{z}{l}} c\left(z - \tilde{d}\right) dz = N_0 c e^{\frac{-\tilde{d}}{l}} l .$$

Now, if the rigid plane is brought to the height d, then all of the springs with heights in the non-deformed state larger than $d - \Delta d_{crit}$ and larger than $\tilde{d}$ will remain in contact. The force acting on the plane is equal to

$$F = \begin{cases} \int_{\tilde{d}}^{\infty} \frac{N_0}{l} e^{-\frac{z}{l}} c\left(z - d\right) dz = N_0 c e^{\frac{-\tilde{d}}{l}} (l + \tilde{d} - d), & \text{for} \quad d - \Delta d_{crit} < \tilde{d} \\ \int_{d - \Delta d_{crit}}^{\infty} \frac{N_0}{l} e^{-\frac{z}{l}} c\left(z - d\right) dz = N_0 c e^{\frac{\Delta d_{crit} - d}{l}} \left(l - \Delta d_{crit}\right), & \text{for} \quad d - \Delta d_{crit} > \tilde{d} \end{cases} .$$

For $l > \Delta d_{crit}$, the force acting on the plane is *always positive*, meaning that there is no *macroscopic adhesion*. For $l < \Delta d_{crit}$, the absolute value of the negative force reaches its maximum value for $d = \tilde{d} + \Delta d_{crit}$. This value is the adhesive force:

$$\left|F_A\right| = N_0 c e^{\frac{-\tilde{d}}{l}} \left(\Delta d_{crit} - l\right).$$

In this model, the ratio of adhesive force to compressive force,

$$\frac{\left|F_A\right|}{F_N} = \frac{\Delta d_{crit} - l}{l},$$

is not dependent on the compressive force and is called the *adhesion coefficient*. For $l = \Delta d_{crit}$, the adhesive force becomes zero.

Problem 6: Determine the normal force similarly to Problem 5, but using the height distribution

$$\Phi(z) = \left(\frac{1}{2\pi l^2}\right)^{1/2} e^{-\frac{z^2}{2l^2}} .$$

Solution: The force is calculated as

$$F_N = \int_{d-\Delta d_{crit}}^{\infty} N_0 \left(\frac{1}{2\pi l^2}\right)^{1/2} e^{-\frac{z^2}{2l^2}} c(z-d)\,dz\,.$$

The results from numerical integration are shown in Fig. 7.12 as plots of $F_N(d)$. For $\Delta d_{crit} < 0.3l$, there is no distance at which F_N takes a negative value (no macroscopic adhesion).

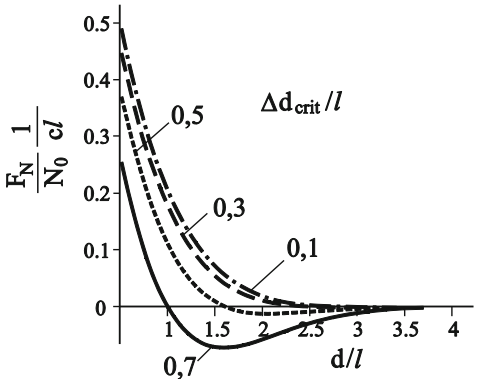

Fig. 7.12 Dependence of normal force on the normalized distance parameterized by $\frac{\Delta d_{crit}}{l}$.

Problem 7: Estimate the average pressure in the real contact area between an elastic half-space and a rough surface composed of cone-shaped asperities with the same inclination angle θ (Fig. 7.13).

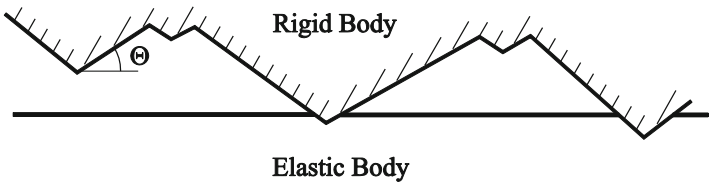

Fig. 7.13 Contact between a rough surface composed of cone-shaped asperities and an elastic body.

Solution: It follows from Equations (5.37) and (5.39) that a relationship exists between the normal force F_N and the contact radius a for the indentation of *one* rigid cone into an elastic half-space:

$$F_N = \frac{1}{2} E^* \pi a^2 \tan\theta\,.$$

The average pressure in *one* micro-contact is, therefore,

$$\langle \sigma \rangle = \frac{F_N}{\pi a^2} = \frac{1}{2} E^* \tan\theta = \frac{1}{2} E^* \nabla z \,,$$

where $\nabla z = \tan\theta$ is the gradient of the surface profile (in this case constant). This pressure is independent of the penetration depth and, therefore, is valid for the average pressure in the entirety of the contact area. Thus, we come to the same result, Equation (7.16), for both "abrasive" surfaces with sharp asperities as well as the contact between two stochastically rough surfaces.

8 Tangential Contact Problems

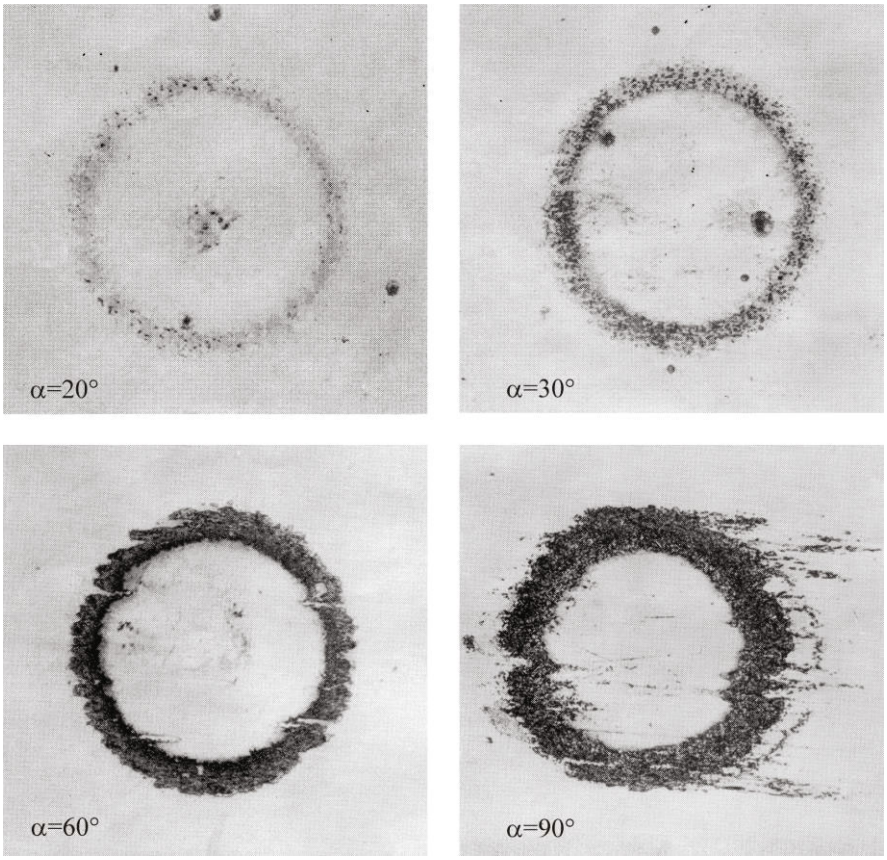

In the contact problems up to now, we have assumed that the contacting bodies have absolutely smooth, frictionless surfaces. According to this, there exist no shear forces in the contact area. If the contact point is also loaded in the tangential direction, then static and kinetic frictional forces become of interest. In this chapter, we investigate shear stresses in tangentially loaded contacts.

It is worth mentioning that, in general, shear stress is generated even in *normal contact* if we take friction into account. If two bodies with different elastic properties are brought into contact, then there exists in the contact a relative displacement in the tangential direction due to the transverse expansion of both bodies. Consequently, the frictional stresses come into play. The shear stresses play no role only in normal contact problems in which the two bodies have the *same elastic properties,* because both bodies deform in the same way in the lateral direction. Under these conditions, shear stresses do not emerge even if one takes static friction into account.

V.L. Popov, *Contact Mechanics and Friction*,
DOI 10.1007/978-3-662-53081-8_8

In this chapter, we will initially consider a tangential contact problem for a case in which complete sticking exists in the contact area and then we will expand our considerations to include contacts in which partial or complete sliding takes place.

8.1 Deformation of an Elastic Half-Space being Acted upon by Tangential Forces

The contact under investigation is shown schematically in Fig. 8.1: Two elastic solid bodies are pressed together and subsequently moved in the tangential direction. In the first step, we assume that in tangential loading, there exists no sliding in the contact. This means either that the bodies are "glued together" or the coefficient of friction tends to infinity.

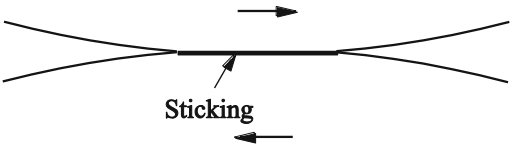

Fig. 8.1 Tangential contact between two elastic solid bodies.

As with normal contact problems, we will work with the *half-space approximation*: The gradient of the surface of the contacting bodies should be small in the vicinity relevant to the contact problem.

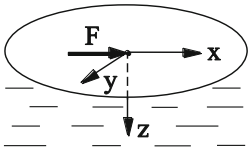

Fig. 8.2 Tangential unit force on the surface of a half-space.

As a preparatory step, we consider the deformation of an elastic half-space being acted upon by a concentrated force at a point on the surface, which we will choose as the origin. The force has only one component in the x-direction. The displacements of the surface $z = 0$ are given by the following equations[1]:

[1] L.D. Landau, E.M. Lifschitz, Theory of elasticity (Theoretical Physics, Vol7), 3rd edition, 1999, Butterworth-Heinemann, Oxford, §§ 8,9.

$$u_x = F_x \frac{1}{4\pi G}\left\{2(1-\nu)+\frac{2\nu x^2}{r^2}\right\}\frac{1}{r} \quad ,$$

$$u_y = F_x \frac{1}{4\pi G}\cdot\frac{2\nu}{r^3}xy \quad , \tag{8.1}$$

$$u_z = F_x \frac{1}{4\pi G}\cdot\frac{(1-2\nu)}{r^2}x \quad ,$$

where G is the shear modulus.

8.2 Deformation of an Elastic Half-Space being Acted upon by a Tangential Stress Distribution

1. Now, we consider the displacement of the surface being acted upon by the following tangential force distribution (in the x-direction):

$$\sigma_{zx}(x,y) = \tau(x,y) = \tau_0\left(1-r^2/a^2\right)^{-1/2}, \tag{8.2}$$

with $r^2 = x^2 + y^2 \le a^2$. The tangential displacement in the x-direction is calculated as

$$u_x = \frac{1}{4\pi G}\cdot 2\iint_A\left\{\frac{1-\nu}{s}+\nu\frac{(x-x')^2}{s^3}\right\}\tau(x',y')dx'dy', \tag{8.3}$$

with

$$s^2 = (x-x')^2 + (y-y')^2. \tag{8.4}$$

By integrating, we obtain the following displacement inside of the loaded area[2] $(r \le a)$:

$$u_x = \frac{\pi(2-\nu)}{4G}\tau_0 a = const. \tag{8.5}$$

Simple considerations of symmetry lead to the conclusion that

$$u_y = 0. \tag{8.6}$$

In contrast, u_z is non-zero and is an odd function of the coordinate x. For a concentrated force, it is calculated directly using (8.1). However, this property is also

[2] Details can be found in K.L. Johnson, Contact mechanics. Cambridge University Press, Ninth printing 2003.

valid for every symmetric stress distribution. The total force acting on the contact area is calculated as

$$F_x = \int_0^a \tau(r) 2\pi r dr = 2\pi\tau_0 a^2 . \tag{8.7}$$

2. Similarly, it can be shown that the stress distribution

$$\tau(x,y) = \tau_0 \left(1 - r^2 / a^2\right)^{1/2} \tag{8.8}$$

leads to a displacement of the surface points inside of the loaded area $(r \le a)$ of

$$u_x = \frac{\tau_0 \pi}{32Ga}\left[4(2-\nu)a^2 - (4-3\nu)x^2 - (4-\nu)y^2\right]. \tag{8.9}$$

The total force, thereby, is

$$F_x = \tfrac{2}{3}\pi\tau_0 a^2 . \tag{8.10}$$

3. If an elastic body is acted on by a shear stress of

$$\tau(x,y) = \tau_0 \left(1 - x^2 / a^2\right)^{1/2} \tag{8.11}$$

in the x-direction within a strip with a width of $2a$ (Fig. 8.3), then the displacement of the surface points is given by

$$u_x = const - \tau_0 \frac{x^2}{aE^*} . \tag{8.12}$$

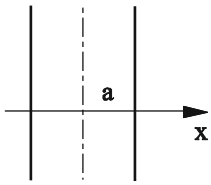

Fig. 8.3 Strip of width $2a$, which is loaded by the shear stress distribution in Equation (8.11).

4. A special case of tangential loading is presented by *torsion*. If the tangential forces in a round contact area with radius a are directed perpendicular to the respective polar radius r and the corresponding stresses are given by

$$\sigma_{zx} = -\tau(r)\sin\varphi , \quad \sigma_{zy} = \tau(r)\cos\varphi \tag{8.13}$$

with

$$\tau(r) = \tau_0 \frac{r}{a}\left(1 - \left(\frac{r}{a}\right)^2\right)^{-1/2} , \tag{8.14}$$

then the polar components of the displacement of the surface are equal to[3]

$$u_\varphi = \frac{\pi\tau_0 r}{4G}, \quad u_r = 0, \quad u_z = 0. \tag{8.15}$$

Therefore, the total contact area rigidly turns by an angle of $\pi\tau_0 / 4G$. Thus, this stress distribution is produced by the torsion of the rigid cylindrical indenter sticking to the surface. The total torsional moment is

$$M_z = \tfrac{4}{3}\pi a^3 \tau_0. \tag{8.16}$$

8.3 Tangential Contact Problems without Slip

Now, we will move on to the discussion of tangential contact problems. We visualize that we have two opposing bodies, and we generate a *constant* displacement of u_x in one of them and $-u_x$ in the other, respectively. The corresponding stress distribution (8.2) must exist on one side and the same distribution, with a negative sign, on the other. If we were to now glue both stress areas together, then they remain in equilibrium due to Newton's third law of motion (*action-reaction*). It is important that the "adhering" surfaces exactly match in the z-direction due to the asymmetry of the displacements in the z-direction with respect to x. These considerations show that the relative movement of $2u_x$ of two bodies with the same elastic properties results in exactly the stress distribution (8.2):

$$\tau(x,y) = \tau_0 \left(1 - r^2 / a^2\right)^{-1/2}. \tag{8.17}$$

It can be noticed that the shear stress in the boundary of a sticking area approaches infinity, while the normal stress approaches zero. That means that in most cases, the no-slip condition near the boundary is not met and relative sliding occurs. We will discuss this partial movement – slip – in the next section.

We define the *shear stiffness* of a contact between two elastic bodies k_x as the ratio of the tangential force to the relative tangential displacement of the two bodies. From equations (8.5) and (8.7) the tangential stiffness is

$$k_x = \frac{F_x}{2u_x} = \frac{4Ga}{(2-\nu)} = 2G^* a, \tag{8.18}$$

[3] K.L. Johnson, Contact mechanics. Cambridge University Press, Ninth printing 2003.

where we have inserted the effective shear modulus, $G^* = \frac{2G}{(2-\nu)}$. Just as with the normal stiffness, the shear stiffness (8.18) is proportional to the *diameter* of the contact.

Note that the mentioned equations are not *exact* in the application to a contact between an elastic half-space and a rigid body, because in this case, the displacements in the vertical direction vanish, which is not true in the case of the stress distribution in (8.2). However, they present a good approximation. For a contact between two elastic bodies with the elastic constants G_1, G_2, ν_1, and ν_2, the following good approximation is valid for the shear stiffness:

$$k_x = \frac{F_x}{u_{rel}} \approx 2G^* a \tag{8.19}$$

with

$$\frac{1}{G^*} = \frac{2-\nu_1}{4G_1} + \frac{2-\nu_2}{4G_2} . \tag{8.20}$$

In (8.19), u_{rel} is the relative displacement of the two bodies. Equation (8.5), in the case of two bodies with different elastic properties, takes the form

$$u_{rel} \approx \frac{\pi \tau_0 a}{G^*} . \tag{8.21}$$

8.4 Tangential Contact Problems Accounting for Slip

Now, we consider a combined contact problem characterized by tangential and normal forces acting simultaneously. We visualize, for example, that two spheres are pressed together with a normal force F_N and subsequently pulled in the tangential direction with a force F_x. It is assumed that between the two bodies, there exists dry friction according to Coulomb's law of friction in its simplest form: the maximum static friction stress $\tau_{\max}$ is equal to the kinetic friction stress τ_k and this, in turn, is equal to the normal stress p multiplied with a constant coefficient of friction μ:

$$\tau_{\max} = \mu p , \quad \tau_k = \mu p . \tag{8.22}$$

The condition for sticking yields

$$\tau \le \mu p\,. \tag{8.23}$$

If we were to assume that the bodies completely adhere in the contact area, then we would get the following equations for the distributions of normal and tangential stresses:

$$p = p_0\left(1-\left(r/a\right)^2\right)^{1/2}, \quad F_N = \frac{2}{3}p_0\pi a^2, \tag{8.24}$$

$$\tau = \tau_0\left(1-\left(r/a\right)^2\right)^{-1/2}, \quad F_x = 2\pi\tau_0 a^2\,. \tag{8.25}$$

These distributions are shown in Fig. 8.4. Since the normal stress at the boundary of the area approaches zero and the tangential stress tends to infinity, the condition (8.23) is *always invalid* near the boundary of the contact area: at the boundary of the contact area there is always slip, even for small tangential loadings. Inside of the area, however, the condition (8.23) is met for sufficiently small tangential forces. In general, the total contact area is divided into an inner no-slip (sticking) domain and an outer sliding domain (Fig. 8.5). The radius c of the boundary between the two domains is found using the condition $\tau = \mu p$.

The distribution of the shear stress (8.25) in the contact is, needless to say, only valid under the assumption that there exists no sliding in the contact. We can prove with this distribution that the assumption is contradictory and, therefore, sliding at the boundary will always exist, but we cannot calculate the new stress distribution or the radius of the no-slip domain.

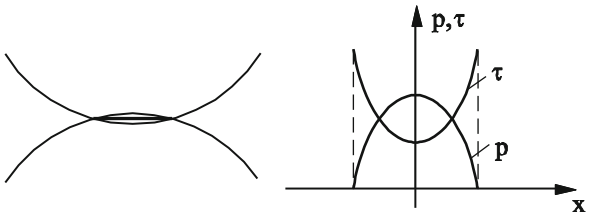

Fig. 8.4 Normal and tangential stresses in a contact.

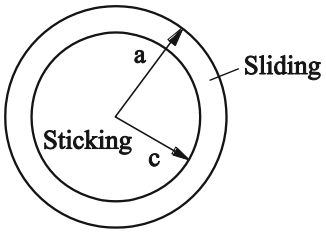

Fig. 8.5 Sticking and sliding domains in a round tangential contact.

However, as in many other "classical contact problems," it is possible to construct a correct stress distribution as the combination of known distributions. In this case, it is possible to fulfill all of the contact boundary conditions through superposition of two "Hertzian" stress distributions (8.8). The stress distributions of the Hertzian type together with the stress distributions of the type in (8.25) prove to be universal "building blocks" of contact mechanics allowing all classical contact mechanical problems to be solved. We look for a tangential stress distribution in the contact of the form

$$\tau = \tau^{(1)} + \tau^{(2)}, \tag{8.26}$$

with

$$\tau^{(1)} = \tau_1 \left(1 - r^2 / a^2\right)^{1/2} \tag{8.27}$$

and

$$\tau^{(2)} = -\tau_2 \left(1 - r^2 / c^2\right)^{1/2}, \tag{8.28}$$

(see Fig. 8.6). The surface displacement caused by this stress, according to (8.9), is equal to

$$\begin{aligned} u_x = {} & \frac{\tau_1 \pi}{32Ga}\left[4(2-\nu)a^2 - (4-3\nu)x^2 - (4-\nu)y^2\right] \\ & - \frac{\tau_2 \pi}{32Gc}\left[4(2-\nu)c^2 - (4-3\nu)x^2 - (4-\nu)y^2\right] . \end{aligned} \tag{8.29}$$

The corresponding pressure distribution is given by the Hertzian equation (8.24).

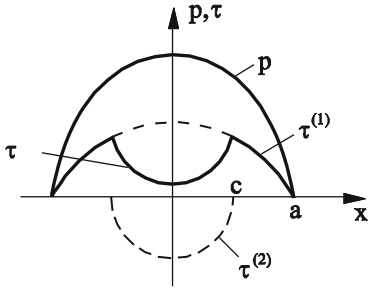

Fig. 8.6 Normal and tangential stress in a tangential contact.

The sticking inside of the circle of radius c means that in this domain, the displacement is *constant*:

$$u_x(r) = const \quad \text{if } r < c . \tag{8.30}$$

The sliding in the remaining domain means that there, Coulomb's law of friction is met:

$$\tau(r) = \mu p(r), \quad \text{if } c < r < a\,. \tag{8.31}$$

The second condition leads to the claim that

$$\tau_1 = \mu p_0\,. \tag{8.32}$$

From the condition (8.30), it follows that

$$\tau_2 = \mu p_0 \frac{c}{a}\,. \tag{8.33}$$

The displacement in the sticking domain is, thereby, equal to

$$u_x = \frac{(2-\nu)\pi\mu p_0}{8Ga}\left(a^2 - c^2\right). \tag{8.34}$$

Before complete sliding starts ($c = 0$), the body can be displaced in the tangential direction by at the most

$$u_x = \frac{(2-\nu)\pi\mu p_0 a}{8G} = \frac{3(2-\nu)\mu F_N}{16Ga}\,. \tag{8.35}$$

The total tangential force in the contact area is calculated using (8.26), (8.27) and (8.28):

$$F_x = \frac{2}{3}\pi\left(\tau_1 a^2 - \tau_2 c^2\right) = \frac{2\pi}{3a}\mu p_0\left(a^3 - c^3\right). \tag{8.36}$$

Taking into account the relationship $F_N = \frac{2}{3} p_0 \pi a^2$, this force can be written in the form

$$F_x = \mu F_N\left(1 - \left(\frac{c}{a}\right)^3\right). \tag{8.37}$$

Therefore, we obtain a radius for the static area of

$$\frac{c}{a} = \left(1 - \frac{F_x}{\mu F_N}\right)^{1/3}. \tag{8.38}$$

The tangential force at which complete sliding is introduced is, as expected, $F_x = \mu F_N$. We must emphasize, however, that the sliding domain already dominates a large portion of the contact area before this force is reached. Upon reaching the force $F_x = \mu F_N$, there is no longer a transition from sticking to sliding, rather a transition from partial sliding to complete sliding.

We have shown that by applying an arbitrarily small tangential force to a Hertzian contact generated by a normal force, we create a ring-shaped sliding do-

main. By periodic loading, only the material in this domain would be worn. This phenomenon is known as *fretting* (see Problem 2 of Chapter 17).

8.5 Absence of Slip for a Rigid Cylindrical Indenter

If a flat, rigid, cylindrical indenter presses into an elastic half-space, then the normal stress distribution is given by $p = p_0\left(1-r^2/a^2\right)^{-1/2}$. Upon subsequently applying a tangential force, a shear stress distribution of $\tau = \tau_0\left(1-r^2/a^2\right)^{-1/2}$ is produced. Therefore, the no-slip condition, $\tau < \mu p$, is either met or not met in the total contact area. In this case, there is no partial slip domain.

8.6 Tangential Contact of Axially Symmetrical Bodies

In Section 5.6 of Chapter 5, a method for the mapping of any axially-symmetric normal contact problems onto a contact with a one-dimensional Winkler foundation was introduced (method of dimensionality reduction, MDR). The basic feature that enables this reduction is the proportionality of the incremental stiffness to the diameter of the contact area. This property is valid for both normal and tangential contact. The idea of dimensionality reduction can, therefore, be transferred directly to tangential contacts. In this chapter, we will restrict ourselves to the case of "elastically similar" materials, for which the condition

$$\frac{1-2\nu_1}{G_1} = \frac{1-2\nu_2}{G_2}\,. \tag{8.39}$$

is satisfied. This condition guarantees the independence of the normal and tangential contact problems[4].

The tangential stiffness of a circular contact with the diameter D between two elastic half-spaces is given by (8.19):

$$k_x = DG^*\,, \tag{8.40}$$

where G^* is defined by (8.20). This stiffness is trivially replicated with a foundation consisting of springs with tangential stiffness

$$\Delta k_x = G^*\Delta x\,, \tag{8.41}$$

where Δx is the distance between the springs. In this section, we will show how tangential contact problems with Coulomb friction between any rotationally sym-

[4] K.L. Johnson, Contact Mechanics, Cambridge University Press, Ninth printing 2003.

metric profiles can be exactly described by means of Winkler foundation with the normal stiffness defined in Chapter 5, Eq. (5.51), and the tangential stiffness (8.41). We describe only the calculation steps. The proof of the correctness of the procedure is given in Appendix D.

We consider an axially symmetric indenter with the profile $z = f(r)$, which is firstly pressed in the elastic half-space with a normal force F_N, and then loaded by a tangential force F_x in the x direction. We assume that in the contact, Coulomb's law of friction is valid in its simplest form: as long as the tangential stress τ is smaller than the friction coefficient μ multiplied with the normal stress p, the surfaces are in a state of sticking. Once slipping starts, the tangential stress remains constant and equals μp:

$$\tau(r) \le \mu p(r), \text{ for stick,} \tag{8.42}$$

$$\tau(r) = \mu p(r), \text{ for slip.} \tag{8.43}$$

If a small tangential force is applied, a ring-shaped slip domain is generated at the edge of the contact, and it expands inwards for increasing force until complete slip is exhibited. We denote the inner radius of the slip domain (or the radius of the stick domain) with c.

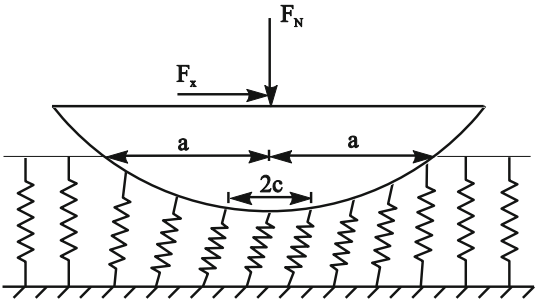

Fig. 8.7 Equivalent model for tangential contact.

The MDR is applied to the tangential contact as follows. In the first step the modified profile is calculated according to transformation (5.52). In the second step, it is pressed with a normal force F_N into the Winkler foundation with stiffnesses defined according to (5.51) and (8.41), and then tangentially displaced by $u_x^{(0)}$ (Fig. 8.7). Each spring sticks to the indenter and is displaced along with it as long as the tangential force $\Delta F_x = k_x u_x^{(0)}$ is smaller than $\mu \Delta F_z$. After the maximum static friction force is reached, the spring begins to slip and the force remains constant and equal to $\mu \Delta F_z$. This rule can also be incrementally formulated so that it can be applied for arbitrary loading histories: for a small displacement of the indenter of $\Delta u_x^{(0)}$, the following relations are valid

$$\begin{aligned} \Delta u_x(x) &= \Delta u_x^{(0)}, \quad \text{if } \left|k_x u_x(x)\right| < \mu \Delta F_z \\ u_x(x) &= \pm \frac{\mu \Delta F_z(x)}{k_x}, \quad \text{in slip state} \end{aligned} \quad . \tag{8.44}$$

The sign of the last equation is dependent on the direction of motion of the indenter. By following the incremental changes in the position of the indenter, we can explicitly determine the displacement of all of the springs in the contact area; with this, all tangential forces

$$\Delta F_x = k_x u_x(x) = G^* \Delta x \cdot u_x(x) \tag{8.45}$$

and the linear force density (distributed load)

$$q_x(x) = \frac{\Delta F_x}{\Delta x} = G^* u_x(x) \tag{8.46}$$

are also calculated. The distribution of tangential stress $\tau(r)$ and the displacement $u_x(r)$ in the original three-dimensional contact are determined by transformations which are very similar to (5.59) and (5.60)[5]:

$$\tau(r) = -\frac{1}{\pi} \int_r^\infty \frac{q_x'(x)\mathrm{d}x}{\sqrt{x^2 - r^2}}, \tag{8.47}$$

$$u_x(r) = \frac{2}{\pi} \int_0^r \frac{u_x(x)\mathrm{d}x}{\sqrt{r^2 - x^2}}. \tag{8.48}$$

Let us illustrate the application of this procedure in the case when the indenter is displaced in one direction from the equilibrium position. Then the radius c of the stick domain is determined from the condition that the tangential force $k_x u_x^{(0)}$ is equal to μ times the normal force $k_z u_z(c)$:

$$G^* u_x^{(0)} = \mu E^* \left(d - g(c)\right). \tag{8.49}$$

The tangential displacement is equal to

$$u_x(x) = \begin{cases} u_x^{(0)}, & \text{for } x < c \\ \mu \left(\dfrac{E^*}{G^*}\right)\left(d - g(x)\right), & \text{for } c < x < a \end{cases}, \tag{8.50}$$

The distributed load is equal to

[5] We stress that all macroscopic quantities obtained with the help of the method described above represent the exact three-dimensional solutions of Cattaneo, Mindlin, Jäger and Ciavarella.

$$q_x(x)=\begin{cases} G^* u_x^{(0)}, & \text{for } x<c \\ \mu E^*\left(d-g(x)\right), & \text{for } c<x<a \end{cases} \tag{8.51}$$

and the resulting tangential force is

$$F_x = 2\int_0^a q_x(x)\,\mathrm{d}x = 2\mu E^*\left[c\left(d-g(c)\right)+\int_c^a \left(d-g(x)\right)\mathrm{d}x\right] = 2\mu E^*\int_c^a xg'(x)\mathrm{d}x\,. \tag{8.52}$$

The normal force is still given by (5.57),

$$F_N = 2E^*\int_0^a \left(d-g(x)\right)\mathrm{d}x\,, \tag{8.53}$$

and the ratio of $F_x/\left(\mu F_N\right)$ is given as

$$\frac{F_x}{\mu F_N} = \frac{\int_c^a xg'(x)\mathrm{d}x}{\int_0^a xg'(x)\mathrm{d}x}\,. \tag{8.54}$$

This equation determines the relation between the ratio $F_x/(\mu F_N)$ and the stick radius (generalization of (8.37) for an arbitrary axially-symmetric indenter).

There is an interesting and very general conclusion from Eq. (8.49). The maximum tangential displacement $u_{x,\max}^{(0)}$, for which the stick area *just disappears* (or the minimum displacement, for which complete sliding occurs) can be obtained if we set $c=0$ into (8.49) (hence $g(c)=0$):

$$u_{x,\max}^{(0)} = \mu\frac{E^*}{G^*}d\,. \tag{8.55}$$

The displacement until complete sliding occurs depends only on the indentation depth (not on the shape of the indenter).

Problems

Problem 1: We consider two elastic bodies which respectively fill the half-spaces $z>0$ and $z<0$ (Fig. 8.8). The upper body moves in the horizontal direction with a velocity of $du_{rel}/dt = v_c$. The bodies form a circular, no-slip domain with a radius of $a(t)=a_0+v_1 t$ which increases with time; in the remaining areas, the tan-

gential stress is equal to zero[6]. Determine the tangential stress distribution in the contact area.

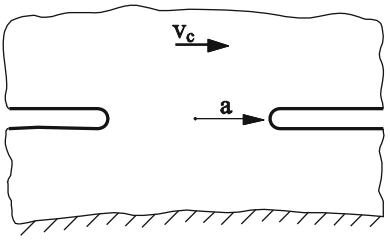

Fig. 8.8 Two elastic bodies in a contact in which the upper body moves with a constant velocity v_c relative to the lower body.

Solution: From the equations $du_{rel}/dt = v_c$ and $da/dt = v_1$, we get

$$du_{rel} = \frac{v_c}{v_1} da \, .$$

The *change* of the shear stress in the contact area, $r < a(t)$, caused by a tangential movement of du_{rel} is, according to (8.17) and (8.5), calculated as

$$d\tau(r) = \frac{G^*}{\pi a} du_{rel} \left(1 - \left(\frac{r}{a}\right)^2\right)^{-1/2} = \frac{G^*}{\pi a} \frac{v_c}{v_1} \left(1 - \left(\frac{r}{a}\right)^2\right)^{-1/2} da \, , \quad \text{for} \quad r < a \, ,$$

where G^* is defined by (8.20). At the point in time at which the contact front expands from the initial radius a_0 to the radius a_1, the stress is calculated as follows:

$$\tau = \frac{G^*}{\pi} \frac{v_c}{v_1} \int_{a_0}^{a_1} \frac{1}{a} \left(1 - \left(\frac{r}{a}\right)^2\right)^{-1/2} da, \qquad \text{for} \quad r < a_0,$$

$$\tau = \frac{G^*}{\pi} \frac{v_c}{v_1} \int_{r}^{a_1} \frac{1}{a} \left(1 - \left(\frac{r}{a}\right)^2\right)^{-1/2} da, \qquad \text{for} \quad a_0 < r < a_1 \, .$$

Calculating the integrals provides

[6] One such situation can exist if two bodies are separated by a sheet of liquid which solidifies. It is typical with solidification that the boundary between the solid and liquid phases spreads at a constant speed.

$$\tau = \frac{G^*}{\pi}\frac{v_c}{v_1}\ln\frac{a_1+\sqrt{a_1^2-r^2}}{a_0+\sqrt{a_0^2-r^2}}, \quad \text{for} \quad r < a_0$$

$$\tau = \frac{G^*}{\pi}\frac{v_c}{v_1}\ln\frac{a_1+\sqrt{a_1^2-r^2}}{r}, \quad \text{for} \quad a_0 < r < a_1 \ .$$

This dependence is shown in Fig. 8.9 for $a_0 / a_1 = 0.1$.

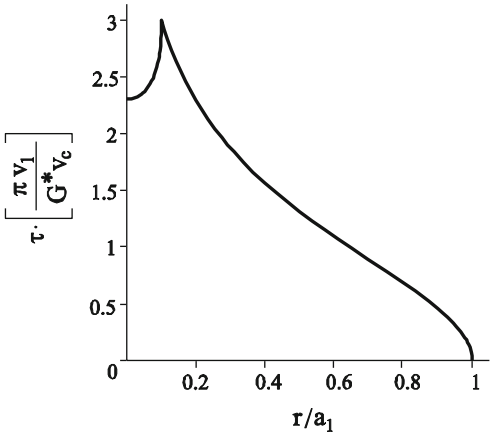

Fig. 8.9 Tangential stress distribution in the contact area.

Problem 2: An elastic sphere is pressed into a rigid plane. The direction of the compression force always remains the same (Fig. 8.10). Determine the circumstances at which no-slip conditions exists for the entire contact area.

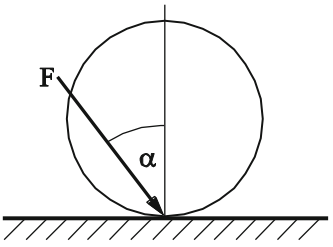

Fig. 8.10 Elastic sphere that is pressed into a rigid plane at an inclined angle.

Solution: We begin with the assumption that no sliding takes place in the contact area and verify afterwards the validity of this assumption. We can separate the continuous increase of the force into infinitesimally small steps, where in every step the normal force is increased by dF_N and the tangential force by dF_x. There is a geometric relationship between the increments dF_N and dF_x, namely, $dF_x / dF_N = \tan\alpha$. An increase in the tangential force of dF_x, considering the no-slip condition, causes an increase in the shear stress of

$$d\tau(r) = \frac{dF_x}{2\pi a^2}\left(1-\frac{r^2}{a^2}\right)^{-1/2} = \frac{dF_N \tan\alpha}{2\pi a^2}\left(1-\frac{r^2}{a^2}\right)^{-1/2}, \quad r < a\,.$$

From the relationship between the normal force and the contact radius, $F_N = \frac{4}{3}\frac{E^* a^3}{R}$, we obtain $dF_N = 4\frac{E^* a^2 da}{R}$. Thus, the shear stress increase can be written in the form

$$d\tau(r) = \frac{2E^*}{\pi R}\tan\alpha\left(1-\frac{r^2}{a^2}\right)^{-1/2} da, \quad r < a\,.$$

If the radius of the contact area increases from a_0 to a_1 due to the applied force, the tangential stress experiences a total increase of

$$\tau(r) = \frac{2E^*}{\pi R}\tan\alpha\int_{a_0}^{a_1}\left(1-\frac{r^2}{a^2}\right)^{-1/2} da, \qquad r < a_0\,,$$

$$\tau(r) = \frac{2E^*}{\pi R}\tan\alpha\int_{r}^{a_1}\left(1-\frac{r^2}{a^2}\right)^{-1/2} da, \qquad a_0 < r < a_1\,.$$

Calculation of the integral yields

$$\tau(r) = \frac{2E^*}{\pi R}\tan\alpha\cdot\left[\left(a_1^2-r^2\right)^{1/2} - \left(a_0^2-r^2\right)^{1/2}\right], \qquad r < a_0\,,$$

$$\tau(r) = \frac{2E^*}{\pi R}\tan\alpha\cdot\left(a_1^2-r^2\right)^{1/2}, \qquad a_0 < r < a_1\,.$$

The Hertzian pressure distribution is calculated as

$$p(r) = \frac{p_0}{a_1}\left(a_1^2-r^2\right)^{1/2} = \frac{3F_N}{2\pi a_1^3}\left(a_1^2-r^2\right)^{1/2} = \frac{2E^*}{\pi R}\left(a_1^2-r^2\right)^{1/2}.$$

No sliding exists if the condition $\tau(r) \le \mu p(r)$ is met over the entire contact area. This is the case when

$$\tan\alpha \le \mu\,.$$

If the angle at which the force acts is smaller than the critical angle, then there is no sliding in the contact. Note that the critical angle is equal to the *friction angle* (see Chapter 10), consequently, these results agree with the macroscopic results in that no sliding takes place at an application angle smaller than the friction angle.

Problem 3: Solve Problem 2 with the Method of Dimensionality Reduction.

Solution: The solution to this problem using MRD is trivial. Since each sticking spring is loaded with the force with the angle α, there is no slip when the angle α is smaller than the friction angle (see (10.5) in Chapter 10):

$$\tan\alpha \le \mu .$$

Problem 4: A rigid, axially-symmetrical profile with the form $z = Ar^n$ is firstly pressed into an elastic half-space with the force F_N and then loaded with the tangential force F_x. Determine the relation between the tangential force, tangential displacement and radius of the stick area c.

Solution: The MDR-transformed profile in this case has the form $g(x) = A\kappa_n |x|^n$ with $\kappa_n = \frac{\sqrt{\pi}}{2}\frac{n\Gamma(\frac{n}{2})}{\Gamma(\frac{n}{2}+\frac{1}{2})}$, where $\Gamma(n) = \int_0^\infty t^{n-1}e^{-t}\mathrm{d}t$ is the Gamma-function (see Chapter 5, Problem 7). Substituting $g(x)$ into (8.54) it gives

$$\frac{F_x}{\mu F_N} = 1 - \left(\frac{c}{a}\right)^{n+1},$$

where a is the contact radius. The relation between tangential displacement of the indenter and the radius of the stick area is obtained by substitution of $g(x)$ into (8.49):

$$G^* u_x^{(0)} = \mu E^* \left(d - A\kappa_n c^n\right).$$

Problem 5: A flat cylindrical indenter with rounded corners (Fig. 8.11) is firstly pressed into an elastic half-space by the normal force F_N and then loaded with a tangential force F_x which causes a tangential relative movement $u_x^{(0)}$ between the two bodies. The contacting materials are assumed to be elastically similar and the profile of the indenter (Fig.8.11) is given by

$$f(r) = \begin{cases} 0 & \text{for} \quad 0 \le r < b \\ \dfrac{1}{2R}(r-b)^2 & \text{for} \quad b \le r \le a \end{cases}.$$

With the MDR, determine the dependence of indentation depth and the normal force on the contact radius. Furthermore, calculate the tangential displacement and the tangential force as a function of the radius of the stick area.

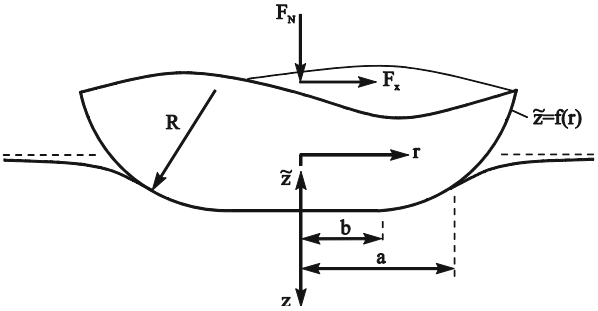

Fig. 8.11 Tangential contact of a flat indenter with rounded corners (radius R).

Solution: Firstly the equivalent one-dimensional profile will be determined according to (5.52):

$$g(x) = x\int_0^x \frac{f'(r)}{\sqrt{x^2 - r^2}}\,\mathrm{d}r = \begin{cases} 0 & \text{for} \quad 0 \le x < b \\ \dfrac{x}{R}\displaystyle\int_b^x \frac{r-b}{\sqrt{x^2-r^2}}\,\mathrm{d}r & \text{for} \quad b \le x \le a \end{cases}.$$

The calculation of the integral provides

$$\int_b^x \frac{r-b}{\sqrt{x^2-r^2}}\,dr = \sqrt{x^2-b^2} - b\arccos\left(\frac{b}{x}\right),$$

so that

$$g(x) = \begin{cases} 0 & \text{for} \quad |x| < b \\ \dfrac{|x|}{R}\sqrt{x^2-b^2} - \dfrac{b|x|}{R}\arccos\left(\dfrac{b}{|x|}\right) & \text{for} \quad b \le |x| \le a \end{cases}.$$

The normalized original and the equivalent profiles are compared in Fig. 8.12.

The indentation depth as a function of the contact radius is derived from the one-dimensional profile by

$$d = g(a) = \frac{a}{R}\sqrt{a^2-b^2} - \frac{ba}{R}\arccos\left(\frac{b}{a}\right)$$

and the dependence of normal force on the contact radius by

$$\begin{aligned} F_N &= 2E^*\int_0^a \left[d - g(x)\right]\mathrm{d}x \\ &= 2E^*\int_0^b d\,\mathrm{d}x + 2E^*\int_b^a \left[d - \left(\frac{x}{R}\sqrt{x^2-b^2} - \frac{bx}{R}\arccos\left(\frac{b}{x}\right)\right)\right]\mathrm{d}x \end{aligned}.$$

Integration and consideration of the relation between the indentation depth and the contact radius result in

$$F_N = \frac{4}{3} E^* \frac{a^3}{R} \left[\left(1 - \frac{1}{4} \left(\frac{b}{a} \right)^2 \right) \sqrt{1 - \left(\frac{b}{a} \right)^2} - \frac{3}{4} \frac{b}{a} \arccos\left(\frac{b}{a} \right) \right] .$$

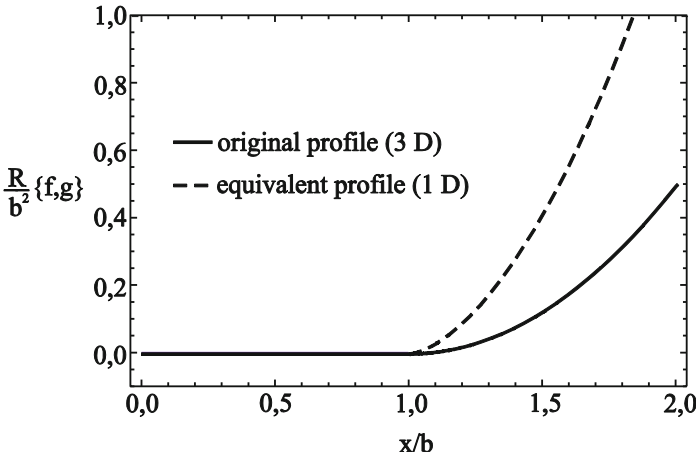

Fig. 8.12 Flat indenter with rounded corners: three-dimensional and one-dimensional MDR-transformed profile.

The limiting case $b = 0$ corresponds to a parabolic profile. As expected, Hertzian relations will be found by substituting it into the equations.

The boundary between stick and slip, is determined from (8.49)

$$u_x^{(0)} = \mu \frac{E^*}{G^*} \frac{a}{R} \left[\sqrt{a^2 - b^2} - b \arccos\left(\frac{b}{a} \right) - \frac{c}{a} \left(\sqrt{c^2 - b^2} - b \arccos\left(\frac{b}{c} \right) \right) \right] .$$

The tangential force is calculated using (8.52) as

$$F_x = \mu \frac{E^*}{3R} \left[\left(4a^2 - b^2 \right) \sqrt{a^2 - b^2} - 3a^2 b \arccos\left(\frac{b}{a} \right) \right] - \mu \frac{E^*}{3R} \left[\left(4c^2 - b^2 \right) \sqrt{c^2 - b^2} - 3c^2 b \arccos\left(\frac{b}{c} \right) \right] .$$

Fig. 13.8 shows the dependence of the sticking radius on the tangential force for different values of the geometrical factor b/a in normalized form. The limiting case $b = 0$ provides the classic result of Cattaneo and Mindlin for a parabolic indenter. If the rounded area is very small ($b = 0.95a$), then the curve approaches that of a flat indenter.

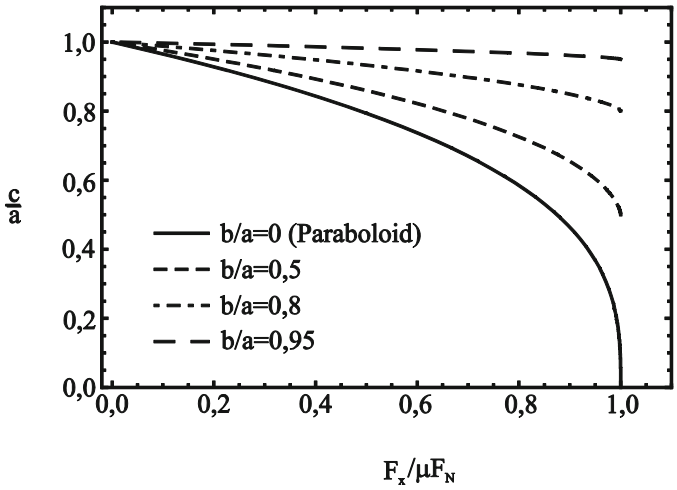

Fig. 8.13 Contact radius of the sticking area c as a function of the applied tangential force for a flat indenter with rounded corners.

9 Rolling Contact

Rolling contacts are found in innumerable technical applications. Wheel-rail or tire-street contacts, roll bearings, gears, and diverse feeding or transportation mechanisms (e.g. in a printer) are the most known examples.

Reynolds investigated rolling contact mechanics early on[1]. He established through experimental investigations that in rolling contact both sliding and sticking domains exist in the contact area. For increasing driving or braking moments, the sliding domain expands until finally the entire contact area is sliding. This sliding leads to the translational speed of the wheel no longer being equal to the circumferential speed ΩR. The difference in the two speeds is called the *creep speed* and plays an important role in contact mechanics.

Sliding in the contact area, however, is not the only cause for the difference between the translational and circumferential speeds. For small driving or braking moments there is almost no sliding in the contact area. The difference between the translational and rotational speeds exists, nevertheless, and is proportional to the moment. This relationship was first discovered by Carter in 1916 through his calculations[2]. This small creep can be attributed to the elastic deformations in the wheel.

[1] O. Reynolds, On rolling friction. Philosophical Transactions of the Royal Society of London, 166 (I): 155-174, 1876.

[2] F.W. Carter, The electric locomotive. Proc. Inst. Civil Engn., 201, 221-252, 1916, Discussion pages 253-289.

V.L. Popov, *Contact Mechanics and Friction*,
DOI 10.1007/978-3-662-53081-8_9

Of special interest for technical applications is the partial sliding that takes place in the contact area, because it leads to wear even though full sliding is not yet taking place.

9.1 Qualitative Discussion of the Processes in a Rolling Contact

The fact that in a driven or braking wheel, there must be both stick and slip domains can already be derived from the analogy between rolling and tangential contact. If we bring a wheel into contact with a rigid plane and apply a moment, then the contact area is loaded in the tangential direction. In the previous chapter, however, we saw that when a Hertzian contact is loaded in the tangential direction, a sliding domain is always produced. This is also valid for contacts involving driven rolling wheels. As with a tangential contact, a rolling contact initially forms a small sliding domain which grows with increasing moment until it encompasses the entire contact area.

We will now qualitatively discuss the processes that transpire in a rolling wheel. In order to better understand these processes, we consider a simplified model of an elastic wheel composed of a rigid inner ring and a series of elements that are elastically coupled both to the ring and to one another, as shown in Fig. 9.1. Between the elements and the base, there is friction characterized by the coefficient of friction μ. If we initially press the wheel onto a rigid base (Fig. 9.1 b) and subsequently apply a moment (Fig. 9.1 c), then the springs to the right of the contact area are in compression and the springs to the left are in tension. Thus, the inner rigid ring rotates a specific angle, which is dependent on the number and stiffness of the springs. Now, let us allow the wheel to roll to the right (Fig. 9.1d). The elements which are under pressure, but have not yet contacted the rigid surface, enter the contact area in the same equilibrium state as they were in before contact. The elements are "carried" through the contact area in the same equilibrium state. When they reach the trailing edge, where the normal force decreases, they are unloaded and relax. Therefore, as an element slips out of the contact area towards the rear, the wheel turns a bit further.

For a braking wheel, the springs on the leading edge are in tension, and on the trailing edge in compression. The springs on the leading edge, however, are already in equilibrium before they reach the contact area and remain in this state until they reach the trailing edge. From this, we come to the following realization:

> For a driven or braking wheel there is always a sticking domain that exists in the leading edge and a slip domain that exists in the trailing edge.

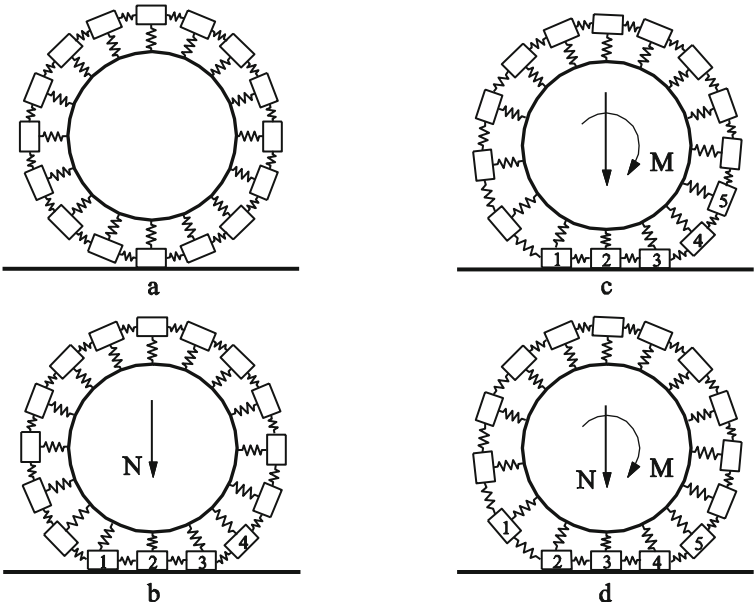

Fig. 9.1 Simplified model of a wheel in traction.

For every rotation of an angle corresponding to an individual element, the wheel experiences an "elastic rotation" in addition to the "rigid rotation." Therefore, the circumferential speed of the wheel is faster than the translational speed. For a braking wheel (traction moment and rolling direction in opposition), however, the circumferential speed is smaller than the translational speed. It is clear that the incremental elastic rotation on transition from one element to another is always the same. For this reason, the difference in speeds, $v_{creep} = v - \Omega R$, will be proportional to the translational speed v. Therefore, in order to characterize the creep, it is often sensible to adopt a dimensionless quantity

$$s = \frac{v - \Omega R}{v} = 1 - \frac{\Omega R}{v}, \tag{9.1}$$

which we call the *creep ratio*. It is negative for a driven wheel and positive for a braking wheel. It is easy to see that the creep ratio is equal to the *deformation* ε_{xx} in the sticking domain of the contact. One can establish this most easily by observing the mass transfer through the contact area. The density of the material in the sticking domain is $\rho_0/(1+\varepsilon_{xx})$. The contact area moves with the translational speed v. The mass flow density in the contact area is $v\rho_0/(1+\varepsilon_{xx})$. Otherwise, according to the definition, it is equal to $\rho_0 \Omega R$. Therefore, it follows that

$$\Omega R = \frac{v}{(1+\varepsilon_{xx})} \tag{9.2}$$

and the creep ratio is

$$s = \frac{\varepsilon_{xx}}{1+\varepsilon_{xx}} \approx \varepsilon_{xx} \,. \tag{9.3}$$

9.2 Stress Distribution in a Stationary Rolling Contact

A. Preparatory Step

In the following, we use the results from the theory of elasticity which are already known to us (see Section 8.2). If a tangential stress of

$$\tau(r) = \sigma_{zx}(r) = \tau_0 \sqrt{1 - r^2/a^2} \tag{9.4}$$

is applied to a circular area (Fig. 9.2 a), then it leads to a displacement of

$$u_x = \frac{\pi\tau_0}{32Ga}\left[4(2-\nu)a^2 - (4-3\nu)x^2 - (4-\nu)y^2\right] \tag{9.5}$$

in the tangential direction. A stress distribution of

$$\tau = \sigma_{zx}(x) = \tau_0 \sqrt{1 - x^2/a^2} \tag{9.6}$$

on a strip with a width of $2a$ (Fig. 9.2 b) causes a displacement of

$$u_x = const - \tau_0 \frac{x^2}{aE^*} \,. \tag{9.7}$$

With these stress distributions, the stress distribution in a rolling wheel is able to be constructed.

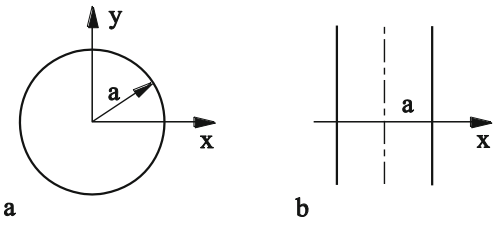

Fig. 9.2 Various contact areas loaded with tangential stresses: (a) circular, (b) strip.

B. Theory of Carter

The two-dimensional rolling contact problem, meaning the rolling motion of a cylinder on a plane was solved in 1926 by Carter. As in many other solutions of normal and tangential problems, his solution is based on the hypothesis that one can "construct" the stress distribution in a rolling contact from the superposition of two "Hertzian" stress distributions for which the analytical solutions of the displacement fields on the surface of the continuum are known. Let us search for the stress distribution of a driven wheel in the form

$$\tau = \tau^{(1)}(x) + \tau^{(2)}(x) \tag{9.8}$$

with

$$\tau^{(1)}(x) = \tau_1 \left(1 - \frac{x^2}{a^2}\right)^{\frac{1}{2}} \tag{9.9}$$

and

$$\tau^{(2)}(x) = -\tau_2 \left(1 - \frac{(x-d)^2}{c^2}\right)^{\frac{1}{2}}, \tag{9.10}$$

where a is half of the width of the total contact and c is half the width of the sticking domain of the leading edge. The definition of value of d can be taken from Fig. 9.3: $d = a - c$. The pressure distribution is given for the total contact by the Hertzian expression

$$p(x) = p_0 \left(1 - \frac{x^2}{a^2}\right)^{\frac{1}{2}} \quad . \tag{9.11}$$

In order for the given stress distribution to be actually consistent with a *rolling contact*, certain kinematic and dynamic relationships must be met. First, we notice that the leading edge of the wheel is already in a deformed state before it enters the contact area. As soon as the elements come into contact with the base, they can no longer move relative to one another until they leave the sticking domain. Hence, it follows that:

1. In the sticking domain, the deformation is constant. (9.12)

Under the assumption that Coulomb's law of friction is valid in the sliding domain, it is true that

2. In the complete sliding domain, the condition must be fulfilled that

$$\tau(x) = \mu p(x) \, . \tag{9.13}$$

These two conditions guarantee that we have a stationary rolling contact. Now, our task is to show that these two conditions can be met in assuming the stress distribution from (9.8).

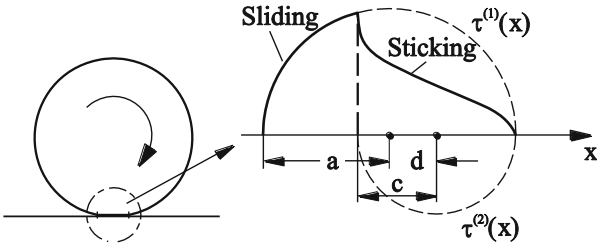

Fig. 9.3 Distribution of the tangential stresses in the contact area for the rolling contact of a driven elastic cylinder.

The displacements caused by the stresses $\tau^{(1)}(x)$ and $\tau^{(2)}(x)$ are equal to $u_x^{(1)} = C^{(1)} - \tau_1 \frac{x^2}{aE^*}$ and $u_x^{(2)} = C^{(2)} + \tau_2 \frac{(x-d)^2}{cE^*}$, respectively. The total displacement is

$$u_x = const - \tau_1 \frac{x^2}{aE^*} + \tau_2 \frac{(x-d)^2}{cE^*} \tag{9.14}$$

and the deformation is

$$\frac{\partial u_x}{\partial x} = -\tau_1 \frac{2x}{aE^*} + \tau_2 \frac{2(x-d)}{cE^*}. \tag{9.15}$$

For the condition (9.12) to be met, then the expression

$$\tau_2 = \frac{c}{a}\tau_1 \tag{9.16}$$

must be valid. From condition (9.13), it follows that

$$\tau_1 = \mu p_0. \tag{9.17}$$

The deformation is constant in the sticking domain and equal to

$$\frac{\partial u_x}{\partial x} = -\frac{2\mu p_0 d}{aE^*}. \tag{9.18}$$

The total lateral force in the contact area is calculated as

$$F_x = \int_{-a}^{a} L \cdot \tau(x) dx = = \left(\frac{\pi}{2} a\mu p_0 - \frac{c}{a}\frac{\pi}{2} c\mu p_0 \right) L = \mu F_N \left(1 - \frac{c^2}{a^2} \right). \tag{9.19}$$

The radius of the sticking domain is

$$\frac{c}{a}=1-\frac{d}{a}=\left(1-\frac{F_x}{\mu F_N}\right)^{1/2}. \tag{9.20}$$

According to (9.3) and (9.18), we obtain the following creep ratio:

$$s=\frac{\partial u_x}{\partial x}=-\frac{2\mu p_0}{E^*}\left[1-\left(1-\frac{F_x}{\mu F_N}\right)^{1/2}\right]. \tag{9.21}$$

Taking into account the relationships $F_N=\frac{\pi a p_0}{2}L$ and $F_N=\frac{\pi E^* L a^2}{4R}$ (see Equation (5.34)), one can also present the equation for creep ratio in the following form:

$$s=-\frac{\mu a}{R}\left[1-\sqrt{1-\frac{F_x}{\mu F_N}}\right]. \tag{9.22}$$

This relationship is illustrated in Fig. 9.4. It is called the traction-creep curve.

For small tangential forces, the slip can be expanded as a Taylor series of $F_x/\mu F_N$. In the first order,

$$s\approx-\frac{aF_x}{2RF_N}\quad\text{for}\quad F_x\ll\mu F_N. \tag{9.23}$$

According to this, the slip is not dependent on the coefficient of friction μ for small tangential forces. The linear dependence $|s|=\frac{aF_x}{2RF_N}$ is shown in Fig. 9.4 with the dotted line. The deviation of the actual slip from the dotted line shows the amount of "real sliding" in the contact area. The entire contact area slides when $F_x=\mu F_N$. At this moment the creep is equal to $s=-\frac{\mu a}{R}$. According to this, the maximum creep is equal to two times the "elastic creep" (9.23) at the same force. The difference between the two,

$$s_{sliding}=-\frac{\mu a}{2R}, \tag{9.24}$$

gives the part of the creep which is caused by slip. The characteristic value of the sliding speed in the rolling contact for "critical traction" (immediately before the beginning of complete sliding) is, therefore,

$$v_{sliding}\approx\frac{\mu a}{2R}v, \tag{9.25}$$

where v is the translational speed of the wheel. For small traction forces, the creep can be estimated from the difference between the complete creep (9.22) and the elastic part of the creep (9.23) as

$$s_{sliding} = -\frac{\mu a}{8R}\left(\frac{F_x}{\mu F_N}\right)^2 . \tag{9.26}$$

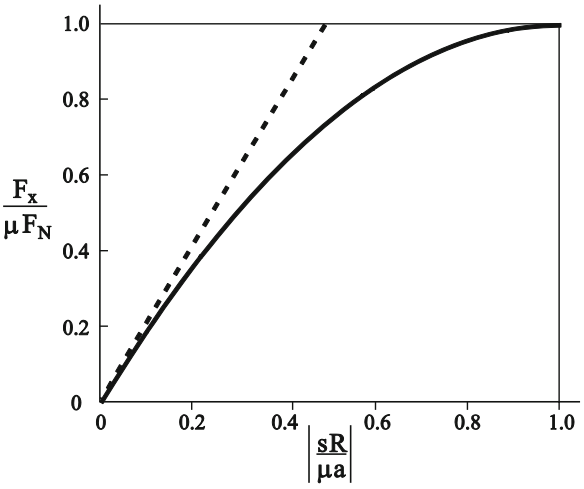

Fig. 9.4 Traction-creep curve.

C. Three-dimensional Rolling Contact Problem

One can also determine the stress distribution in a rolling contact for a three-dimensional case by a similar procedure as that of Carter, where one superimposes two stress distributions of the forms

$$\tau^{(1)}(x,y) = \tau_1\sqrt{1-\frac{x^2+y^2}{a^2}} \tag{9.27}$$

and

$$\tau^{(2)}(x,y) = -\tau_2\sqrt{1-\frac{(x-d)^2+y^2}{c^2}} . \tag{9.28}$$

The stress distribution in Equation (9.28) is only defined in the sticking domain. The displacement of the surface caused by the superimposed stresses, according to (9.5), is

$$u_x = \frac{\pi}{32G}\begin{Bmatrix} \frac{\tau_1}{a}\left[4(2-\nu)a^2 - (4-3\nu)x^2 - (4-\nu)y^2\right] \\ -\frac{\tau_2}{c}\left[4(2-\nu)c^2 - (4-3\nu)(x-d)^2 - (4-\nu)y^2\right] \end{Bmatrix}. \tag{9.29}$$

The deformation component, $\varepsilon_{xx} = \partial u_x / \partial x$, is equal to

$$\frac{\partial u_x}{\partial x} = \frac{\pi(4-3\nu)}{16G}\left\{-\frac{\tau_1}{a}x + \frac{\tau_2}{c}x - \frac{\tau_2}{c}d\right\}. \tag{9.30}$$

From the requirements (9.12) and (9.13), the same conditions follow as in the cylindrical contact, (9.16) and (9.17). The deformation and, therefore, the creep ratio is equal to

$$\frac{\partial u_x}{\partial x} = -\frac{\pi(4-3\nu)}{16G}\mu p_0 \frac{d}{a}. \tag{9.31}$$

The tangential force is

$$F_x = \frac{2}{3}\pi a^2 \tau_1 - \frac{2}{3}\pi c^2 \tau_2 = \mu F_N\left(1 - \left(\frac{c}{a}\right)^3\right). \tag{9.32}$$

The radius of the sticking domain has the same form as in pure tangential contact:

$$\frac{c}{a} = \left(1 - \frac{F_x}{\mu F_N}\right)^{1/3} \tag{9.33}$$

and the creep ratio[3],

$$s = \frac{\partial u_x}{\partial x} = -\frac{3(4-3\nu)\mu F_N}{32Ga^2}\left[1 - \left(1 - \frac{F_x}{\mu F_N}\right)^{1/3}\right]. \tag{9.34}$$

Taking the relationship $F_N = \frac{4}{3}E^* \frac{a^3}{R}$ into account, the creep ratio can also be written in the form

$$s = -\frac{(4-3\nu)\mu}{4(1-\nu)}\frac{a}{R}\left[1 - \left(1 - \frac{F_x}{\mu F_N}\right)^{1/3}\right]. \tag{9.35}$$

[3] This equation is valid for an elastic wheel on a rigid plane. For contact between the same materials, the slip is two times that of (9.34).

For small driving forces, we obtain the following for the first order approximation:

$$s \approx -\frac{(4-3\nu)F_x}{32Ga^2}\,. \tag{9.36}$$

Problems

Problem 1: Estimate the sliding speed (a) in a locomotive wheel (b) in an automobile tire.

Solution: (a) For a locomotive wheel, the creep is calculated according to (9.35):

$$s = -\frac{(4-3\nu)\mu}{4(1-\nu)}\frac{a}{R}\left[1-\left(1-\frac{F_x}{\mu F_N}\right)^{1/3}\right].$$

We obtain the creep at the critical traction by inserting $F_x = \mu F_N$:

$$|s| = \frac{(4-3\nu)\mu}{4(1-\nu)}\frac{a}{R}\,.$$

The sliding speed is calculated by multiplying the creep with the translational speed v. At $\mu \approx 0.3$, $a \approx 7$ mm, $R = 0.5$ m, and $\nu = 1/3$, the sliding speed is $v_{sliding} \approx 5 \cdot 10^{-3} v$. At a translational speed of 30 m/s (108 km/h), it has a characteristic value of $v_{sliding} \approx 0.14$ m/s.

(b) For an automobile tire in "critical traction" with $\mu \approx 1$, $a \approx 5$ cm, $R = 0.3$ m and $\nu = 1/2$, we obtain $v_{sliding} \approx 0.2v$ for the sliding speed. At a translational speed of 15 m/s (54 km/h), the sliding speed is around 3 m/s. At "normal operating conditions" (constant speed of 15 m/s), the sliding speed in a rolling contact between a rubber tire and the street is much smaller and, as a rule, around 1 cm/s.

Problem 2: Estimate the energy loss in a driven or braking wheel.

Solution: We obtain the following estimation for the frictional power $\dot{W}$ in the contact by multiplying the tangential force acting on the contact with the average sliding speed:

$$\dot{W} \approx |s| F_x v = |s| \dot{W}_0\,,$$

where $\dot{W}_0 = F_x v$ is the "power" of the frictional force.

Problem 3: If a force is applied to a rolling, elastic wheel perpendicular to the rolling direction, then the wheel receives a velocity component in the direction of the force (*transverse creep*) due to elastic deformations and partial sliding. Find the transverse creep of a rolling elastic sphere.

Solution: The axis of rotation of the sphere should be parallel to the x-axis; without the transverse force, the sphere would roll exactly in the y-direction. The sticking domain is always at the leading edge, independent of the type of loading (Fig. 9.5).

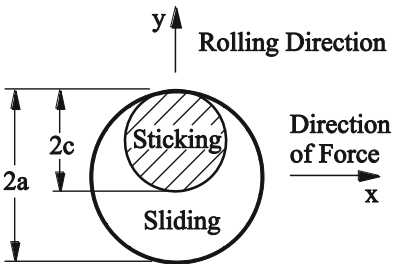

Fig. 9.5 Stick and slip domains for a rolling, elastic wheel which is acted on by a force applied perpendicular to the rolling direction.

We look for the stress in the form

$$\tau(x,y)=\mu p_0\sqrt{1-\frac{x^2+y^2}{a^2}}-\mu p_0\frac{c}{a}\sqrt{1-\frac{x^2+(y-d)^2}{c^2}}\ .$$

The corresponding displacement field, according to (9.5), is

$$u_x=\frac{\pi}{32G}\left\{\begin{array}{l}\dfrac{\mu p_0}{a}\left[4(2-\nu)a^2-(4-3\nu)x^2-(4-\nu)y^2\right]\\ -\dfrac{\mu p_0}{a}\left[4(2-\nu)c^2-(4-3\nu)x^2-(4-\nu)(y-d)^2\right]\end{array}\right\}$$

and the relevant component of the deformation tensor is

$$\varepsilon_{xy}=\frac{\partial u_x}{\partial y}=-\frac{\pi\mu p_0(4-\nu)}{16G}\frac{d}{a}\ .$$

This value specifies the angle at that the sphere will actually roll, relative to the direction of ideal rolling. Similarly to how we did in the derivation of the Equations (9.32) - (9.35), we obtain a transverse creep of

$$s_\perp=\varepsilon_{xy}=-\frac{3\mu(4-\nu)}{32Ga^2}\mu F_N\left[1-\left(1-\frac{F_x}{\mu F_N}\right)^{1/3}\right]=-\frac{(4-\nu)\mu}{4(1-\nu)}\frac{a}{R}\left[1-\left(1-\frac{F_x}{\mu F_N}\right)^{1/3}\right].$$

Problem 4: Let us examine the belt transmission shown in Fig. 9.6. The right disk is powered with the moment M so that it rotates with the constant angular velocity of ω_1. However, the driven disk (left) only turns at an angular velocity of $\omega_2 < \omega_1$. The sticking domain, in which the force in the belt F_1 is constant, as well as the sliding domain, in which the force decreases to F_2, are shown on the powered disk. A corresponding change from sticking to sliding is present in the left disk as well. Determine the creep s and the loss of mechanical energy.

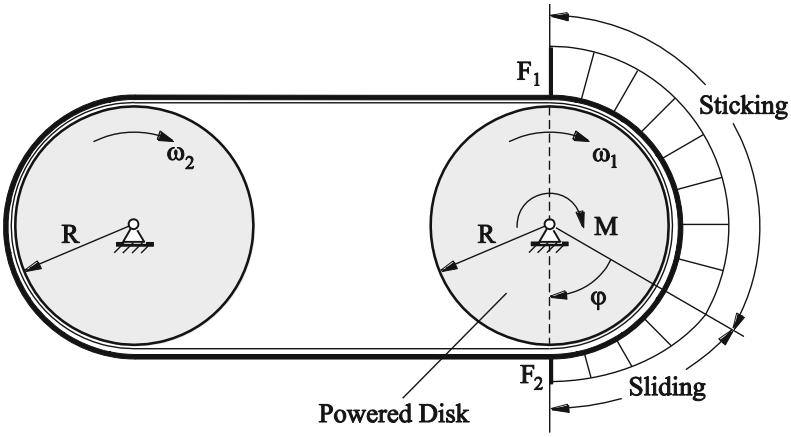

Fig. 9.6 Elastic belt, which transfers a moment M between two rotating disks.

Solution: The force moment transferred by the belt transmission is equal to

$$M = (F_1 - F_2)\,R\,.$$

Because the extension of the belt in the sticking domain remains constant, the tension force in the entire sticking domain is constant and equal to F_1. In the sliding domain, the force decreases to the value F_2, for which the following equation is valid (see Chapter 10 Problem 4):

$$F_1 / F_2 = e^{\mu\varphi}\,.$$

The elastic deformation of the belt is equal to $\varepsilon = F / EA$, where E is the module of elasticity and A is the cross-sectional area. In the two sections between the disks (above and below), the following equations are valid:

$$\varepsilon_1 = \frac{F_1}{EA}\,, \qquad \varepsilon_2 = \frac{F_2}{EA}\,.$$

The mass flow must remain constant at every point. From this, it follows that

$$\frac{v_1}{1+\varepsilon_1} = \frac{v_2}{1+\varepsilon_2}\,.$$

The creep ratio is

$$s = 2\frac{v_1 - v_2}{v_1 + v_2} \approx \varepsilon_1 - \varepsilon_2 = \frac{F_1 - F_2}{EA} = \frac{M}{REA}.$$

The dissipated power is

$$\dot{W} = M\left(\omega_1 - \omega_2\right),$$

with

$$\omega_1 = \frac{v_1}{R}, \quad \omega_2 = \frac{v_2}{R}.$$

For small differences in the angular velocities of the disks, it holds true that

$$\dot{W} \approx \frac{M^2 \bar{\omega}}{REA}.$$

Here, $\bar{\omega} = \frac{1}{2}\left(\omega_1 + \omega_2\right)$ is the average angular velocity.

Problem 5: A wheel rolls with the angular velocity ω and, at the same time, is turned at an angular velocity Ω about the vertical axis[4] (for example, consider the steering of an automobile). Determine the torsional creep, which we define as the ratio $s = \Omega / \omega$, as a function of the torsional moment assuming an infinitely large coefficient of friction.

Solution: The stress distributions

$$\tau_x = \frac{8G(3-\nu)}{3\pi(3-2\nu)}\frac{s}{R}\frac{(a+x)y}{\left(a^2 - r^2\right)^{1/2}},$$

$$\tau_y = \frac{8G(1-\nu)}{3\pi(3-2\nu)}\frac{s}{R}\frac{\left(a^2 - 2x^2 - ax - y^2\right)}{\left(a^2 - r^2\right)^{1/2}}$$

lead to a surface displacement which fulfills the sticking condition (constant deformation in the entire contact area)[5]. This results in a tangential force of zero ($F_x = F_y = 0$), while the torsional moment is

$$M_z = \frac{32\left(2-\nu\right)}{9(3-2\nu)}\frac{a^4}{R}Gs.$$

---

[4] The rotation about an axis perpendicular to the base is called s*pin*.

[5] K.L. Johnson, The effect of spin upon the rolling motion of an elastic sphere on a plane. Transactions ASME, Journal of Applied mechanics, 1958, v. 25, p.332.

The resulting creep ratio is

$$s = \frac{9(3-2\nu)}{32(2-\nu)} \frac{R}{a^4} \frac{M_z}{G} .$$

10 Coulomb's Law of Friction

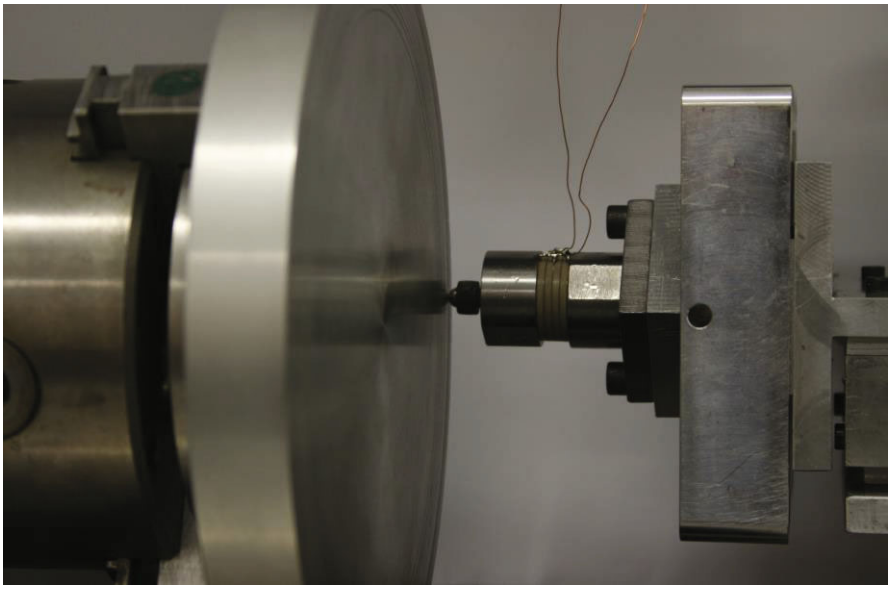

10.1 Introduction

In this chapter, we will only investigate the *dry friction* or *Coulomb friction* between two solid bodies. Friction between solid bodies is an extremely complicated physical phenomenon. It encompasses elastic and plastic deformations of the surface layers of the contacting bodies, interactions with wear particles, microfractures and the restoration of the continuity of materials, excitation of electrons and phonons, chemical reactions, and the transfer of particles from one body to the other. What is astonishing is the fact that it is possible to formulate a very simple law for dry friction. This first order approximation is sufficient for many engineering applications: The frictional force is proportional to the normal force and as good as independent from the speed. The astounding property of dry friction lies in the fact that in a first order approximation, it is dependent neither on contact area nor on roughness. This property allows us to use the notion of the coefficient of friction. The coefficient of friction, however, gives only a very rough first approximation of the quotient of frictional force to normal force.

Leonardo da Vinci was the first to experimentally investigate the law of friction and formulate the most important principles (e.g. that the frictional resistance is proportional to the weight and independent from the contact area). He derived the latter with the help of the experiments shown in Fig. 10.1.

V.L. Popov, *Contact Mechanics and Friction*,
DOI 10.1007/978-3-662-53081-8_10

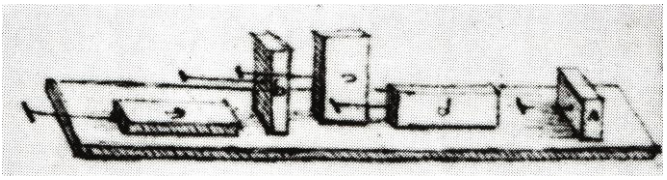

Fig. 10.1 Drawing from the notebooks of Leonardo da Vinci which illustrates the independence of the frictional force from the footprint.

10.2 Static and Kinetic Friction

Through detailed experimental investigations, Coulomb (1736-1806) determined that the frictional force F_R between two bodies which are pressed together with a normal force F_N (Fig. 10.2) exhibit the following simple properties in a rough approximation[1]:

A. *Static Friction*. In order to set in motion a body lying on an even surface in a state of rest, a critical force, the *force of static friction* F_s, must be overcome. This force is roughly proportional to the normal force F_N [2]:

$$F_s = \mu_s F_N . \tag{10.1}$$

The coefficient μ_s is called the *coefficient of static friction*. It is dependent on the pairing of the contacting materials, however, shows almost no dependence on contact area or roughness.

B. *Kinetic Friction* F_R is the resisting force which acts on a body after the force of static friction has been overcome. Coulomb experimentally determined the following properties of kinetic friction:

- Kinetic friction is proportional to the normal force F_N :

$$F_R = \mu_k F_N . \tag{10.2}$$

- It shows no considerable dependence on the contact area or roughness of the surface.

- The *coefficient of kinetic friction* is approximately equal to the coefficient of static friction:

---

[1] A more detailed description of Coulomb's findings can be found in: E. Popova, V. L. Popov, The research works of Coulomb and Amontons and generalized laws of friction, Friction, 2015, v. 3, N.2, pp. 183-190.

[2] This proportionality is known as Amontons' law.

$$\mu_k \approx \mu_s \,. \tag{10.3}$$

- The kinetic friction is independent of, or rather very weakly dependent on, the sliding velocity.

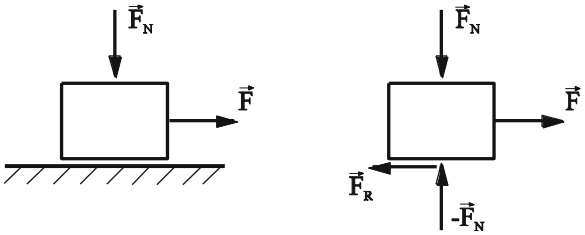

Fig. 10.2 A block being acted upon by normal and tangential force on a plane; in the corresponding free body diagram, the reaction force and the frictional force can be seen.

This law gives only a rough outline of the properties of dry friction. A more detailed analysis shows that static and kinetic frictional forces have the same origin and are not able to be considered separately in many mechanical problems. We have already seen that when a contact is tangentially loaded, as a rule, partial sliding takes place, even when "macroscopic sliding" has not yet occurred. Thus, the difference between the static and kinetic coefficients of friction prove to be relative: often the transition from static to sliding contact is continuous (as is the case in a driven wheel) or the "static friction" emerges as sliding friction at very low velocities (as is the case with rubber friction, e.g. a rubber tire on the street)[3].

10.3 Angle of Friction

The simplest experimental method to determine the coefficient of friction, which is practically always feasible, is the measurement of the inclination angle at which a body lying on an inclined plane begins to slide. This angle is called the *angle of friction*. The forces acting on such a body are shown in Fig. 10.3 b.

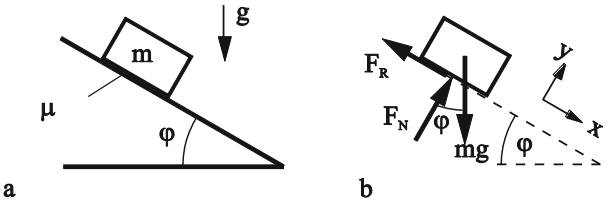

Fig. 10.3 A body on an inclined plane.

[3] See section 20.3.

Upon reaching the angle of friction, the static force reaches its maximum value, $F_s = \mu_s F_N$. The equilibrium of the forces in this critical state yields (for the coordinate system shown in Fig. 10.3 b):

$$\begin{aligned} \text{x:} \quad & mg\sin\varphi - \mu_s F_N = 0 \\ y: \quad & F_N - mg\cos\varphi = 0 \ . \end{aligned} \tag{10.4}$$

Hence, it follows that

$$\tan\varphi = \mu_s \, . \tag{10.5}$$

According to this, the tangent of the angle of friction is equal to the coefficient of static friction.

10.4 Dependence of the Coefficient of Friction on the Contact Time[4]

It was also Coulomb who discovered deviations from the simple law of friction. Among other things, he discovered that the static frictional force increases with the amount of time an object is at rest. The experimental data from Coulomb are provided in Table 10.1. In Fig. 10.4, the frictional force is plotted logarithmically versus time. In this depiction, the plot is a straight line: the static frictional force increases logarithmically with time.

Physical reasons for this time dependence can be very diverse. For metallic materials, the real contact area in the micro-contacts increases with time due to the always present creep processes. At higher temperatures, this increase is faster. When the contact area increases, this process slows, leading to a logarithmic dependence of contact area and, thus, a logarithmic dependence of the static frictional force. This increase begins at the instant of first contact on the atomic scale – in the subnanosecond domain – and does not stop even after very long time periods. For elastomers, this effect is tied to the increase in contact area due to the viscoelasticity of the material. Also, capillary forces attribute to frictional forces and lead to the approximate logarithmic time dependence of the static frictional force.

It should be mentioned that the time dependence of the coefficient of "static" friction results in friction being a dynamic process. If the coefficient of friction is dependent on the contact time, then it would also apply to a rolling contact, because "rolling" can be considered a continuous reestablishment of new contacts on the underlying surface. For larger rolling speeds, the contact time is small and one can expect a smaller "static" frictional force in the contact.

[4] See also section 20.3.

Table 10.1 Static frictional force for oak against oak smeared with tallow as a function of the resting time.

t, min	F_s, arb. units
0	5.02
2	7.90
4	8.66
9	9.25
26	10.36
60	11.86
960	15.35

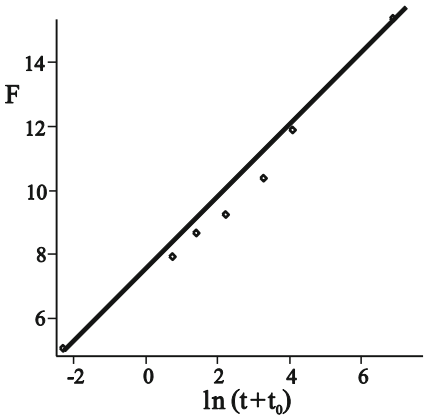

Fig. 10.4 The data of Coulomb from Table 10.1: The static frictional force plotted as a logarithmic function of time: $F = a + b\ln(t + t_0)$ with $a = 7.28$, $b = 1.10$, and $t_0 = 0.101$ min.

Also, during kinetic friction, micro-asperities come into contact and as the duration of the contact is dependent on the sliding speed, the force of kinetic friction is also dependent on the sliding speed. These examples show that the difference between the "static" and "kinetic" friction is relative and only provides us a very rough picture. In reality, kinetic and static friction are closely related to one another and with contact dynamics.

10.5 Dependence of the Coefficient of Friction on the Normal Force

Also, the linear dependence of the frictional force on the normal force, (10.1) or (10.2), is only met in a specific force domain – for not too large or too small of a

normal force. For metallic materials, this domain can contain several orders of magnitude, as Fig. 10.5 illustrates[5].

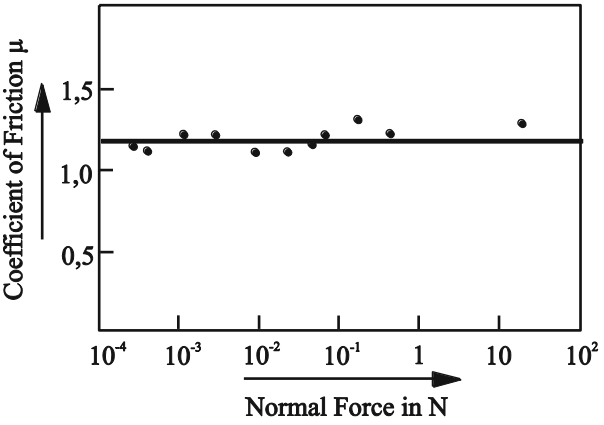

Fig. 10.5 Coefficient of Friction for steel on electro-polished Aluminum. The coefficient of friction remains constant for loads from 10 mg to 10 kg, in other words, for a change in the load by a factor of 10^6.

This dependence is no longer valid when the real contact area is comparable to the apparent contact area. This limit is easily reached for soft metals such as indium or lead, but particularly easy for polymers and elastomers, which due to this reason, considerably deviate from Amontons' law in behavior. In Fig. 10.6, the frictional force between steel and teflon is presented as a function of the normal force. As a good approximation, the frictional force is proportional to $F_N^{0.85}$. Therefore, the coefficient of friction decreases with the normal force.

[5] F.P. Bowden, D. Tabor, The Friction and Lubrication of Solids. Clarendon Press, Oxford, 2001.

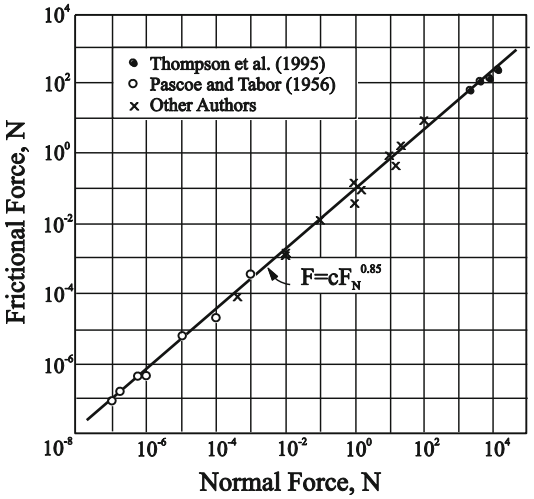

Fig. 10.6 Dependence of the coefficient of friction on normal force between steel and teflon. Source: E. Rabinowicz, Friction and wear of materials. Second Edition. John Wiley & Sons, inc., 1995.

10.6 Dependence of the Coefficient of Friction on Sliding Speed[6]

For the sake of simplicity, it is often assumed that the coefficient of kinetic friction is independent of sliding speed. Also, this is a good, but rough, approximation that is valid for not too high and not too low speeds. The exact dependence of the frictional force on sliding speed is important in many applications. If the frictional force decreases with the speed, then stationary sliding is unstable and, as a rule, leads to frictional instabilities[7].

10.7 Dependence of the Coefficient of Friction on the Surface Roughness

Frequently, the origins of friction are explained through the roughness of the surfaces. In mechanics, one describes the surfaces for which friction exists as "rough," while "smooth" surfaces are usually categorized as frictionless. Every tribologist knows that these definitions are not valid: In a large domain of rough-

[6] See also section 20.3.

[7] Frictional instabilities are discussed in Chapter 12 in detail.

nesses, the frictional force is independent or only very slightly dependent on the roughness. Contrary to expectations, the coefficient of friction for especially smooth metal surfaces can be even larger than for rough surfaces. The influence of roughness on friction is dependent on many factors, for instance, the presence of impurities or liquid films in the tribological contact, among others.

Experimentation dealing with the transfer of radioactive elements between two contact partners offers an impressive verification for the weak dependence of friction (and wear) on the surface roughness. In Fig. 10.7, the results of the experiment are presented, in which a radioactive copper block is drug over a copper plate which has a roughness of 25 nm on one part and a roughness 20 times larger on the other (500 nm). The large difference in the roughness has almost no influence on the frictional force and the material transfer from one of the bodies to the other (which one can see by the subsequent radioactivity measurement). The roughness does not even have an impact on the size of contact areas.

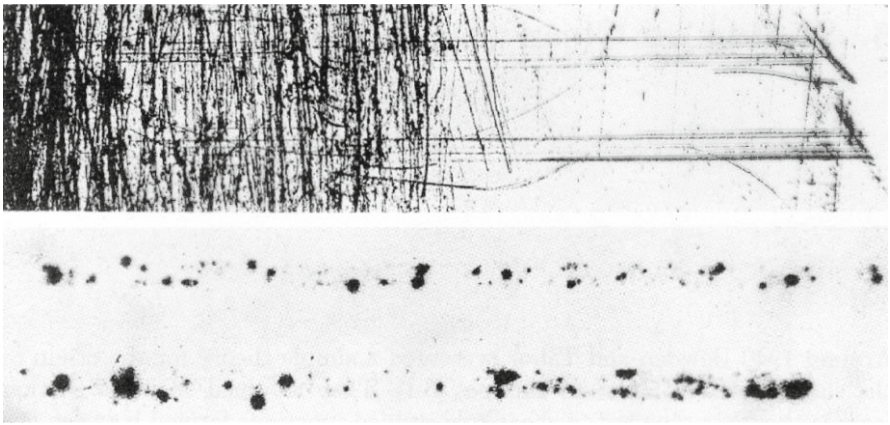

Fig. 10.7 Photograph and radiograph of a copper surface, of which one part has a roughness of 25 nm and the other 20 times larger with 500 nm, after a friction experiment with a load of 40 N and a sliding speed of 0.01 cm/s. The frictional force as well as the wear are almost independent from the roughness[8].

10.8 Coulomb's View on the Origin of the Law of Friction

Coulomb proposed the first model for the physical origin of friction, which explained some of the important properties of dry friction in a simple way. According to his view, the interaction between micro-roughnesses of both contacting sur-

[8] E. Rabinowicz, Friction and wear of materials. Second Edition. John Wiley & Sons, inc., 1995.

faces is responsible for the force of friction, which is shown schematically in his sketch (Fig. 10.8). As aforementioned, the influence of the roughness of the surfaces on friction, in reality, is much more complicated. Nevertheless, even very detailed modern analysis continues to lead to the simplest view that was already suggested by Coulomb. We will, therefore, quickly discuss this view.

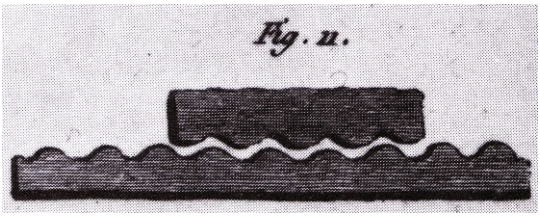

Fig. 10.8 Interactions between roughnesses as the origin of frictional force (sketch from Coulomb).

Following Coulomb, we consider a body that is pressed onto a corrugated surface as a model for dry friction. In order to simplify the problem further, we reduced the body to a single point mass. The resulting model is presented in Fig. 10.9.

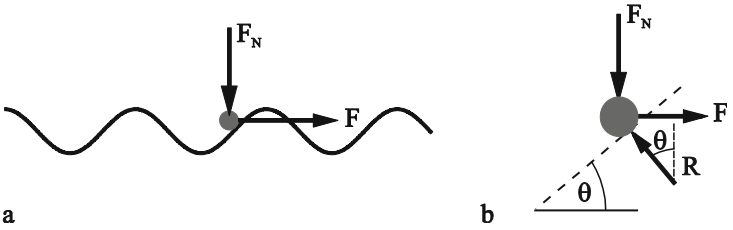

Fig. 10.9 Coulomb's simplified model for dry friction.

Between the corrugated surface and the point mass, there should no longer be static friction stemming from even smaller scale. The equilibrium conditions are determined from the free-body diagram shown in Fig. 10.9 b:

$$R\cos\theta = F_N\,, \quad R\sin\theta = F\,. \tag{10.6}$$

It follows that

$$F = F_N \tan\theta\,. \tag{10.7}$$

The force of static friction F_s is, by definition, equal to the maximum force F, at which equilibrium is still possible:

$$F_s = F_{\max} = F_N \tan\theta_{\max}\,. \tag{10.8}$$

The coefficient of static friction is, therefore, equal to the maximum slope of the surface:

$$\mu_s = \tan\theta_{\max} . \tag{10.9}$$

This model provides, in a simple way, one of the most important properties of dry friction – its proportionality to normal force – and gives a simple geometric explanation for the coefficient of friction. If this is applied to sufficiently large bodies with periodic "corrugations," as in the sketch from Coulomb, then the model also explains the independence of the coefficient of friction from the contact area. It does not explain, however, the observable independence (or relatively weak dependence) of the frictional force on the surface roughness.

10.9 Theory of Bowden and Tabor

There have been many investigations in order to explain the universality and simplicity of Coulomb's law of friction. It appears that the robustness of Coulomb's law of friction has several contributing factors. One important reason for the proportionality of the frictional force to the normal force lies in the contact properties of rough surfaces. We saw in Chapter 7 that contact properties such as the real contact area and the contact length increase approximately linearly with the normal force and are independent of the apparent contact area. In contrast, the slope of the surface in the micro-contact is independent of the normal force (or very weakly dependent). If we were to explain frictional force according to the belief of Coulomb with the gradient of the surfaces in the contact, then the coefficient of friction would be independent of normal force. The coefficient of friction would, however, be very different for ground and polished surfaces, which is usually not the case.

In 1949, Bowden and Tabor proposed a simple theory, which explains the origin of kinetic friction between pure metallic surfaces through the formation of cold-weld junctions. If two bodies are pressed together, then in a few places, they come so close to one another that the atoms of one body come into contact with the atoms of the second body, while extensive regions exist in which the distance between the bodies is so large that any atomic interactions can be neglected. We call the contact areas bridges; the total area of all of the bridges is the real contact area A. The remaining area is usually much larger than the real contact area, but has almost no contribution to the frictional force.

For metals, the real contact area can be fairly closely approximated in most practical cases, by assuming that all micro-contacts are plastically deformed and the stress is equal to the penetration hardness σ_0 of the material. This assumption provides a real contact area of

$$A \approx F_N / \sigma_0 . \tag{10.10}$$

If a tangential stress of τ_c is necessary to shear a cold-weld junction, then the maximum force of static friction is equal to

$$F_s = F_N \frac{\tau_c}{\sigma_0}. \tag{10.11}$$

Because the shear strength for an isotropic plastic body is around $1/\sqrt{3}$ of the tensile strength and this, in turn, is around 1/3 of the penetration hardness, there should be, as a rule, a universal dependence, $F_s \approx \left(\frac{1}{6} \div \frac{1}{5}\right) F_N$, leading to a coefficient of friction of $\mu \approx \frac{1}{6} \div \frac{1}{5}$. For many non-lubricated metal pairings (e.g. steel on bronze, steel on brass, or steel on cast iron), the coefficient of friction is effectively on the order of $\mu \sim 0.16 - 0.2$. For larger compressive forces, the coefficient of friction between pure metals can reach higher values, which is probably related to the larger plastic deformations and, therefore, the resulting considerable changes in surface topography.

Coefficients of friction between different materials are dependent on many parameters. However, based on the ideas of Bowden and Tabor, it is possible to formulate a rough classification. Initially, we notice that for strong adhesion in a tribological contact there exist both contacts in compression and contacts in tension. The stress in the compressive areas is roughly equal to the hardness, $\sigma_0 \approx 3\sigma_c$. In the tensile areas, $\sigma_0 \approx \zeta\sigma_c$ is valid, where ζ in generally smaller than 3. Thus, the normal force is equal to

$$F_N = \sigma_c \left(3A_{comp} - \zeta A_{ten}\right). \tag{10.12}$$

If all of the cold welds are sheared, then the static force of friction is

$$F_s \approx \tau_c \left(A_{comp} + A_{ten}\right). \tag{10.13}$$

The following approximation results for the coefficient of friction:

$$\mu \approx \frac{\tau_c \left(A_{comp} + A_{ten}\right)}{\sigma_c \left(3A_{comp} - \zeta A_{ten}\right)}. \tag{10.14}$$

Assuming $\tau_c \approx \sigma_c / \sqrt{3}$, which is valid for plastic isotropic substances, we obtain the approximation

$$\mu \approx \frac{1}{\sqrt{3}} \left(\frac{A_{comp} + A_{ten}}{3A_{comp} - \zeta A_{ten}} \right). \tag{10.15}$$

We consider the following cases:

1. *Pure metals in the presence of the smallest amount of lubrication, which has no lubricating effect, however, inhibits metallic adhesion.* In this case, $A_{ten} = 0$ and the coefficient of friction has the aforementioned universal value on the order of

$$\mu \approx \frac{1}{3\sqrt{3}} \approx 0.19 \,. \tag{10.16}$$

This coefficient of friction is characteristic for dry friction between metals under "normal conditions," in which the surfaces are covered with oxides as well as other impurities in small amounts.

2. *Pure metals with surfaces free of lubricants, but where oxides are present.* In this case, one can assume that the adhesion is strong and that the areas being stressed by compression and tension are about the same. The fact that the microcontacts bear the load is still true because of the difference between the plastic properties in tension and compression. The coefficient of friction is approximated as

$$\mu \approx \frac{1}{\sqrt{3}} \left(\frac{2}{3-\zeta} \right). \tag{10.17}$$

For $\zeta = 1$ to 2, this equation yields coefficients of friction in the range of $\mu \approx 0.6$ to 1.2. We have made this estimation for isotropic media. Pure metals with cubic crystal lattices (e.g. Fe, Al, Cu, Ni, Pb, Sn) have such coefficients of friction. For metals with hexagonal lattices (Mg, Ti, Zn, Cd), the coefficient of friction is around 0.6.

3. *Pure metals with a thin sheet of a soft metal* (e.g. lead or tin on steel, copper, silver, …). As long as the sheet is thin enough (around 100 nanometers), Equation (10.11) is valid, where σ_0 is the hardness of the harder material and τ_c is the shear strength of the softer material. The coefficient of friction is, in this case, smaller than it is with pure metals and can be 0.1 or smaller.

4. *Multi-phase materials*. Most materials that are used in tribological applications are not pure materials, rather multi-phase alloys, which, as a rule, consist of a harder matrix and softer inclusions. For example, tin bronze and lead bronze have this structure and are used as materials for bearings. One can assume that the function of these alloys is based on the extrusion of the softer metals which forms a thin layer on the sliding surface and reduces the friction according to the mechanism described in Case 3.

5. *Surfaces that are only elastically deformed.* In the case of diamond or amourphous carbon coatings, Equation (10.11) is not applicable, because the surface deforms purely elastically.

10.10 Dependence of the Coefficient of Friction on Temperature

Because the relationship of shear strength to hardness is not dependent on temperature, the coefficient of friction between pure metals is also independent from temperature. This is valid as long as the conditions do not change so that a transition takes place between the categories mentioned above. In the presence of a thin, soft sheet on a hard surface, the coefficient of friction increases quickly if the melting temperature of the sheet is reached. For metal sheets, this occurs abruptly upon reaching the melting temperature of the softer material. For grease or metallic soaps formed on the sliding surfaces, it occurs at the softening temperature of the grease or metallic soap.

Under "normal conditions," which are described in "Case 1" in the previous section, the coefficient of friction is only weakly dependent on the temperature for many metal pairings. Between 200°C and 300°C, a sharp increase occurs. Here, the coefficient of friction can increase twofold or threefold. At higher temperatures, it remains almost constant or increases at a slower rate. A typical temperature traverse is shown in Fig. 10.10. It is apparent that the reason for this is the softening or decomposition of the layers of impurities, typically small amounts of grease.

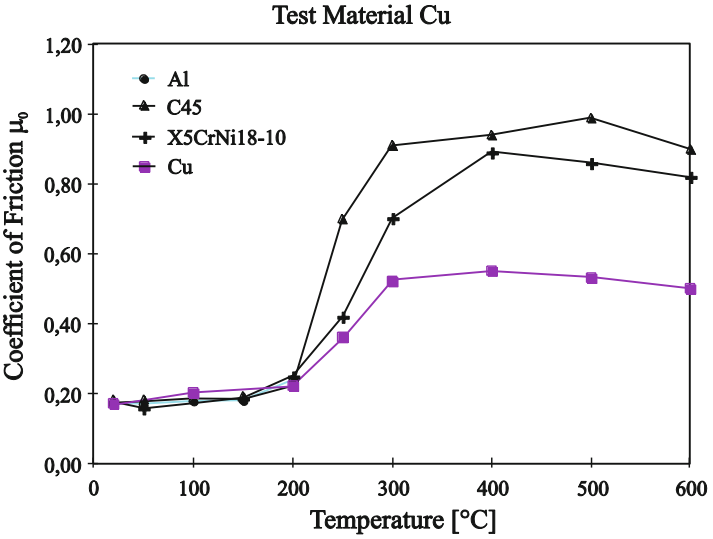

Fig. 10.10 Coefficient of static friction as a function of temperature for copper probes over aluminum, steel, and copper. Data from: Martin Köhler. Beitrag zur Bestimmung des Coulombschen Haftreibungskoeffizienten zwischen zwei metallischen Festkörpern. Cuvillier Verlag Göttingen, 2005.

For low temperatures, the coefficient of friction is constant, relatively small, and only weakly dependent on material combination. Characteristic values are on the order of 0.16-0.22. It is characteristic in this domain that oxide layers or other

layers of impurities remain on the surface during the frictional process. The domain of higher coefficients of friction is characteristic for conditions in which metal contact occurs.

Problems[9]

Problem 1: Self-locking. An arm is attached to a bushing which can move vertically on a pole. A movable weight is slid onto this arm (Fig. 10.11 a). As long as the weight is far enough away from the vertical pole, it is held up by the frictional forces that act on the corner points of the bushing (self-locking). Determine the necessary distance for this self-locking.

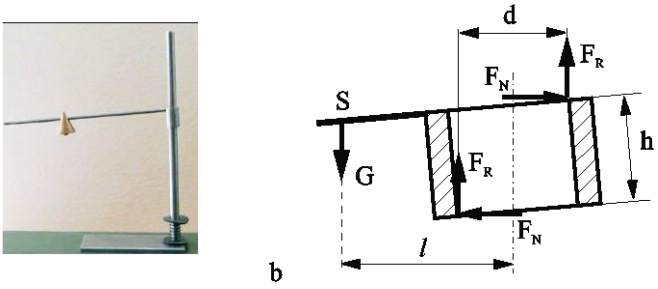

Fig. 10.11 Simple, self-locking system with the corresponding free-body diagram.

Solution: From the equilibrium condition in the horizontal direction, it follows that both reaction forces F_N at the corner points have the same magnitude (as shown in Fig. 10.11 b). At the limit between sliding and self-locking, the frictional forces reach their maximum value, $F_s = \mu_s F_N$. From the force equilibrium in the vertical direction, we obtain

$$2\mu_s F_N - G = 0 .$$

The moment equilibrium with respect to the center of the bushing is

$$Gl - 2F_N \frac{h}{2} = 0 .$$

Thus, it follows that the necessary distance is

$$l_c = \frac{h}{2\mu_s} .$$

[9] In the problems in this chapter, Coulomb's law of friction is used in its simplest forms (10.1) and (10.2).

Problem 2: Transverse Force. An automobile is accelerated or braked due to the frictional force between the tires and the street. This frictional force F_R should be smaller than the maximum force of static friction[10]: $F_R < F_s = \mu_k F_N$. Determine the transverse force $F_\perp$ at which the automobile begins to skid to one side.

Solution: Both the braking force and the transverse force are components of the frictional force in the rolling contact. Complete sliding occurs when $F_R^2 + F_\perp^2 > F_s^2$. Therefore, it follows that

$$F_\perp > \sqrt{\left(\mu_k F_N\right)^2 - F_R^2}\ .$$

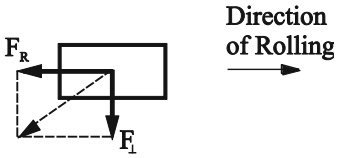

Fig. 10.12 Resulting forces in a rolling contact.

Problem 3: During complete braking of an automobile, the tires lock and they slide along the street at a velocity of v_0. What transverse velocity would a small force $F_\perp$ acting in the transverse direction cause?

Solution: The magnitude of the kinetic frictional force is not dependent on velocity, however, its direction is exactly opposite that of the velocity. From this, it follows that $\dfrac{v_\perp}{v_0} \approx \dfrac{F_\perp}{\mu_k F_N}$ and

$$v_\perp \approx F_\perp \left(\frac{v_0}{\mu_k F_N}\right).$$

The transverse velocity is proportional to the transverse force.

[10] For rolling contact, the maximum frictional force is determined using the coefficient of *kinetic* friction $F_S = \mu_k F_N$, because it deals with the transition from partial to complete sliding.

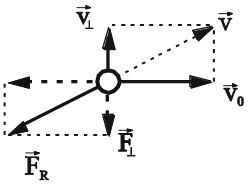

Fig. 10.13 Force and velocity components of a sliding wheel that is acted upon by a small transverse force $F_\perp$.

Problem 4: Belt/Cable Friction. A cable is slung around a pole (Fig. 10.14 a). The angle between the first and last contact points is $\alpha = \varphi_2 - \varphi_1$. The cable is pulled from one end with a force F_2. Determine the force F_1 that is necessary to keep the cable from moving.

Solution: We consider an infinitely small element of the cable (Fig. 10.14 b). Equilibrium of forces on the element yields

$$F(\varphi + d\varphi) - F(\varphi) - dF_R = 0$$

or

$$\frac{dF}{d\varphi} d\varphi - dF_R = 0 .$$

In the perpendicular direction, we have

$$dN - F d\varphi = 0 .$$

Here, dN is the reaction force acting on the element and dF_R is the frictional force acting on the element. The cable does not slide only up to the point when the frictional force reaches its maximum value $dF_R = \mu dN$. From these three equations, we obtain

$$\frac{dF}{d\varphi} = \mu F .$$

After separating the variables, $dF / F = \mu d\varphi$, and integrating, we obtain $\ln F\big|_{F_1}^{F_2} = \mu(\varphi_2 - \varphi_1) = \mu\alpha$. It then follows that

$$F_2 = F_1 e^{\mu\alpha} \text{ or } F_1 = F_2 e^{-\mu\alpha} .$$

Numerical Example: For $\mu = 0.4$, $\alpha = 2\pi$ (a full loop), $F_2 \approx 12 \cdot F_1$. For two loops, we would have $F_2 \approx 152 \cdot F_1$.

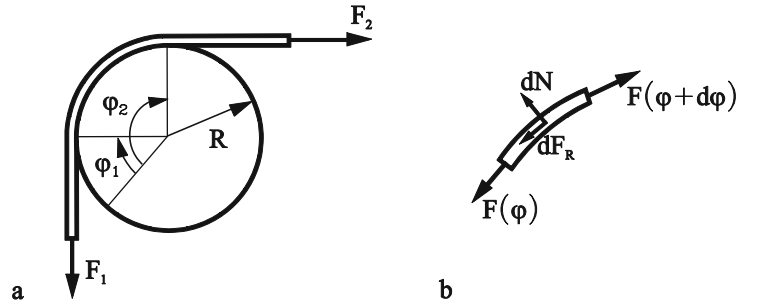

Fig. 10.14 A cable slung around a pole as well as the corresponding free-body diagram of an infinitesimal cable element.

Problem 5: A cylindrical tank (radius R) is filled with sand. Let the coefficient of friction of the sand on the wall be μ. Determine the pressure in the sand as a function of height.

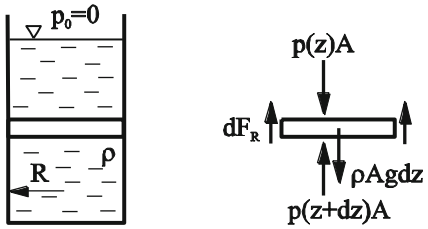

Fig. 10.15 Infinitely thin slice from the sand column.

Solution: If the coefficient of friction is not too large, then the pressure in the sand is "almost isotropic" (as it is for a liquid). In this approximation, we consider the force equilibrium of an infinitely thin slice of the sand column (Fig. 10.15):

$$\rho g \pi R^2 dz + \big(p(z) - p(z+dz)\big)\pi R^2 - dF_R = 0$$

or

$$\rho g \pi R^2 dz - \frac{dp}{dz} dz \cdot \pi R^2 - dF_R = 0\,.$$

According to Coulomb's law, the frictional force is $dF_R = \mu p 2\pi R dz$. From the two equations, one obtains

$$\rho g - \frac{dp}{dz} - 2\frac{\mu p}{R} = 0\,.$$

Separating the variables, $dz = \dfrac{dp}{\big(\rho g - 2\mu p / R\big)}$, and integrating yields

$$p = \frac{\rho g R}{2\mu}\left(1 - e^{-\frac{2\mu z}{R}}\right).$$

For large values of z, the pressure reaches the saturation value of $p_\infty = \rho g R / 2\mu$.

Problem 6: Wishbones, which are used to control the front wheels of automobiles, are manufactured using the following method. In the first step, a wishbone is stamped from sheet metal (Fig. 10.16 a). The rubber-metal bearing (Fig. 10.16 b) is pressed into the wishbone in the second step (Fig. 10.16 c). For quality control, the force required in order to once again remove the bearing must be at least 5.5 kN. Calculate the force required to remove the bearing. Which factors influence this force? Use the following data: the height of the cylindrical eyelet $L = 2$ cm, the radius of the eyelet $R = 1.6$ cm, the thickness of the sheet metal $t = 1.6$ mm, the yield strength of the metal $\sigma_c = 300$ MPa, and the coefficient of friction $\mu = 0.16$.

Fig. 10.16 (a) Wishbone with sheet-metal eyelet; (b) Slotted rubber-metal bearing; (c) Finished wishbone with press-fitted bearing.

Solution: The radial stress σ_r working on the eyelet leads to tensile stress in the sheet σ_φ (Fig. 10.17). The interdependence of these stresses is given by the formula for stress in a *thin walled pressure vessel*, $\sigma_\varphi = \sigma_r R / t$. By pressing in the bearing, the sheet metal is plastically deformed: $\sigma_\varphi = \sigma_c$.

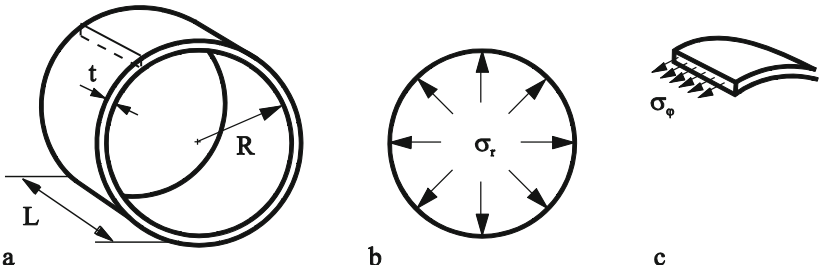

Fig. 10.17 (a) Thin-walled cylinder; (b) Constant radial stress caused by the surface compressions; (c) Circumferential stress σ_φ made visible with a suitable cut.

According to this, the radial stress is

$$\sigma_r = \sigma_c \frac{t}{R}.$$

The maximum static friction is calculated as the product of this stress with the surface of the eyelet, $2\pi RL$, and the coefficient of friction:

$$F_{removal} = 2\pi L \mu \sigma_c t.$$

For the parameters given in the problem statement, the required force to remove the bearing is $F_{removal} \approx 9.6$ kN.

Problem 7: Thermocyclic Creep. A plate of length L lies on a surface with which there is a coefficient of friction of μ. A force F, which is smaller than the force of kinetic friction, acts in the horizontal direction. If the plate is heated, then it expands asymmetrically due to the applied force F relative to the underlying surface. If the temperature is brought back down to its original value, then the plate again contracts. Determine the displacement of the plate after one full thermal cycle (Fig. 10.18).

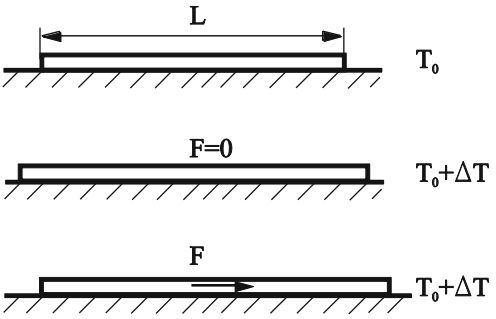

Fig. 10.18 Thermal creep process of a plate on a surface with which there is a coefficient of friction of μ.

Solution: We assume that the plate is sufficiently rigid. If the plate is heated, then it expands symmetrically by the length $\Delta L = \alpha \Delta T L$, its centroid remaining at the same point. If a force F acts on the plate during the heating, then the plate would move asymmetrically. Now, instead of the centroid, the point at a distance Δl to the *left* will remain stationary, because the part of the frictional force that acts to the right must be smaller than that which acts to the left in order for the resultants to be in equilibrium with the force F (Fig. 10.19).

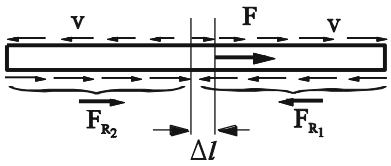

Fig. 10.19 Dynamics of the creep process.

Because the frictional forces oppose the direction of motion, a larger portion of the frictional force must act towards the left than towards the right. So, the equilibrium condition during heating is

$$F - \mu mg\left(\frac{L/2+\Delta l}{L}\right) + \mu mg\left(\frac{L/2-\Delta l}{L}\right) = 0 .$$

From this, it follows that

$$\Delta l = \frac{F}{\mu mg}\frac{L}{2} .$$

Therefore, during heating, the centroid is displaced by

$$u_S = \varepsilon_{th}\Delta l = \frac{FL}{2\mu mg}\alpha\Delta T .$$

During cooling, the centroid moves the *same* distance in the *same* direction: The stationary point must now lie to the *right* of the centroid, because the expansion or contraction direction and the direction of the frictional forces are exactly opposite. The total displacement during the cycle is, therefore, equal to

$$u_{tot} = \frac{FL}{\mu mg}\alpha\Delta T .$$

The displacement is proportional to the force, even for very small forces. Similar processes at the interface between phases with different thermal expansion coefficients are the cause of the thermocyclic creep of multi-phase materials and composites.

Problem 8: Determine the coefficient of static friction of a corrugated surface with a maximum slope of $\mu_1 = \tan\theta_1$ (Fig. 10.20) in the presence of "microscopic" friction which is characterized by a coefficient of friction of μ_0.

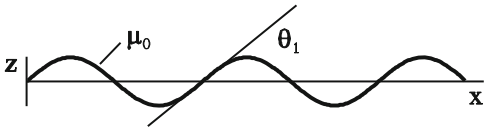

Fig. 10.20 Corrugated surface with coefficient of friction μ_0.

Solution: We can form the following equilibrium equations (for the x' and z' directions), based on the diagram shown in Fig. 10.21:

$$F_N \cos\theta_1 + F\sin\theta_1 = R\,,$$

$$F_N \sin\theta_1 + \mu_0 R = F\cos\theta_1\,.$$

From which, it follows that

$$\mu = \frac{F}{F_N} = \frac{\mu_0 + \mu_1}{1-\mu_0\mu_1}\,.$$

Notice that this "superposition law" has a simple geometric interpretation for coefficients of friction on different scales, meaning that the friction angles on these scales are summed. Actually, when we write $\mu_1 = \tan\theta_1$, $\mu_0 = \tan\theta_0$ and $\mu = \tan\theta$ with $\theta = \theta_1 + \theta_2$, we come to the same conclusion

$$\mu = \tan\theta = \frac{\sin(\theta_0+\theta_1)}{\cos(\theta_0+\theta_1)} = \frac{\sin\theta_0\cos\theta_1 + \cos\theta_0\sin\theta_1}{\cos\theta_0\cos\theta_1 - \sin\theta_0\sin\theta_1} = \frac{\tan\theta_0 + \tan\theta_1}{1-\tan\theta_0\cdot\tan\theta_1} = \frac{\mu_0+\mu_1}{1-\mu_0\mu_1}\,.$$

Hence, we can formulate the following general rule to superimpose coefficients of friction on different scales:

$$\mu_{tot} = \tan\left(\sum_i \arctan\mu_i\right),$$

where μ_i are the coefficients of friction on various spatial scales.

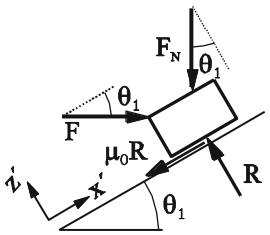

Fig. 10.21 Free-body diagram of a body on a corrugated surface with friction.

Problem 9: Two disks with masses m_1 and m_2 and coefficients of kinetic friction of μ_1 and μ_2 are connected by a massless rigid rod of length l (Fig. 10.22). Determine the conditions under which the sliding of the system in the direction of the rod is stable.

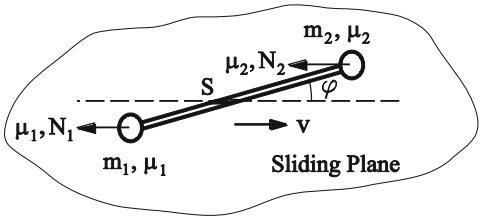

Fig. 10.22 Two disks connected with a light, rigid rod.

Solution: We assume that the orientation of the rod with respect to the sliding direction is deflected by a small angle φ and we calculate the component of the moment that attempts to turn the rod in the sliding plane. The movement is stable when the moment is negative so that the angle φ decreases, while a positive moment leads to an increase in the angle. We will call the distances from the disks to the centroid a_1 and a_2:

$$a_1 = \frac{m_2}{m_1 + m_2} l, \qquad a_2 = \frac{m_1}{m_1 + m_2} l .$$

The normal forces N_1 and N_2 are defined as

$$N_1 = m_1 g, \qquad N_2 = m_2 g .$$

The total moment of the frictional forces with respect to the centroid S is equal to

$$M^{(s)} = \left(-\mu_1 N_1 a_1 + \mu_2 N_2 a_2\right) \sin\varphi = \left(-\mu_1 + \mu_2\right) \frac{m_1 m_2}{m_1 + m_2} g l \sin\varphi .$$

The moment is negative and the movement is stable when

$$\mu_1 > \mu_2 .$$

Therefore, the system is stable when the disk with the smaller coefficient of friction slides in front. Otherwise, the system is unstable: the rod turns and eventually slides with the disk with the smaller coefficient of friction at the front.

11 The Prandtl-Tomlinson Model for Dry Friction

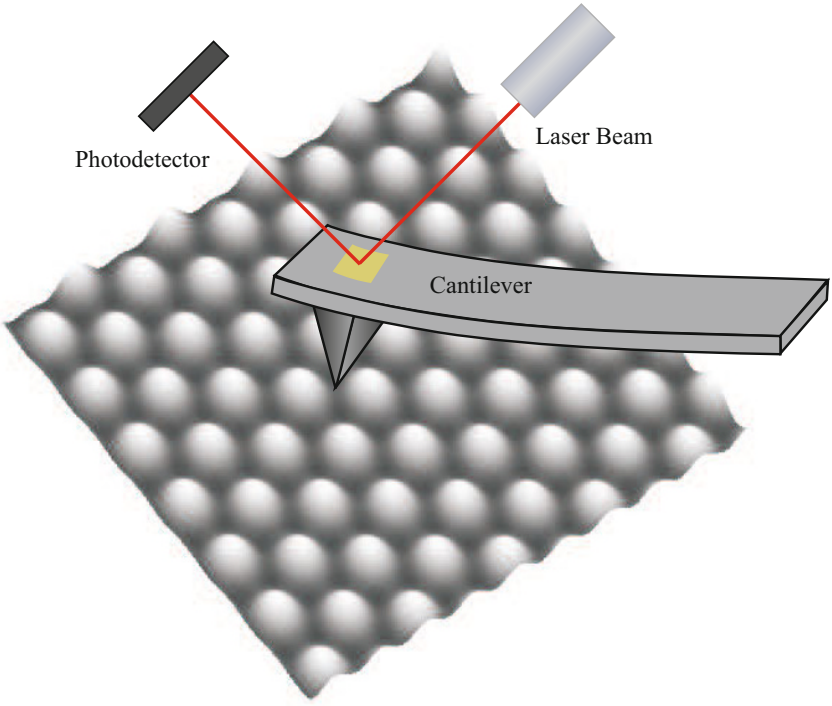

11.1 Introduction

The development of experimental methods to investigate frictional processes on the atomic scale and numerical simulation methods has heralded in a drastic growth in the number of studies in the area of friction of solid bodies on the atomic scale. A simple model, known as the "Tomlinson model," can be used as the basis for many investigations of frictional mechanisms on the atomic scale. It was suggested by Prandtl in 1928 to describe the plastic deformations in crystals[1]. The paper by Tomlinson[2] that is often cited in this context did not contain the model today known as the "Tomlinson model" and suggests an adhesive contribution to friction. In the following, we will call this model the "Prandtl-Tomlinson model."

[1] L. Prandtl, Ein Gedankenmodell zur kinetischen Theorie der festen Körper. ZAMM, 1928, Vol. 8, p. 85-106.

[2] G.A. Tomlinson, A molecular theory of friction. The London, Edinburgh, and Dublin philosophical magazine and journal of science, 1929, Vol. 7 (46 Supplement), p. 905.).

V.L. Popov, *Contact Mechanics and Friction*,
DOI 10.1007/978-3-662-53081-8_11

Prandtl considered the one dimensional movement of a point mass in a periodic potential with the wave number k being acted upon by an external force and being damped proportional to velocity[3] (Fig. 11.1):

$$m\ddot{x} = F - \eta\dot{x} - N\sin kx\,. \tag{11.1}$$

Here, x is the coordinate of the body, m its mass, F the external force acting upon it, η the damping coefficient, N the amplitude of the periodic force, and k the wave number.

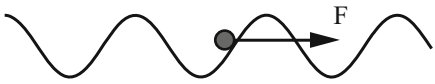

Fig. 11.1 Prandtl-Tomlinson model: A point mass in a periodic potential.

The model from Prandtl-Tomlinson describes many fundamental properties of dry friction. Actually, we must apply a minimum force to the body so that a macroscopic movement can even begin. This minimum force is none other than the macroscopic force of static friction. If the body is in motion and the force reduced, then the body will generally continue to move, even with a smaller force than the force of static friction, because it already possesses a part of the necessary energy due to its inertia. Macroscopically, this means that the kinetic friction can be smaller than the static friction, which is a frequently recurring characteristic of dry friction. The force of static friction in the model in Fig. 11.1 is equal to N.

The success of the model, variations and generalizations of which are investigated in innumerable publications and are drawn on to interpret many tribological processes, is due to the fact that it is a simplistic model that accounts for two of the most important fundamental properties of an arbitrary frictional system. It describes a body being acted upon by a periodic conservative force with an average value of zero in combination with a dissipating force which is proportional to velocity. Without the conservative force, no static friction can exist. Without damping, no macroscopic sliding frictional force can exist. These two essential properties are present in the Prandtl-Tomlinson model. In this sense, the Prandtl-Tomlinson model is the simplest usable model of a tribological system. Essentially, the Prandtl-Tomlinson model is a restatement and further simplification of the view of Coulomb about the "interlocking" of surfaces as the origin of friction.

Obviously, the model cannot represent all of the subtleties of a real tribological system. For instance, there is no change of the surface potential caused by wear in this model. It should be noted, however, that it is fundamentally possible to expand the model to take plastic deformations into account. In this context, it should be mentioned once more that the model from L. Prandtl in 1928 was proposed precisely to describe plastic deformations in crystals.

[3] In this way, for example, the movement of the tip of an atomic force microscope over a crystalline surface can be described.

In this chapter, we investigate the Prandtl-Tomlinson model as well as several applications and generalizations of it.

11.2 Basic Properties of the Prandtl-Tomlinson Model

If a body is at rest and a force F is applied to it, then its equilibrium position moves to the point x, which satisfies the equation

$$F = N \sin kx . \tag{11.2}$$

This equation has a solution only when $F \leq N$. So, the force of static friction, in this model, is equal to

$$F_s = N . \tag{11.3}$$

For a larger force, no equilibrium is possible and the body enters into macroscopic motion[4]. In this model, every macroscopic movement of the body, from a microscopic point of view, is a superposition of a constant speed and a periodic oscillation, as is shown in Fig. 11.2 a. In this figure, the results of the numerical integration of Equation (11.1) are presented. The tangential force changes slowly from zero to some maximum value larger than the force of static friction and then decreases afterwards. The curve shows the instantaneous speed as a function of the instantaneous force. After the critical force is reached, the body begins to move with a finite velocity. If the force is decreased, the body can continue to move when acted upon by forces smaller than the force of static friction. At a specific critical velocity, the macroscopic movement stops, the body oscillates about a potential minimum, and then comes to a standstill.

On the macroscopic scale, we do not perceive the microscopic oscillations. The movement described above is described from a macroscopic point of view as a quasi-stationary frictional process. The dependence of the average velocity on the applied force is perceived as the *macroscopic law of friction* to a macroscopic observer (Fig. 11.2 b).

[4] Here, we call "macroscopic" the movement of a body in a spatial domain much larger than the potential period. Conversely, we call the length scale smaller than, or comparable to, the wavelength of the potential "microscopic."

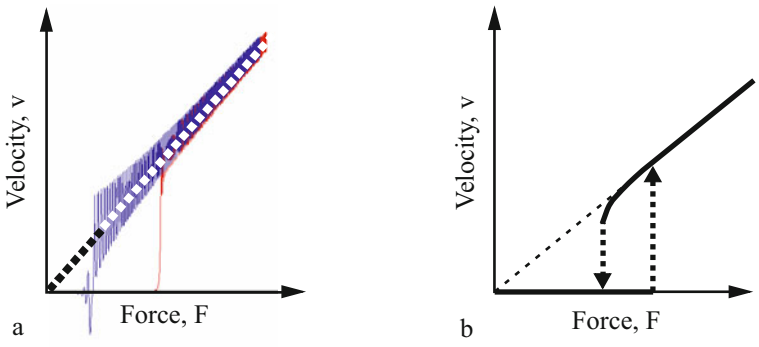

Fig. 11.2 (a) Dependence of instantaneous velocity on the force (increasing linearly with time) in the Prandtl-Tomlinson model. (b) Macroscopic law of friction: dependence of the average velocity on the force.

Case of small damping

If the damping is $\eta = 0$ and the body is put into motion, then it will continue to move indefinitely, even in the absence of an external force ($F = 0$). Thereby, conservation of energy is valid

$$E_0 = \frac{mv^2}{2} - \frac{N}{k}\cos kx = const, \quad \text{for } \eta = 0, \quad F = 0 . \tag{11.4}$$

In this case, the resulting velocity as a function of the x-coordinate is

$$v = \sqrt{\frac{2}{m}\left(E_0 + \frac{N}{k}\cos kx\right)}, \quad \text{for } \eta = 0, \quad F = 0 . \tag{11.5}$$

In the presence of a small damping, a small force must be applied in order to maintain periodic motion. The motion is periodic if the work performed by an external force F over a period of $a = 2\pi / k$ is equal to the energy loss, $\int_0^T \eta v^2(t)dt$:

$$\frac{2\pi F}{k} = \int_0^T \eta v^2(t)dt = \int_0^a \eta v(x)dx = \eta \int_0^a \sqrt{\frac{2}{m}\left(E_0 + \frac{N}{k}\cos kx\right)}dx . \tag{11.6}$$

The smallest force F_1 at which a macroscopic movement still exists is given by (11.6) with $E_0 = N / k$:

$$\frac{F_1}{N} = \frac{4}{\pi}\frac{\eta}{\sqrt{mkN}} . \tag{11.7}$$

The damping at which the force of kinetic friction would be equal to the force of static friction has the order of magnitude of

$$\frac{\eta}{\sqrt{mkN}} \approx 1 \tag{11.8}$$

and indicates the boundary between the considered case with little damping (*under-damped* system) and the case with much damping (*over-damped* system).

Case of large damping
For large damping, one can neglect the inertia term in (11.1):

$$0 = F - \eta\dot{x} - N\sin kx\,. \tag{11.9}$$

This is known as *over-damped* motion. The equation of motion in this case is a first-order differential equation. It can be written in the form

$$\dot{x} = \frac{dx}{dt} = \frac{F}{\eta} - \frac{N}{\eta}\sin kx\,. \tag{11.10}$$

One spatial period is traversed in the time

$$T = \int_0^{2\pi/k} \frac{dx}{\frac{F}{\eta} - \frac{N}{\eta}\sin kx} = \frac{\eta}{kN}\int_0^{2\pi} \frac{dz}{\frac{F}{N} - \sin z} = \frac{\eta}{kN}\frac{2\pi}{\sqrt{\left(\frac{F}{N}\right)^2 - 1}}\,. \tag{11.11}$$

The average speed is, therefore,

$$\overline{v} = \frac{a}{T} = \frac{\sqrt{F^2 - N^2}}{\eta}\,. \tag{11.12}$$

The force, as a function of the average speed, is

$$F = \sqrt{N^2 + \left(\eta\overline{v}\right)^2}\,. \tag{11.13}$$

This dependence is presented in Fig. 11.3.

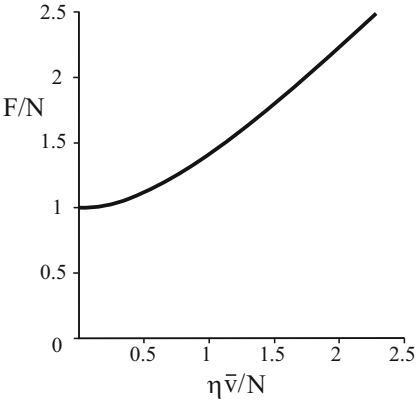

Fig. 11.3 The law of friction for the Prandtl-Tomlinson model in the over-damped case.

The "phase diagram" for the Prandtl-Tomlinson model
In order to investigate the properties of the Prandtl-Tomlinson model for arbitrary parameters, we will introduce the dimensionless variables into (11.1)

$$x = \xi \tilde{x}\,, \quad t = \tau \tilde{t}\,. \tag{11.14}$$

From this, the equation of motion assumes the form

$$\frac{m\xi}{N}\frac{\tilde{x}''}{\tau^2} = \frac{F}{N} - \frac{\eta\xi}{N}\frac{\tilde{x}'}{\tau} - \sin(k\xi\tilde{x})\,, \tag{11.15}$$

where the prime indicates the derivative $\partial / \partial \tilde{t}$. We choose

$$k\xi = 1\,, \quad \tau^2 \frac{N}{m\xi} = 1 \tag{11.16}$$

and write Equation (11.15) in the form

$$\tilde{x}'' + \frac{\eta}{\sqrt{mkN}}\tilde{x}' + \sin\tilde{x} = \frac{F}{N}\,. \tag{11.17}$$

It now only contains two dimensionless parameters,

$$\kappa_1 = \frac{\eta}{\sqrt{mkN}}\,, \quad \kappa_2 = \frac{F}{N}\,. \tag{11.18}$$

In Fig. 11.4, the "phase portrait" of the system is presented. The nature of the motion in the dimensionless coordinates is dependent only on the region in which the system lies on the parameter plane (κ_1, κ_2) in this figure.

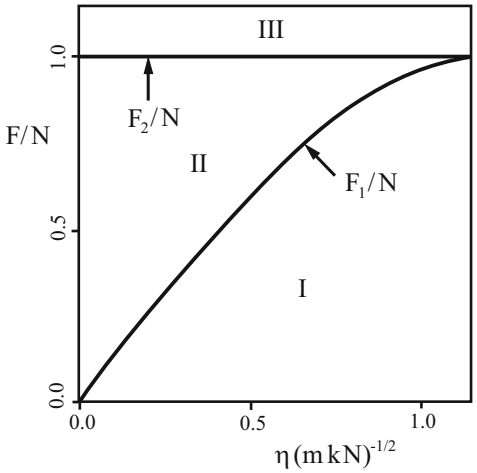

Fig. 11.4 Two critical forces, F_1 and F_2, as a functions of the damping coefficient.

For $\kappa_1 = \dfrac{\eta}{\sqrt{mkN}} < 1.193$, there are three force domains (shown in Fig. 11.4 as I, II and III), which are separated by the critical forces F_1 and F_2. For $F > F_2$, there is no equilibrium solution and the body moves unrestricted. If the force decreases, the body comes to a standstill when $F < F_1$. Between the domains in which only the static state ($F < F_1$) or only motion ($F > F_2$) exist, there is a domain of *bistability*, in which the body can exist in a static state or a state of motion, depending on its initial condition. This domain of bistability does not exist if the damping is larger than a critical value:

$$\frac{\eta}{\sqrt{mkN}} > 1.193 . \tag{11.19}$$

For small damping coefficients, the critical force F_1 is given by (11.7).

11.3 Elastic Instability

The simplest generalization of the Prandtl-Tomlinson model is presented in Fig. 11.5. Instead of being acted upon by a constant force, the body is connected to a spring (stiffness c) which is fastened to a sliding sled that moves in the horizontal direction. This model is more suited to describe the movement of the tip of an atomic force microscope than the original model from Prandtl-Tomlinson, because it takes into account the stiffness of the arm of the microscope in the simplest manner.

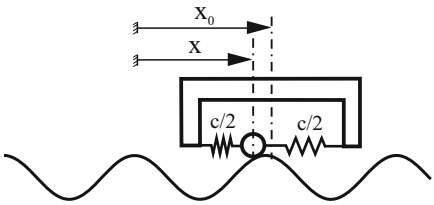

Fig. 11.5 A body in a periodic potential pulled with a spring.

In this case, the equation of motion is

$$m\ddot{x} + \eta\dot{x} + \frac{\partial U}{\partial x} = c(x_0 - x)\,. \tag{11.20}$$

If the sled is pulled slowly with a constant velocity, then the body can be found at every point in time at an equilibrium position $x(x_0)$, where $x_0 = x_0(t)$ is the coordinate of the sled. The average value of the spring force is equal to the (macroscopic) force of friction. If there is only one equilibrium position $x(x_0)$ for *every* x_0, then the average value of the force acting on the body is *exactly zero*. In order to show that, we investigate the total potential energy of the body:

$$U_{tot}(x, x_0) = U(x) + \frac{1}{2}c\left(x - x_0\right)^2. \tag{11.21}$$

The equilibrium position is determined from the condition

$$U'_{tot}(x, x_0) = U'(x) + c\left(x - x_0\right) = 0\,, \tag{11.22}$$

where the prime indicates the derivative $\partial / \partial x$. The average value of this force (over time, which in this case, is the same as over x_0) is equal to

$$\bar{F}_{base} = -\frac{1}{L}\int_0^L U' dx_0\,. \tag{11.23}$$

Here, L is the spatial period of the potential. If we differentiate Equation (11.22), we obtain

$$\left(U''(x) + c\right) dx = c dx_0\,. \tag{11.24}$$

With this, one can replace the integration of (11.23) over dx_0 with integration over dx:

$$\bar{F}_{base} = -\frac{1}{L}\int_0^L U'\left(1 + \frac{U''}{c}\right) dx = -\frac{1}{L}\left[U(x) + \frac{U'^2(x)}{2c}\right]_0^L = 0\,. \tag{11.25}$$

The resulting average force is zero, because both $U(x)$ and $U'^2(x)$ are periodic functions of x. From this, it follows that *the force of friction under these conditions is exactly zero*. This is valid for arbitrarily defined periodic potentials.

The situation changes considerably if the equilibrium coordinate x is a non-continuous function of x_0, so that in some points, Equation (11.24) is not satisfied. As an example, we will investigate the system shown in Fig. 11.5 with a potential of the form

$$U(x) = -\frac{N}{k}\cos kx\,. \tag{11.26}$$

The equilibrium condition (11.22) takes the form

$$-\sin kx = \frac{c}{N}(x - x_0)\,. \tag{11.27}$$

The functions $-\sin kx$ and $\frac{c}{N}(x - x_0)$ are shown in Fig. 11.6 for various x_0. Their intersection indicates the equilibrium coordinate of the body. If $c/Nk > 1$, then x is a continuous function of the coordinate x_0 of the sled, which is illustrated through example calculations in Fig. 11.6 b with $c/Nk = 1.5$. If, on the other hand, the stiffness of the spring is smaller than a critical value:

$$c/Nk < 1\,, \tag{11.28}$$

then the dependence of the equilibrium coordinate on x_0 has jump discontinuities (Fig. 11.6 d). In this case, the time-averaged force is not equal to zero. The dependence of the spring force on the coordinate x_0 for the case of a weak spring ($c/Nk = 0.1$) is presented in Fig. 11.7.

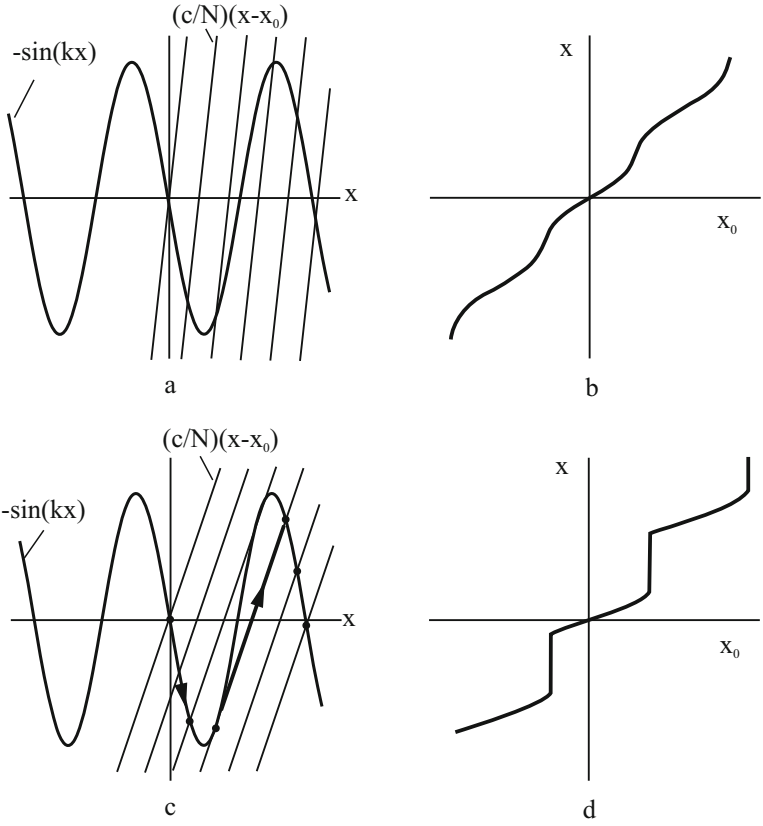

Fig. 11.6 The functions $-\sin kx$ and the linear function $\frac{c}{N}(x-x_0)$ are plotted in (a) for $c/Nk=1.5$ and in (c) for $c/Nk=0.5$. If x_0 increases, the linear function shifts to the right. The equilibrium coordinate is a continuous function of x_0, when $c/Nk>1$ (b) and has jump discontinuities when $c/Nk<1$ (d).

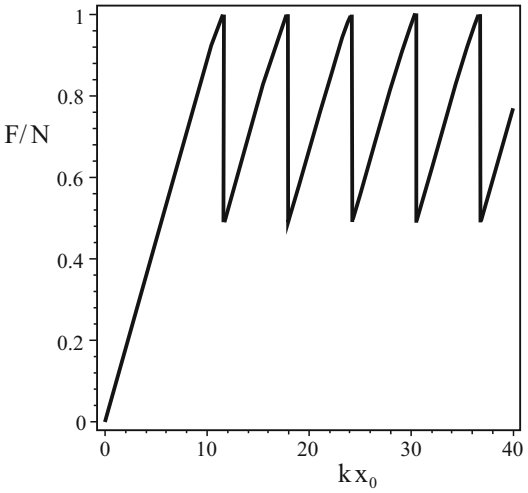

Fig. 11.7 Dependence of the force acting on the body in model (11.20) as a function of the coordinate of the sliding sled x_0 for the case $c/Nk = 0.1$. Because of the emergence of elastic instabilities, the average value of the force is not equal to zero.

11.4 Superlubricity

Experimental and theoretical investigations in recent years have led to the conclusion that in an "atomically close" contact between two crystalline solid bodies, it is possible to have no friction, provided that the periods of the crystal lattices are incompatible (as shown in Fig. 11.8). An additional requirement is that no elastic instabilities may appear in the contact between both bodies. The cause for the absence of static friction is that the atoms of one of the crystal lattices are placed in all possible relative energy states in relation to the other lattice. Therefore, the movement of the body leads merely to another distribution of the atoms that sit in the positions of low and high energy, but it causes no change in the average (macroscopic) energy of the body. Because of this, even an infinitesimally small force can put the body into motion.

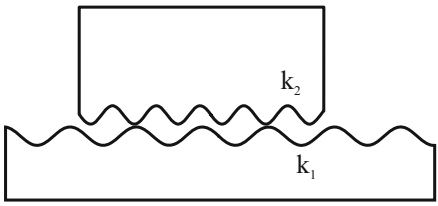

Fig. 11.8 Contact between two periodic surfaces (e.g. two crystals) with different lattice periods.

These considerations are, of course, independent of the scale. They are valid for the contact between two macroscopic structured surfaces, for example, between corrugated rubber base and a corrugated steel plate. *As long as the periods of the structures of both surfaces are different and no elastic instabilities occur, the structures give no contribution to static friction.*

11.5 Nanomachines: Concepts for Micro and Nano-Actuators

Because of the tendency to miniaturize mechanical devices, one must ask oneself the question of what the theoretical limit of miniaturization is. An important aspect thereby is whether or not it is possible to transfer thermal or chemical potential energy into the energy of directional movement even on the smallest, atomic scales. Many researchers have taken the motion of the so-called motor protein along periodically built microfibers as an example for many investigations on nano-machines. All motor proteins have a similar structure consisting of two "heads" and a connecting element. The length of the connection can be changed through the burning of "energy molecules." By heating the protein molecule, it transforms from a globular state to that of a random coil, whereby the length of the bond increases. After cooling, the bond again takes its original length.

Most of the methods to produce directed motion of microscopic or molecular objects which are discussed in literature are based on the interactions between a moving object and a heterogeneous, and in most cases periodic, substrate. The driven object can consist of one or more bodies whose separation distances are controllable. The underlying substrate can be symmetric as well as asymmetric. For non-symmetric bases, one uses the "ratchet-and-pawl" principle[5]. A directional movement, however, is also possible in symmetric potentials[6].

In this section, we will illustrate the idea behind nano-machines using the example of a "three-body machine." From a mathematical point of view, we are dealing with the movement of a multi-body system in a (spatially) periodic potential which is a simple generalization of the Prandtl-Tomlinson model.

Below, we show how controlling the length of the connections between the bodies in a periodic potential can lead to a directional movement of the system for which the movement direction as well as speed are arbitrarily controllable.

---

[5] These machines are often just called "ratchets."

[6] A general classification of various oscillation-based methods for actuation on micro- and nano-scales can be found in: V.L. Popov, R. Wetter, Symmetry breaking as a general design principle of oscillation-based methods for fixation and manipulation of nano-objects, Advanced Biomaterials and Devices in Medicine, 2016, v. 3, No. 1, pp. 10-18.

Singular points and bifurcation sets of a three-body machine

We consider a mass point in a periodic potential (Fig. 11.9) that is connected by two massless rods of lengths l_1 and l_2. The potential energy of the system is equal to

$$U = U_0\left(\cos(k(x-l_1)) + \cos(kx) + \cos(k(x+l_2))\right), \tag{11.29}$$

where $k = 2\pi / a$ is the wave number and a is the spatial period of the potential. The potential energy can be rewritten in the form

$$U = U_0\sqrt{\left(\sin kl_1 - \sin kl_2\right)^2 + \left(1 + \cos kl_1 + \cos kl_2\right)^2}\,\cos(kx - \varphi), \tag{11.30}$$

where

$$\tan\varphi = \frac{\sin kl_1 - \sin kl_2}{1 + \cos kl_1 + \cos kl_2}. \tag{11.31}$$

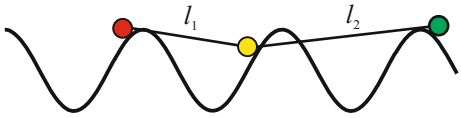

Fig. 11.9 Three-body machine.

The phase φ is a continuous function of the parameters l_1 and l_2 over an arbitrary path on the parameter plane (l_1, l_2), as long as this path does not cross any *singular points*, in which the amplitude of the potential (11.30) approaches zero and the phase (11.31) is undefined. The position of these points is determined by the conditions

$$\sin kl_1 - \sin kl_2 = 0 \tag{11.32}$$

and

$$1 + \cos kl_1 + \cos kl_2 = 0. \tag{11.33}$$

From this, it follows that

$$kl_1 = \pi \pm \pi/3 + 2\pi n, \quad kl_2 = \pi \pm \pi/3 + 2\pi m, \tag{11.34}$$

where m and n are integers. The position of singular points on the (l_1, l_2)-plane is shown in Fig. 11.10. All of these points can be obtained by periodically repeating the two points $(kl_1, kl_2) = (2\pi/3, 2\pi/3)$ and $(kl_1, kl_2) = (4\pi/3, 4\pi/3)$ as multiples of 2π.

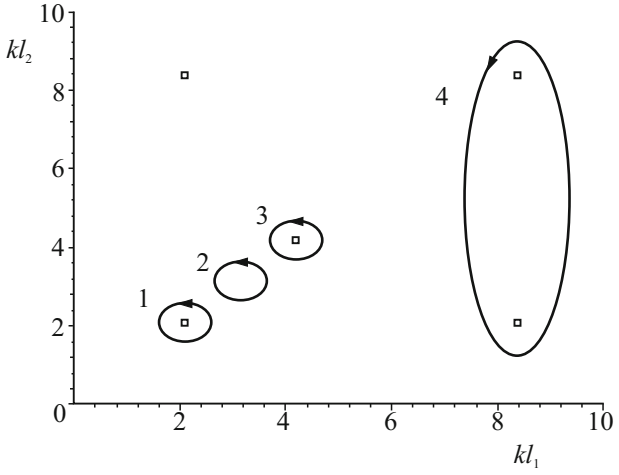

Fig. 11.10 Positions of singular points of a "three-body machine."

Conditions for controlled directional motion

Now, we assume that the lengths l_1 and l_2 are arbitrarily controllable. When they change so that one singular point in Fig. 11.10 is encircled by a closed path (path 1), then the phase is decreased by 2π. By closing a loop about a second point (path 3), it is increased by 2π. We assign the first point the topological index -1 and the second point the index +1. Generally, the phases of a closed-path on the (l_1, l_2)-plane change by $2\pi i$, where i is the sum of the indices of all of the points enclosed by the path. Path 2 in Fig. 11.10, for example, surrounds no singular point. Therefore, the phase does not change along the path. Path 4 surrounds two points with the index -1 and, therefore, the phase changes by -4π over the complete path. A phase change of 2π corresponds to the movement of the three-body machine over one spatial period.

A periodic change in the rod lengths l_1 and l_2 on a path which encloses singular points with the non-zero sum of the topological indices leads to directional motion of the system. If a path in the (l_1, l_2)-plane is traversed at an angular frequency of ω, then the system would move at the macroscopic (average) velocity $v = \dfrac{\omega i}{k}$.

An interesting question is if this "machine" can move even when being opposed by an external force and, therefore, be used to carry loads. In order to answer this question, we allow an external force of $-F$ to act on the system. This leads to an additional term Fx in the potential energy so that the total potential energy assumes the form

$$U_{tot} = U_0 \left(\cos(k(x-l_1)) + \cos(kx) + \cos(k(x+l_2))\right) + Fx \,. \tag{11.35}$$

We determine the bifurcation set (also called the "catastrophe set") for this potential. The bifurcation set is understood to be the parameter set for which the number of equilibrium points of the potential changes and, therefore, the equilibrium position is generally no longer a continuous function of the parameters l_1 and l_2. It is determined by two conditions:

$$\frac{\partial U_{tot}}{\partial x} = 0 \tag{11.36}$$

and

$$\frac{\partial^2 U_{tot}}{\partial x^2} = 0 \,. \tag{11.37}$$

The first condition means that we are dealing with an equilibrium position. The second condition indicates that it is exactly the moment in which the equilibrium loses its stability. In our case, (11.36) yields

$$\frac{\partial U_{tot}}{\partial x} = U_0 k \left(-\sin(k(x-l_1)) - \sin(kx) - \sin(k(x+l_2))\right) + F = 0 \tag{11.38}$$

and (11.37)

$$\frac{\partial^2 U_{tot}}{\partial x^2} = U_0 k^2 \left(-\cos(k(x-l_1)) - \cos(kx) - \cos(k(x+l_2))\right) = 0 \,. \tag{11.39}$$

By applying the addition theorems of trigonometry and subsequently summing the squares, this equation can be written in the form

$$\left(1 + \cos kl_1 + \cos kl_2\right)^2 + (\sin kl_1 - \sin kl_2)^2 = \left(F / U_0 k\right)^2 . \tag{11.40}$$

The bifurcation set determined by this equation is shown in Fig. 11.11 for 4 different values of the parameter $f = F / U_0 k$. A translational movement is induced when the lengths l_1 and l_2 vary over a closed path that completely surrounds a closed bifurcation set so that the phase in every point remains a continuous function of l_1 and l_2. This is obviously only possible for $f < 1$. The maximum driving force is, therefore, equal to $F_{\max} = U_0 k$.

With certain special variations in time of the lengths of l_1 and l_2, the directional motion of the system can be especially clearly seen. By choosing

$$l_1 = (4/3)\pi / k + l_0 \cos(\omega t) \text{ and } l_2 = (4/3)\pi / k + l_0 \cos(\omega t + \varphi) \tag{11.41}$$

with

$$\varphi = (2/3)\pi \tag{11.42}$$

and $l_0 \ll 1/k$, the potential energy (11.29) takes the following form:

$$\begin{aligned} &U_0 k l_0 \left[\sin(kx+\pi/3)\cos(\omega t+2\pi/3)-\sin(kx-\pi/3)\cos\omega t\right] \\ &= U_0 k l_0 \left(\sqrt{3}/2\right)\cos(kx+\omega t+\pi/3)\ . \end{aligned} \tag{11.43}$$

This is a periodic profile that propagates at a constant velocity ω/k in the negative x-direction. The system moves together with the potential wave in one of its minima.

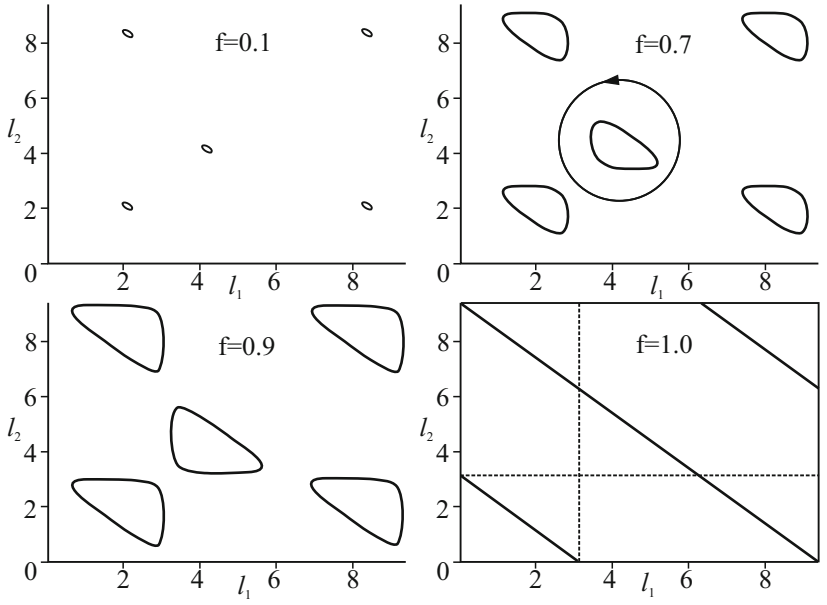

Abb. 11.11 Bifurcation sets of the potential (11.35) for various external forces $f = F/U_0 k$. Directional motion is possible as long as the bifurcation sets form closed forms that can be surrounded by a path without it intersecting them.

The ideas discussed in this section are used actively in nano-tribology in order to describe, among others things, the molecular motors in cells, muscular contraction, and the design of nano-motors.

Problems

Problem 1: Investigate a somewhat modified Prandtl-Tomlinson model: a point mass m moves under the applied force F in a periodic potential that is formed by repeating the domain of a parabola shown below (Fig. 11.12):

$$U(x) = \frac{1}{2}cx^2 \text{ for } -\frac{a}{2} \le x \le \frac{a}{2}$$

with

$$U(x+a) = U(x).$$

Furthermore, there is damping proportional to velocity with the damping coefficient η. Determine: (a) the force of static friction, (b) the minimum velocity at which macroscopic movement ceases, (c) the force of kinetic friction as a function of the average sliding velocity and damping, and (d) the "phase diagram" of a system similar to the classical Prandtl-Tomlinson model.

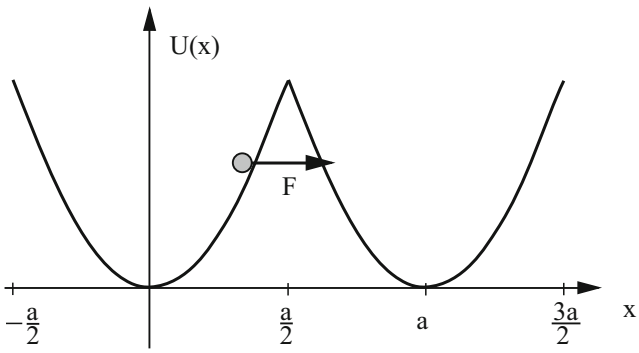

Fig. 11.12 Modified Prandtl-Tomlinson model with parabolic potential.

Solution: The force of static friction is equal to the maximum slope of the potential, which is reached at the end of the period (e.g. at $x = a/2$):

$$F_s = \frac{ca}{2}.$$

The equation of motion within the period of the potential is

$$m\ddot{x} + \eta\dot{x} + cx = F.$$

The minimum force at which macroscopic movement still exists obviously corresponds to the situation at which the body starts moving (at $x = -a/2$ with a velocity $\dot{x} = 0$) and stops (at $x = a/2$ with the velocity $\dot{x} = 0$ again). This is exactly half of one damped oscillation period in a parabolic potential. The vibration frequency of damped oscillations is generally known to be equal to

$$\omega^* = \sqrt{\omega_0^2 - \delta^2}$$

with $\omega_0^2 = c/m$ and $\delta = \eta/2m$. According to this, a spatial period of the potential is repeated after the time

$$T = \frac{\pi}{\omega^*}.$$

The smallest average velocity possible for a steady state unbounded movement is equal to

$$v_{\min} = \frac{a}{T} = \frac{a\omega^*}{\pi} = \frac{a}{\pi}\sqrt{\frac{c}{m} - \left(\frac{\eta}{2m}\right)^2}.$$

The minimal force at which macroscopic movement is still possible can be established most easily by using the following considerations. The total potential energy of the body, taking into account the external force F, is equal to

$$U = \frac{cx^2}{2} - Fx = \frac{c}{2}\left[\left(x - \frac{F}{c}\right)^2 - \left(\frac{F}{c}\right)^2\right].$$

The change in the potential energy between the point $x = -a/2$ and the minimum potential energy is $\Delta U_0 = \frac{c}{2}\left(\frac{a}{2} + \frac{F}{c}\right)^2$, and the change in the potential energy between the minimum and the point $x = a/2$ is $\Delta U_1 = -\frac{c}{2}\left(\frac{a}{2} - \frac{F}{c}\right)^2$. At the minimum force, the body traverses exactly half of the damped oscillation period: from $-a/2$ to $a/2$. It is known from vibration theory that the energy of a damped oscillation decreases exponentially according to $e^{-2\delta t}$. The ratio of the aforementioned energies is, therefore, $e^{-2\delta T}$:

$$\left(\frac{a - 2F/c}{a + 2F/c}\right)^2 = e^{-2\delta T}.$$

From this, it follows that

$$F = \frac{ac}{2}\frac{1 - e^{-\delta T}}{1 + e^{-\delta T}} = F_s\frac{1 - e^{-\delta T}}{1 + e^{-\delta T}}$$

with

$$\delta T = \frac{\pi\eta}{\sqrt{4mc - \eta^2}} = \frac{\pi}{\sqrt{\frac{4mc}{\eta^2} - 1}}.$$

The dependence of the normalized force F/F_s on the dimensionless parameter $\eta/\sqrt{4mc}$ is shown in Fig. 11.13.

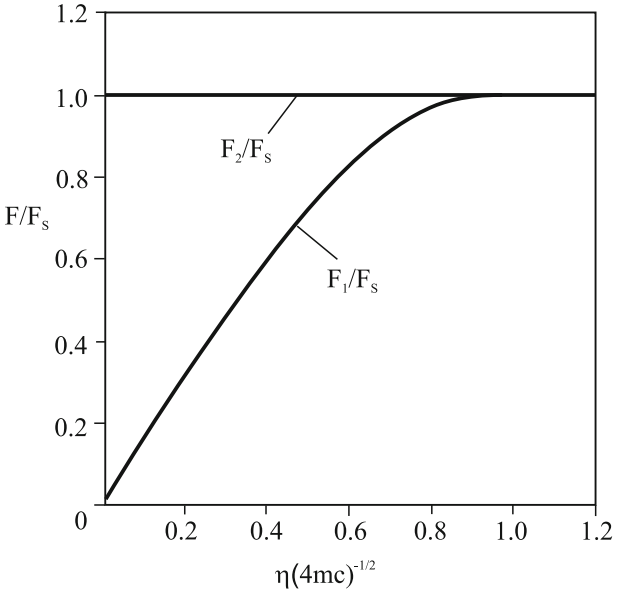

Fig. 11.13 Phase diagram of a modified Prandtl-Tomlinson model with parabolic sections with two critical forces F_1 and F_2.

Problem 2: A point mass is coupled with a rigid slide, by means of springs which have a "vertical stiffness" $c_\perp$ and a "tangential stiffness" $c_\parallel$[7]. It is placed on a sinusoidal profile ($y = h_0 \cos kx$) as shown in Fig. 11.14. Then, the slide moves to the right. Determine the conditions required for elastic instabilities to occur in this system.

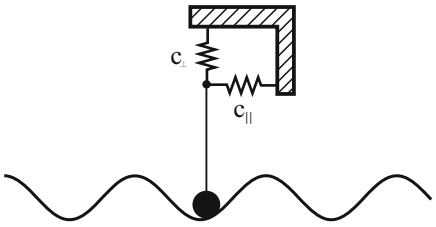

Fig. 11.14 A body that is elastically coupled in the vertical and horizontal directions sliding on a corrugated surface.

Solution: The potential energy of the system is equal to

$$U(x, y, x_0, y_0) = \frac{c_\perp}{2}(y - y_0)^2 + \frac{c_\parallel}{2}(x - x_0)^2 .$$

[7] This model can describe, for example, an element of the elastic profile of a rubber sole.

For the system described in the problem statement, the relationships $y = h_0 \cos kx$ and $y_0 = -h_0$ are valid. The potential energy assumes the form

$$U(x, x_0) = \frac{c_\perp}{2}\left(h_0 \cos kx + h_0\right)^2 + \frac{c_\parallel}{2}\left(x - x_0\right)^2 .$$

The condition for an elastic instability to occur is

$$\frac{\partial^2 U}{\partial x^2} = -c_\perp h_0^2 k^2 \left[\cos kx + \cos 2kx\right] + c_\parallel = 0 .$$

This equation has solutions and, therefore, the system exhibits instabilities when

$$c_\parallel < 2c_\perp h_0^2 k^2 .$$

12 Frictionally Induced Vibrations

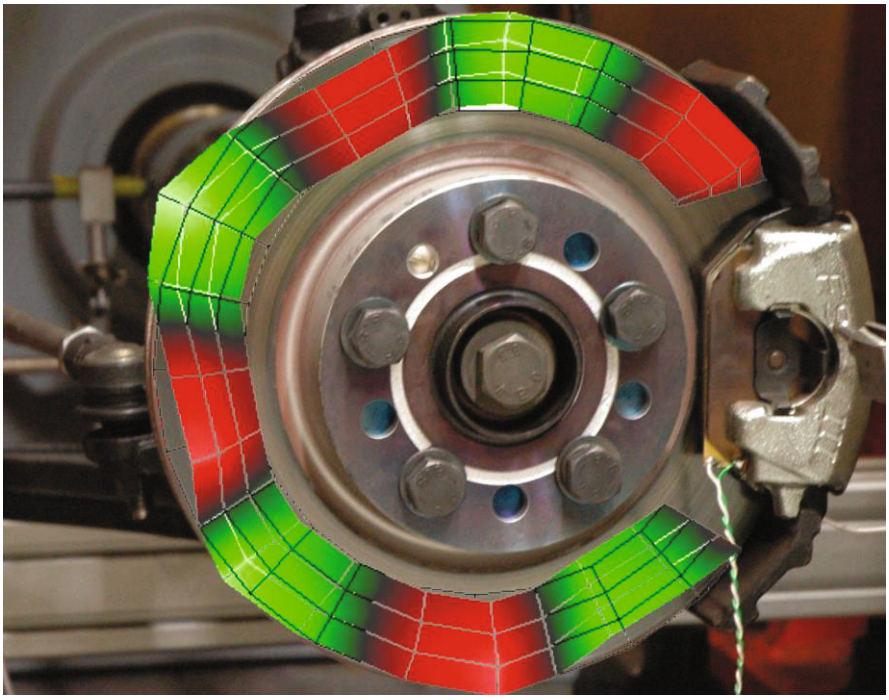

From a system dynamics point of view, technical systems with friction are nonlinear dissipative open systems. Even if it is possible for a system to be in a state of steady motion, it can only practically take place if it is stable relative to small disturbances. Otherwise, the perturbations intensify, resulting in a periodic or chaotic vibration. If the amplitude of the vibrations is large enough for the relative velocity of the surfaces in friction to be occasionally zero, then the movement consists of the alternating phases from rest (stick) to sliding (slip) and is called *stick-slip-movement*.

An instability in the uniform steady-state movement is not, however, the only mechanism for frictionally induced vibrations. Under certain conditions, it is possible for the steady movement of a tribological system to be completely nonexistent. In this case, only an oscillating movement is possible. An example is presented by the so-called *sprag-slip* movement.

The frictional vibrations that occur in many technical frictional systems (brakes, bush bearings, wheel-rail contact, etc.) can on one side lead to higher wear and the formation of unwanted structures on the surface in friction (corrugations on rails, formation of cracks, polygonization of locomotive wheels, washboarding), and on the other side, can lead to subjective uncomfortable sounds or vibrations of a varying nature (chattering, howling, whistling, or squealing). Today, there are still no solutions in many fields for the squealing of brakes or of

V.L. Popov, *Contact Mechanics and Friction*,
DOI 10.1007/978-3-662-53081-8_12

wheels around curves that can be reliably and technically cost-worthily implemented. Even in applications where squealing does not influence the function of a system, some technological processes cannot be used solely due to squeal and its associated comfort disturbances. For this reason, in many areas of bush bearing technology, bearings made from manganese steel, despite their excellent wear resistance, are not used because they cause squealing.

In this chapter, we investigate a few models of frictionally induced vibrations which allow a better understanding of the conditions that produce a stable or unstable movement and practical recommendations to reduce these vibrations.

12.1 Frictional Instabilities at Decreasing Dependence of the Frictional Force on the Velocity

First, we will consider the simplest model of a frictional pair, in which one of the partners is modeled as a rigid plane and the other as a rigid block of mass m. The total elasticity of the system is represented as a spring with the stiffness c. The block is dragged over a rigid surface with a velocity v_0 using a spring-damper combination. It is assumed that the frictional force in the contact area is a function defined for all sliding velocities $F(\dot{x})$. The equation of motion for the block is

$$m\ddot{x} + F(\dot{x}) + \eta\dot{x} + cx = cv_0 t + \eta v_0 , \tag{12.1}$$

where $F(\dot{x})$ is the velocity dependent force of kinetic friction.

The equation (12.1) has a steady-state solution

$$x = x_0 + v_0 t \tag{12.2}$$

with

$$x_0 = -\frac{F(v_0)}{c} . \tag{12.3}$$

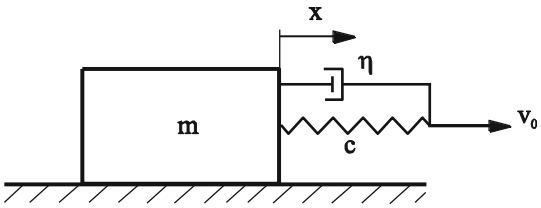

Fig. 12.1 A block is pulled over a surface using a spring-damper combination.

Whether or not the steady-state solution can be realized in an actual process is dependent on the stability of this solution with respect to the existing disturbances.

In order to investigate the stability, we assume that the steady-state solution (12.2) is weakly disturbed:

$$x = x_0 + v_0 t + \delta x \tag{12.4}$$

with $\delta \dot{x} \ll v_0$. Substituting (12.4) into the equation of motion (12.1) and linearizing it with respect to δx, we obtain the following equation for the disturbance:

$$m\delta\ddot{x} + \left(\eta + \left. \frac{dF(\dot{x})}{d\dot{x}} \right|_{\dot{x}=v_0} \right) \delta\dot{x} + c\delta x = 0 . \tag{12.5}$$

This equation describes the oscillations of a body with a mass of m and a spring with a stiffness of c in the presence of damping that is proportional to velocity and having a damping coefficient of

$$\alpha = \eta + \left. \frac{dF(\dot{x})}{d\dot{x}} \right|_{\dot{x}=v_0} . \tag{12.6}$$

Even without formal stability analysis, it is clear that Equation (12.5) with positive damping,

$$\alpha = \eta + \left. \frac{dF(\dot{x})}{d\dot{x}} \right|_{\dot{x}=v_0} > 0, \quad \text{(stable motion)} \tag{12.7}$$

describes a damped oscillation: the steady-state movement is stable. In the opposite case,

$$\alpha = \eta + \left. \frac{dF(\dot{x})}{d\dot{x}} \right|_{\dot{x}=v_0} < 0, \quad \text{(unstable motion)} \tag{12.8}$$

when we are dealing with a *negative damping* and a *divergent* oscillation: the steady-state solution is unstable.

The frequency of the weakly damped oscillation is equal to

$$\omega^* = \sqrt{\omega_0^2 - (\alpha/2)^2} , \tag{12.9}$$

where $\omega_0 = \sqrt{c/m}$ is the undamped natural frequency of the body. For cases of weak damping, $\omega^* \approx \omega_0$.

From this, the following conclusions can be drawn:

I. In a system without damping ($\eta = 0$), the stability criterion is dependent only on the relation of the frictional force to the velocity:
- If the frictional force increases with the sliding velocity, then the sliding motion is stable.
- If the frictional force decreases with velocity, then an instability develops.

If the frictional force decreases with velocity at low velocities and again increases at higher velocities[1], as is shown in Fig. 12.2, then the motion is unstable at low velocities $v < v_{min}$ and stable at higher velocities.

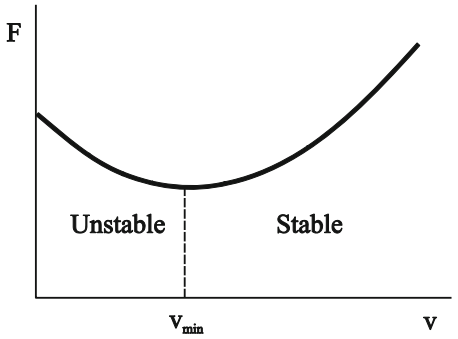

Fig. 12.2 In many tribological systems, the frictional force initially decreases as the velocity increases and then again increases at higher velocities.

II. The characteristic frequency, according to this mechanism of exciting vibrations, is practically determined only by the natural frequency of the "resonator" (of the complete tribological system). This is verified in many tribological systems and machining processes experimentally. Thus, in many cases, all of the parameters of a tribological system, such as its composition, the relative speed of the bodies, and the roughness of the surfaces, influence the intensity of the acoustic emissions with friction, but not their frequency spectrum.

III. This type of instability can be suppressed when sufficiently large damping is introduced into the system: the stability criterion (12.7) is then met at sufficiently large damping even if the derivative $dF / d\dot{x}$ has a negative value.

12.2 Instability in a System with Distributed Elasticity

The model of a sliding body as a rigid mass being pulled by a spring, which was investigated in the last section, is a strong simplification of reality. This poses the question of what influence distributed elasticity has on the condition of stability. It is especially of interest to verify if the introduction of damping to the system can prevent the development of instabilities even if it is introduced "far away" from the frictional surface.

As an initial generalization, we will investigate a system composed of a rigid body and an elastic body[2] (Fig. 12.3). The rigid body moves in the horizontal di-

[1]Such a trend is typical, for example, for lubricated systems during the transition from mixed friction to hydrodynamic friction (Stribeck-Curve).

rection with a constant velocity. An elastic sheet is bound to a rigid base. For the sake of simplicity, we investigate only the shear vibrations in the elastic sheet, meaning that we assume that the displacement field only has an x-component and that this is only dependent on the z-coordinate. The equation of motion is

$$\frac{\partial^2 u}{\partial t^2} = \frac{G}{\rho}\frac{\partial^2 u}{\partial z^2} \tag{12.10}$$

with the boundary conditions

$$G\frac{\partial u}{\partial z}\bigg|_{z=0} = \sigma_{fric}(v_0 - \dot{u}|_{z=0}) \tag{12.11}$$

and

$$u(z=-l)=0\,. \tag{12.12}$$

$\sigma_{fric}(v)$ is the frictional stress (frictional force per unit area), which is assumed to be dependent on the velocity. For weak velocity dependence of the frictional stress, we can expand it in the first order for $\dot{u}$:

$$\sigma_{fric}(v_0 - \dot{u}|_{z=0}) = \sigma_{fric}(v_0) - \frac{d\sigma_{fric}}{dv}\bigg|_{v=v_0} \dot{u}\big(z=0\big)\,. \tag{12.13}$$

The boundary condition (12.11) then assumes the form

$$G\frac{\partial u}{\partial z}\bigg|_{z=0} = \sigma_{Fric}(v_0) - \frac{d\sigma_{Fric}}{dv}\bigg|_{v=v_0} \dot{u}(z=0)\,. \tag{12.14}$$

The solution of the wave equation (12.10) with the boundary conditions (12.12) and (12.14) can be written as the sum

$$u(z,t) = u^{(0)}(z,t) + u^{(1)}(z,t)\,, \tag{12.15}$$

where

$$u^{(0)}(z,t) = \frac{\sigma_{Fric}(v_0)}{G}\big(z+l\big) \tag{12.16}$$

is the static solution of the equation of motion that meets the boundary conditions $u^{(0)}(-l)=0$ and $G\dfrac{\partial u^{(0)}}{\partial z}\bigg|_{z=0} = \sigma_{fric}(v_0)$ and $u^{(1)}(z,t)$ is the solution to the wave equation

[2] A generalization to the contact between two elastic bodies is easily possible; however, it would unnecessarily complicate our examinations.

$$\frac{\partial^2 u^{(1)}}{\partial t^2} = \frac{G}{\rho}\frac{\partial^2 u^{(1)}}{\partial z^2} \tag{12.17}$$

with the boundary conditions

$$G\frac{\partial u^{(1)}}{\partial z}\bigg|_{z=0} = -\frac{d\sigma_{fric}}{dv}\bigg|_{v=v_0} \dot{u}^{(1)}(0) \quad \text{and} \quad u^{(1)}(-l) = 0\,. \tag{12.18}$$

The sum $u^{(0)}(z,t) + u^{(1)}(z,t)$ fulfills the wave equation as well as the boundary conditions (12.12) and (12.14), and is, therefore, the solution to our problem.

If the frictional stress were independent of the velocity ($d\sigma_{fric}/dv = 0$), then $u^{(1)}$ would be the solution to the wave equation for the free vibrations of a sheet fixed on one end and free to move on the other. In the presence of a weak velocity dependence with $d\sigma_{fric}/dv > 0$, we would be dealing with free oscillations of the sheet which is weakly damped at the surface, proportional to velocity. Even without a formal solution of the equation of motion, it is intuitively clear that, in this case, we are dealing with damped oscillations of a layer. Conversely, if the force decreases with the velocity, it means that a weak *negative damping* has been introduced at the surface. In this case, we would be dealing with divergent oscillations. From these considerations, it follows that the stability criteria in the distributed system are the same as in the simple system with a mass and spring. Furthermore, it is clear that the instability can be mitigated by the introduction of damping at an *arbitrary* position in the system. It is only important that for a given form of oscillation, the energy increase due to negative damping (caused by the decreased dependence of the frictional forces on velocity) must be compensated for by positive damping.

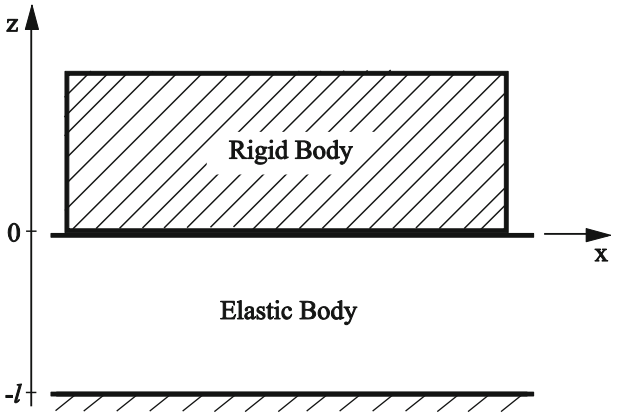

Fig. 12.3 A tribological system consisting of a rigid body and an elastic body. The elastic body is rigidly embedded on the lower surface. The rigid body is dragged in the horizontal direction with a constant velocity v_0.

For weak velocity dependence in a first order approximation, we are dealing with oscillations at the natural frequency of the system, whose amplitude changes only slowly with time (it either increases or decreases depending on which damping – positive or negative – is prevalent in the system). One can consider these oscillations in "d'Alembert's picture" of the natural oscillation as the propagation of an elastic wave, which is reflected multiple times from boundaries of the medium and in doing so loses (positive damping) or gains (negative damping) a certain part of its energy with every reflection. It is clear that the damping is determined by how large the energy loss is for every reflection of the wave on the boundary of the medium.

12.3 Critical Damping and Optimal Suppression of Squeal

Based on the view of d'Alembert of natural oscillations, we can argue that we have a case of "ideal damping" if a wave is *absorbed in its entirety* when it impacts a boundary. We will investigate the conditions under which this is possible.

We consider an elastic sheet whose bottom surface is connected to a rigid base by a damping layer (Fig. 12.4). The stress in this layer should be proportional to the relative velocities between the elastic body and the rigid base. From this, we obtain the boundary condition for the elastic sheet on the lower surface:

$$G\left.\frac{\partial u}{\partial z}\right|_{z=-l} = \beta\left.\frac{\partial u}{\partial t}\right|_{z=-l}, \tag{12.19}$$

where β is the damping coefficient.

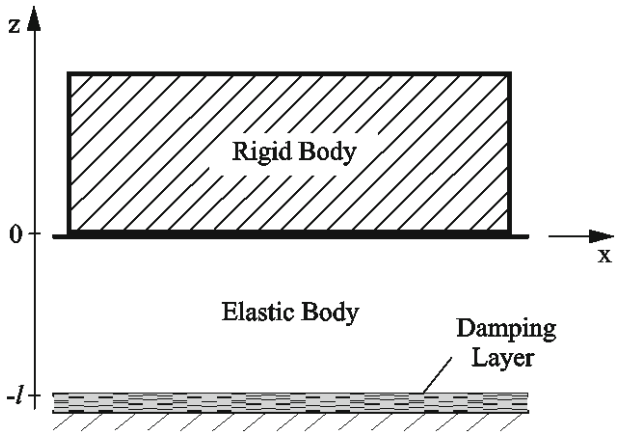

Fig. 12.4 Elastic sheet, which is connected to a rigid base by a damping layer.

The requirement of complete absorption of the wave on the bottom surface means that the equation of motion (12.10) with the boundary condition (12.19) has a solution in the form of a propagating wave in the z-direction:

$$u(z,t) = f(z+ct)\,, \tag{12.20}$$

where $c = \sqrt{G/\rho}$ is the transverse velocity of the elastic wave. By inserting this special solution of the wave equation into the boundary condition (12.19), we obtain

$$\beta = \sqrt{G\rho}\,. \tag{12.21}$$

For this damping there is no reflection of the wave coming from above: Therefore, we have perfect damping. Note that for either a smaller or larger damping coefficient, there is a reflection[3]. In the cases in which $\beta \to 0$ and $\beta \to \infty$, we would actually be dealing with a dissipation free system.

The effect of complete absorption has many applications in physics and technology, the most important of which are listed here:
1. Suppression of squeal.
2. The prevention of acoustic reflections: A so-called "anechoic chamber" should have exactly perfect critical damping on the walls.
3. For molecular dynamics, as well as other numerical simulations, the critical damping at the boundary of the simulation domain must be established in order to suppress the non-physical reflections which are dependent on the size of the simulated domain.
4. In high frequency technologies, the same idea is used to suppress the reflections in waveguides.

We estimate the required parameters of the damping layer that are necessary to suppress squeal in a steel bearing. According to (12.21) for steel ($G \approx 78$ GPa, $\rho \approx 7.8 \cdot 10^3$ kg/m^3), complete damping is achieved with $\beta \approx 2.5 \cdot 10^7$ Pa·s/m. A 1 cm thick polymer sheet with a viscosity somewhat close to that of thick honey, for example, has such a damping coefficient. Experimental investigations show that the installation of a properly dimensioned polymer sheet actually leads to practically complete suppression of squeal (Fig. 12.5).

[3] See problem 2 of this chapter.

Fig. 12.5 Part of a bush bearing made of manganese steel for which the installation of a correctly dimensioned polymer lining has suppressed squeal.

12.4 Active Suppression of Squeal

Besides passive suppression of squeal by the introduction of damping into the tribological system, it is possible to *actively* suppress the instabilities by the design of an appropriate control loop. We will explain the fundamental ideas behind active suppression of instabilities by investigating the simple model in Fig. 12.6.

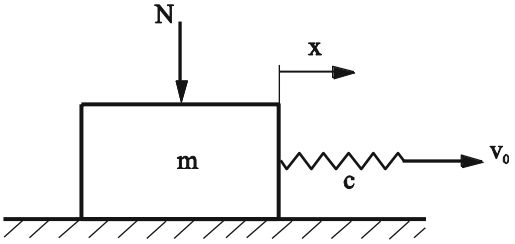

Fig. 12.6 Simple model to illustrate the fundamental ideas behind the active suppression of instabilities.

We assume that the normal force is a periodic function of time with the same frequency as the natural frequency ω_0 of the system:

$$N = N_0 + N_1 \cos(\omega_0 t + \varphi) \tag{12.22}$$

with $N_1 \ll N_0$. For weak damping in a first order approximation, the body experiences free, undamped oscillations with the velocity

$$v = v_0 + v_1 \cos \omega_0 t \,. \tag{12.23}$$

For a qualitative stability investigation, we calculate the change in energy of the moving body over one oscillation period. Thereby we assume that the frictional force can be presented as product of the normal force and the velocity dependent coefficient of friction:

$$F_{fric} = N\mu(v) \,. \tag{12.24}$$

The change in the energy of oscillations is determined by the average power of the frictional force in the reference system that moves with the average velocity v_0:

$$\bar{P} = -\overline{F_{fric} \cdot \left(v - v_0\right)} = -\overline{N\left(\mu_0 + \frac{d\mu}{dv} v\right) \cdot \left(v - v_0\right)} \,. \tag{12.25}$$

Inserting (12.22) and (12.23) into (12.25) yields

$$\begin{aligned} \bar{P} &= -\overline{\left(N_0 + N_1 \cos\left(\omega_0 t + \varphi\right)\right)\left(\mu_0 v_1 \cos \omega_0 t + \frac{d\mu}{dv}\left(v_0 + v_1 \cos \omega_0 t\right) v_1 \cos \omega_0 t\right)} \\ &= -\frac{1}{2} v_1 \left(N_0 v_1 \frac{d\mu}{dv} + N_1 \left(\mu_0 + \frac{d\mu}{dv} v_0\right) \cos \varphi\right) \end{aligned} \tag{12.26}$$

or for weak damping

$$\bar{P} \approx -\frac{1}{2} v_1 \left(N_0 v_1 \frac{d\mu}{dv} + N_1 \mu_0 \cos \varphi\right) . \tag{12.27}$$

If there are no oscillations in the normal force, then the average power would be equal to $-\frac{1}{2} N_0 v_1^2 \frac{d\mu}{dv}$. We would then come to the already known result: for decreasing frictional force as a function of velocity $\left(d\mu / dv < 0\right)$, the energy increases and the process is unstable. By changing the normal force, however, the power can be made negative and, therefore, the oscillations damped. For this to occur, the following condition must be met:

$$N_0 v_1 \frac{d\mu}{dv} + N_1 \mu_0 \cos \varphi > 0 \,. \tag{12.28}$$

This can only be met when $\cos \varphi > 0$, ideally $\cos \varphi = 1$ and therefore $\varphi = 0$. In other words, the normal force (12.22) should oscillate, as far as possible, in phase with the velocity (12.23). This can be realized using a control loop in which the velocity is measured and the normal force is varied proportionally to the measured velocity $\Delta N = \xi\left(\dot{x} - v_0\right)$. In this case, the equation of motion is

$$m\ddot{x} + \left(N_0 + \xi\left(\dot{x} - v_0\right)\right)\mu(\dot{x}) + \eta \dot{x} + cx = cv_0 t + \eta v_0 \,. \tag{12.29}$$

The linearized equation for a small perturbation of the steady-state solution (12.2) is

$$m\delta\ddot{x}+\left(N_0\frac{d\mu}{dv}+\mu_0\xi+\eta\right)\delta\dot{x}+c\delta x=0\,. \tag{12.30}$$

In order for the steady state sliding to remain stable, the total damping in (12.30) must be positive:

$$N_0\frac{d\mu}{dv}+\mu_0\xi+\eta>0\,. \tag{12.31}$$

For decreasing frictional force as a function of velocity, this can be achieved either through sufficiently large damping η or through a sufficiently strong coupling $\mu_0\xi$ between the velocity and the normal force. One can see from Equation (12.31) that the control loop has the same effect as a damper. The advantage of active suppression lies in the simple controllability of a control loop compared to passive damping, whose parameters can only be adjusted by material choice and dimensioning.

12.5 Strength Aspects during Squeal

We want to estimate the stress introduced into a system experiencing squeal in order to determine under what conditions the strength of the material can be compromised. We investigate the system shown in Fig. 12.3. For weak damping, we can find a first order approximation solution to the perturbation equation (12.17) with the boundary conditions

$$G\left.\frac{\partial u^{(1)}}{\partial z}\right|_{z=0}=0 \quad \text{and} \quad u^{(1)}(-l)=0\,. \tag{12.32}$$

The solution for the eigenmode with the smallest natural frequency is

$$u(z,t)=A\sin\left(\frac{\pi}{2l}(z+l)\right)\cdot\sin\frac{\pi c}{2l}t\,, \tag{12.33}$$

where $c=\sqrt{G/\rho}$ is the velocity of the transverse elastic wave. The oscillation amplitude of the velocity $\dot{u}$ is then $\bar{v}=A\frac{\pi c}{2l}$, and that of the stress $G\frac{\partial u}{\partial z}$ is equal to $\bar{\sigma}=AG\frac{\pi}{2l}$. According to this, the following relationship exists between the amplitude of the stress and the amplitude of the velocity:

$$\bar{\sigma} = G\frac{\bar{v}}{c} = \bar{v}\sqrt{G\rho}\,. \tag{12.34}$$

As a rule, the oscillation amplitude of the velocity will have the same order of magnitude as the sliding velocity v_0 in the stationary cycle. The order of magnitude of the stresses in a squealing system can, thus, be estimated with

$$\bar{\sigma} = G\frac{\bar{v}_0}{c} = \bar{v}_0\sqrt{G\rho}\,. \tag{12.35}$$

This is a very general result which remains valid also for oscillations with higher natural frequencies: the stresses in a limit-cycle are essentially only dependent on velocity! The critical velocity, at which the stress reaches the critical shear stress σ_F of the material, is given by

$$v_c = \frac{\sigma_F}{\sqrt{\rho G}}\,. \tag{12.36}$$

For steel with $\sigma_F = 300\ MPa$ (which corresponds to a tensile strength of around 500 MPa), we obtain the critical velocity of $v_0 \simeq 12$ m/s. For larger sliding velocities, the squeal would lead to the failure of a part made of such a steel!

12.6 Dependence of the Stability Criteria on the Stiffness of the System

In the previous section, we considered the mechanisms for the development of instabilities caused only by the decrease of frictional force with velocity. The stability criteria are, in this case, independent of the stiffness of the system. In the example shown in Fig. 12.2, the motion at an average velocity lower than the velocity $v_{\min}$ is always unstable. The stiffness of the system influences the frequency of the frictionally induced oscillations, but not the stability criteria. In practice, however, it is seen that by changing the stiffness of a system, it can be stabilized. This property, which has been established in numerous experimental investigations means that the simple explanation of instabilities being caused by decreasing frictional force with the velocity may not always be correct.

The reason for this, from the mathematical point of view, lies in the invalid assumption that the frictional force is determined only by the instantaneous state of the frictional contact – essentially by the normal force and the sliding velocity. For the force of static friction, this assumption would mean that it always remains constant. Since Coulomb, however, it is known that this is not completely correct. Even if the normal force does not change and the “sliding velocity” remains con-

stant (equal to zero), the force of static friction changes over time. The change can have varying physical causes. In metallic substances, creep processes lead to a change in the real contact area and, thereby, account for the change in the frictional force. In elastomers, it is the viscosity that is responsible for the delayed reaction. In lubricated systems, the film thickness changes with time even with no change in the normal force. Furthermore, the temperature of the contact partners changes, and with it that of the lubricating oil, which also has an impact on the frictional force. The contribution to the frictional force through the building of capillary bridges is also explicitly time dependent.

All of these processes could be described in every individual case by the introduction of additional appropriate variables, called "internal variables," which sufficiently characterize the state of the frictional layer and the intermediate material (also called third body). The idea of internal variables was originally applied to earthquake dynamics by A. Ruina[4]. In some cases, these variables have clear physical meanings (e.g. temperature); in others, empirical experiences are summarized in the internal variables.

We will investigate the simplest phenomenological model that describes the typical dynamics of the "contact state[5]." We once again consider the model shown in Fig. 12.1, which is described by the equation of motion

$$m\ddot{x} + F(\dot{x},\theta) + \eta\dot{x} + cx = cv_0 t + \eta v_0 , \tag{12.37}$$

where the frictional force $F(\dot{x},\theta)$ is now not only dependent on the velocity, but also on the internal state variable θ. For this dependence, we assume

$$F(\dot{x},\theta) = F_k + (F_s - F_k)\theta . \tag{12.38}$$

Here, θ is the internal variable that describes the state of the contact zone and changes from $\theta = 0$, at the initial moment of contact, to $\theta = 1$ after a long time at rest. Consequently, F_s is the force of static friction and F_k, that of kinetic friction. For the variable of state θ, we assume the following simple kinetic equation

$$\dot{\theta} = \left(\frac{1}{\tau}(1-\theta) - \frac{1}{D}\dot{x} \right), \quad 0 < \theta < 1 . \tag{12.39}$$

For vanishing velocity, $\dot{x} = 0$, θ increases with time until a saturation value, $\theta = 1$. If the body is put into motion, then the variable of state decreases faster at higher velocities. The physical meaning of τ in (12.39) is the characteristic relaxation time of the parameter θ when the system is at rest, while D is the characteristic "relaxation length" of this parameter at the initiation of motion. In a physical view of the contact between two rough surfaces, τ can be understood to be the

[4] A. Ruina, Slip Instability and State Variable Friction Laws. Journal of Geophysical Research, 1983, v.88, N.B12, pp. 10359-10370.

[5] A more complicated and realistic rate- and state -dependent frictional law is discussed in Chapter 20.

characteristic time of the creep process and D, as the average contact diameter between two micro-contacts, however, other interpretations are also possible depending on the system.

The system of equations formed by (12.37), (12.38), and (12.39) has a steady-state solution with

$$\dot{x} = v_0 , \tag{12.40}$$

$$\theta = \theta_0 = \begin{cases} 1 - v_0 / v_c, & \text{for } v_0 < v_c, \\ 0, & \text{for } v_0 > v_c, \end{cases} \tag{12.41}$$

$$F = \begin{cases} F_k + (F_s - F_k)(1 - v_0 / v_c), & \text{for } v_0 < v_c, \\ F_k, & \text{for } v_0 > v_c, \end{cases} \tag{12.42}$$

where

$$v_c = D / \tau . \tag{12.43}$$

The dependence of the steady-state frictional force (12.42) on the velocity is presented in Fig. 12.7.

Thus, the system of equations in (12.37)-(12.39) correctly qualitatively reproduces the known properties of friction. The most important of these are the decrease of the frictional force from the static value to the kinetic value within some velocity interval as well as the growth of the force of static friction with time after the body is at rest.

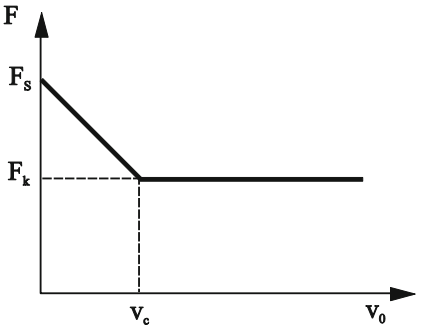

Fig. 12.7 Steady-state frictional force as a function of the sliding velocity according to Equation (12.42).

If we use the dependence of the frictional force on the sliding velocity (12.42) in a steady-state sliding process for a stability analysis, we would come to the conclusion that sliding at $v_0 < v_c$ is unstable. In reality, this conclusion is only valid if the oscillation time is much larger than the characteristic relaxation time τ, because only under this premise can the dependence (12.42) be used for dynamic processes as well. From this, it follows that at *sufficiently small stiffnesses,* and the

correspondingly large oscillation periods, sliding is unstable in reality. Conversely, for large stiffnesses, and the correspondingly small oscillation periods, the parameter θ has no time to change. The frictional force is then, according to (12.38) , completely independent from the velocity, and instability does not occur. In order to investigate the stability of the steady-state solution (12.40)-(12.42) in the generalized case and to obtain the stability limit, dependent on the sliding velocity and the stiffness of the system, we consider a small disturbance to the steady-state solution:

$$x = x_0 + v_0 t + \delta x\,, \qquad \theta = \theta_0 + \delta\theta\,. \tag{12.44}$$

The linearized equations are

$$m\delta\ddot{x} + \eta\delta\dot{x} + c\delta x + \left(F_s - F_k\right)\delta\theta = 0 \tag{12.45}$$

and

$$\delta\dot{\theta} = -\frac{1}{\tau}\delta\theta - \frac{1}{D}\delta\dot{x}\,. \tag{12.46}$$

We look for a solution to this system of equations in the exponential form

$$\delta x = Ae^{\lambda t}\,, \qquad \delta\theta = Be^{\lambda t}\,. \tag{12.47}$$

Insertion into (12.45) and (12.46), provides us

$$\left(\lambda^2 m + \eta\lambda + c\right)A + \left(F_s - F_k\right)B = 0 \tag{12.48}$$

and

$$\frac{1}{D}\lambda A + \left(\lambda + \frac{1}{\tau}\right)B = 0\,. \tag{12.49}$$

This linear system of equations has a non-trivial solution, when the determinant vanishes:

$$\begin{vmatrix} \left(\lambda^2 + \dfrac{\eta}{m}\lambda + \dfrac{c}{m}\right) & \dfrac{\left(F_s - F_k\right)}{m} \\ \dfrac{1}{D}\lambda & \left(\lambda + \dfrac{1}{\tau}\right) \end{vmatrix} = 0 \tag{12.50}$$

or

$$\lambda^3 + \lambda^2 P + \lambda Q + R = 0 \tag{12.51}$$

with

$$P = \left(\frac{1}{\tau} + \frac{\eta}{m}\right), \quad Q = \left(\frac{c}{m} + \frac{\eta}{\tau m} - \frac{(F_s - F_k)}{Dm}\right), \quad R = \frac{c}{\tau m}. \tag{12.52}$$

On the limit of stability, the system experiences undamped oscillations. That means that two of the three solutions of the third order algebraic equation of λ are purely imaginary and complex conjugates and the third is real and negative:

$$\lambda_1 = -\Lambda, \quad \lambda_2 = +i\omega_c, \quad \lambda_3 = -i\omega_c. \tag{12.53}$$

In this case, the general solution is

$$\delta x = x_1 e^{-\Lambda t} + x_2^* e^{i\omega_c t} + x_3^* e^{-i\omega_c t} = x_1 e^{-\Lambda t} + x_2 \cos\omega_c t + x_3 \sin\omega_c t, \tag{12.54}$$

which describes a periodic oscillation with a constant amplitude, given a sufficiently long period of time.

A third order algebraic equation with given roots has the following form:

$$(\lambda + \Lambda)(\lambda - i\omega_c)(\lambda + i\omega_c) = \lambda^3 + \lambda^2\Lambda + \lambda\omega_c^2 + \Lambda\omega_c^2 = 0. \tag{12.55}$$

A comparison between (12.51) and (12.55) results in

$$P = \Lambda, \quad Q = \omega_c^2, \quad R = \Lambda\omega_c^2. \tag{12.56}$$

From this, it follows that on the limit of stability, the condition $R = PQ$ must be fulfilled or, taking (12.52) into consideration,

$$\frac{c}{\tau m} = \left(\frac{1}{\tau} + \frac{\eta}{m}\right)\left(\frac{c}{m} + \frac{\eta}{\tau m} - \frac{(F_s - F_k)}{Dm}\right). \tag{12.57}$$

Thus, the critical stiffness is defined as

$$c_c = \frac{m}{\eta}\left(\frac{1}{\tau} + \frac{\eta}{m}\right)\left(\frac{(F_s - F_k)}{D} - \frac{\eta}{\tau}\right). \tag{12.58}$$

For very small damping coefficients, this expression is simplified to

$$c_c = \frac{(F_s - F_k)m}{\eta D\tau}. \tag{12.59}$$

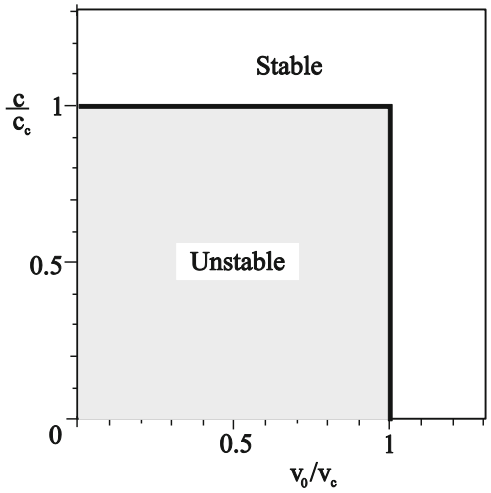

Fig. 12.8 Stability diagram of a tribological system on the "velocity-stiffness" plane.

For stiffnesses smaller than c_c, the sliding is unstable and for stiffnesses larger than c_c, stable. The movement is also stable for $v_0 > v_c$. This can be seen in the stability diagram presented in Fig. 12.8. In this case, the movement can be stabilized by increasing the velocity as well as increasing the stiffness. In reality, the stability diagram is never so rectangular. The qualitative conclusion about the existence of a domain of instability for small velocities and stiffnesses, however, is very general and is observed in systems with various mechanisms of friction.

12.7 Sprag-Slip

In all of the preceding models, only the movement of the system in the sliding direction was investigated. In reality, movement in the direction perpendicular to the surface can also significantly influence the behavior of a tribological system. To illustrate this, we investigate the model shown in Fig. 12.9.

If the force F acting in the horizontal direction is larger than $\mu_s N$, where N is the normal force on the base caused by the springs, then the system will slide. However, if the body is made to oscillate in the vertical direction, then the compression force changes periodically. Every time that the value F/μ_s is reached, the "foot" sticks. In the time interval in which the compressive force is less than F/μ_s, the system slides: the movement consists of alternating phases of sticking and slipping.

In the system shown in Fig. 12.9 a, the movements in the horizontal and vertical directions are independent. After the oscillations are damped out in the vertical direction, the system remains in either a static or sliding state. The system in Fig.

12.9 b is different. Every time that the compressive force exceeds the value F / μ_s due to the oscillations, the foot of the system sticks, whereby the system is suddenly braked. Therefore, due to the inclination, the braking will induce oscillations of the body.

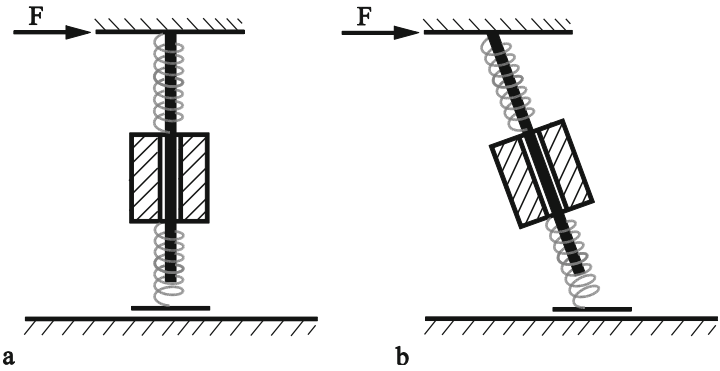

Fig. 12.9 Simple model for the explanation of the sprag-slip mechanism.

Fig. 12.10 At rest, this system is "self-braking." If one swings the bird, the self-braking is intermittently removed and the fastener slides down the rod. This alternating change between sticking and sliding is an example of a sprag-slip movement.

The oscillations due to this mechanism and the associated stick-slip movement are referred to as *sprag-slip*. This term is always used when the system sticks due

to changes in the compressive force. Examples are the chattering of a windshield wiper or the toy shown in Fig. 12.10. For this toy, the condition of self-locking (Chapter 10, Problem 1) is fulfilled. However, if the system is brought to the oscillation, the bird starts to "walk" down supporting self excited oscillations. A more detailed theoretical analysis shows that sliding is not stable also in the vicinity of the point of self-locking in the parameter space of the system. A detailed analysis can be found in[6].

Problems

Problem 1: Stick-slip. The difference between static and kinetic friction that was known to Coulomb is, as a matter of fact, only an extreme case of velocity dependence of the frictional force: For very small velocities ($v \approx 0$), the frictional force is equal to F_s and then falls almost instantly to the level of the force of kinetic friction F_k (Fig. 12.11). Determine the unstable movement in this case. As a model, we once again use a rigid block being pulled over a rigid surface by means of a spring.

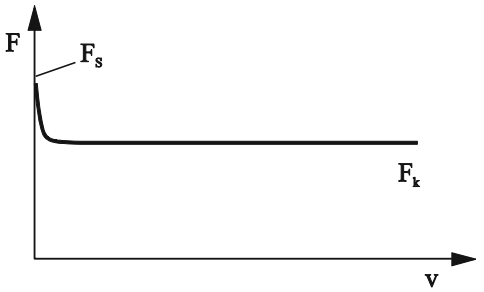

Fig. 12.11 Law of friction with a quick decrease in the frictional force from the static value F_s to the kinetic value F_k.

Solution: If a body is initially at rest at $x = 0$ and the spring is pulled with a constant velocity v_0, then the spring force increases according to the law

$$F_{spring} = cv_0 t$$

until it reaches the static force F_s at the time

$$t_0 = F_s / cv_0 .$$

[6] R Wetter, V.L Popov, The influence of system dynamics on the frictional resistance: insights from a discrete model, Tribology Letters, 2016, v. 61, N. 2, pp. 1-20.

At this moment, the body begins to move and at the same time, the frictional force falls to the value F_k. The equation of motion in the sliding phase is

$$m\ddot{x} + cx = cv_0 t - F_k .$$

The initial conditions are

$$x(t_0) = 0 , \quad \dot{x}(t_0) = 0 .$$

The general solution of the equation of motion is

$$x = a \sin \omega t + b \cos \omega t + v_0 t - \frac{F_k}{c},$$
$$\dot{x} = a\omega \cos \omega t - b\omega \sin \omega t + v_0 .$$

Inserting the initial conditions yields the solution

$$x = a \sin \omega t + b \cos \omega t + v_0 t - F_k / c = A \sin(\omega t + \varphi) + v_0 t - F_k / c,$$
$$\dot{x} = a\omega \cos \omega t - b\omega \sin \omega t + v_0 = A\omega \cos(\omega t + \varphi) + v_0 ,$$
$$\ddot{x} = -a\omega^2 \sin \omega t - b\omega^2 \cos \omega t = -A\omega^2 \sin(\omega t + \varphi).$$

with

$$a = \frac{1}{\omega}\left(-v_0 \cos \frac{\omega F_s}{c v_0} - \omega \frac{F_s - F_k}{c} \sin \frac{\omega F_s}{c v_0} \right),$$

$$b = \frac{1}{\omega}\left(v_0 \sin \frac{\omega F_s}{c v_0} - \omega \frac{F_s - F_k}{c} \cos \frac{\omega F_s}{c v_0} \right)$$

and

$$A = \frac{1}{\omega}\sqrt{v_0^2 + \left(\omega \frac{F_s - F_k}{c} \right)^2} .$$

The body once again comes to rest when $\dot{x} = A\omega \cos(\omega t + \varphi) + v_0 = 0$. From this, it follows that $\cos(\omega t + \varphi) = -v_0 / A\omega$. The associated acceleration is equal to

$$\ddot{x} = -A\omega^2 \sin(\omega t + \varphi) = -A\omega^2 \sqrt{1 - \cos^2(\omega t + \varphi)} = -\left(F_s - F_k \right) / m ,$$

the force acting on the body is equal to $-\left(F_s - F_k \right)$, and the force of the spring is equal to

$$F_{spring} = -F_s + 2F_k < F_s .$$

Because this force is smaller than the force of static friction, the body sticks until the spring force once again reaches the value F_s.

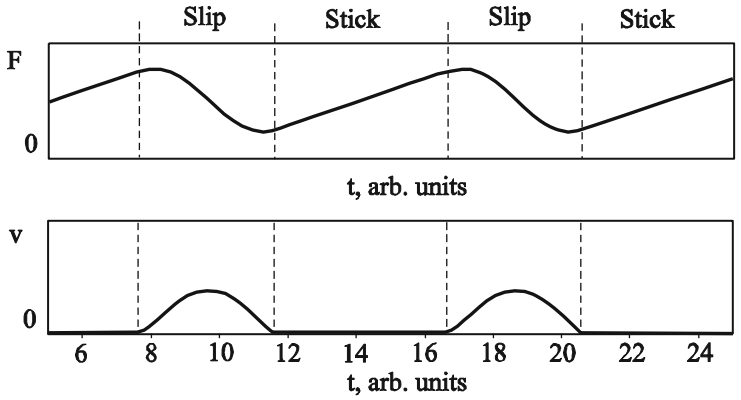

Fig. 12.12 Spring force (above) and sliding speed (below) as functions of time for a stick-slip motion in the case of the frictional force shown in Fig. 12.11. The body does not move, and the spring force increases linearly with time (stick phase) until the spring force reaches the force of static friction. At this moment, the body begins to move and oscillate until the velocity is once again zero. Then, the next stick phase begins.

Then, the slip phase repeats itself. The movement consists of alternating phases of rest (stick) and sliding (slip) and is termed *stick-slip* motion. The temporal dependence of velocity and spring force for an example of stick-slip motion is presented in Fig. 12.12 with respect to time. The duration of a slip phase is given by

$$t_{slip} = \frac{2}{\omega} \arctan\left(\frac{\omega}{v_0} \frac{F_s - F_k}{c} \right).$$

In the limiting case $v_0 \to 0$, this time approaches π / ω (half of the oscillation period). The slip length for very small values of v_0 is

$$\Delta x_{slip} = 2 \frac{F_s - F_k}{c}.$$

Problem 2: Determine the reflection coefficient for the damping sheet in the system shown in Fig. 12.4 for an arbitrary damping coefficient.

Solution: We are looking for the solution to the wave equation (12.10) with the boundary condition (12.19) as the superposition of an incident and a reflecting wave in complex form:

$$u = u_0 e^{ikct} \left(e^{ikz} + B e^{-ikz} \right).$$

The amplitude of the incident wave we assume to be 1. The amplitude of the reflected wave is B. Insertion into the boundary condition (12.19) yields

$$B = e^{-2ikl}\frac{G-\beta c}{G+\beta c}.$$

We define the reflection coefficient as the ratio of the intensity of the incident wave to that of the reflected wave; it is, therefore, equal to $|B|^2$:

$$|B|^2 = \left(\frac{G-\beta c}{G+\beta c}\right)^2.$$

The reflection coefficient becomes zero for $\beta = G/c = \sqrt{G\rho}$. For $\beta \to 0$ and $\beta \to \infty$, it approaches 1.

Problem 3: Determine the reflection coefficient between an elastic sheet and a liquid film with a dynamic viscosity[7] $\bar{\eta}$.

Solution: The equations of motion to be solved are the wave equation

$$\frac{\partial^2 u}{\partial t^2} = \frac{G}{\rho}\frac{\partial^2 u}{\partial z^2}$$

in the elastic continuum and the Navier-Stokes equation for the liquid medium, which for purely transverse motion has the form

$$\rho\frac{\partial v}{\partial t} = \bar{\eta}\frac{\partial^2 v}{\partial z^2}.$$

We place the surface $z = 0$ at the boundary between the elastic medium and the liquid medium. Let the positive z-direction be defined in the direction of the elastic layer. The boundary conditions at the interface are

$$\dot{u}(0,t) = v(0,t) \qquad \text{(no-slip condition)}$$

and

$$G\left.\frac{\partial u}{\partial z}\right|_{z=0} = \bar{\eta}\left.\frac{\partial v}{\partial z}\right|_{z=0} \qquad \text{(equilibrium condition).}$$

We look for the solution to the wave equation, as we did in Problem 2, in the form of a superposition of an incident and a reflected wave

[7] The dynamic viscosity $\bar{\eta}$ should not be confused with the damping coefficient η, which is used earlier in this chapter or in other chapters and has other units.

$$u = e^{i\omega t}\left(e^{i\frac{\omega}{c}z} + Be^{-i\frac{\omega}{c}z} \right).$$

The solution to the Navier-Stokes equation with the frequency ω, which approaches zero at infinity, is

$$v = Ce^{\frac{1+i}{\sqrt{2}}\sqrt{\frac{\rho\omega}{\bar{\eta}}}z} e^{i\omega t}.$$

The application of the boundary conditions at the interface results in the following system of equations:

$$i\omega(1+B) = C,$$

$$iG\frac{\omega}{c}(1-B) = \bar{\eta}\frac{1+i}{\sqrt{2}}\sqrt{\frac{\rho\omega}{\bar{\eta}}}C.$$

The reflection coefficient is

$$|B|^2 = \frac{(1-\zeta)^2 + \zeta^2}{(1+\zeta)^2 + \zeta^2}$$

with

$$\zeta = \frac{c}{G}\sqrt{\frac{\rho\omega\bar{\eta}}{2}} = \sqrt{\frac{\omega\bar{\eta}}{2G}}.$$

The reflection coefficient reaches its minimum $|B|^2 \approx 0.17$ for $\zeta = 1/\sqrt{2}$. We see that the oscillations can be damped very efficiently by liquid layers (or polymers with corresponding rheological properties), however, only in specific frequency domains. In both limiting cases, a viscosity of zero or infinity, the reflection coefficient is equal to 1 as expected.

13 Thermal Effects in Contacts

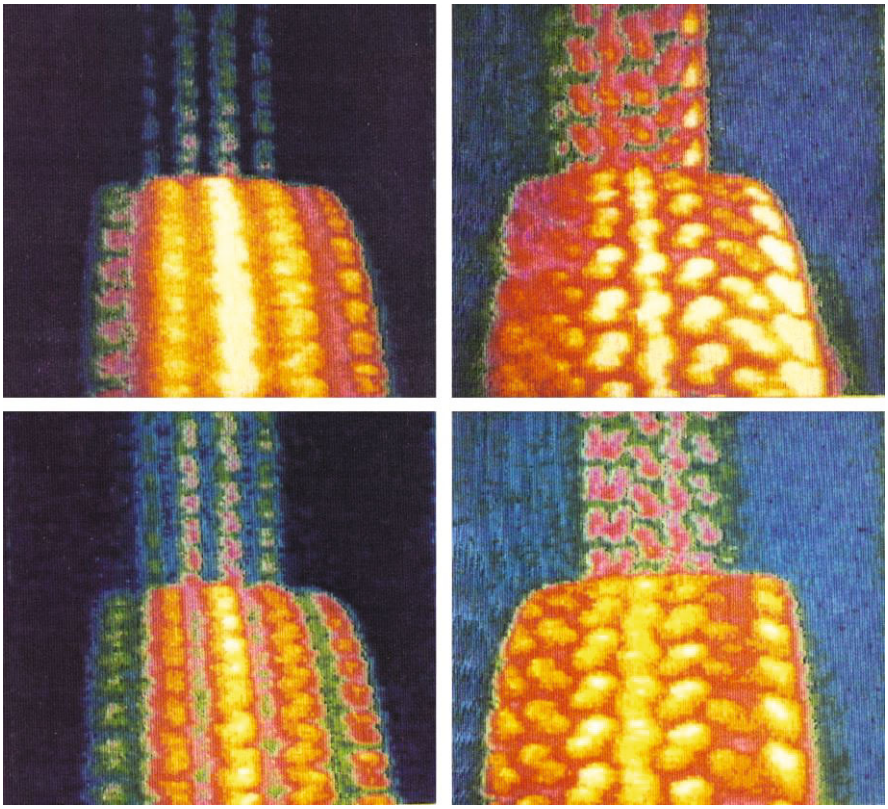

On the contact interface between two bodies in frictional contact with one another, heat energy is released. Because the real contact area is, as a rule, only a fraction of the apparent contact area, the heat released in a tribological contact is very heterogeneous. The local temperature increases can be so high that they may influence the material properties and can even cause the material to melt. Furthermore, a local change in the temperature leads to a local heat expansion and, thus, a corresponding change in the contact conditions. This feedback reaction can, under certain conditions, lead to the development of thermo-mechanical instabilities in the contact. In this chapter, we investigate the various aspects of the frictionally caused heat release in tribological contacts.

V.L. Popov, *Contact Mechanics and Friction*,
DOI 10.1007/978-3-662-53081-8_13

13.1 Introduction

The first systematic investigation of temperature distributions in frictional contacts was carried out in 1935 by F.P. Bowden and K. Riedler[1]. In the course of these investigations, they used the tribological contact as a natural thermocouple. This approach remains today one of the simplest and most dependable methods to experimentally determine the temperature distribution in a tribological contact. In further studies with Tabor, Bowden measured very high temperatures (around the same magnitude as the melting temperature) in parts of the contact.

By investigating thermal effects in contacts, one can differentiate between three scales: (1) the tribological system as a whole, (2) the "macroscopic contact area," and (3) the micro-contacts between the rough surfaces. While the temperature of the entire system changes slowly during the process, the temperature in a sliding contact (e.g. between two gears) can change very quickly and reach high values. This is referred to as the "flash temperature." The theoretical investigation of flash temperatures in "macroscopic contact areas" is, above all, associated with the name H. Blok[2]. For these conditions, a large *Péclet number* is characteristic. The temperature dynamics for small *Péclet numbers* was investigated by J.K. Jaeger[3]. This theory, as a rule, is applicable to micro-contacts. It has been shown, however, that Jaeger's theory for small *Péclet numbers* remains relatively accurate even in the area of validity of Blok's theory. We limit ourselves in this chapter, therefore, to the case of small *Péclet numbers*.

13.2 Flash Temperatures in Micro-Contacts

We consider the contact between two rough surfaces in the scope of the model from Greenwood and Williamson (see Chapter 7). At the same time, we assume that there is friction between micro-asperities with the coefficient of friction μ. We calculate the temperature increase in a micro-contact by assuming that the characteristic propagation length of the heat, $D \approx \sqrt{2\alpha t}$, during the existence of a contact, $t \approx a / v$, is much larger than the contact radius: $\sqrt{2\alpha t} \gg a$ or

$$\frac{va}{2\alpha} \ll 1 . \tag{13.1}$$

[1] F.P. Bowden, K.E.W. Riedler, A note on the surface temperature of sliding metals. Proc. Cambridge Philos. Soc., 1935, v. 31, Pt.3, p.431.

[2] H. Blok, The Dissipation of Frictional Heat. Applied Scientific Research, Section A, 1955, N. 2-3, pp. 151-181.

[3] J.K. Jaeger, Moving Sources of Heat and the Temperature of Sliding Contacts. Journal and Proc. Royal Society, New South Walls, 1942, v. 76, Pt. III, pp. 203-224.

Here, α is the *thermal diffusivity*, a the contact radius, and v the sliding speed. The ratio $va/2\alpha$ is known as the *Péclet number*. If the condition (13.1) is met, one can consider the heat propagation at every point in time as a stationary process with a given heat production on the surface. For metallic substances ($\alpha \approx 10^{-4}$ m$^2/s$, $a \approx 10^{-5} - 10^{-4}$ m), this means that the sliding speed may not be larger than $2\alpha/a \approx 2 - 20$ m/s, which is true in most applications. For ceramics and polymers ($\alpha \approx 10^{-7} - 10^{-6}$ m$^2/s$, $a \approx 10^{-5}$ m), this approximation is valid for sliding speeds under $0.02 - 0.2$ m/s.

A homogeneous temperature increase ΔT in a round area with the radius a on the surface of a half-space with the thermal conductivity λ produces a heat flux $\dot{W}$ that is associated with ΔT by the thermal resistance R_w:

$$\dot{W} = \frac{\Delta T}{R_w}. \tag{13.2}$$

The thermal resistance for a round contact is equal to

$$R_w = \frac{1}{2a\lambda}. \tag{13.3}$$

We can also use this with equation (13.2) in order to estimate the temperature increase of the surface for a given heat flow:

$$\Delta T = \frac{\dot{W}}{2a\lambda}. \tag{13.4}$$

Under the assumption that the total heat flows only into one body, we get for one single elastic micro-contact

$$\Delta T = \frac{\mu \Delta F_N v}{2a\lambda}. \tag{13.5}$$

By inserting the Hertzian formula $\Delta F_N = \frac{4}{3} E^* R^{1/2} d^{3/2}$ and taking into account that $a = \sqrt{Rd}$, we obtain

$$\Delta T = \frac{2}{3} \frac{\mu E^* d v}{\lambda}. \tag{13.6}$$

As we saw in Chapter 7, the average penetration depth $\bar{d}$ is practically independent from the compressive force and is approximately equal to l/π.
Therefore, we obtain an average temperature increase in the micro-contact of

$$\overline{\Delta T} \approx 0.2 \frac{\mu E^* l v}{\lambda}. \tag{13.7}$$

For a contact between steel and sapphire ($E^* \approx 140$ GPa , $\mu \approx 0.15$, $l \approx 1\ \mu$m and $\lambda \approx 40\ \frac{W}{m \cdot K}$) at a sliding speed of 1 m/s , the average temperature increase in the micro-contacts reaches $\overline{\Delta T} \approx 110$ K . For copper, with $E^* \approx 100$ GPa and $\lambda \approx 400\ \frac{W}{m \cdot K}$, we would have an average temperature increase of $\overline{\Delta T} \approx 8$ K under the same assumptions. In applications where the flash temperature must be kept as low as possible[4], it is advantageous to choose a pairing between a polymer and a ceramic. In this way, both the (small) modulus of elasticity E^* of the polymer and, as a rule, the much larger thermal conductivity λ of the ceramic contribute to the minimization of the temperature increase.

13.3 Thermo-Mechanical Instability

If two planar bodies are pressed together and put into motion relative to one another, an instability can come about through the interaction between the release of frictional energy and thermal expansion: areas with higher temperatures and, therefore, larger expansions are put under higher stress and, thus, heated even more (Fig. 13.1). We would like to investigate the conditions for the development of such an instability.

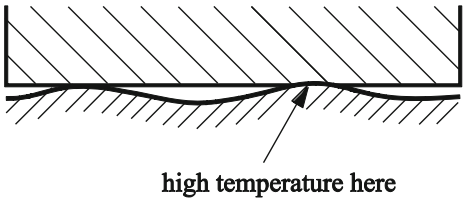

Fig. 13.1 The areas with increased temperatures bulge out due to thermal expansion. This leads to an increased frictional power and further heating of this area. This can lead to instability and the formation of a permanent pattern.

First, we make a rough estimation. If an instability with a wave number k develops on the surface, then stress and temperature distributions with the same wave number would develop on this area of the surface. The "characteristic decay depth" of these stress and temperature fluctuations and, therefore, the deformed zone of the surface has the order of magnitude of $1/k$. If the surface is heated (in the area of compression) by ΔT , then it leads to a thermal stress of

[4] In artificial hips, the temperature may not exceed the temperature of the dissociation of protein. The allowable temperature increase is, therefore, limited to 2-4 K.

$$\Delta\sigma \approx \gamma \Delta T E^* , \tag{13.8}$$

where γ is the volumetric thermal expansion coefficient and E^*, the modulus of elasticity. The frictional power per unit area, $\mu \Delta\sigma v$, must be the same as the heat flux into the trough of the material in steady state:

$$\mu \Delta\sigma v \approx \lambda \frac{\Delta T}{1/k} . \tag{13.9}$$

Taking Equation (13.8) into account, we calculate a wave vector for which the heat production and heat flux are in equilibrium,

$$k_c \approx \frac{E^* \mu \gamma v}{\lambda} . \tag{13.10}$$

Temperature disturbances with smaller wave numbers than the critical wave number are unstable.

Thermo-mechanical instabilities can, among other things, be responsible for the phenomenon known as "washboard type" wear in the contact areas of compression rings of very highly loaded motors (see Fig. 13.2).

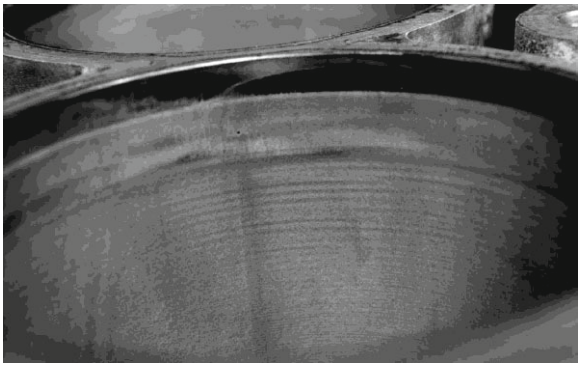

Fig. 13.2 Photograph of a cylinder in a combustion engine with "washboarding."

Problems

Problem 1: Determine the stability criterion for a thermo-mechanical instability in a contact between an elastic and a rigid body.

Solution: This problem is treated the same as the estimation that we have already done above. We consider the system shown in Fig. 13.3. The upper body should be absolutely rigid and not thermally conductive.

At the boundary between a stable and an unstable state, the disturbances are stationary. To determine the instability criterion we thus use the equilibrium equation for the elastic body taking into account the thermal expansion:

$$\frac{3}{2}\frac{(1-2\nu)}{(1+\nu)}\Delta\vec{u}+\frac{3}{2}\frac{1}{(1+\nu)}\nabla\mathrm{div}\vec{u}=\gamma\nabla T$$

and the steady-state equation for the thermal conduction

$$\Delta T=0\,.$$

Here, $\vec{u}$ is the displacement vector, ν is the Poisson's ratio, T is the variation of the temperature from its stationary value far from the surface, and $\Delta=\frac{\partial^2}{\partial x^2}+\frac{\partial^2}{\partial z^2}$ is the Laplace operator. The stress tensor is calculated as

$$\sigma_{ik}=-\frac{2}{3}\frac{G(1+\nu)}{(1-2\nu)}\gamma T\delta_{ik}+\frac{2}{3}\frac{G(1+\nu)}{(1-2\nu)}\frac{\partial u_l}{\partial x_l}\delta_{ik}+G\left(\frac{\partial u_i}{\partial x_k}+\frac{\partial u_k}{\partial x_i}-\frac{2}{3}\frac{\partial u_l}{\partial x_l}\delta_{ik}\right),$$

where G is the shear modulus.

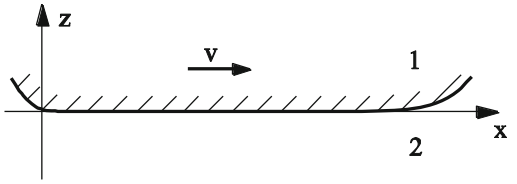

Fig. 13.3 A rigid, non-conductive body 1 in contact with an elastic continuum 2. The bodies move relative to each other with a tangential velocity v.

Because of the rigidity assumption of the upper body, the surface of the elastic body cannot experience any displacement in the vertical direction:

$$u_z(z=0)=0\,.$$

For simplification, we assume that the coefficient of friction is very small and the normal stress component σ_{zz} dominates so that the tangential stress in the mechanical equilibrium condition may be assumed to be negligibly small:

$$\sigma_{xz}(z=0)=0\,.$$

The solution to the equations $\frac{3}{2}\frac{(1-2\nu)}{(1+\nu)}\Delta\vec{u}+\frac{3}{2}\frac{1}{(1+\nu)}\nabla\mathrm{div}\vec{u}=\gamma\nabla T$ and $\Delta T=0$ that meets the conditions $u_z(z=0)=0$ and $\sigma_{xz}(z=0)=0$ is[5]

$$T=T_0\cos kx\cdot e^{kz},\quad \vec{u}=-\frac{\gamma T_0(1+\nu)}{6(1-\nu)k}\left((-1+kz)\sin kx,\ 0,\ -kz\cos kx\right)\cdot e^{kz}\ .$$

In steady state, the heat that is released at the surface must be equal to the heat flux out of the surface (which, according to our assumption, goes only into the lower body):

$$\lambda\left.\frac{\partial T}{\partial z}\right|_{z=0}=-\mu\nu\sigma_{zz}(z=0)\,.$$

λ is the thermal conductivity coefficient. From this, it follows that the critical value of the wave number is

$$k_c=\frac{\nu\mu G\gamma(1+\nu)}{3\lambda(1-\nu)}\,.$$

For $\nu=1/3$, we have a wave number of $k_c=\frac{2}{3}\frac{\nu\mu G\gamma}{\lambda}$. Temperature disturbances with smaller wave numbers than the critical wave number are unstable.

[5] The choice of the dependence of $\cos kx$ of the solution on the coordinate x means that we are investigating the development of a harmonic disturbance. An arbitrary disturbance can always be presented as the superposition of Fourier components with various wave numbers due to the linearity of the problem.

14 Lubricated Systems

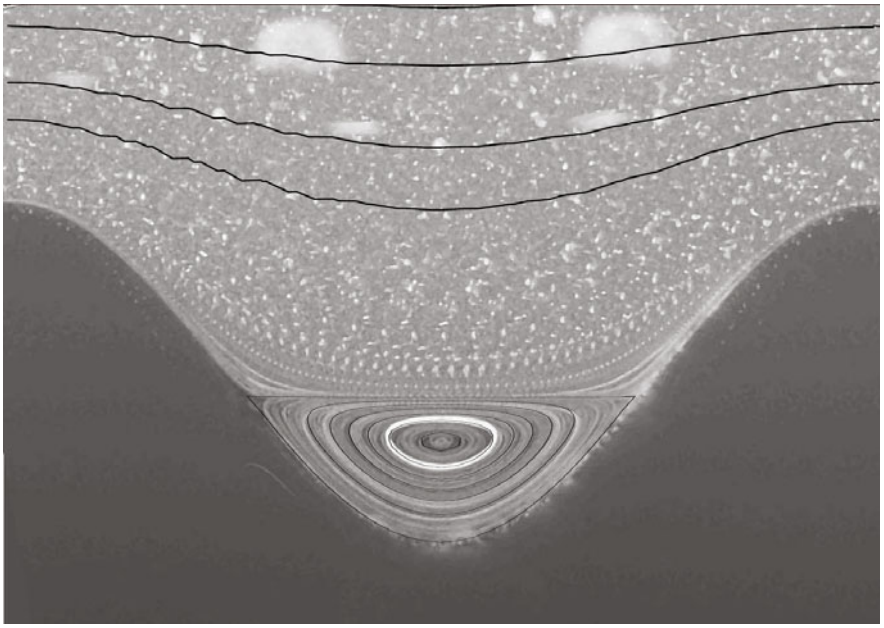

In order to reduce frictional forces and wear, lubrication has been used for thousands of years. It inhibits direct contact between two bodies and, thereby, replaces dry friction with fluid friction. The presence of liquid between two bodies influences not only the tangential, but also the normal forces: two dry sheets of glass can effortlessly be taken apart from one another, while in order to take two wet sheets apart one needs a considerable force. This phenomenon can be attributed, on the one hand, to capillary forces, and on the other, to pure hydrodynamic nature: a viscous liquid requires a given time in order to flow in the small space between two sheets. During dynamic loading, this phenomenon leads to an apparent "adhesion" between two lubricated bodies, which we describe as "viscous adhesion."

In most cases in lubricated tribological systems, we deal with non-turbulent flows. Furthermore, the lubricant can be soundly approximated as incompressible. We begin our considerations of hydrodynamic lubrication and viscous adhesion with the investigation of a steady-state flow between two parallel plates, which forms the foundations of lubrication theory.

V.L. Popov, *Contact Mechanics and Friction*,
DOI 10.1007/978-3-662-53081-8_14

14.1 Flow between two parallel plates

The dynamics of a linearly viscous (Newtonian) fluid is given by the Navier-Stokes equation, which takes the following form for incompressible fluids:

$$\rho \frac{d\vec{v}}{dt} = -\nabla p + \eta \Delta \vec{v}\,, \tag{14.1}$$

where ρ is the density, η the dynamic viscosity of the fluid, and p the pressure in the fluid. Moreover, an incompressible fluid satisfies the equation

$$\mathrm{div}\vec{v} = 0\,. \tag{14.2}$$

For quasi-static flows (so-called creeping flows), which we deal with in most lubrication problems, the inertial term can be neglected and the equation takes the form

$$\eta \Delta \vec{v} = \nabla p\,. \tag{14.3}$$

We consider two plates separated by a liquid film. In the general case, the plates can move relative to each other. Without restricting the generality, we can assume that the upper plate has a velocity of zero. We define the velocity of the lower plate as $-v_0$.

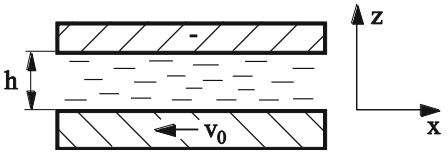

Fig. 14.1 Flow between two parallel plates.

We consider a steady-state flow in the x-direction. According to this, the velocity has only an x-component, which is dependent on the z-coordinate $\vec{v} = \big(v(z), 0\big)$. Equation (14.3) takes the following form:

$$\frac{\partial p}{\partial x} = \eta \left(\frac{\partial^2}{\partial x^2} + \frac{\partial^2}{\partial z^2} \right) v_x = \eta \frac{\partial^2 v}{\partial z^2}\,, \tag{14.4}$$

$$\frac{\partial p}{\partial z} = \eta \left(\frac{\partial^2}{\partial x^2} + \frac{\partial^2}{\partial z^2} \right) v_z = 0\,. \tag{14.5}$$

From (14.5), it follows that the pressure is independent of the vertical coordinate z: $p = p(x)$. Integrating (14.4) twice yields

$$\eta v = \frac{\partial p}{\partial x} \cdot \frac{z^2}{2} + C_1 z + C_2\,. \tag{14.6}$$

Using the boundary conditions $v(0) = -v_0$ and $v(h) = 0$, we obtain $C_2 = -\eta v_0$ and $C_1 = \frac{\eta v_0}{h} - \frac{\partial p}{\partial x}\frac{h}{2}$. Therefore, the velocity distribution is given by

$$\eta v = \frac{\partial p}{\partial x}\frac{z(z-h)}{2} + \frac{\eta v_0}{h}(z-h). \tag{14.7}$$

14.2 Hydrodynamic Lubrication

Now, we consider the two bodies sketched in Fig. 14.2. Let the surface of one be somewhat slanted relative to the other. We assume that the surfaces of both bodies are smooth and even. Furthermore, we assume that the lower body moves to the left at a velocity $-v_0$. For small angles of inclination, one can consider the flow at every point to be like the flow between two parallel plates and use the velocity distribution equation (14.7):

$$v = p'\frac{z(z-h)}{2\eta} + \frac{v_0}{h}(z-h). \tag{14.8}$$

Here, we have denoted the pressure gradient with p'.

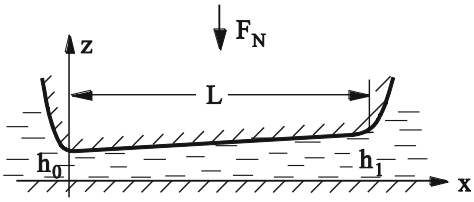

Fig. 14.2 Two bodies sliding past one another separated by a lubricating film.

Due to conservation of mass, it follows that the mass flow through every cross-section per unit time must be constant:

$$\frac{Q}{D} = \int_0^h v(z)dz = \int_0^h \left(p'\frac{z(z-h)}{2\eta} + \frac{v_0}{h}(z-h) \right) dz = -p'\frac{h^3}{12\eta} - \frac{v_0 h}{2} = C, \tag{14.9}$$

where D is the width of the sliding body and C is a constant. According to this, we obtain a pressure gradient of

$$\frac{dp}{dx} = -6\eta v_0 \left(\frac{1}{h^2} - \frac{C}{h^3} \right). \tag{14.10}$$

By multiplying by h^3 and derivating by x, this equation can be written in the differential form

$$\frac{\mathrm{d}}{\mathrm{d}x}\left(h^3\frac{\mathrm{d}p}{\mathrm{d}x}\right)=-6\eta v_0\frac{\mathrm{d}h}{\mathrm{d}x}. \tag{14.11}$$

This equation represents the one-dimensional special case of the Reynolds equation[1]

$$\frac{\mathrm{d}}{\mathrm{d}x}\left(h^3\frac{\mathrm{d}p}{\mathrm{d}x}\right)+\frac{\mathrm{d}}{\mathrm{d}y}\left(h^3\frac{\mathrm{d}p}{\mathrm{d}y}\right)=-6\eta v_0\frac{\mathrm{d}h}{\mathrm{d}x} \tag{14.12}$$

derived by Reynolds in 1886, which carries his name and is today regarded as the basis of the hydrodynamic lubrication theory. In the Reynolds equation x and y are coordinates in the sliding plane: x in the moving direction and y perpendicular to it.

With a linear increase in height $h=h_0+ax$, (14.10) can be explicitly integrated, giving us a pressure of

$$\begin{aligned} p &= p_{ext}-6\eta v_0\int_0^x\left(\frac{1}{h^2}-\frac{C}{h^3}\right)dx = p_{ext}-\frac{6\eta v_0}{a}\int_{h_0}^{h}\left(\frac{1}{h^2}-\frac{C}{h^3}\right)dh \\ &= p_{ext}+\frac{3\eta v_0}{a}\left(2\left(\frac{1}{h}-\frac{1}{h_0}\right)-C\left(\frac{1}{h^2}-\frac{1}{h_0{}^2}\right)\right). \end{aligned} \tag{14.13}$$

When calculating the definite integral, we take into account that $p(0)=p_{ext}$. On the other side $(x=L)$, the pressure is also the same as the external pressure p_{ext}, where it follows that $C=2h_0h_1/(h_0+h_1)$. Thus, we obtain a pressure distribution of

$$p=p_{ext}+\frac{6\eta v_0}{a}\left(\left(\frac{1}{h}-\frac{1}{h_0}\right)-\frac{h_0h_1}{h_0+h_1}\left(\frac{1}{h^2}-\frac{1}{h_0{}^2}\right)\right). \tag{14.14}$$

The velocity field is given by

$$v=v_0(z-h)\left[\frac{1}{h}+3z\left(-\frac{1}{h^2}+\frac{2}{h^3}\cdot\frac{h_0h_1}{h_0+h_1}\right)\right]. \tag{14.15}$$

[1] O. Reynolds, On the Theory of Lubrication and its Applications to Mr. Beauchamp Tower's Experiments, including an Experimental Determination of the Viscosity of Olive Oil, Philosophical Transactions of the Royal Society, 1886, v. 177, part 1, 157-234.

This velocity profile and the pressure distribution for $p_{ext} = 0$ (14.14) are shown in Fig. 14.3.

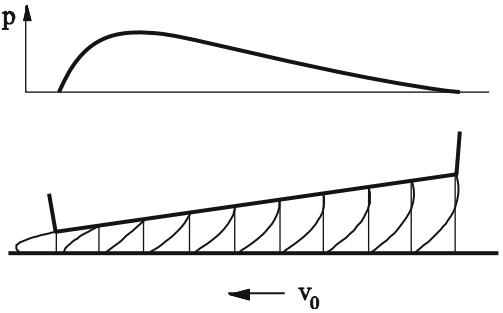

Fig. 14.3 Velocity profile and pressure distribution between two hydrodynamically lubricated even sliding plates.

As soon as the velocity and pressure distributions are known, one can easily calculate the x- and z-components of the forces acting on the upper body. The vertical force component is calculated as follows:

$$F_N = \int dxdy\left(p - p_{ext}\right) = \frac{\eta A L v_0}{h_0^2}\alpha \tag{14.16}$$

with $\alpha = \frac{6}{\left(\xi - 1\right)^2}\left[\ln\xi - \frac{2(\xi - 1)}{\xi + 1}\right]$ and $\xi = h_1 / h_0$; $A = LD$ is the apparent "contact area." The horizontal force component is caused by the viscous stress $\sigma_{xz} = \eta \partial v / \partial z$ and is calculated as

$$F_R = \eta \int_A dxdy \left.\frac{\partial v}{\partial z}\right|_{z=0} = \frac{\eta A v_0}{h_0}\beta\,, \tag{14.17}$$

with $\beta = \frac{1}{\xi - 1}\left[4\ln\xi - \frac{6(\xi - 1)}{\xi + 1}\right]$. We obtain a coefficient of friction of

$$\mu = \frac{F_R}{F_N} = \left(\frac{h_0}{L}\right)\frac{\beta}{\alpha}. \tag{14.18}$$

The coefficient of friction is dependent on the average pressure acting on the contact area. If we calculate the slot width h_0 from (14.16) and insert it into (14.18), we obtain

$$\mu = \frac{\beta}{\sqrt{\alpha}}\sqrt{\frac{A\eta v_0}{L F_N}} = \frac{\beta}{\sqrt{\alpha}}\sqrt{\frac{\eta v_0}{LP}}\,. \tag{14.19}$$

Here, $P = F_N / A$ is the average pressure in the contact area. The dependence of the parameter β/α, as well as $\beta/\sqrt{\alpha}$, on ξ is shown in Fig. 14.4. In the relevant domain of ξ-values, the ratio β/α lies between 5 and 10. Thus, the following rough estimation for the coefficient of friction is obtained:

$$\mu \approx 10\left(\frac{h_0}{L}\right). \tag{14.20}$$

The coefficient of friction is around 10 times the ratio of the smallest width of the slot (i.e. the film thickness) to the length of the contact area. In the large domain of relevant film thickness ratios ξ, the ratio $\beta/\sqrt{\alpha}$ changes only slightly and is roughly equal to 2 (see Fig. 14.4). Hence, a good approximation of (14.19) is

$$\mu \approx 2\sqrt{\frac{\eta v_0}{LP}}. \tag{14.21}$$

For the same length of the contact area, the coefficient of friction is a function of the parameter combination $\eta v_0 / P$.

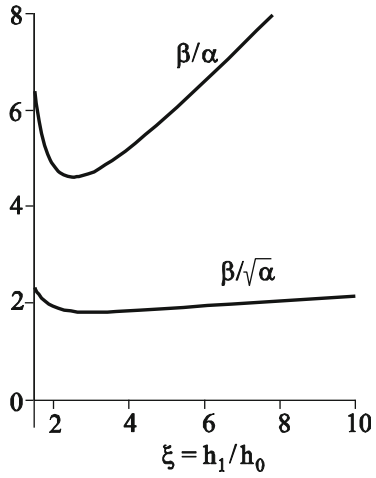

Fig. 14.4 The parameters that influence the coefficient of friction, β/α and $\beta/\sqrt{\alpha}$, as functions of the slot width ratio ξ.

The larger the pressure is, the smaller the coefficient of friction. One must take into consideration, however, that as the pressure increases, the slot width decreases: $h_0 = \sqrt{\alpha L \frac{\eta v_0}{P}}$. At a sufficiently small film thickness, the assumption that the surfaces are smooth is no longer valid; the influence of roughness becomes signifi-

cant and the system transitions into the domain of *mixed friction*. Because of this, at even larger pressures the coefficient of friction increases once again. The dependence of the coefficient of friction on the parameter $\eta v_0 / P$ is called the “Stribeck curve”. It describes the dependence of the coefficient of friction on all of the mentioned parameters. In particular, it describes the dependence of the frictional force on the speed in a lubricated system. For large values of $\eta v_0 / P$, this dependence has a universal character. In the domain of mixed friction, on the other hand, the curve is dependent on the properties of the surfaces and the lubricant. We enter the domain of mixed friction as the sliding velocity decreases. The higher the speed is, the larger the film thickness of the lubricant and the more seldom the surfaces come into direct contact with asperities.

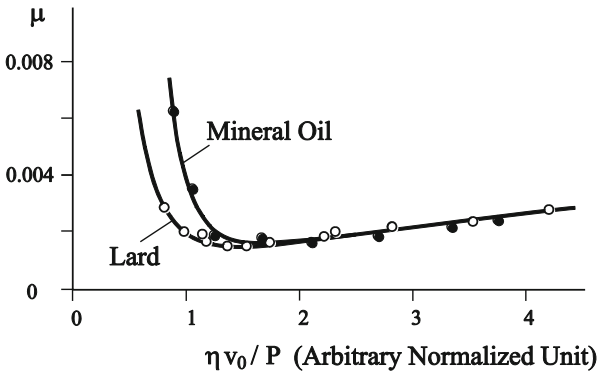

Fig. 14.5 Stribeck curves for two different oils as lubricants. At high speeds, they converge. At small values of $\eta v_0 / P$, however, the systems exhibit different behavior for the different lubricants[2].

14.3 “Viscous Adhesion”

If a liquid film exists between two bodies, then they can be neither quickly pressed together nor quickly separated. The last effect is often perceived as a type of “adhesion.” During dynamic processes, it is often difficult to differentiate between “genuine” adhesion (which is caused by either surface forces between solid bodies or capillary bridges) and “viscous adhesion.” The convergence of two bodies separated by a liquid film can only happen if the liquid is “squeezed out.” In order for the bodies to separate, the liquid must once again flow into the slot, except in the case that cavitation occurs (formation and growth of steam bubbles). However, both processes require a certain time.

[2] A.E. Norton, Lubrication. McGraw-Hill, New York, 1942.

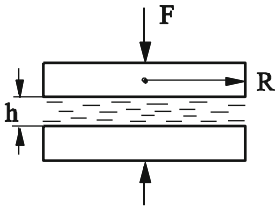

Fig. 14.6 The expulsion of a fluid film from between two round plates.

Let us consider the convergence of two round plates with the radius R, between which a liquid film exists (Fig. 14.6). The fluid that is expelled by the vertical convergence forms a radial flow. Due to symmetry, it is clear that the flow velocity is radially symmetric. If the thickness of the film is much smaller than the radius of the plates, then the radial component of the velocity is much larger than the convergence speed of the plates and we are essentially dealing with a flow being acted upon by a pressure gradient, which we investigated in the first section. According to this, the velocity is equal to

$$v = p' \frac{z(z-h)}{2\eta}, \tag{14.22}$$

where $p' = \partial p / \partial r$. The volume flow through the cylindrical surface with the radius r is

$$Q = \int_0^h 2\pi r v(z) dz = p' \frac{\pi r}{\eta} \int_0^h z(z-h) dz = -p' \frac{\pi r h^3}{6\eta}. \tag{14.23}$$

This flow must be equal to the volume flow $Q = -\pi r^2 \dot{h}$, due to the vertical movement of the upper plate:

$$-\pi r^2 \dot{h} = -p' \frac{\pi r h^3}{6\eta}. \tag{14.24}$$

From this, the pressure gradient is

$$p' = \frac{6\eta r \dot{h}}{h^3}, \tag{14.25}$$

or, after one integration,

$$p = \frac{6\eta \dot{h}}{h^3} \int r dr = \frac{3\eta \dot{h}}{h^3} r^2 + C. \tag{14.26}$$

The constant of integration is determined using the boundary condition $p(r = R) = p_{ext}$ (external pressure):

$$C = p_{ext} - \frac{3\eta \dot{h}}{h^3} R^2 . \tag{14.27}$$

Therefore, in the end, the pressure distribution assumes the form:

$$p = \frac{3\eta \dot{h}}{h^3}\left(r^2 - R^2\right) + p_{ext} . \tag{14.28}$$

We calculate the normal force acting vertically on the plate as

$$F = \int_0^R 2\pi r\left(p(r) - p_{ext}\right) dr = \frac{6\eta\pi \dot{h}}{h^3}\int_0^R \left(r^2 - R^2\right) r dr = -\frac{3\eta\pi \dot{h}}{2h^3} R^4 . \tag{14.29}$$

For a given force, we can now calculate the time that is required for the plates to converge from a distance of h_0 to a distance of h:

$$\int_0^t \frac{2F}{3\eta\pi R^4} dt = -\int_{h_0}^{h} \frac{dh}{h^3} , \tag{14.30}$$

$$\frac{2F}{3\eta\pi R^4} t = \frac{1}{2}\left(\frac{1}{h^2} - \frac{1}{h_0^2}\right). \tag{14.31}$$

For large initial separation distances, this time is practically only dependent on the minimum separation distance, in this case the final separation distance:

$$t = \frac{3\eta\pi R^4}{4Fh^2} . \tag{14.32}$$

If the force is dependent on the time, then the following is valid:

$$\int_0^t F(t) dt = \frac{3\eta\pi R^4}{4h^2} . \tag{14.33}$$

This means that the minimum obtainable film thickness is only dependent on the *impulse*.

In order to illustrate this idea, we consider a body covered with a viscous fluid which is thrown against a ceiling with a velocity v (Fig. 14.7). How long afterwards will it remain hanging on the ceiling? Immediately before the impact, the momentum of the body is equal to Mv. During the impact, the momentum is brought to zero due to the impulse of the reaction force of the ceiling. Thus, the impulse is also equal to Mv. Because the impulse needed to bring the plates together to a distance of h is equal to the impulse needed to separate the plates from a distance of h, then the impulse from gravity, Mgt, must attain a value of Mv in order to “tear” the plate from the ceiling. From this, it follows that $t = v/g$. This is only valid for Newtonian fluids.

From (14.33) it follows that viscous adhesion with Newtonian fluids cannot be used to walk on the ceiling. The situation changes if the viscosity of the liquid is dependent on the velocity gradient. As one can see in Equation (14.33), the impulse needed to bring the plates together to a film thickness of h (or to separate the plates to a distance of h) is proportional to viscosity. For non-linearly viscous liquids, the viscosity is dependent on the velocity (as a rule, it is smaller at larger velocities). If the plates are initially shoved very quickly together and then slowly taken apart, then the positive impulse during impact is smaller than the negative during separation. This difference can be used to hold a moving body in equilibrium on the ceiling.

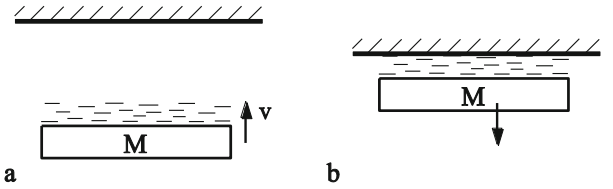

Fig. 14.7 A plate thrown against the "ceiling" that is covered with a liquid film will hang from it for a time.

14.4 Rheology of Lubricants

Until now, we have assumed that a lubricant is a linearly viscous (Newtonian) fluid. This means that the viscosity is a constant which is dependent on neither the velocity gradient nor the pressure. In practice, deviations from linearly viscous behavior are often desired and are brought about by the introduction of special additives. In this section, we will qualitatively discuss the most important deviations from linearly viscous behavior.

In the spatial scale of the diameters of a few atoms and the time scale of 10^{-13} to 10^{-10} s, the liquid is presented as an amorphous body in which every molecule lies in the minimum created by its neighbors and moves from it only seldom due to thermal fluctuations. These very rare jumps from the microscopic point of view are, however, the physical cause for the fluidity of liquids being acted upon by shear stresses. If the shear stress in the medium is not equal to zero, then every molecule can jump in every direction with the same probability P, which is given by the Boltzmann factor

$$P \propto e^{-\frac{U_0}{kT}}, \tag{14.34}$$

where U_0 is the activation energy, T is the absolute temperature, and k is the Boltzmann constant. In the absence of macroscopic stresses, no macroscopic motion takes place in the liquid. If a stress τ is applied to the medium, then the

height of the potential barrier changes for the molecules to "jump to the right" $\left(U_r = U_0 - \tau V_0\right)$ and "to the left" $\left(U_l = U_0 + \tau V_0\right)$. Here, V_0 is the so-called activation volume. In addition, the activation energy U_0 is dependent on the pressure p acting on the fluid. As a rule, it increases with pressure: $U_0 = E_0 + pV_1$, where V_1 is another constant with the same dimensions as volume. Thus, the activation energies for molecular motion in the opposing directions can be written as

$$\begin{aligned} U_r &= E_0 + pV_1 - \tau V_0 \ , \\ U_l &= E_0 + pV_1 + \tau V_0 \ . \end{aligned} \tag{14.35}$$

Both activation volumes V_0 and V_1 have an order of magnitude of an atomic volume a^3, where a is the atomic radius. The velocity of the macroscopic shear deformation is proportional to the difference between molecular flows in opposing directions:

$$\dot{\gamma} = \frac{dv_x}{dz} = const\left\{ e^{-\frac{E_0 + pV_1 - \tau V_0}{kT}} - e^{-\frac{E_0 + pV_1 + \tau V_0}{kT}} \right\} = Ce^{-\frac{E_0 + pV_1}{kT}} \sinh\left(\frac{\tau V_0}{kT}\right). \tag{14.36}$$

This equation presents a compact form of the most important typical deviations of the rheology of real fluids from those of Newtonian fluids. The following limiting cases provide a more differentiated view of the properties which are described by Equation (14.36):

I. If the stress is very small: $\frac{\tau V_0}{kT} \ll 1$, then one can replace $\sinh\left(\frac{\tau V_0}{kT}\right)$ with $\frac{\tau V_0}{kT}$ neglecting higher order terms. For the velocity of the shear deformation, we obtain

$$\dot{\gamma} = \frac{dv_x}{dz} = Ce^{-\frac{E_0 + pV_1}{kT}} \frac{\tau V_0}{kT} \ . \tag{14.37}$$

This equation indicates that the shear deformation rate is proportional to the shear stress. The proportionality coefficient between τ and $\dot{\gamma}$ is none other than the dynamic viscosity of the medium:

$$\eta = \frac{kT}{CV_0} e^{\frac{E_0 + pV_1}{kT}} \ . \tag{14.38}$$

For the condition $kT \ll E_0$, which is valid at room temperatures, the viscosity decreases exponentially as the temperature increases. A decrease in viscosity of about 50 percent is typical for a temperature increase of 30 K. Furthermore, vis-

cosity features an exponential pressure dependence. The coefficient $\alpha = V_1 / kT$ in the pressure dependence relationship $\eta \propto e^{\alpha p}$ is called the *pressure viscosity coefficient.* At room temperature, the pressure viscosity coefficient is on the order of magnitude of $\alpha \sim 10^{-8}\ Pa^{-1}$.

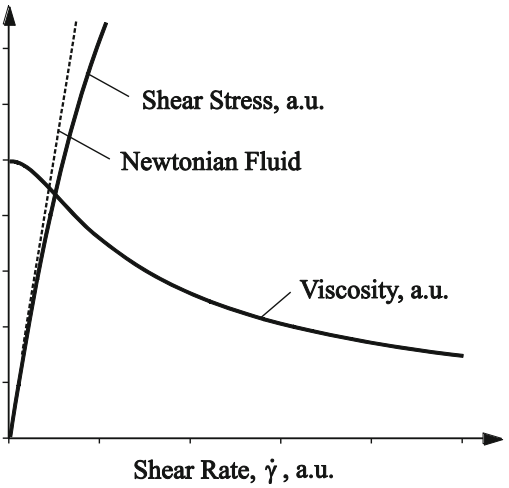

Fig. 14.8 Dependence of shear stress on the velocity of shear deformations (velocity gradients) according to (14.36) and the viscosity defined as $\tau / \dot{\gamma}$. The viscosity decreases with the deformation velocity.

II. In general, the dependence in (14.36) is non-linear. The deformation velocity increases with the shear stress faster than if it had a linear dependence. This means that at larger stresses or velocity gradients, the viscosity is smaller (see Fig. 14.8).

14.5 Boundary Layer Lubrication

If the thickness of the film is comparable to the roughness of the surface, then the system enters into the domain of *mixed friction*, where parts of the surface are separated by a liquid layer while in other parts, the micro-roughnesses come into close contact. At these points, the surfaces can be plastically deformed and come into an atomically close contact. Hardy (1919-1922) found experimentally that under these conditions the lubrication with greases protects the surfaces better than with more fluidic oils. He showed that even a single molecular layer of grease can dramatically reduce friction as well as wear. Hardy also recognized that the boundary layer adheres to the metal surface. Under conditions in which the surfaces are characterized by very thin, but strongly adhering, surface layers of lubrication, the friction is known as *boundary layer friction.* According to Hardy, the coefficient of friction as well as the wear decreases as the molecular weight of

the grease increases. It is important for the effectiveness of the boundary layer that the fatty acids form a *metal soap* with the metal surfaces. The protection mechanism of boundary layer lubrication is very similar to that of thin metal sheets (see Chapter 10), according to Bowden and Tabor. In particular, the film remains effective only up to the melting temperature or the softening temperature of the metal soap that has formed on the surface.

The most important difference between a lubricating grease and a lubricating oil consists of the fact that oil is a liquid, while greases and metal soaps are solid bodies with small, but finite, yield points. Thus, an oil can be completely pressed out of a contact point, but a plastic film cannot. So, between two round plates (radius R) being pressed together and separated by a lubricating material with a yield point τ_0, a film remains with a thickness[3]

$$h = \frac{2\tau_0}{3}\frac{\pi R^3}{F}\,. \tag{14.39}$$

14.6 Elastohydrodynamics

In highly loaded lubricated contacts such as rolling bearings, gears or cam followers, the surfaces of the contact partners are elastically deformed. The problem of the dynamics of the lubricant with account of elastic deformation is called elastohydrodynamics. It was essentially solved in 1945 by A. Ertel. In this section we discuss the most important aspects of elastohydrodynamic lubrication with Ertel's approximation[4].

We consider an elastic, cylindrical body $z = x^2/(2R)$ moving along a rigid plane at the speed v in the negative x-direction. Equation (14.10) in this case has the following form:

$$\frac{\mathrm{d}p}{\mathrm{d}x} = 6\eta v\frac{h(x)-h_0}{h(x)^3}\,, \tag{14.40}$$

where h_0 is the thickness of the lubricant at the point where the pressure reaches its maximum: $\mathrm{d}p/\mathrm{d}x = 0$. In highly loaded lubricated contacts, the pressure in the contact region can be so high that the dependence of viscosity on pressure (14.38) must be considered that we write here in the form

---

[3] See Problem 5 of this chapter.

[4] We follow the solution of A. Ertel described in the paper: E. Popova, V.L. Popov, On the history of elastohydrodynamics: The dramatic destiny of Alexander Mohrenstein-Ertel and his contribution to the theory and practice of lubrication. ZAMM· Z. Angew. Math. Mech., 2015, v. 96, N. 7, pp. 652-883.

$$\eta = \eta_0 e^{\alpha p} . \tag{14.41}$$

Then the Reynold's equation (14.40) has the form

$$e^{-\alpha p} \frac{\mathrm{d}p}{\mathrm{d}x} = 6\eta_0 v \frac{h(x) - h_0}{h(x)^3} . \tag{14.42}$$

With an introduction of the "effective pressure"

$$\Pi = \frac{1 - e^{-\alpha p}}{\alpha} \tag{14.43}$$

we can re-write (14.42) as

$$\frac{\mathrm{d}\Pi}{\mathrm{d}x} = 6\eta_0 v \frac{h(x) - h_0}{h(x)^3} , \tag{14.44}$$

which is similar to Eq.(14.40): only the pressure p is now replaced by the "effective pressure" Π. If the pressure in the contact area is very high, then the effective pressure according to (14.43) is constant in almost the entire contact area and equal to $\Pi = 1/\alpha$. From (14.44) it follows that in this part of the contact area, the thickness of lubricant film is practically constant and equal to h_0. The pressure distribution therefore corresponds to the Hertzian pressure distribution in a first approximation.

The film thickness h_0 is determined by processes at the inlet edge of the contact, where the surfaces can still be regarded as not deformed and the gap between them is given by the Hertzian solution[5]:

$$\delta = \frac{P}{\pi E^*} \hat{h} \tag{14.45}$$

with the dimensionless thickness

$$\hat{h}(\xi) = \left[2\xi\sqrt{\xi^2 - 1} - \ln \frac{\xi + \sqrt{\xi^2 - 1}}{\xi - \sqrt{\xi^2 - 1}} \right] \tag{14.46}$$

where $\xi = |x| / a$ is the x-coordinate normalized by the half length of the contact width

$$a = 2\sqrt{\frac{PR}{\pi E^*}} . \tag{14.47}$$

[5] K.L. Johnson, Contact mechanics, Cambridge University Press, 2001.

We introduced here the parameter P which is equal to the normal force divided by the contact length in the transverse direction $P = F / L$. In the inlet area (14.44) takes the form

$$\frac{\mathrm{d}\Pi}{\mathrm{d}x} = 6\eta_0 v \frac{\delta(x)}{\left(\delta(x) + h_0\right)^3}. \tag{14.48}$$

Integration over x from $-\infty$ to $-a$ results

$$\Pi(-a) = \frac{1}{\alpha} = 6\eta_0 v \int_{-\infty}^{-a} \frac{\delta(x)}{\left(\delta(x) + h_0\right)^3} \mathrm{d}x = \frac{6\eta_0 v a \pi^2 E^{*2}}{P^2} \Sigma, \tag{14.49}$$

where we introduced the notation

$$\Sigma = \int_1^{\infty} \frac{\hat{h}(\xi)}{\left(\hat{h}(\xi) + \hat{h}_0\right)^3} \mathrm{d}\xi, \quad \hat{h}_0 = \frac{\pi E^*}{P} h_0. \tag{14.50}$$

As seen in Fig.14.9, this function can be approximated very well as follows

$$\Sigma \approx 0.0986 \cdot \hat{h}_0^{-1.375}. \tag{14.51}$$

Substituting into (14.49) and solving the equation with respect to h_0 results in

$$h_0 = 1.25 \cdot \alpha^{0.727} \left(\eta_0 v\right)^{0.727} R^{0.364} E^{*0.091} P^{-0.091}. \tag{14.52}$$

This result of Ertel is very close to the later numerical solution of Hamrock and Dowson[6]:

$$h_0 = 3.06 \cdot \alpha^{0.56} \left(\eta_0 v\right)^{0.69} R^{0.41} E^{*-0.03} P^{-0.1}. \tag{14.53}$$

[6] B.J. Hamrock, D. Dowson, Ball Bearing Lubrication, Wiley, New York, p.386, 1981.

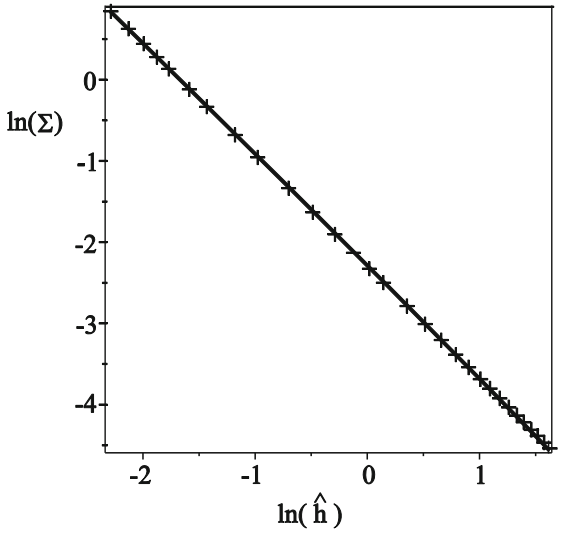

Fig. 14.9 Comparison of the function (14.50) (solid line) with the approximation (14.51) (crosses).

At the outlet edge the pressure gradient is negative, therefore, the film thickness decreases according to (14.44) and becomes smaller than h_0.

Finally, we briefly discuss the pressure distribution at the outlet edge. After Ertel, one can consider the lubricant film as practically incompressible in the inner high-pressure contact region and as compressible in the outer region. This means that the pressure distribution in the vicinity of the outlet edge can be considered as a superposition of the Hertzian pressure distribution and the singular pressure distribution generated by a rigid flat punch:

$$p(x) = c_1 \left(1 - x^2 / a'^2\right)^{1/2} + c_2 \left(1 - x^2 / a'^2\right)^{-1/2} \tag{14.54}$$

with $a' < a$. This distribution is exemplary illustrated in Fig. 14.10.

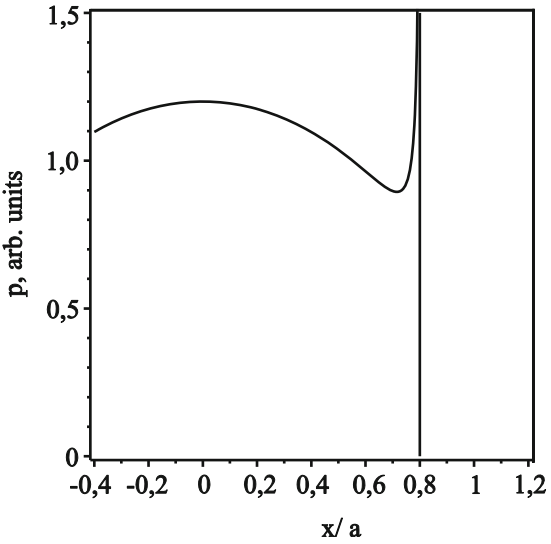

Fig. 14.10 Schematic representation of the pressure distribution at the outlet edge of an elasto-hydrodynamically lubricated contact.

14.7 Solid Lubricants

Under certain conditions, liquid lubricants cannot be applied to reduce friction and wear. Space flight applications are one example where tribological systems must function reliably in either vacuum or in extremely high or low temperatures. In these cases, solid lubricants can be used.

Precursors of today's solid lubricants – lead, graphite, and molybdenite (MoS_2) – have been known for ages. All three substances have similar colors (from grayish-blue to black) and are easily spread on a counter body. Until the 18th century, they were often mistaken for one another. Lead was replaced by graphite and graphite with molybdenite. The name "molybdenite" itself stems from the Greek Μόλυβδος, which means lead. In England, graphite was known as "plumbago," which can also be traced back to lead.

The extensive propagation of graphite and molybdenite as solid lubricants was only possible after methods to produce highly pure substances were developed. Both substances were applied at the end of the 19th century and during the 1930's, respectively, in the form of suspensions.

The most important properties of a solid lubricant are its strong adhesion to surfaces in friction and its easy deformability. Apart from the layered structure of graphite and molybdenite, other factors may be important. For example, graphite has good lubricating properties only in the presence of a small amount of water or

oxygen, but loses its lubricating properties in a vacuum. In contrast, the lubricating properties of molybdenite improve under "water-free" conditions.

As a rule, materials used in modern industry as solid lubricants have a layered structure similar to that of graphite and molybdenite. It is apparent that the mechanism of the lubricating action of solid lubricants is similar to that of boundary layer lubrication.

Problems

Problem 1: Calculate the force of friction between a corrugated surface with a periodic profile of $a\cos kx$ and an even plane which are separated by a liquid film.

Solution: We will define the separation distance between the two surfaces as $h = h(x)$. The gradient h' is assumed to be very small. Let the slot in between the surfaces be filled with a lubricant with a viscosity of η. The velocity profile of a creeping flow in a parallel slot has the form (14.7):

$$v = p'\frac{z(z-h)}{2\eta} + \frac{v_0}{h}(z-h)$$

with a pressure gradient (14.10)

$$\frac{dp}{dx} = -6\eta v_0\left(\frac{1}{h^2} - \frac{C}{h^3}\right).$$

Integrating over a spatial period Λ yields

$$p(\Lambda) - p(0) = -6\eta v_0 \int_0^{\Lambda}\left(\frac{1}{h(x)^2} - \frac{C}{h(x)^3}\right)dx = 0.$$

Here, we set this integral equal to zero, because the pressure distribution is assumed to be a periodic function with the same period Λ as the profile of the corrugated surface. From this, it follows that

$$C = \frac{\int_0^{\Lambda}\frac{dx}{h(x)^2}}{\int_0^{\Lambda}\frac{dx}{h(x)^3}}.$$

The shear stress acting in the liquid on the even (lower) surface is equal to

$$\tau = \eta\left.\frac{\partial v}{\partial z}\right|_{z=0} = -\frac{p'h}{2} + \frac{\eta v_0}{h} = \eta v_0\left(\frac{4}{h} - \frac{3C}{h^2}\right).$$

For the tangential stress averaged over the period, which we perceive as macroscopic friction τ_R, we obtain

$$\tau_R = \frac{1}{\Lambda}\int_0^{\Lambda} \tau dx = \frac{\eta v_0}{\Lambda}\int_0^{\Lambda}\left(\frac{4}{h(x)} - \frac{3C}{h(x)^2}\right)dx\,,$$

or after substituting C,

$$\tau_R = \frac{\eta v_0}{\Lambda}\left(4\int_0^{\Lambda}\frac{dx}{h(x)} - 3\left(\int_0^{\Lambda}\frac{dx}{h(x)^3}\right)^{-1}\left(\int_0^{\Lambda}\frac{dx}{h(x)^2}\right)^2\right).$$

For a constant slot width, this equation becomes the elementary formula $\tau_R = \eta v_0 / h$. Now, we assume that the corrugated surface is given through the equation

$$h(x) = h_0 + a\left(1-\cos(kx)\right)$$

so that the minimum slot width is h_0, the amplitude of the corrugations a, and the wave number $k = 2\pi/\Lambda$. In this case, it follows that

$$\tau_R = \frac{\eta v_0}{h_0}\frac{1}{\sqrt{1+2a/h_0}}\frac{h_0^2+2h_0a+3a^2}{h_0^2+2h_0a+\frac{3}{2}a^2}\,.$$

In the limiting case $h_0 \ll a$, it is

$$\tau_R \approx \sqrt{2}\,\frac{\eta v_0}{\sqrt{ah_0}}\,.$$

Problem 2: Calculate the force that acts between a plane and a sphere (radius R**)** approaching this plane. The distance between the sphere and the plane should be much smaller than R.

Solution: In this case, we are dealing purely with the squeezing of a fluid caused by a pressure gradient. The pressure gradient is calculated according to Equation (14.25):

$$p' = \frac{6\eta r\dot{h}}{h^3}\,.$$

In our case, the slot height is given by

$$h \approx h_0 + r^2/2R\,.$$

Integrating the pressure gradient, we obtain

$$p = p_{ext} - \int_r^\infty 6\eta\dot{h}\frac{rdr}{\left(h_0 + r^2/2R\right)^3} = p_{ext} - \frac{3\eta R\dot{h}}{\left(h_0 + r^2/2R\right)^2}.$$

(Because the integral converges on the upper boundary, we have replaced it with ∞). The force acting on the sphere is, therefore, equal to

$$F_N = \int_0^\infty 2\pi r\left(p(r) - p_{ext}\right)dr = -\frac{6\pi\eta R^2\dot{h}}{h_0}.$$

Problem3: A cylindrical profile $z = x^2/(2R)$ is moving along a rigid plane in the negative x-direction at the speed v with distance $h_{\min}$. Determine the pressure distribution in the lubrication gap, the normal and the tangential force and the coefficient of friction considering cavitation.

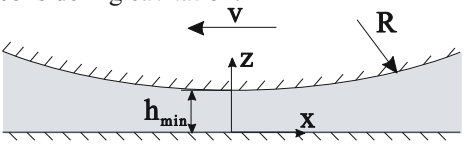

Fig. 14.11 Hydrodynamic lubrication between a rigid body cylindrical profile and a rigid plane.

Solution[7]*:* Equation (14.10) in this case has a following form:

$$\frac{\mathrm{d}p}{\mathrm{d}x} = 6\eta v\frac{h(x) - h_0}{h(x)^3},$$

where h_0 is the film thickness at the point where the pressure reaches its maximum $\mathrm{d}p/\mathrm{d}x = 0$. The thickness of the lubrication gap is

$$h = h_{\min} + \frac{x^2}{2R}.$$

Introducing dimensionless variables

$$\tilde{x} = x/\sqrt{2Rh_{\min}}, \quad \tilde{h} = h/h_{\min}, \quad \tilde{p} = p\cdot\frac{h_{\min}^2}{3\eta v\sqrt{2Rh_{\min}}}$$

one can rewrite the both equations in the form:

$$\frac{\mathrm{d}\tilde{p}}{\mathrm{d}\tilde{x}} = 2\frac{\tilde{h} - \tilde{h}_0}{\tilde{h}^3},$$

[7] We follows the solution of A. Ertel described in the paper: E. Popova, V.L. Popov, On the history of elastohydrodynamics: The dramatic destiny of Alexander Mohrenstein-Ertel and his contribution to the theory and practice of lubrication. ZAMM· Z. Angew. Math. Mech., 2015, v. 96 N. 7, pp. 652-883.

$$\tilde{h} = 1 + \tilde{x}^2 .$$

Integration of the first equation results in

$$\tilde{p} = \frac{\pi}{2} + \arctan\tilde{x} + \frac{\tilde{x}}{1+\tilde{x}^2} - \frac{3}{4}\tilde{h}_0\left[\frac{\pi}{2} + \arctan\tilde{x} + \frac{\tilde{x}}{1+\tilde{x}^2} + \frac{2}{3}\frac{\tilde{x}}{\left(1+\tilde{x}^2\right)^2}\right] + \tilde{p}_0 \ ,$$

where $\tilde{p}_0$ is the dimensionless outlet pressure for $x \to -\infty$. Here, we assume it to be zero. The pressure distribution for different values of $\tilde{h}_0$ is shown in Fig. 14.12.

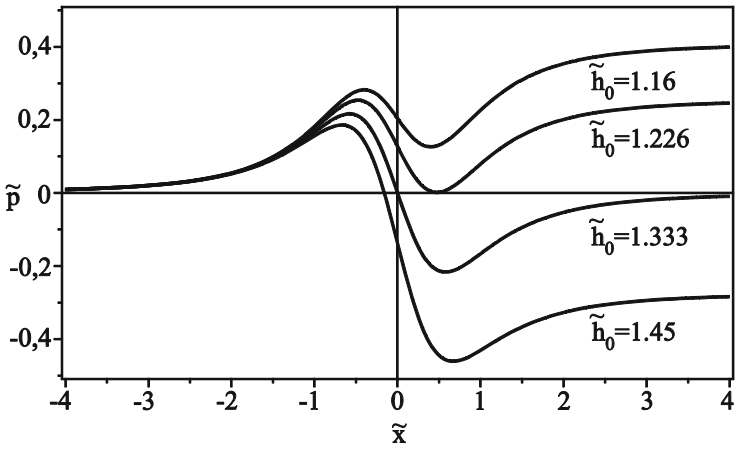

Fig. 14.12 Normalized pressure distribution in the lubrication gap.

We assume that fluids cannot bear negative pressures[8]. This condition means that the curves in Fig. 14.12 are valid only to the point where the pressure disappears (after which it remains equal to zero). This assumption does not unambigously determine the choice of the integration constant. A further condition is the disappearance of the pressure gradient at the cavitation point, which ensures the stability of the separation line. In Fig. 14.12 we see that this condition is fulfilled only by the curve with $\tilde{h}_0 = 1.226$. The normal force per unit length of the cylinder $\tilde{f}_N$ is given by integration of the pressure to the cavitation point and is equal to $\tilde{f}_N = 0.408$. With the original variables, it gives

$$f_N = 2.447\frac{\eta v R}{h_{\min}} .$$

[8] If the pressure is smaller than the pressure of saturated vapor, liquids are in a thermodynamically unstable state and will "boil" (cavitation). Since the saturated vapor pressure of lubricating oils at operating temperature is usually very small, it can be assumed to be zero.

The integration of the tangential force results in the tangential force per unit length, q,

$$q = 5.149\eta v\sqrt{\frac{R}{h_{\min}}}\,.$$

The coefficient of friction is

$$\mu \approx 2\sqrt{\frac{h_{\min}}{R}} \approx 3\sqrt{\frac{\eta v}{f_N}}\,,$$

which coincides with (14.21) up to a constant coefficient and is an additional illustration of the robustness of this equation.

Problem 4: Consider a sliding bearing in the form of a step (Rayleigh step-bearing, Fig 14.13). Determine the pressure distribution in the lubrication gap, the normal and the tangential force, and the coefficient of friction. The external pressure is assumed to be negligibly small.

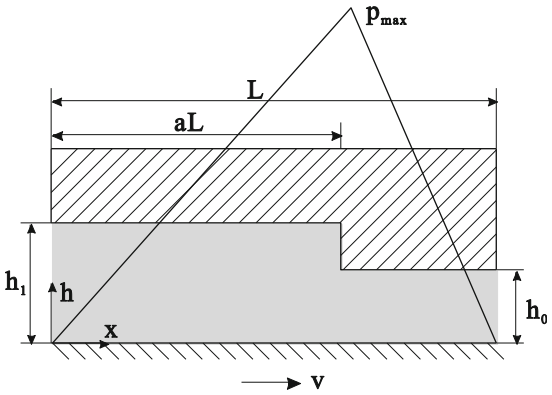

Fig. 14.13 Rayleigh step-bearing: a stepped profile moves with respect to a flat surface with speed v. The geometric parameters of the object and the pressure distribution are shown in the figure.

Solution: In this case, the thickness of the lubricant layer is constant in the each field $x \in [0, aL]$ and $[aL, L]$, so that equation (14.11) for each section takes the most simple form $\mathrm{d}^2 p / \mathrm{d}x^2 = 0$. Thus, the pressure in each region of constant height is a linear function of the coordinate x: $p(x) = C_1 x + C_2$, where the coefficients C_1 and C_2 are different for the left and right regions. Since the pressure at the outer edges of the gap vanishes, it is clear that the pressure initially increases linearly from the front edge, reaches its maximum at the step point and then linearly decreases down to the value zero at the back edge, as shown in Fig. 14.13:

$$p(x)=\begin{cases}\dfrac{p_{\max}}{aL}\cdot x, & x\le aL\\ -\dfrac{p_{\max}}{L-aL}\cdot(x-L), & x\ge aL\end{cases}.$$

To determine the value of $p_{\max}$, the continuity equation must be used: the flow density q is given by the equation (14.9) (here with a change in sign of the speed), $q=-\dfrac{h^3}{12\eta}\cdot\dfrac{\mathrm{d}p}{\mathrm{d}x}+\dfrac{vh}{2}$ in the left and right region must be same:

$$-\frac{h_1^{\,3}}{12\eta}\cdot\left.\frac{\mathrm{d}p}{\mathrm{d}x}\right|_{x=aL-}+\frac{vh_1}{2}=-\frac{h_0^{\,3}}{12\eta}\cdot\left.\frac{\mathrm{d}p}{\mathrm{d}x}\right|_{x=aL+}+\frac{vh_0}{2}.$$

Calculating the pressure gradient to the left and to the right from the step

$$\left.\frac{\mathrm{d}p}{\mathrm{d}x}\right|_{x=aL-}=\frac{p_{\max}}{aL},\quad \left.\frac{\mathrm{d}p}{\mathrm{d}x}\right|_{x=aL+}=-\frac{p_{\max}}{L-aL},$$

substituting these values into the continuity equation and solving it with respect to $p_{\max}$ results in

$$p_{\max}=\frac{6v\eta L}{h_0^2}\cdot\frac{a(1-a)m}{a+(1-a)(1+m)^3},$$

where we introduced the notation $m=h_1/h_0-1$.

The normal force F_N is determined by the integration of the pressure:

$$F_N=\int_0^L p(x)\mathrm{d}x=\frac{3v\eta L^2}{h_0^2}\cdot\frac{a(1-a)m}{a+(1-a)(1+m)^3}=\frac{p_{\max}L}{2}$$

and the tangential force F_x, by the integration of the viscous stress

$$F_x=\int_0^L\tau\mathrm{d}x=\int_0^L\left(\frac{h}{2}\frac{\mathrm{d}p}{\mathrm{d}x}+\eta\frac{v}{h}\right)\mathrm{d}x=\frac{p_{\max}h_0}{2}m+\frac{\eta vL}{h_0}\cdot\left(\frac{a}{1+m}+1-a\right).$$

The coefficient of friction μ is

$$\mu=\frac{F_x}{F_N}=\frac{h_0}{L}\left[m+\frac{1}{3m}\left(\frac{a}{1+m}+1-a\right)\left(\frac{1}{1-a}+\frac{(1+m)^3}{a}\right)\right].$$

The coefficient of friction reaches its minimum $\mu=4h_0/L$ when $m=1$ and $a=0.8$.

Problem 5: Mohrenstein bearing. Determine the coefficient of friction in the contact between a bearing and an elastic moving surface, in which the pressure distribution in the lubricating gap is given by a preload (as shown schematically in Fig. 14.14).

Solution: We consider an elastic profile, which moves along a rigid plane in the positive x-direction with the speed v. For this elastohydrodynamic problem (14.40) is valid:

$$\frac{\mathrm{d}p}{\mathrm{d}x} = 6\eta v \frac{h(x) - h_0}{h(x)^3} .$$

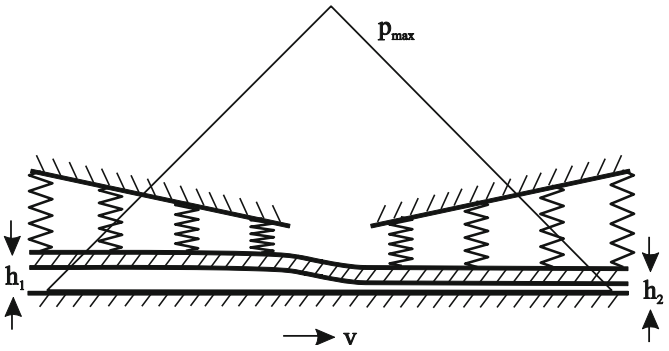

Fig. 14.14 Schematic representation of the "Mohrenstein bearing". The figure depicts the patent (A. von Mohrenstein, US patent 2738241, Hydrodynamic bearing. Application July 16, 1952, patented March 13, 1956).

If the preload pressure is given by means of appropriately distributed springs and it can be assumed that small changes of the lubricating gap do not affect the pressure distribution in the contact area, then the pressure distribution in the Reynolds equation can be considered to be a known function of the coordinate. In contrast, the lubrication gap is unknown and must be determined from the Reynolds equation. Through constructive measures, one can create a pressure distribution which linearly increases from one end of the film to the center and then decreases linearly (as shown in Fig. 14.14). Then, the pressure gradient is constant in both the left and right areas and equal to $\pm\nabla p$. From the Reynold's equation, it follows that in the area left of the center, the thickness of the lubricating layer is constant and equal to h_1, and in the area right of the center constant and equal to h_2. The layer thicknesses are determined by the equations

$$\nabla p = 6\eta v \frac{h_1 - h_0}{h_1^3} \quad \text{and} \quad -\nabla p = 6\eta v \frac{h_2 - h_0}{h_2^3} .$$

From the first equation we can easily deduce that the pressure gradient reaches the maximum value of $\nabla p_{\max} = \frac{8}{9}\frac{\eta v}{h_0^2}$ at $h_1 = \frac{3}{2}h_0$. By substitution of the maximum pressure gradient into the second equation and solving for h_2 it follows that $h_2 = 0.894h_0 = 0.596h_1$. The layer thickness in the outlet area is roughly equal to half the layer thickness in the inlet region. Unlike the Rayleigh-step bearing, the Mohrenstein bearing is symmetric: It works in the same way regardless of the direction of movement. The layer thicknesses are set according to the sliding direction automatically. The coefficient of friction of the Mohrenstein bearing corresponds to that of the Rayleigh bearing (see Problem 4) with $a = 0.5$ and $m = 0.678$ and is equal to $\mu_0 = 5.17h_2 / L$, where L is the total length of the bearing.

Problem 6: A shaft of radius r rotates in a cylindrical cavity with a constant angular velocity ω (Fig. 14.15), while the outer cylinder does not move and has a radius of $R = r + a$. Let the length of the cylinders be L. The space in between the cylinders is filled with a liquid of viscosity η. In general, the shaft lies eccentrically in the cylindrical cavity, because it is loaded. Assuming that $a \ll r$, calculate the friction moment acting on the cam shaft and the coefficient of friction.

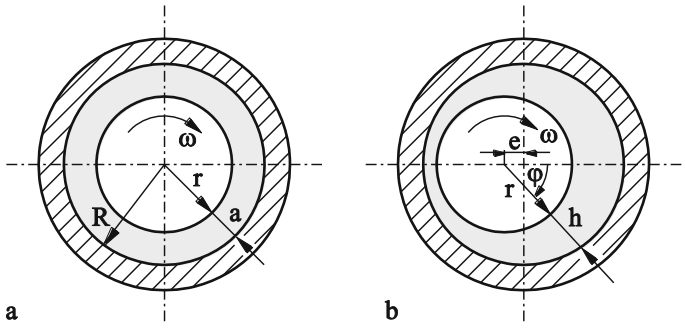

Fig. 14.15 Hydrodynamic bearing: (a) without load, (b) with load.

Solution: Assuming that $a \ll r$, the flow between the shaft and the cylinder can be seen as a parallel flow. The velocity, thereby, has only the circumferential component v_φ and the pressure p is only dependent on the angle. Equation (14.8) is valid for the flow profile, which in our case takes the following form:

$$v_\varphi = \frac{1}{r}\frac{dp}{d\varphi}\frac{\tilde{z}(\tilde{z} - h(\varphi))}{2\eta} + \frac{\omega r}{h(\varphi)}(h(\varphi) - \tilde{z})$$

with

$$h(\varphi) \approx a + e\cos\varphi\,.$$

The pressure distribution is given by

$$p(\varphi)-p(0)=+6\eta\omega r^2\int_0^{\varphi}\left(\frac{1}{h(\varphi)^2}-\frac{C}{h(\varphi)^3}\right)d\varphi,$$

where

$$C=\frac{\int_0^{2\pi}\frac{d\varphi}{h(\varphi)^2}}{\int_0^{2\pi}\frac{d\varphi}{h(\varphi)^3}}$$

(see analogous equations in Problem 1). It is an odd function of the angle φ. The horizontal component of the force $F_x=Lr\int_0^{2\pi}p(\varphi)\cos\varphi d\varphi$ vanishes, because $p(\varphi)$ is an odd function. The vertical component of the force is calculated as[9]

$$F_z=Lr\int_0^{2\pi}p(\varphi)\sin\varphi d\varphi=-Lr^3 6\eta\omega\int_0^{2\pi}(1-\cos\varphi)\left(\frac{1}{h(\varphi)^2}-\frac{C}{h(\varphi)^3}\right)d\varphi=\frac{12\pi eLr^3\eta\omega}{\left(2a^2+e^2\right)\sqrt{a^2-e^2}}.$$

The tangential stress is calculated in exactly the same way as in Problem 1 and is

$$\tau=-\eta\omega r\left(\frac{4}{h(\varphi)}-\frac{3C}{h(\varphi)^2}\right).$$

The moment is

$$M=Lr^2\int_0^{2\pi}\tau(\varphi)d\varphi=-L\eta\omega r^3\int_0^{2\pi}\left(\frac{4}{h(\varphi)}-\frac{3C}{h(\varphi)^2}\right)d\varphi=-\frac{4\pi\eta\omega r^3L\left(a^2+2e^2\right)}{\sqrt{a^2-e^2}\left(2a^2+e^2\right)}.$$

For the ratio $\mu=|M|/rF_z$, which plays the role of the coefficient of friction in this case, we obtain

$$\mu=\frac{\left(a^2+2e^2\right)}{3er}.$$

For larger loads, when $e\to a$, the coefficient of friction assumes the limiting value

$$\mu=\frac{a}{r}.$$

[9] In reality, the viscous stress also contributes to the vertical force. One can show, however, that this contribution is small under the assumed conditions and can be neglected.

Problem 7: a) Calculate the velocity profile and pressure distribution in a squeezing flow of a non-linearly viscous liquid between two round plates. We assume that the rheological law is

$$\dot{\gamma} = \dot{\gamma}_0 \left(\frac{\tau}{\tau_0} \right)^n ,$$

where γ is the shear deformation, $\dot{\gamma}_0$ is the characteristic shear velocity, n is an odd number, and τ_0 is the characteristic stress (in the limiting case of $n \to \infty$, the yield stress).
b) Calculate the remaining film thickness in the case of an ideally plastic material with the critical shear stress τ_0 ($n \to \infty$).

Solution: (a) We choose the coordinate axes so that the origin lies at the middle of the film and the z-axis is perpendicular to the film (Fig. 14.16). The pressure is independent of the z-coordinate.

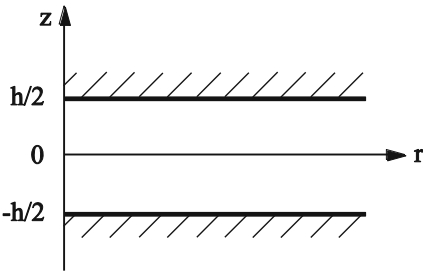

Fig. 14.16

Due to axial symmetry, it is sufficient to consider only the r-component of the equilibrium equation:

$$-\frac{\partial p}{\partial r} + \frac{\partial \tau}{\partial z} = 0 .$$

Integrating once with respect to z yields

$$\tau = C_1 + p'z$$

and inserting this into the rheological law, we obtain the following flow profile

$$\dot{\gamma} = \dot{\gamma}_0 \left(\frac{C_1 + p'z}{\tau_0} \right)^n .$$

The constant C_1 must vanish, because $\dot{\gamma}(z = 0) = 0$ must be fulfilled due to reasons of symmetry. The equation can now be written in the form

$$\frac{\partial v}{\partial z} = \dot{\gamma}_0 \left(\frac{p'z}{\tau_0} \right)^n .$$

Integration yields

$$v = \frac{\dot{\gamma}_0}{n+1} \left(\frac{p'}{\tau_0} \right)^n z^{n+1} + C_2 .$$

Taking into account the no-slip condition $v(h/2) = v(-h/2) = 0$ on the solid surface, we ultimately come to the following flow profile in the slot:

$$v = \frac{\dot{\gamma}_0}{n+1} \left(\frac{-p'}{\tau_0} \right)^n \left(\left(\frac{h}{2} \right)^{n+1} - z^{n+1} \right).$$

The volume flow through a cylinder barrel with the radius r is calculated as

$$Q = 2\pi r \int_{-h/2}^{h/2} v(z)\mathrm{d}z = 2\pi r \frac{\dot{\gamma}_0}{n+2} \left(\frac{-p'}{\tau_0} \right)^n \frac{h^{n+2}}{2^{n+1}} .$$

From continuity, it follows that

$$-\pi r^2 \dot{h} = 2\pi r \frac{\dot{\gamma}_0}{n+2} \left(\frac{-p'}{\tau_0} \right)^n \frac{h^{n+2}}{2^{n+1}} .$$

For the pressure gradient we get

$$-\frac{\partial p}{\partial r} = 2\tau_0 \left(-\dot{h} \frac{n+2}{\dot{\gamma}_0 h^{n+2}} r \right)^{1/n} .$$

Integrating this equation with the boundary condition $p(R) = p_0$, we obtain the pressure distribution in the film:

$$p - p_0 = 2\tau_0 \left(-\dot{h} \frac{n+2}{\dot{\gamma}_0 h^{n+2}} \right)^{1/n} \frac{1}{\frac{1}{n}+1} \left(R^{\frac{1}{n}+1} - r^{\frac{1}{n}+1} \right).$$

The normal force acting on the plate is equal to

$$F = \int_0^R 2\pi r \left(p - p_0 \right) \mathrm{d}r = \frac{2\tau_0 n}{3n+1} \frac{\pi R^{3+\frac{1}{n}}}{h^{1+\frac{2}{n}}} \left(-\dot{h} \frac{n+2}{\dot{\gamma}_0} \right)^{1/n} .$$

For $n = 1$ (linearly viscous fluid), we again call upon Equation (14.27).
(b) In the limiting case of $n \to \infty$, the equations for pressure distribution and force simplify to

$$p - p_0 = 2\tau_0 \frac{R-r}{h}$$

and

$$F = \frac{2\tau_0}{3} \frac{\pi R^3}{h}.$$

In this case, we are dealing with an ideally plastic behavior with a yield point of τ_0. From this equation, the thickness of the film, which remains in the slot and is not pressed out, can be calculated:

$$h = \frac{2\tau_0}{3} \frac{\pi R^3}{F}.$$

15 Viscoelastic Properties of Elastomers

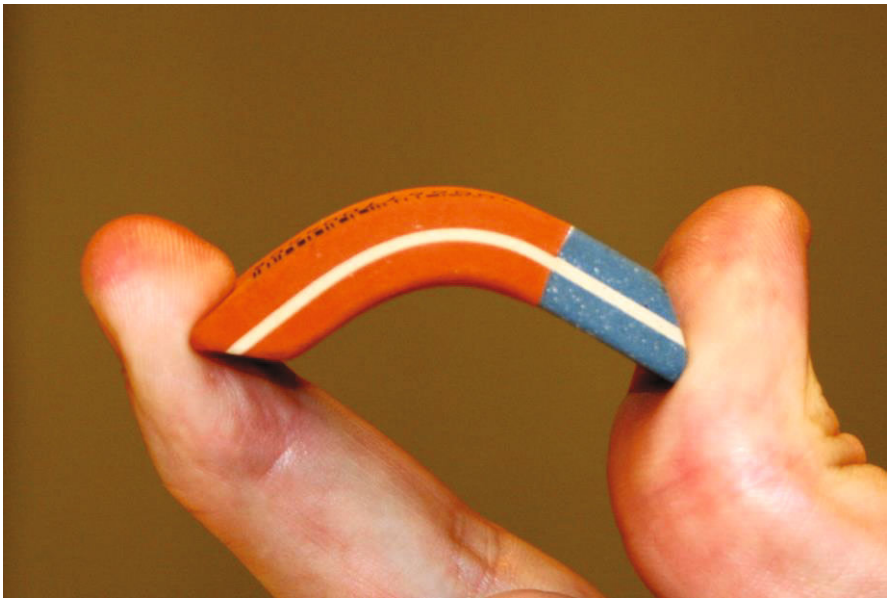

15.1 Introduction

Rubber and other elastomers play an important role in many tribological applications. They are used where large frictional forces are demanded. In particular, they find applications as materials for tires, feed rollers (e.g. in printers), sports shoes, seals, rubber bands, and materials in electronic devices (e.g. keyboard contacts), as well as adhesive fixtures.

The two most important properties of elastomers are: (1) an extremely small modulus of elasticity (ca. 1 to 10 MPa, meaning 4 to 5 orders of magnitude smaller than normal "solid bodies") and (2) extremely high deformability: elastomers can often be stretched to multiple times their original length.

The cause for these two fundamental properties of elastomers lies in their structure. Elastomers consist of polymer molecules which interact relatively weak with one another. In thermodynamic equilibrium, they are in a statistically favored coiled state. If a mechanical stress is applied to an elastomer, then the polymer molecules begin to untangle (Fig. 15.1). If the stress is then removed, then the polymer molecules relax once again to their coiled state. While for "normal solid bodies" the equilibrium state primarily corresponds to a minimum in potential en-

V.L. Popov, *Contact Mechanics and Friction*,
DOI 10.1007/978-3-662-53081-8_15

ergy, for elastomers equilibrium is reached primarily when entropy reaches its maximum. This has become known as *entropy elasticity*[1].

In order to prevent the complete disentanglement of the chains under tensile loading, the rubber chains are connected to each other by sulfur bridges – this treatment is known as *vulcanization*[2]. By the addition of a large amount of sulfur during vulcanization, hard rubber is formed; by adding less sulfur we get softer rubber. In order to achieve an optimization between elasticity, wear resistance, and adhesive ability, rubber is mixed with soot during the manufacture of automobile tires. The composite material that results is known as "soot-filled rubber."

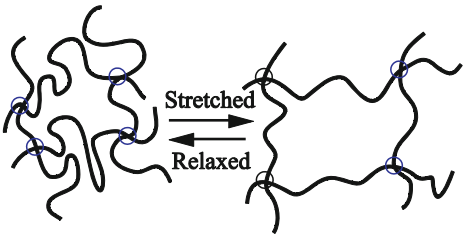

Fig. 15.1 Schematic representation of the changes that occur in the structure of an elastomer during tensile loading.

It is generally accepted that the contact and frictional properties of elastomers are due primarily to their rheological properties. In other words, the tribological properties of elastomers are largely determined not by their surface properties, but rather by their volume properties. This is the reason why, in this chapter, we initially devote ourselves to the detailed analysis of the rheological properties of rubber as well as methods to describe them. The terms and methods introduced in this chapter will be used in the next chapter in order to discuss the friction of elastomers. Thereby, we treat elastomers as *linearly* viscoelastic materials. The treatment of non-linearities is beyond the scope of this book.

15.2 Stress-Relaxation

We consider a rubber block that is being acted upon by shear forces (Fig. 15.2). If it is quickly deformed by the shear angle[3] ε_0, then the stress reaches a high level $\sigma(0)$ in the first moment and afterwards slowly relaxes to a much lower level $\sigma(\infty)$ (Fig. 15.3), whereby with elastomers, $\sigma(\infty)$ can be 3 to 4 orders of magni-

[1] In this sense, the elasticity of rubber is similar to the "elasticity" of an ideal gas, where the interactions between the molecules play no role and the elasticity is, likewise, of pure entropic nature.

[2] Vulcanization was developed by Charles Goodyear in 1839.

[3] Note that the shear angle ε_0 is equal to twice the shear component of the deformation tensor.

tude smaller than $\sigma(0)$. The physical cause for this behavior is clear: in the first moment, the polymer molecules do not yet have the time to untangle and the rubber responds like a "normal solid material." The respective shear modulus of $G(0) = \sigma(0)/\varepsilon_0$ has the same order of magnitude as the shear modulus of glass and is called the *glass modulus*. The ratio $G(\infty) = \sigma(\infty)/\varepsilon_0$ describes the behavior of the material after a sufficiently long waiting time and is called the *static shear modulus*. Over time, the molecules twist apart and the internal stress in the material eases. The ratio

$$G(t) = \frac{\sigma(t)}{\varepsilon_0} \tag{15.1}$$

is called the *time-dependent shear modulus*. It is easy to see that this function completely describes the mechanical properties of a material, assuming that the material exhibits a linear behavior:

We assume that the block is deformed according to an arbitrary strain function $\varepsilon(t)$. An arbitrary time-dependent function $\varepsilon(t)$ can always be presented as the sum of chronological step functions, as is schematically shown in Fig. 15.4. In this diagram, an "elementary step function" at time t' has an amplitude of $d\varepsilon(t') = \dot{\varepsilon}(t')dt'$. Its stress contribution is equal to $d\sigma = G(t-t')\dot{\varepsilon}(t')dt'$, and the total stress at every point in time is, therefore, calculated as

$$\sigma(t) = \int_{-\infty}^{t} G(t-t')\dot{\varepsilon}(t')dt' . \tag{15.2}$$

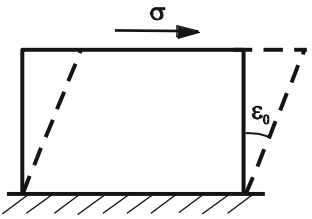

Fig. 15.2 Shear deformation of a rubber block.

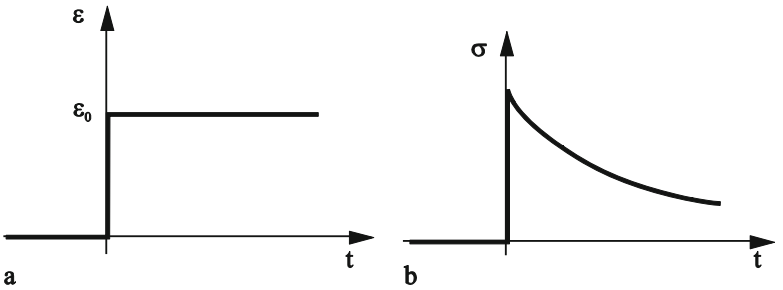

Fig. 15.3 If a rubber block is quickly deformed by ε_0 at time $t = 0$, then the stress increases initially to a high level and afterwards, relaxes with time to a much lower level.

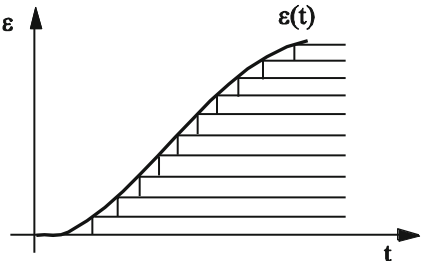

Fig. 15.4 Presentation of a time-dependent function as the superposition of several chronological step functions.

Equation (15.2) shows that the time-dependent shear modulus can be understood, in a mathematical sense, as a weighting function which describes how previous strain changes contribute to the stress at the current time. Because of this, $G(t)$ is also sometimes called the *memory function*.

15.3 Complex, Frequency-Dependent Shear Moduli

If $\varepsilon(t)$ changes according to the harmonic function

$$\varepsilon(t) = \tilde{\varepsilon}\cos(\omega t), \tag{15.3}$$

then after the transient time, there will also be a periodic change in stress at the same frequency ω. The connection between the change in deformation and stress can be presented quite simply when the real function $\cos(\omega t)$ is presented as the sum of two complex exponentials:

$$\cos(\omega t) = \frac{1}{2}\left(e^{i\omega t} + e^{-i\omega t}\right). \tag{15.4}$$

Due to the principal of superposition, one can initially calculate the stresses which result from the complex oscillations

$$\varepsilon(t) = \tilde{\varepsilon} e^{i\omega t} \quad \text{and} \quad \varepsilon(t) = \tilde{\varepsilon} e^{-i\omega t} \tag{15.5}$$

and sum them afterwards. If we insert $\varepsilon(t) = \tilde{\varepsilon} e^{i\omega t}$ into (15.2), then we obtain a stress of

$$\sigma(t) = \int_{-\infty}^{t} G(t-t') i\omega \tilde{\varepsilon} e^{i\omega t'} dt' . \tag{15.6}$$

By substituting $\xi = t - t'$, we bring the integral into the following form:

$$\sigma(t) = \int_{-\infty}^{t} G(t-t') i\omega \tilde{\varepsilon} e^{i\omega t'} dt' = i\omega \tilde{\varepsilon} e^{i\omega t} \int_{0}^{\infty} G(\xi) e^{-i\omega \xi} d\xi , \tag{15.7}$$

or, in other words,

$$\sigma(t) = \hat{G}(\omega) \tilde{\varepsilon} e^{i\omega t} = \hat{G}(\omega) \varepsilon(t) . \tag{15.8}$$

For a harmonic excitation in the form of a complex exponential $e^{i\omega t}$, the stress is proportional to deformation. The proportionality coefficient

$$\hat{G}(\omega) = i\omega \int_{0}^{\infty} G(\xi) e^{-i\omega \xi} d\xi \tag{15.9}$$

is generally a complex quantity and is called the *complex shear modulus*. Its real part, $G'(\omega) = \mathrm{Re}\, \hat{G}(\omega)$, is called the *storage modulus* and its imaginary part, $G''(\omega) = \mathrm{Im}\, \hat{G}(\omega)$, the *loss modulus.*

The amplitude of the oscillations is given respectively by the magnitude of the complex stress or deformation:

$$\left|\sigma(t)\right| = \left|\hat{G}(\omega) \tilde{\varepsilon} e^{i\omega t}\right| = \left|\hat{G}(\omega)\right| \left|\tilde{\varepsilon}\right| \left|e^{i\omega t}\right| . \tag{15.10}$$

Because the magnitude is $\left|e^{i\omega t}\right| = 1$, it follows that

$$\left|\sigma(t)\right| = \left|\hat{G}(\omega)\right| \left|\tilde{\varepsilon}\right| . \tag{15.11}$$

According to this, the oscillation *amplitudes* of the stress and deformation are connected by the *magnitude of the complex shear modulus*.

In order to illustrate the term complex modulus more clearly, we consider two simple examples:

(a) For a *linearly-elastic body*, the shear deformation behaves according to Hooke's law: $\sigma = G\varepsilon$. In this case, the complex modulus has only a real part and this is equal to G.

(b) For a *linearly-viscous fluid* in pure shear (Fig. 15.5) the following is valid:

$$\sigma = \eta \frac{dv}{dz}. \tag{15.12}$$

Therefore, for a periodic movement $\hat{u}(l,t) = u_0 e^{i\omega t}$ is

$$\hat{\sigma}(t) = \eta \left.\frac{dv}{dz}\right|_{z=l} = \eta \frac{\hat{v}(t)}{l} = \eta i\omega \frac{u_0}{l} e^{i\omega t} = i\omega\eta\hat{\varepsilon}(t). \tag{15.13}$$

In this case, the complex modulus

$$\hat{G}(\omega) = i\omega\eta \tag{15.14}$$

has only an imaginary part: $\mathrm{Re}\,\hat{G} = 0$, $\mathrm{Im}\,\hat{G} = \omega\eta$.

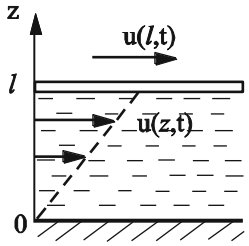

Fig. 15.5 Uniform shear flow of a linearly-viscous fluid.

15.4 Properties of Complex Moduli

According to definition (15.9), it follows that

$$\hat{G}(-\omega) = \hat{G}^*(\omega) \quad . \tag{15.15}$$

Here, "*" means that the value is a complex conjugate. The real and imaginary parts of the modulus, therefore, have the following properties:

$$\begin{aligned} G'(-\omega) &= G'(\omega), \\ G''(-\omega) &= -G''(\omega). \end{aligned} \tag{15.16}$$

Real and imaginary parts of complex moduli are not independent from one another, rather they must satisfy the so-called *Kramers-Kronig relations*:

$$G'(\omega) = G_0 + \frac{2\omega^2}{\pi}\int_0^\infty \frac{1}{z}\frac{G''(z)}{\left(\omega^2 - z^2\right)}dz\,,$$
$$G''(\omega) = -\frac{2\omega}{\pi}\int_0^\infty \frac{G'(z)}{\omega^2 - z^2}dz\,. \tag{15.17}$$

The integrals in these equations are understood to be Cauchy principal values (i.e. one approaches the poles symmetrically so that the singularities can be canceled out).

If the complex modulus is known in the entire frequency domain, then the time-dependent modulus can be calculated. By multiplying (15.9) with $\frac{1}{i\omega 2\pi}e^{i\omega t}$, and subsequently integrating over ω (from $-\infty$ to ∞), we obtain

$$\frac{1}{2\pi}\int_{-\infty}^{\infty}\frac{1}{i\omega}\hat{G}(\omega)e^{i\omega t}d\omega = \frac{1}{2\pi}\int_0^\infty G(\xi)\int_{-\infty}^{\infty}e^{i\omega(t-\xi)}d\omega d\xi\,. \tag{15.18}$$

The step function shown in Fig. 15.3 a corresponds to $\dot{\varepsilon}(t) = \varepsilon_0\delta(t)$, where $\delta(t)$ is the Dirac delta function. By using the identity

$$\int_{-\infty}^{\infty}e^{i\omega t}d\omega = 2\pi\delta(t)\,, \tag{15.19}$$

the right side of the equation (15.18) is simplified and only the time-dependent shear modulus remains. Therefore, taking (15.1) into account validates the following relation

$$\begin{aligned} G(t) = \frac{\sigma(t)}{\varepsilon_0} &= \frac{1}{2\pi}\int_{-\infty}^{\infty}\frac{\hat{G}(\omega)}{i\omega}e^{i\omega t}d\omega \\ &= \frac{1}{2\pi}\int_{-\infty}^{\infty}\frac{1}{\omega}\left(G'(\omega)\sin\omega t + G''(\omega)\cos\omega t\right)d\omega\,. \end{aligned} \tag{15.20}$$

15.5 Energy Dissipation in a Viscoelastic Material

The deformation of a material according to the relation $\varepsilon_1 = \varepsilon_0 e^{i\omega t}$ leads to the stress $\sigma_1 = \varepsilon_0\hat{G}(\omega)e^{i\omega t}$, according to the definition of complex shear moduli. For a deformation $\varepsilon_2 = \varepsilon_0 e^{-i\omega t}$, we only have to change the sign of the frequency: $\sigma_2 = \varepsilon_0\hat{G}(-\omega)e^{-i\omega t} = \varepsilon_0\hat{G}^*(\omega)e^{-i\omega t}$. If the total deformation can be represented over the sum of ε_1 and ε_2 as

$$\varepsilon = \varepsilon_0 \cos \omega t = \frac{\varepsilon_0}{2}\left(e^{i\omega t} + e^{-i\omega t}\right), \tag{15.21}$$

then, due to the linearity of the system, the stress is calculated as the sum σ_1 and σ_2:

$$\sigma = \frac{1}{2}\varepsilon_0 \left(G(\omega)e^{i\omega t} + G(\omega)^* e^{-i\omega t}\right) = \varepsilon_0 \left(G'(\omega)\cos \omega t - G''(\omega)\sin \omega t\right). \tag{15.22}$$

Now, we can calculate the power $\bar{P}$ of this stress in a unit volume:

$$\bar{P} = \left\langle \sigma(t)\dot{\varepsilon}(t)\right\rangle = \tfrac{1}{2}\omega\varepsilon_0^2 G''(\omega). \tag{15.23}$$

The energy dissipation is directly determined by the imaginary part of the complex modulus. Associated with it, is the term *"loss modulus"* for the imaginary part of the modulus of elasticity.

For a given stress, we take the property (15.11) into account and write $\sigma_0^2 = \left|\hat{G}(\omega)\right|^2 \varepsilon_0^2$. With this, we can bring (15.23) into the form

$$\bar{P} = \tfrac{1}{2}\omega\sigma_0^2 \frac{\operatorname{Im}\hat{G}(\omega)}{\left|\hat{G}(\omega)\right|^2} = -\tfrac{1}{2}\omega\sigma_0^2 \operatorname{Im}\left(\frac{1}{\hat{G}(\omega)}\right). \tag{15.24}$$

15.6 Measuring Complex Moduli

If a linearly viscoelastic material is deformed periodically at a frequency ω according to the relation (15.21) and the stress (15.22) is recorded in a steady oscillating state, then one can determine the complex modulus, by determining the average values

$$\bar{E} = \left\langle \sigma(t)\varepsilon(t)\right\rangle \text{ and } \bar{P} = \left\langle \sigma(t)\dot{\varepsilon}(t)\right\rangle. \tag{15.25}$$

We have already calculated the average power above and related it to the loss modulus. Now, the average value $\bar{E}$ can be tied to the *storage modulus*, because

$$\bar{E} = \frac{1}{2}G'\varepsilon_0^2. \tag{15.26}$$

So, the real part of the modulus G can be determined from

$$\operatorname{Re}\hat{G} = G' = \frac{2\bar{E}}{\varepsilon_0^2}, \tag{15.27}$$

while the imaginary part is calculated from (15.23):

$$\operatorname{Im}\hat{G} = G'' = \frac{2\bar{P}}{\omega\varepsilon_0^2}. \tag{15.28}$$

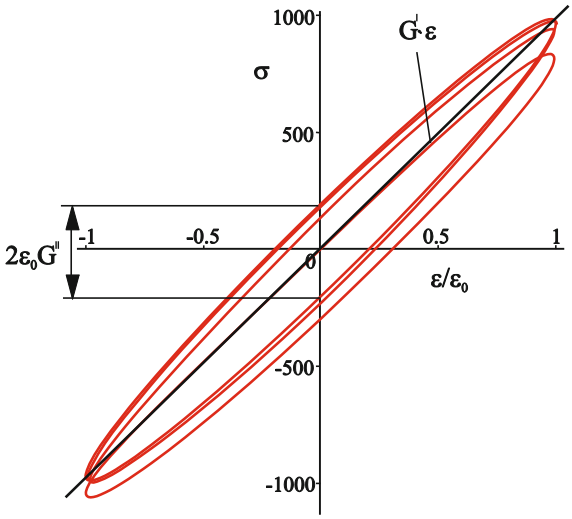

Fig. 15.6 Stress-strain diagram for a viscoelastic material.

The Equations (15.21) and (15.22) describe, in parameterized form, the dynamic stress-strain diagram, which has an elliptical form. The corresponding average slope of the diagram is equal to G'. For $\varepsilon = 0$, we obtain $\sigma = \pm\varepsilon_0 G''$. Therefore, the imaginary part can be determined from the width of the hysteresis loop.

15.7 Rheological Models

For spatially homogeneous deformations, one can frequently work with stiffnesses instead of moduli. The two fundamental elements for this are linearly elastic springs and dampers. From these elements, complicated combinations can be composed which can represent practically arbitrary viscoelastic behavior.

First, we consider the fundamental elements under periodic excitation. For a *linearly elastic spring*, without internal dissipation (Fig. 15.7 a), the relation generally known as Hooke's law is valid:

$$F = cx. \tag{15.29}$$

We call the proportionality coefficient c the *spring constant* or *spring stiffness*. Now, we consider a *linear damper* (Fig. 15.7 b):

$$F = d\dot{x}\,. \tag{15.30}$$

For a harmonic excitation in complex form, $\hat{F} = F_0 e^{i\omega t}$, we look for the solution in the form $\hat{x} = x_0 e^{i\omega t}$. The result is $\hat{F}(t) = id\omega\hat{x}(t)$, meaning *the force is proportional to the displacement at every point in time, as it is in a spring*. The coefficient

$$\hat{c}_d = id\omega\,, \tag{15.31}$$

which relates the force to the displacement, however, is now complex and is dependent on the frequency. We call this the *complex, frequency-dependent spring constant or stiffness*.

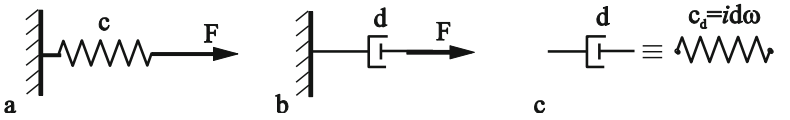

Fig. 15.7 (a) Linearly elastic spring, (b) velocity proportional damper, (c) complex stiffness of a damper.

For a general linear mechanical system (meaning an arbitrarily complex system composed of linear spring and dampers), we have a linear relationship for an excitation force $F_0 e^{i\omega t}$:

$$\hat{F}(t) = \hat{c}(\omega)\hat{x}(t)\,, \tag{15.32}$$

where $\hat{c}(\omega)$ is now the complex spring number of the system. This equation is valid, however, only for an excitation with the frequency ω. In explicit form, it reads $F_0 e^{i\omega t} = \hat{c}(\omega)x_0 e^{i\omega t}$.

A parallel connection of two springs with the spring constants c_1 and c_2 is equivalent to a spring with the spring constant $c = c_1 + c_2$. The relationship for a series connection is $\frac{1}{c} = \frac{1}{c_1} + \frac{1}{c_2} \Rightarrow c = \frac{c_1 c_2}{c_1 + c_2}$. Similar connections can also be used for continua. Then, the stiffnesses must be replaced by moduli.

The component of many rheological models that will be important to us in the following is the *Maxwell element*, which is composed of a spring connected in series with a damper. We will investigate the properties of this element and in doing so, we use the continuum version of the model from the beginning and utilize the moduli rather than stiffnesses.

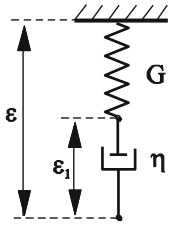

Fig. 15.8 Maxwell element.

The complex moduli of the spring and damper are G and $i\eta\omega$. Due to the series connection, the total modulus is

$$\hat{G}_{Maxwell} = \frac{Gi\eta\omega}{G+i\eta\omega} = \frac{Gi\eta\omega}{(G+i\eta\omega)}\frac{(G-i\eta\omega)}{(G-i\eta\omega)} = \frac{G\left(i\eta\omega G+(\eta\omega)^2\right)}{G^2+(\eta\omega)^2}. \qquad (15.33)$$

The storage modulus and loss moduli are

$$G'_{Maxwell} = \frac{G(\eta\omega)^2}{G^2+(\eta\omega)^2}, \qquad G''_{Maxwell} = \frac{\eta\omega G^2}{G^2+(\eta\omega)^2}. \qquad (15.34)$$

By introducing the quantity

$$\tau = \eta / G, \qquad (15.35)$$

we can also present the Equations (15.34) in the form

$$G'_{Maxwell} = G\frac{(\omega\tau)^2}{1+(\omega\tau)^2}, \qquad G''_{Maxwell} = G\frac{\omega\tau}{1+(\omega\tau)^2}. \qquad (15.36)$$

The parameter τ has the dimension time.

Now, we will investigate the stress relaxation in a medium which is characterized by a Maxwell element. For this, we will use the notation introduced in Fig. 15.8. The stress acting on the connection point between the spring and the damper is equal to $-G(\varepsilon-\varepsilon_1)+\eta\dot{\varepsilon}_1$. Because the connection point is massless, the stress must cancel out: $-G(\varepsilon-\varepsilon_1)+\eta\dot{\varepsilon}_1 = 0$. By dividing this equation by G and substituting (15.35), we can write the equation as

$$\tau\dot{\varepsilon}_1 + \varepsilon_1 = \varepsilon. \qquad (15.37)$$

Were the material to deform *suddenly* at $t=0$ by ε_0, then for every point in time $t>0$,

$$\tau\dot{\varepsilon}_1 + \varepsilon_1 = \varepsilon_0, \qquad (15.38)$$

with the initial condition $\varepsilon_1(0) = 0$. The solution to this equation with this initial condition is

$$\varepsilon_1 = \varepsilon_0 \left(1 - e^{-t/\tau}\right). \tag{15.39}$$

The stress is

$$\sigma = G\left(\varepsilon_0 - \varepsilon_1\right) = G\varepsilon_0 e^{-t/\tau}. \tag{15.40}$$

The stress decays exponentially with the characteristic time τ, which is called the *relaxation time*.

15.8 A Simple Rheological Model for Rubber ("Standard Model")

Now, we would like to construct a spring-damper model that has the most important dynamic properties of rubber during periodic loading. These are:
1. $\omega \approx 0$: For low frequencies, a small modulus (quasi-static deformation) is measured as well as almost no dissipation (i.e. the damping component is very small).
2. $\omega \to \infty$: For very high frequencies, a very large modulus is measured (typically 3 orders of magnitude larger than for quasi-static loading) and, likewise, no appreciable dissipation.
3. For frequencies in between, an intermediate modulus is measured and at the same time, strong dissipation.

These properties result from the fact that the molecular chains can only coil and uncoil in a finite amount of time.

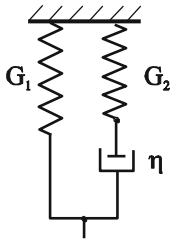

Fig. 15.9 A simple rheological model for rubber.

These properties of a rubber block should now be qualitatively described using the rheological model presented in Fig. 15.9. Because we are dealing with the parallel connection of a spring and a Maxwell element, we can immediately write

$$G' = G_1 + G_2 \frac{(\omega\tau)^2}{1+(\omega\tau)^2}, \qquad G'' = G_2 \frac{\omega\tau}{1+(\omega\tau)^2} \tag{15.41}$$

with $\tau = \eta / G_2$. The dependence of the moduli on frequency is presented logarithmically for the case of $G_2 / G_1 = 1000$ in Fig. 15.10.

At low frequencies, $\omega < G_1 / \eta$ (quasi-static loading), the modulus approaches G_1. At very high frequencies, $\omega > G_2 / \eta$, it approaches $G_2 \gg G_1$. This means that for very slow loading, rubber is soft. On the other hand, for very quick loading, it is hard. Typical shear moduli of filled rubbers at low frequencies are around 10 MPa, while at higher frequencies they are about 1000 times larger. In the area in between, the imaginary part is predominant: $G''(\omega) \approx \eta\omega$, meaning that the rubber behaves like a viscous fluid during periodic loading.

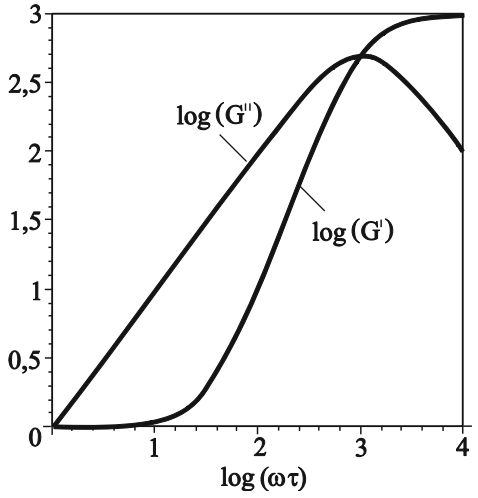

Fig. 15.10 Real and imaginary parts of the frequency-dependent modulus for the rheological model shown in Fig. 15.9 with $G_2 / G_1 = 1000$.

Due to the fact that we are dealing with a parallel connection of a spring and a Maxwell element, we can once again immediately write

$$\sigma(t) = \varepsilon_0 \left(G_1 + G_2 e^{-t/\tau} \right). \tag{15.42}$$

The normalized stress, which we have called the *time-dependent modulus*, can be obtained by dividing this equation by ε_0:

$$G(t) = \sigma / \varepsilon_0 = \left(G_1 + G_2 e^{-t/\tau} \right). \tag{15.43}$$

It relaxes from the value $G_0 = G_1 + G_2 \approx G_2$ for $t = 0$ to the value $G_\infty = G_1$ for $t \to \infty$.

15.9 Influence of Temperature on Rheological Properties

The physical reason for the finite time of the stress-relaxation is the kinetic process of the "uncoiling" of the polymer molecules. This is a thermally activated process and, therefore, is strongly dependent on temperature. Because the relaxation time in the complex modulus (15.41) only appears as the combination $\omega\tau(T)$, and in the time-dependent modulus (15.43) only as the combination $t/\tau(T)$:

$$G(t) = F(t/\tau(T)), \quad \hat{G}(\omega) = Q(\omega\tau(T)), \tag{15.44}$$

then the time-dependent moduli for different temperatures, plotted as a function of the logarithm of time, are the same curves, only shifted by the value $\log(\tau(T_2)/\tau(T_1))$ (Fig. 15.11). This is also valid for the frequency-dependent moduli plotted as a function of the logarithm of frequency. Because of these reasons, $\log\tau(T)$ is also called the *shift-function.*

It is often assumed when describing the rheological properties of elastomers that the assumption made above (15.44) is valid even when the rheology is not described using the simple model shown above. Williams, Landel, and Ferry proposed an analytical approximation for the shift-function in 1955 which contains two constants C_1 and C_2 and is known as the *WLF-function*. The constants must be determined experimentally for every type of rubber:

$$\log\tau(T) = \frac{C_1(T-T_g)}{C_2+T-T_g} = C_1\left(1-\frac{1}{1+C_2^{-1}\left(T-T_g\right)}\right). \tag{15.45}$$

T_g is the so called *glass transition temperature*.

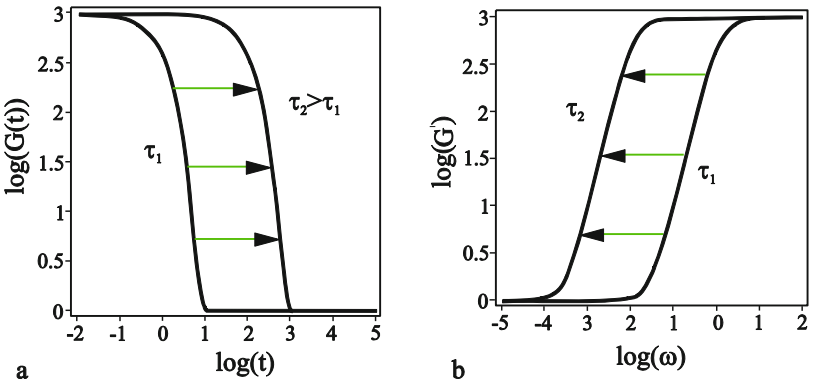

Fig. 15.11 Relaxation function (a) and frequency-dependent modulus (b) at two temperatures. The smaller relaxation time τ_1 corresponds to a higher temperature as that of the relaxation time τ_2 (in this example around 100 times larger).

15.10 Master Curves

The assumption (15.44) is used to experimentally reproduce the entire relaxation curve by use of measurements in a defined time interval. We consider, for example, the stress-relaxation during a tensile test: the probe is quickly deformed by $\varepsilon = 1\%$ and the stress is subsequently measured as a function of time. The length of time of the experiments is limited by a realizable time domain. As an example, we will investigate the stress-relaxation in a time window from 3 to 600 seconds after the sudden deformation: shorter times are difficult to realize, while larger times lead to practically unacceptable duration of the experiment.

Experimental results at various temperatures can be seen when they are presented logarithmically as in Fig. 15.12. From the hypothesis, we assume that at different temperatures, the measured curves are only shifted pieces of the same curve. Now, one attempts to shift the curves so that they form the entire curve (Fig. 15.13).

This method has shown itself to be successful and leads to an "experimental" relaxation curve in a time interval which is inaccessible to direct experimental measurements (e.g. from the sub-millisecond domain to that of years). These curves are called "master curves." The shifting of the individual curve segments for various temperature or time domains is not the same. This is due to the different activation energies of the various scales.

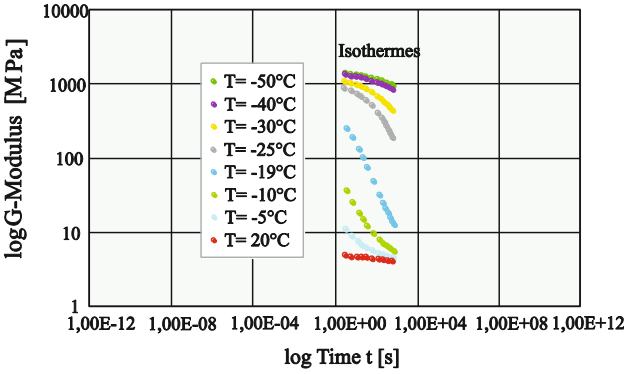

Fig. 15.12 Measurements of stress-relaxation for various temperatures in a given time window. (Data of M. Achenbach)

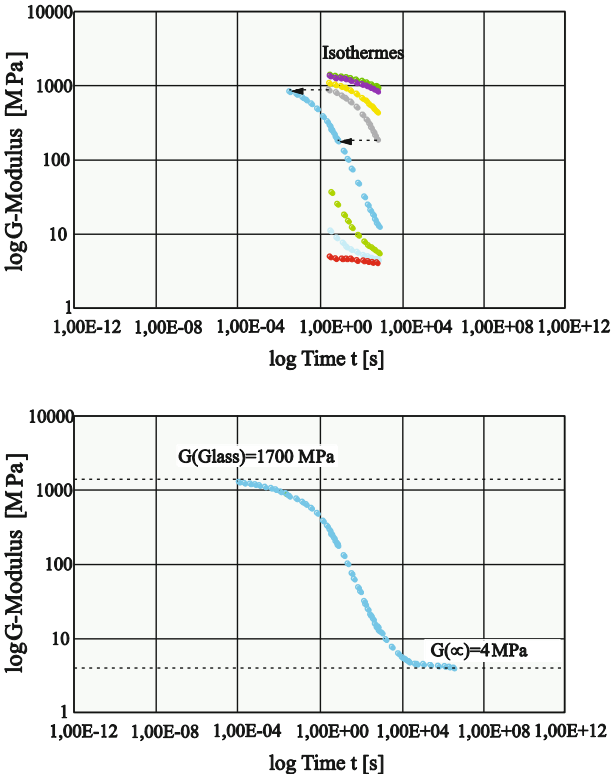

Fig. 15.13 The sections of the stress-relaxation curves at various temperatures (shown logarithmically) are shifted so that they form a single *master curve*. (Data of M. Achenbach)

15.11 Prony Series

The experimental master curves obtained in this way differ significantly from the relaxation curves in the "standard model" of the spring and Maxwell element connected in parallel. The transition from the large "glass modulus" at very small times to the small "rubber modulus" at very large times does not take place in real elastomers over a short time period τ, rather it extends over several orders of magnitude of time. Therefore, the model must be adjusted.

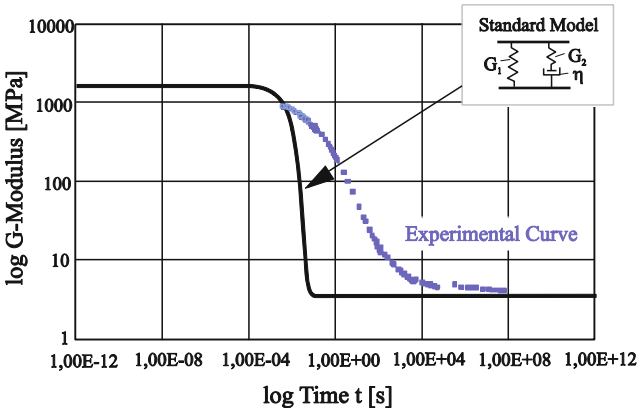

Fig. 15.14 Logarithmic presentation of the time-dependent shear modulus for the simple rheological model (continuous curve) and a real elastomer. (Data of M. Achenbach)

An adjustment can be made in which, instead of a Maxwell element with a relaxation time τ, one attaches a series of elements with various relaxation times in parallel (Fig. 15.15). By use of a sufficiently large number of Maxwell elements, every relaxation function is able to be represented. This model is called the *Prony series*.

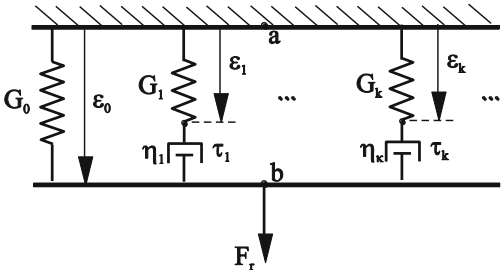

Fig. 15.15 Prony series.

In this model, the relaxation of the G-modulus is given by

$$G(t) = G_0 + \sum_{i=1}^{N} G_i \cdot e^{-t/\tau_i} \,. \tag{15.46}$$

One can also generalize this equation using an integral form:

$$G(t) = G_0 + G_1 \int_{\tau_1}^{\tau_2} g(\tau) e^{-t/\tau} \, d\tau \,. \tag{15.47}$$

The complex shear modulus is given by

$$G'(\omega) = G_0 + \sum_{k=1}^{N_k} G_k \frac{\omega^2 \tau_k^2}{1+\omega^2 \tau_k^2} ,$$
$$G''(\omega) = \sum_{k=1}^{N_k} G_k \frac{\omega \tau_k}{1+\omega^2 \tau_k^2} , \tag{15.48}$$

or in the integral form

$$G'(\omega) = G_0 + G_1 \int_{\tau_1}^{\tau_2} \frac{\omega^2 \tau^2}{1+\omega^2 \tau^2} g(\tau) d\tau ,$$
$$G''(\omega) = G_1 \int_{\tau_1}^{\tau_2} \frac{\omega \tau}{1+\omega^2 \tau^2} g(\tau) d\tau . \tag{15.49}$$

Instead of the exponential decay of stress in terms of time, which is characteristic for a Maxwell element, many elastomers are found to experience a decay in stress that can be described by a power function. In order to describe such a relaxation function, the weight function $g(\tau)$ in Equations (15.47) and (15.49) must also be a power function: $g(\tau) \propto \tau^{-s}$. The relaxation function is then completely parameterized by choosing G_0, G_1, s, τ_1 and τ_2.

To illustrate, we calculate the relaxation of the shear modulus in a model with the following parameters: $G_0 = 1$, $G_1 = 1000$, $\tau_1 = 10^{-2}$, $\tau_2 = 10^2$, $g(\tau) = \tau_1 \tau^{-2}$. Substituting these into (15.47) provides

$$G(t) = G_0 + \frac{G_1 \tau_1}{t} \left(e^{-\frac{t}{\tau_2}} - e^{-\frac{t}{\tau_1}} \right) . \tag{15.50}$$

The result is presented in Fig. 15.16. One can see that in the middle time domain $\tau_1 \ll t \ll \tau_2$, the dependence of $\log G(t)$ on $\log t$ is a linear function with the slope -1: The stress decreases in this domain according to the power function $G \propto t^{-1}$.

The frequency dependence of the complex modulus is given by

$$G'(\omega) = G_0 + G_1 \tau_1 \int_{\tau_1}^{\tau_2} \frac{\omega^2}{1+\omega^2 \tau^2} d\tau = G_0 + G_1 \omega \tau_1 \left(\arctan \omega \tau_2 - \arctan \omega \tau_1 \right) ,$$
$$G''(\omega) = \tfrac{1}{2} G_1 \tau_1 \omega \ln \left(\frac{\tau_2^2}{\tau_1^2} \frac{1+\omega^2 \tau_1^2}{1+\omega^2 \tau_2^2} \right) , \tag{15.51}$$

see Fig. 15.17.

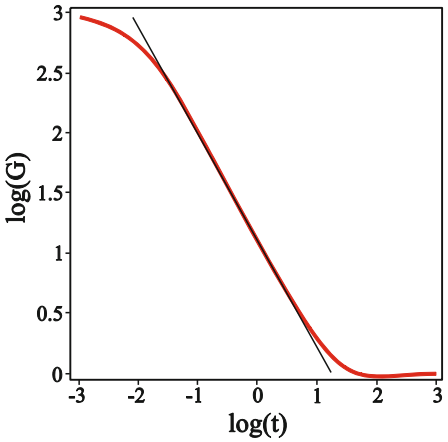

Fig. 15.16 Time-dependent shear modulus according to (15.50).

In the middle frequency domain, $1/\tau_2 \ll \omega \ll 1/\tau_1$, the following equations apply:

$$G'(\omega) = G_0 + \frac{\pi}{2} G_1 \tau_1 \omega$$
$$G''(\omega) = G_1 \omega \tau_1 \ln(1/\omega\tau_1). \tag{15.52}$$

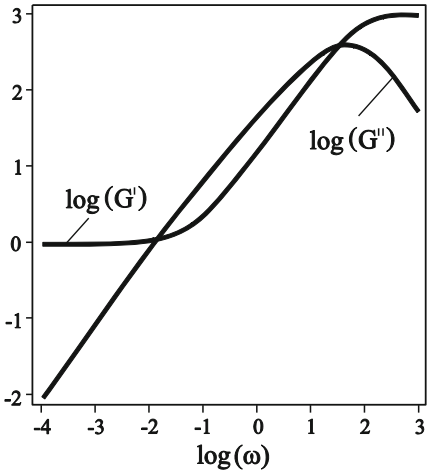

Fig. 15.17 Real and imaginary parts of the frequency-dependent modulus according to Equation (15.51).

15.12 Application of the Method of Dimensionality Reduction to Viscoelastic Media

If the indentation velocity of an elastomer during a dynamic loading is smaller than the smallest speed of sound (which is defined by the smallest relevant elastic module), then the contact can be regarded as being quasi-static. If this condition is met and an area of an elastomer is excited with an angular frequency ω, a linear relationship is valid between the stress and deformation and, consequently, between the force and the displacement. The medium can be considered to be an elastic body with the effective shear modulus $G(\omega)$. All principles that are valid for a purely elastic body must also be valid for the harmonically excited viscoelastic medium. In particular, the incremental stiffness will be proportional to the diameter of the contact area, which is the mathematical basis for the application of the method of dimensionality reduction (MDR) described in Section 5.6. Therefore, elastomers can also be described using the MDR, where the stiffness of the individual spring is selected according to (5.51):

$$\Delta k_z = E^* \Delta x \ . \tag{15.53}$$

The only difference to the elastic contact is that the effective modulus of elasticity is now a function of frequency.

Elastomers can often be regarded as incompressible media, thus $\nu = 1/2$, and

$$\Delta k_z(\omega) = E^*(\omega)\Delta x = \frac{E(\omega)}{1-\nu^2}\Delta x = \frac{2G(\omega)}{1-\nu}\Delta x \approx 4G(\omega)\Delta x : \tag{15.54}$$

For the case of incompressible elastomers, the stiffness of an individual "spring" of Winkler foundation is four times the shear modulus multiplied with the discretization step size.

For a harmonic excitation in the one-dimensional equivalent system, we get the spring force of

$$\Delta F_N(x,\omega) = \frac{2G(\omega)}{1-\nu}\Delta x \cdot u_z(x,\omega) \approx 4G(\omega)\Delta x \cdot u_z(x,\omega) \ . \tag{15.55}$$

The reverse transformation into the time domain gives the force as an explicit function of time

$$\Delta F_N(x,t) = \frac{2}{1-\nu}\Delta x \int_{-\infty}^{t} G(t-t')\dot{u}_z(x,t')\mathrm{d}t' \approx 4\Delta x \int_{-\infty}^{t} G(t-t')\dot{u}_z(x,t')\mathrm{d}t' \ . \tag{15.56}$$

For tangential contacts the tangential stiffness of springs of the equivalent one-dimensional MDR bedding must be defined in accordance with (8.41):

$$\Delta k_x = G^*(\omega)\Delta x = \frac{4G(\omega)}{2-\nu}\Delta x \approx \frac{8}{3}G(\omega)\Delta x\,. \tag{15.57}$$

The corresponding force in the time domain is

$$\Delta F_x(t) = \frac{4}{2-\nu}\Delta x\int_{-\infty}^{t} G(t-t')\dot{z}(t')dt' \approx \frac{8}{3}\Delta x\int_{-\infty}^{t} G(t-t')\dot{z}(t')dt'\,. \tag{15.58}$$

The formal mathematical proof of this method is based on the method of functional equations of Radok and is presented in a recent textbook[4].

The general linear relations (15.56) and (15.57) are often used to represent rheological models, such as a Maxwell body, Kelvin body, or standard model. For non-compressible media, the forces in the spring and damper elements are calculated in accordance with

$$\Delta F_N = 4Gu_z\Delta x \quad \text{and} \quad \Delta F_N = 4\eta\dot{u}_z\Delta x\,, \tag{15.59}$$

where η is the dynamic viscosity of the corresponding element.

Problems

Problem 1: Coefficient of restitution for a viscoelastic material. A block of viscoelastic material impacts a rigid wall with the velocity of v_0 and bounces back with the smaller velocity v_1. Determine the coefficient of restitution $e = v_1 / v_0$. The block should be described as a simplified model of a rigid mass m with a spring-damper combination (stiffness c, damping coefficient η), as is shown in Fig. 15.18.

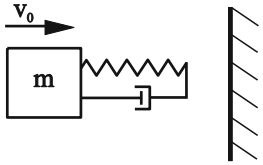

Fig. 15.18 Model of a viscoelastic block impacting a wall.

Solution: From the point in time of the first contact, we are dealing with a damped oscillator. The equation of motion is

$$m\ddot{x} + \eta\dot{x} + cx = 0$$

[4] S. Kürschner, V.L. Popov, M. Heß: Replacing the Material Properties with Radok's Method of Functional Equations. In: V.L. Popov and M. Heß, Method of Dimensionality Reduction in Contact Mechanics and Friction, Springer, 2015, pp.247-256.

or

$$\ddot{x} + 2\delta\dot{x} + \omega_0^2 x = 0$$

with $2\delta = \eta / m$ and $\omega_0^2 = c / m$. The initial conditions are $x(0) = 0$ and $\dot{x}(0) = v_0$. The solution to the equation of motion with the given initial conditions is

$$x(t) = \frac{v_0}{\tilde{\omega}} e^{-\delta t} \sin \tilde{\omega} t\,, \quad \dot{x}(t) = \frac{v_0}{\tilde{\omega}} e^{-\delta t} \left(-\delta \sin \tilde{\omega} t + \tilde{\omega} \cos \tilde{\omega} t\right)$$

with $\tilde{\omega} = \sqrt{\omega_0^2 - \delta^2}$. The block remains in contact with the wall as long as the compressive force on the wall, $F = \eta \dot{x} + cx$, remains positive. The last instant of contact t^* is determined by the equation

$$2\delta \dot{x}(t^*) + \omega_0^2 x(t^*) = \frac{v_0}{\tilde{\omega}} e^{-\delta t} \left[\left(-2\delta^2 + \omega_0^2\right) \sin \tilde{\omega} t^* + 2\delta\tilde{\omega} \cos \tilde{\omega} t^*\right] = 0\,.$$

From this, it follows that

$$\tan \tilde{\omega} t^* = \frac{-2\delta\tilde{\omega}}{\omega_0^2 - 2\delta^2}\,.$$

The velocity at this point in time is equal to

$$\dot{x}(t^*) = \frac{v_0}{\tilde{\omega}} e^{-\delta t^*} \left(-\delta \sin \tilde{\omega} t^* + \tilde{\omega} \cos \tilde{\omega} t^*\right).$$

The coefficient of restitution is, therefore, calculated as

$$e = \frac{\left|\dot{x}(t^*)\right|}{v_0} = \frac{1}{\tilde{\omega}} e^{-\delta t^*} \left|-\delta \sin \tilde{\omega} t^* + \tilde{\omega} \cos \tilde{\omega} t^*\right| = e^{-\frac{\delta}{\tilde{\omega}}\left(\pi \mathrm{H}(\omega_0^2 - 2\delta^2) - \arctan \frac{2\delta\tilde{\omega}}{\omega_0^2 - 2\delta^2}\right)}$$

with

$$\mathrm{H}(\xi) = \begin{cases} 1, & \xi > 0 \\ 0, & \xi < 0 \end{cases}.$$

This dependence is shown in Fig. 15.19.

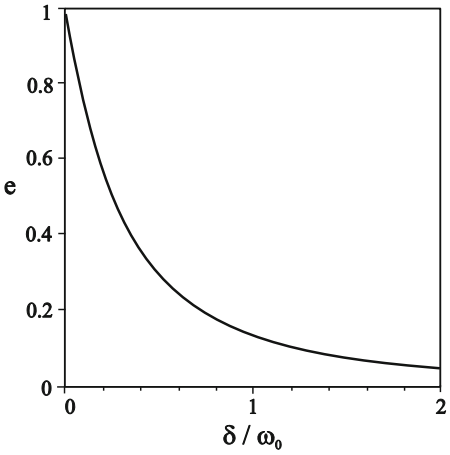

Fig. 15.19 Dependence of the coefficient of restitution on the damping ratio of the viscoelastic material.

Problem 2: Measurement of the Complex G-modulus. A simple method for determining the storage and loss moduli of elastomers is offered by the torsion pendulum (Fig. 15.19). It consists of a cylindrical probe with the radius R and the length l which is immovably fixed on one end and connected to a mass with the rotational moment of inertia Θ on the other end. The pendulum is moved from equilibrium at time $t = 0$ and let go. By measuring the oscillation frequency and damping, the storage and loss moduli can be determined.

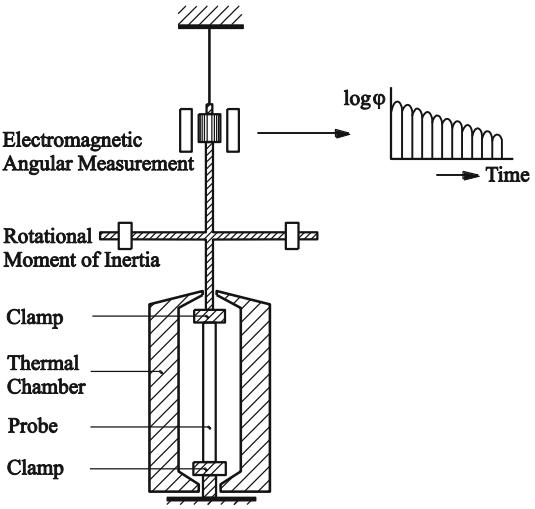

Fig. 15.20 Setup for a torsion pendulum for measuring the complex G-modulus.

Solution: The torsional moment of an elastic rod is

$$M = -\frac{I_p}{l} G\varphi ,$$

where I_p is the polar moment of inertia for the cross-section:

$$I_p = \frac{\pi R^4}{2} .$$

For a periodic excitation at the angular frequency ω, this equation is also valid for a rod made from an elastomer if $G\varphi$ is replaced by

$$G\varphi = G'\varphi + \frac{G''}{\omega}\dot{\varphi} .$$

One can see that this expression is correct, because for a complex excitation, $\varphi(t) = \varphi_0 e^{i\omega t}$, the expression is exactly the product of the complex modulus and the torsional deflection angle: $\hat{G}\varphi = \left(G'(\omega) + iG''(\omega)\right)\varphi$. Thus, using the principle of angular momentum for the pendulum we obtain the equation

$$\Theta\ddot{\varphi} + \frac{I_p}{l}\frac{G''}{\omega}\dot{\varphi} + \frac{I_p}{l}G'\varphi = 0 .$$

This equation describes a damped oscillation with the angular frequency

$$\omega \approx \sqrt{\frac{I_p G'}{\Theta l}}$$

and the logarithmic decrement

$$\delta = \frac{I_p G''}{2l\Theta\omega} .$$

The storage and loss moduli are

$$G'(\omega) = \frac{l\Theta\omega^2}{I_p}, \qquad G''(\omega) = \frac{2l\Theta\omega\delta}{I_p} .$$

Different frequencies can be "sampled" using bodies with different moments of inertia Θ.

Problem 3: A rigid axial-symmetric profile is pressed into a linear viscous half-space (viscosity η, no gravity, no capillary effects) with the constant force F_N. Determine the indentation speed and indentation depth as a function of time for the following profiles:
(a) a cylindrical indenter with the radius a (Fig. 15.21),
(b) a cone $f(r) = \tan\theta \cdot |r|$ (Fig. 15.22),

(c) a paraboloid $f(r) = r^2 / (2R)$ (Fig. 15.23).

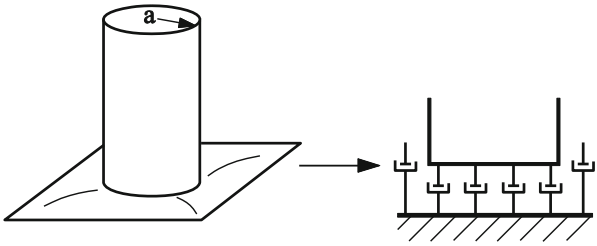

Fig. 15.21 Pressing a cylindrical indenter into a viscous half-space.

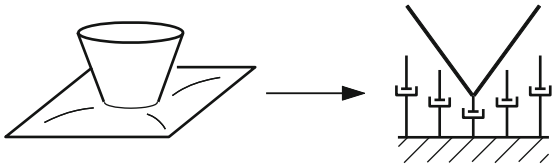

Fig. 15.22 Pressing a cone into a viscous half-space.

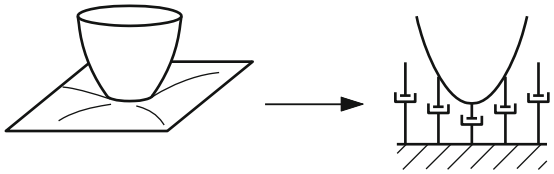

Fig. 15.23 Pressing a parabolid into a viscous half-space.

Solution: In the first step, equivalent one-dimensional profiles are determined by Eq. (5.52). They are given in Problem 7 of Chapter 5:

(a) $g(x) = \begin{cases} 0, & |x| < a \\ \infty, & |x| \geq a \end{cases}$,

(b) $g(x) = \frac{\pi}{2}|x| \tan\theta$,

(c) $g(x) = x^2 / R$.

In the second step, the corresponding Winkler foundation is defined according to (15.59): $\Delta F_N = 4\eta \dot{u}_z \Delta x = 4\eta \dot{d}(t) \Delta x$. In a state of motion with the instantaneous contact radius a, the vertical force is equal to the individual spring force multiplied by the number of springs in contact $2a / \Delta x$:

$$F_N = 8\eta a(t) \dot{d}(t) .$$

The relation between the instantaneous contact radius and indentation depth does not depend on the rheology and can be obtained as in Problem 7 of Chapter 5:

(a) contact radius is constant and equal to a,

(b) $a(t) = \dfrac{2}{\pi}\dfrac{d(t)}{\tan\theta}$,

(c) $a(t) = \sqrt{Rd(t)}$.

Substituting into the equation for the force results in

(a) $F_N = 8\eta a\dot{d}$,

(b) $F_N = \dfrac{16}{\pi\tan\theta}\eta d(t)\dot{d}(t)$,

(c) $F_N = 8\eta R^{1/2}\sqrt{d(t)}\dot{d}(t)$.

Integration with the initial condition $d(0) = 0$ results in

(a) $F_N t = 8\eta a d(t)$,

(b) $F_N t = \dfrac{8}{\pi\tan\theta}\eta d(t)^2$,

(c) $F_N t = \dfrac{16}{3}\eta R^{1/2} d(t)^{3/2}$.

The indentation depth as a function of time is given as:

(a) $d(t) = \dfrac{F_N t}{8\eta a}$,

(b) $d(t) = \left(\dfrac{\pi\tan\theta \cdot F_N t}{8\eta}\right)^{1/2}$,

(c) $d(t) = \left(\dfrac{3F_N t}{16\eta R^{1/2}}\right)^{2/3}$.

Problem 4: A rigid conical indenter $f(r) = \tan\theta \cdot |r|$ is pressed into a viscoelastic half-space (Kelvin body with the shear modulus G and viscosity η) with the constant force F_N. Determine the dependence of the indentation depth with respect to time.

Solution: The equivalent plane shape according to (5.52) is given by the equation $g(x) = \dfrac{\pi}{2}\tan\theta \cdot |x|$ and the contact radius by the equation $a = (2/\pi)(d/\tan\theta)$. For the force, we must use a superposition of the elastic component (see Problem 7 of Chapter 5):

$$F_{N,el} = \frac{8G}{\pi}\frac{d^2}{\tan\theta}$$

and the viscous component (see Problem 3 above):

$$F_N = \frac{8G}{\pi}\frac{d^2}{\tan\theta} + \frac{16\eta}{\pi\tan\theta}d\dot{d}\,.$$

This equation can be written in the form of

$$\frac{\pi \tan\theta \cdot F_N}{8G} = d^2 + 2\tau d\dot{d} = d^2 + \tau \frac{\mathrm{d}\left(d^2\right)}{\mathrm{d}t}$$

where $\tau = \eta / G$ is the relaxation time of the medium. Integration of this equation with the initial condition $d(0) = 0$ gives

$$d^2(t) = \frac{\pi \tan\theta \cdot F_N}{8G}\left(1 - e^{-t/\tau}\right).$$

Problem 5: A rigid cylindrical indenter is pressed into an elastomer, which is described with the "standard model" (Fig. 15.9). Determine the dependence of the indentation depth with respect to time.

Solution: The standard model of elastomers is composed of a Maxwell element (stiffness G_2 and damping coefficient η connected in series) connected in parallel with a stiffness G_1. The one-dimensional counterpart is a foundation composed of elements at a distance Δx, whose individual components are characterized by the parameters $4G_1\Delta x$, $4G_2\Delta x$ and $4\eta\Delta x$. The equivalent one-dimensional indenter is a rectangle whose side has a length of $2a$. The normal force is given by

$$F_N = 8G_1 a u_z + 8G_2 a\left(u_z - u_1\right),$$

where u_1 satisfies the following equation:

$$u_z = u_1 + \tau \dot{u}_1$$

with $\tau = \eta / G_2$. Solving these equations with the initial conditions $u_z(0) = 0$ and $u_1(0) = 0$ results in

$$u_1(t) = \frac{F_N}{8G_1 a}\left(1 - \exp\left(-\frac{G_1 t}{\tau\left(G_1 + G_2\right)}\right)\right),$$

$$u_z(t) = \frac{F_N}{8G_1 a}\left(1 - \frac{G_2}{G_1 + G_2}\exp\left(-\frac{G_1 t}{\tau\left(G_1 + G_2\right)}\right)\right).$$

In the limiting case $G_2 \gg G_1$, we get the result for a Kelvin body:

$$u_z(t) = \frac{F_N}{8G_1 a}\left(1 - \exp\left(-\frac{G_1 t}{\eta}\right)\right).$$

16 Rubber Friction and Contact Mechanics of Rubber

The nature of friction between rubber and a hard substrate is very important for many technical applications. Rubber friction is significantly different from friction between "hard" substances such as metals or ceramics. It was made evident, most notably through the works of Grosch (1962), that rubber friction is very closely related to internal friction. This is proven by the fact that the temperature dependence of the coefficient of friction correlates with the temperature dependence of the complex shear modulus. This is a sign that rubber friction *is a volume property*.

16.1 Friction between an Elastomer and a Rigid Rough Surface

One can determine the frictional force in two ways – either by direct calculation of the tangential force components and then averaging over time or by calculating the energy loss caused by material deformation. If an amount of energy is dissipated per second $\dot{W}$ at a constant macroscopic sliding velocity v, then from a macroscopic point of view, the total energy loss can be considered as being dissipated only by the frictional forces and due to this, can be written as

V.L. Popov, *Contact Mechanics and Friction*,
DOI 10.1007/978-3-662-53081-8_16

$$\dot{W} = F_R v \,. \tag{16.1}$$

The frictional force is determined from the ratio of the energy loss to the sliding velocity

$$F_R = \frac{\dot{W}}{v} \,. \tag{16.2}$$

In a contact between a rigid surface and an elastomer, the energy can only be dissipated through the deformation of the elastomer. Because of this, the roughnesses of the rigid surface and the surface of the elastomer play completely different roles. This is illustrated in Fig. 16.1. If an elastomer slides over a smooth rigid plane (Fig. 16.1 a), then there is no time-dependent change of the deformation state of the elastomer and, therefore, no energy loss: the friction is equal to zero. On the other hand, if the elastomer slides over a rough surface (Fig. 16.1 b), then the local deformation state of every area of the elastomer is dependent on time and energy is dissipated. From this, it follows that during elastomeric friction, the roughness of the surface of the elastomer plays only a small role: the friction is primarily determined by the roughness of the rigid surface. Therefore, we consider the friction between a rough rigid surface and an elastomer, whose surface we assume to be even.

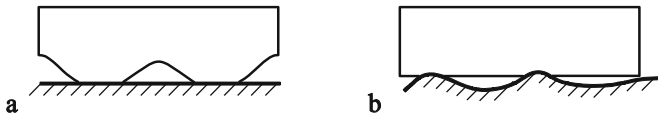

Fig. 16.1 (a) A rough rubber block on a smooth rigid plane and (b) a smooth rubber block on a rough rigid plane.

We want to calculate the deformation and energy dissipation in the elastomer. Thereby, we use the results from the contact mechanics of rough surfaces (Chapter 7). If the rough surface is characterized by the root mean square l of the height distribution of the "peaks" and an average R of the radius of curvature, then the average contact area of an asperity is

$$\Delta A \approx Rl \,. \tag{16.3}$$

According to this, the characteristic diameter of a micro-contact is equal to

$$r \approx \sqrt{\Delta A} \approx \sqrt{Rl} \,. \tag{16.4}$$

At a sliding velocity v, an area with the characteristic dimension r is "traversed" in the time

$$t \approx \frac{r}{v} \approx \frac{\sqrt{Rl}}{v} \,. \tag{16.5}$$

The characteristic frequencies for this process have an order of magnitude of

$$\tilde{\omega} \approx \frac{1}{t} \approx \frac{v}{r}. \tag{16.6}$$

The average pressure in the micro-contacts is

$$\langle \sigma \rangle = \frac{F_N}{A} = \kappa^{-1} E^* \nabla z \tag{16.7}$$

with $\kappa \approx 2$ (see Chapter 7). We denote the root mean square of the gradient of the surface as

$$\nabla z = \sqrt{\langle z'^2 \rangle}. \tag{16.8}$$

The effective modulus of elasticity for rubber is equal to[1]

$$E^* = \frac{E}{1-\nu^2} = \frac{2(1+\nu)G}{1-\nu^2} \approx 4G. \tag{16.9}$$

Because the shear modulus is frequency dependent, the characteristic frequency (16.6) must be substituted into the expression for average pressure (16.7):

$$\langle \sigma \rangle = 4\kappa^{-1} \left| \hat{G}(\tilde{\omega}) \right| \nabla z. \tag{16.10}$$

Thereby, we insert the *magnitude* of the frequency-dependent modulus, because the amplitudes of the stress and deformation are connected by the complex shear modulus. We use the following equation from the previous chapter to calculate the energy dissipation in a unit volume of a micro-contact:

$$\bar{P} = \tfrac{1}{2} \tilde{\omega} \langle \sigma \rangle^2 \frac{G''(\tilde{\omega})}{\left| \hat{G}(\tilde{\omega}) \right|^2}. \tag{16.11}$$

Multiplied with the depth of the significantly deformed volume $\approx r$, it yields the energy loss per unit area and then, when divided by the normal stress, the coefficient of friction:

$$\mu = \xi \nabla z \frac{G''(v/r)}{\left| \hat{G}(v/r) \right|}. \tag{16.12}$$

Here, ξ is a dimensionless coefficient on the order of unity, which is established by more exact calculation. Numerical simulations show that $\xi \approx 1$.

[1] Rubber can be assumed to be a practically incompressible medium which has an approximate Poisson's ratio of $\nu \approx 1/2$.

In the middle frequency domain, it is true for many types of rubber that $G'' \gg G'$. From this, it follows that $\frac{G''(v/r)}{\left|\hat{G}(v/r)\right|} \approx 1$. Then, the coefficient of friction is

$$\mu \approx \nabla z \,. \tag{16.13}$$

Therefore, in the middle frequency domain, we obtain a very simple result: the coefficient of friction is equal to the root mean square of the gradient of the surface. This result has a simple physical reason, which is illustrated in Fig. 16.2: for a purely imaginary shear modulus, the medium can be quickly indented, but only slowly relaxes back to its original form so that the form shown qualitatively in Fig. 16.2 occurs. Because the rubber is in contact with the substrate on only one side of the asperities, it is evident that the coefficient of friction, which we define as the ratio of the horizontal force to the normal force, is approximately equal to the average gradient of the surface in the contact area. As numerical simulations show for stochastically rough surfaces, this average gradient of the surface in the contact area can be associated with the average gradient of the entire surface, whereby we obtain (16.13).

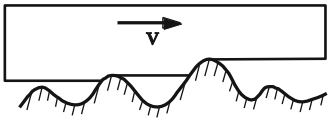

Fig. 16.2 Viscoelastic material in contact with a rough surface.

We will now investigate Equation (16.12) in detail. First, we note that $\frac{G''(v/r)}{\left|\hat{G}(v/r)\right|}$ is always equal to or smaller than 1. *The coefficient of friction can, therefore, never be larger than the average gradient of the surface*[2]. The frequency-dependent modulus for the "standard model" of rubber composed of a spring and a Maxwell element is

$$\hat{G}(\omega) = G_2 \frac{G_1 + i\eta\omega}{G_2 + i\eta\omega}, \tag{16.14}$$

taking into consideration that $G_1 \ll G_2$. With $\tau := \eta / G_2$, we obtain a coefficient of friction of

[2] This is valid when there is no adhesion in the considered contact.

$$\mu \approx \frac{\tilde{\omega}\tau}{\sqrt{\left(1+\left(\tilde{\omega}\tau\right)^2\right)\left(\left(G_1/G_2\right)^2+\left(\tilde{\omega}\tau\right)^2\right)}}\nabla z = \frac{v/\bar{v}}{\sqrt{\left(1+\left(v/\bar{v}\right)^2\right)\left(\left(G_1/G_2\right)^2+\left(v/\bar{v}\right)^2\right)}}\nabla z\ , \tag{16.15}$$

whereby, the characteristic velocity

$$\bar{v} = \frac{r}{\tau} \tag{16.16}$$

is inserted. The dependence (16.15) is presented in Fig. 16.3. The coefficient of friction remains relatively constant and equal to ∇z for velocities in the interval $\bar{v}\left(G_1/G_2\right) < v < \bar{v}$. Notice, however, that the stress acting on the micro-contacts according to (16.10) changes at the same time from $\sigma_1 = 4\kappa^{-1}G_1\nabla z$ for small velocities to $\sigma_2 = 4\kappa^{-1}G_2\nabla z$ for large velocities. Therefore, at larger velocities, the material in the micro-contacts is more strongly loaded.

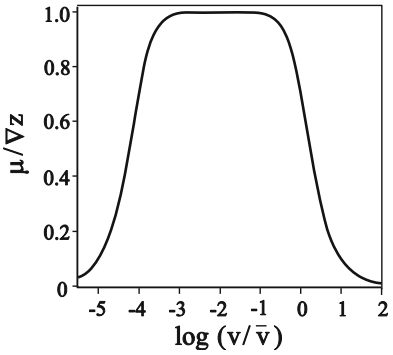

Fig. 16.3 Dependence of the coefficient of friction on the sliding velocity in the "standard model" with $G_2/G_1 = 10^4$.

For the rheological model (15.50-15.51) with a continuous distribution of relaxation times, which was investigated in the previous chapter, we obtain

$$G'(\tilde{\omega}) = G_0 + G_1\tau_1\tilde{\omega}\left(\arctan(\tilde{\omega}\tau_2) - \arctan(\tilde{\omega}\tau_1)\right)\ ,$$
$$G''(\tilde{\omega}) = \frac{1}{2}G_1\tau_1\tilde{\omega}\ln\left(\frac{\tau_2^2}{\tau_1^2}\frac{1+\left(\tilde{\omega}\tau_1\right)^2}{1+\left(\tilde{\omega}\tau_2\right)^2}\right). \tag{16.17}$$

The corresponding coefficient of friction is presented in Fig. 16.4 as a function of sliding velocity. Contrary to the "standard model," the coefficient of friction in a real rubber can remain approximately constant over several orders of magnitude.

In this case as well, it is approximately equal to the average surface slope ∇z in the "plateau area."

The temperature dependence of the coefficient of friction is also determined by the temperature dependence of the complex shear modulus: the curve μ, as a function of $\log(v)$, shifts by changes in temperature in the same direction and by the same magnitude as the frequency-dependent shear modulus. This property is used for "measuring" the coefficients of friction by construction of *master curves* – the same way it is used for the "measurement" of the frequency-dependent modulus (see Chapter 15). Thereby, one can cover the velocity domains that are not directly accessible for measurement. For an increase in temperature, the curve shifts to the right (into the area of higher velocities). Therefore, a master curve constructed for a specific temperature together with the WLF-shift function determines the coefficient of friction for arbitrary temperatures and velocities. Experimental data (master curves) for two elastomers are presented in Fig. 16.5.

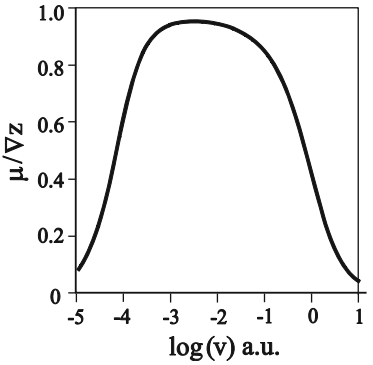

Fig. 16.4 Coefficient of friction as a function of sliding velocity for the Prony series according to Fig. 15.15 using the parameters in the model from Chapter 15.

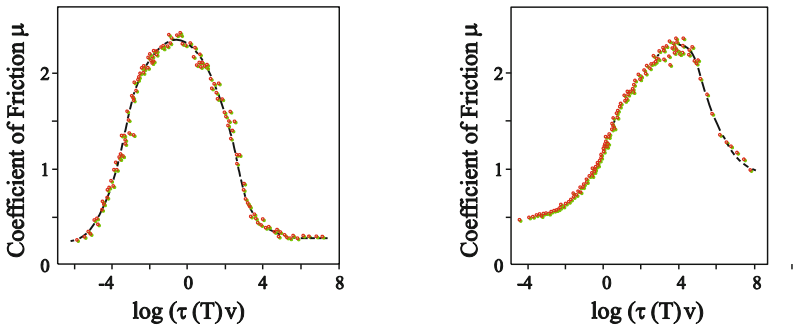

Fig. 16.5 Experimental data from Grosch for the dependence of the coefficient of friction from two types of rubber on various substrates (K. A. Grosch, The relation between the friction and viscoelastic properties of rubber. Proc. Roy. Soc., A2 74, (1963) 21).

16.2 Rolling Resistance

Even for pure rolling without slip, there is energy dissipation in the case of elastomers and with it an associated resistance. As a rule, it is desirable to minimize this resistance, while at the same time maximizing the sliding friction. This is possible, because the characteristic frequency domain for sliding, $\omega_{sliding} \approx v/\lambda$ (where λ is the characteristic wavelength of the roughness profile of the substrate and is on the order of $10-100\ \mu m$), and the characteristic frequency for rolling, $\omega_{rolling} \approx v/a$ (where a is the contact radius on the order of 5 cm), differ by two or three orders of magnitude. For normal operation of a tire, it is desired that in the frequency domain $\omega_{sliding}$, the loss modulus is larger than the storage modulus: $G'' \geq G'$, while in the frequency domain $\omega_{rolling}$, the opposite is desired: $G'' \ll G'$ (Fig. 16.6).

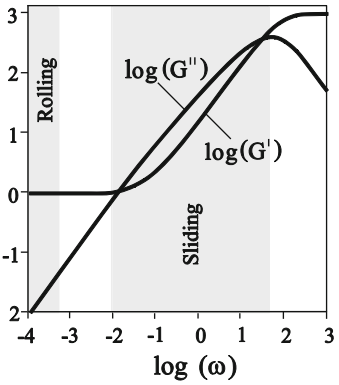

Fig. 16.6 Frequency-dependent storage and loss moduli for a rheological model of an elastomer described in Chapter 15. For the rolling resistance to remain small and the sliding friction to remain large (and constant), we must choose the operating conditions so that the characteristic rolling frequency lies in the frequency domain highlighted on the left and the characteristic sliding frequency lies in the frequency domain highlighted on the right.

In the frequency domain in which the desired condition for rolling is fulfilled, namely $G'' \ll G'$, the storage modulus is practically independent from the frequency and coincides with the static modulus G_∞. Therefore, as a first order approximation, we can assume that we are dealing with a purely elastic Hertzian contact.

We can estimate the energy loss during rolling by considering rolling as the "continuous repetitive placement" of a wheel. The normal force F_N for a sphere with a radius R rolling on a rigid plane as well as the contact radius a, are found using the following Hertzian relations:

$$F_N \approx \frac{4}{3} E^* R^{1/2} d^{3/2} \approx \frac{16}{3} G_\infty R^{1/2} d^{3/2}, \tag{16.18}$$

$$a^2 \approx Rd, \tag{16.19}$$

where d is the penetration depth. We estimate the characteristic frequency with

$$\omega \approx \frac{v}{a} \tag{16.20}$$

and the amplitude of the deformation with

$$\varepsilon_0 \approx \frac{d}{a}. \tag{16.21}$$

According to (15.23), we obtain a power loss per unit volume of

$$\bar{P} = \frac{1}{2} \omega \varepsilon_0^2 G''(\omega) \approx \frac{1}{2} \frac{v}{a} \left(\frac{d}{a} \right)^2 G'' \left(\frac{v}{a} \right) \tag{16.22}$$

and a power loss in the total volume $\sim (2a)^3$ of

$$\dot{W} \approx 4vd^2 G'' \left(\frac{v}{a} \right). \tag{16.23}$$

By dividing the power loss by the velocity, we obtain the resistance force

$$F_w \approx 4d^2 G'' \left(\frac{v}{a} \right). \tag{16.24}$$

At low frequencies, the loss module is always proportional to the frequency and can, therefore, be written in the form

$$G''(\omega) = \bar{\eta} \omega, \tag{16.25}$$

where $\bar{\eta}$ is the dynamic viscosity at low frequencies. Then, the resistance force is

$$F_w \approx 4\bar{\eta} \left(\frac{a^2}{R} \right)^2 \left(\frac{v}{a} \right) = 4\bar{\eta} \frac{a^3}{R^2} v. \tag{16.26}$$

With the Hertzian result (5.24), rewritten using the notation of this section, we get for the deformed volume

$$a^3 = \frac{3RF_N}{16G_\infty}. \tag{16.27}$$

For resistance force we obtain

$$F_w \approx F_N \frac{3}{4}\frac{\bar{\eta}}{G_\infty}\frac{v}{R} = F_N \frac{3}{4}\frac{v\tau}{R} \tag{16.28}$$

and for "coefficient of rolling friction"

$$\mu_{rolling} = \frac{F_W}{F_N} \approx \frac{3}{4}\frac{v\tau}{R}, \tag{16.29}$$

where $\tau = \bar{\eta}/G_\infty$ is the relaxation time of the elastomer. This equation is valid up to a dimensionless constant of magnitude 1. According to this, the rolling friction is proportional to the product of the rolling velocity and the (largest) relaxation time of the rubber and inversely proportional to the radius of curvature of the sphere.

16.3 Adhesive Contact with Elastomers

Until now, we have assumed that there are no adhesive forces between elastomeric and rigid surfaces. This is not the case for sufficiently smooth surfaces. Now, we consider an adhesive contact between a rigid sphere and an elastomer with an even surface (Fig. 16.7). The boundary of the contact can be viewed and treated as the tip of a crack[3]. In equilibrium, the elastomer can be assumed to be an elastic body with the static shear modulus G_∞ and an effective modulus of elasticity of

$$E^* = \frac{2(1+\nu)G_\infty}{1-\nu^2} = \frac{2G_\infty}{(1-\nu)} = 4G_\infty . \tag{16.30}$$

In equilibrium, the JKR equation (6.20) provides us with a relationship between the normal force F_N and the contact radius a:

$$F_N = E^*\left[\frac{4}{3}\frac{a^3}{R} - \left(\frac{8\gamma^*\pi a^3}{E^*}\right)^{1/2}\right]. \tag{16.31}$$

Here, γ^* is the effective surface energy (i.e. the required energy for producing a unit surface). We can present the condition (16.31) in a form in which it is convenient to treat the contact boundary as the tip of a crack. To this end, we first solve Equation (16.31) for γ^*:

$$\gamma^* = \left(F_N - \frac{4}{3}\frac{E^* a^3}{R}\right)^2 \frac{1}{8\pi a^3 E^*} . \tag{16.32}$$

[3] The original theory of Johnson, Kendall, and Roberts is based on exactly this analogy.

Because the effective surface tension γ^* is equal to the force per unit length (line-load) attempting to "close the crack" (i.e. enlarging the contact radius), we can consider Equation (16.32) as an equilibrium condition for the line-loads at the tip of the crack. On the left side, is the line-load which is caused by the van der Waals forces between the surfaces. On the right side, is the corresponding line load, which is caused by the elastic deformation of the continuum and acts in the opposite direction. By denoting the right side of Equation (16.32) with

$$D = \left(F_N - \frac{4}{3}\frac{E^* a^3}{R} \right)^2 \frac{1}{8\pi a^3 E^*}, \tag{16.33}$$

we can write the equilibrium condition in the form

$$\gamma^* = D. \tag{16.34}$$

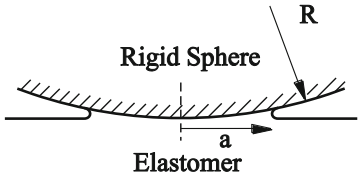

Fig. 16.7 Contact between a rigid sphere and an elastomer. The contact boundary can be viewed as a crack.

The difference $D - \gamma^*$ can be viewed as a "driving force" for the tip of the crack. In equilibrium, it vanishes. If the normal force changes, then the crack is no longer in equilibrium. In a purely elastic body, the tip of a crack being acted upon by a constant "force" $D - \gamma^*$, would accelerate until the velocity reaches the order of magnitude of the surface waves in the elastic continuum (*Rayleigh waves*). In a viscoelastic body, it reaches a finite speed due to the intensive dissipation. For a slow movement, it appears that the largest part of the contact area can be considered as being purely elastic. The total energy losses, on the other hand, are due only to a relatively small "process zone" on the tip of the crack. Maugis and Barquins proposed the following equation that associates the effective uniform load $D - \gamma^*$ with the propagation speed v of the crack:

$$D - \gamma^* = \gamma^* \Phi\left(\tau(T)v\right), \tag{16.35}$$

where $\tau(T)$ is the Williams-Landel-Ferry function. The dimensionless function $\Phi\left(\tau(T)v\right)$ is typically dependent on the velocity v in the middle velocity domain according to a power function:

$$\Phi\left(\tau(T)v\right) = \alpha(T)v^n. \tag{16.36}$$

The exponent n typically lies between 0.25 and 0.7. An example of the function Φ is shown in Fig. 16.8 for a glass sphere on polyurethane. The Equations (16.35) and (16.36) allow us to investigate the kinetics of the adhesion process under various loadings (see, for example, Problem 3 in this chapter).

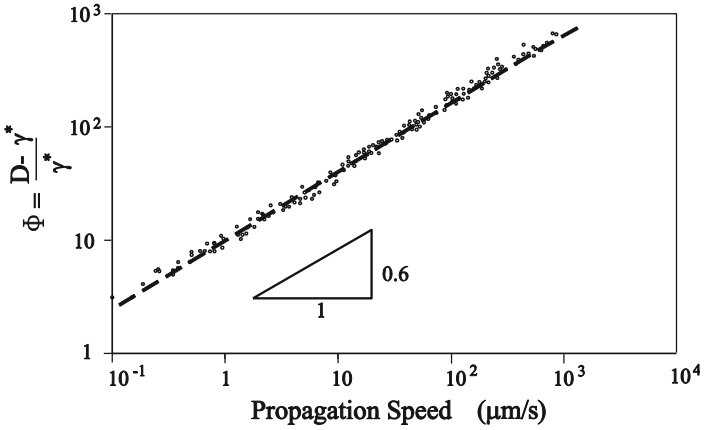

Fig. 16.8 "Dissipation function" Φ as a function of the crack propagation speed for a glass sphere on polyurethane for two radii or curvature and two temperatures. The same master curve can be obtained from peeling experiments with various indenters. From: M. Barquins, Adherence, Friction and Wear of Rubber-Like Materials, Wear, v. 158 (1992) 87-117. The shown dependence can be approximated with $\Phi \approx 10 \cdot \left(v / v_0\right)^{0.6}$ with $v_0 = 1\ \mu m / s$.

Problems

Problem 1: Let a rigid surface be the superposition of two random functions, one having the characteristic wave vector k_1 and the root mean square of the gradient ∇z_1, and the other having the characteristic wave vector $k_2 \gg k_1$ and the root mean square of the gradient ∇z_2. Determine the coefficient of friction between this surface and an elastomer.

Solution: In Chapter 10, we saw that the contributions of the coefficient of friction on different scales are additive – as long as the contribution of every individual scale is much smaller than 1 (practically smaller than 0.3).

First, we investigate a rough surface with a characteristic wave vector k_1 and the standard deviation of the wave vector of the same order of magnitude. The roughness and standard deviation of height l_1 for a surface with such spectral properties have the same order of magnitude: $l_1 \approx h_1$. We can estimate the radius of curvature of the maxima by presenting the surface in the vicinity of each maxi-

mum as $z = h_1 \cos k_1 x \approx h_1 \left(1 - \frac{1}{2} k_1^2 x^2\right)$. The curvature of the maxima have an order of magnitude of $1/R = |z''(0)| \approx h_1 k_1^2$. The characteristic diameter of a micro-contact is estimated using

$$r \approx \sqrt{Rl} \approx \sqrt{\frac{h_1}{h_1 k_1^2}} = \frac{1}{k_1}$$

and, according to this, has the same order of magnitude as the characteristic length of the wave profile of the surface ($\approx \lambda_1 / 2\pi$, where λ_1 is the characteristic wave length).

If there is only one scale with the characteristic wave vector k_1, then Equation (16.12) can be used in order to calculate the coefficient of friction, which we write in the form

$$\mu_1 \approx \nabla z_1 \frac{G''(k_1 v)}{|G(k_1 v)|}.$$

If roughnesses on two scales are present, then the contributions to the coefficients of frictions (as long as these contributions are much smaller than 1) sum to

$$\mu \approx \mu_1 + \mu_2 \approx \nabla z_1 \frac{G''(k_1 v)}{|G(k_1 v)|} + \nabla z_2 \frac{G''(k_2 v)}{|G(k_2 v)|}.$$

Problem 2: Determine the coefficient of rolling resistance of a rigid wheel on an elastic sheet which is composed of a series of the identical viscoelastic elements ("Winkler foundation," see Fig. 16.9). Let every element consist of a spring (spring constant cdx) and a damper (damping constant δdx) connected in parallel.

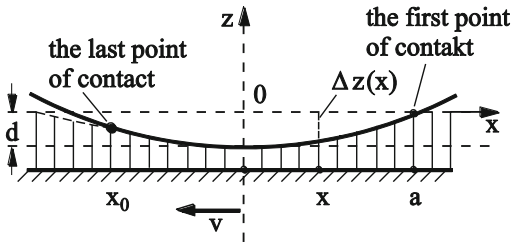

Fig. 16.9 A rigid wheel is regarded as stationary. A rigid plate mounted with an viscoelastic sheet, here modeled as a Winkler foundation, is moved to the left with a velocity v. The "penetration depth" is constant and equal to d.

Solution: We approximate the form of the wheel near the contact point with

$$z = -d + \frac{x^2}{2R},$$

where d is the penetration depth. The gradient in point x is $\tan\theta = z' = x/R$. A movement of the substrate in the negative direction with the velocity v leads to a spring movement in the vertical direction with the velocity $\dot{z} = -vz' = -vx/R$. The force with which an element is acting on the wheel, is equal to

$$dF_z = \left(-cz - \delta\dot{z}\right)dx = \left(-cz + \delta v z'\right)dx = \left(-c\left(-d + \frac{x^2}{2R}\right) + \delta v\frac{x}{R}\right)dx.$$

The z-component of the total force is calculated as

$$F_N = \int_{x_0}^{a}\left(-c\left(-d + \frac{x^2}{2R}\right) + \delta v\frac{x}{R}\right)dx$$

and the x-component of the total force as

$$F_w = \int_{x_0}^{a}\left(-c\left(-d + \frac{x^2}{2R}\right) + \delta v\frac{x}{R}\right)\frac{x}{R}dx,$$

where the coordinate of the first point of contact on the right is denoted with a and the last point of contact on the left with x_0. The coordinate a is calculated using the condition $z = 0$ and x_0 using the condition $dF_z = 0$. From this, it follows that

$$a = \sqrt{2Rd}, \quad x_0 = -\sqrt{2Rd + \left(\frac{v\delta}{c}\right)^2} + \frac{v\delta}{c}.$$

By substituting $\xi = x/\sqrt{2Rd}$, we bring the expressions for F_N and F_w into the following form

$$F_N = 2^{1/2}R^{1/2}d^{3/2}c\int_{\xi_0}^{1}\left(1 - \xi^2 + \kappa\xi\right)d\xi,$$

$$F_w = 2d^2c\int_{\xi_0}^{1}\left(1 - \xi^2 + \kappa\xi\right)\xi d\xi,$$

having defined

$$\kappa = \frac{2^{1/2}\delta v}{cd^{1/2}R^{1/2}} = \frac{2\delta v}{ca}$$

and

$$\xi_0 = -\sqrt{1+\left(\frac{\kappa}{2}\right)^2} + \frac{\kappa}{2}.$$

The coefficient of rolling resistance is calculated as

$$\mu = \frac{F_w}{F_N} = \left(\frac{2d}{R}\right)^{1/2} \frac{\int_{\xi_0}^{1} \left(1-\xi^2+\kappa\xi\right)\xi d\xi}{\int_{\xi_0}^{1} \left(1-\xi^2+\kappa\xi\right) d\xi}.$$

We consider two limiting cases:
(a) $\kappa \ll 1$: very low velocities. In this case, the approximations $F_N = \frac{4}{3} 2^{1/2} R^{1/2} d^{3/2} c$ and $F_w = \frac{4}{3} d^2 c\kappa$ are valid. The coefficient of rolling resistance is, therefore,

$$\mu = \frac{d^{1/2}}{2^{1/2} R^{1/2}} \kappa = \frac{\delta v}{cR} = \frac{\tau v}{R}$$

with $\tau = \delta / c$ (one can compare this result to that of the approximation (16.29)).
(b) $\kappa \gg 1$: very high velocities, or traversing a liquid sheet ($c = 0$). In this case, the approximations $F_N = \delta v d$ and $F_w = \frac{2^{3/2}}{3} \frac{d^{3/2} \delta \cdot v}{R^{1/2}}$ are valid. The coefficient of resistance is, therefore[4],

$$\mu = \frac{2^{3/2}}{3} \left(\frac{F_N}{\delta v R}\right)^{1/2}.$$

Problem 3: Determine the kinetics of the process of the separation of a sphere in contact with an elastomer if the sphere is unloaded before $t = 0$ and at time $t = 0$ a force $F_N = -F_A = -\frac{3}{2}\gamma^* \pi R$, $F_N = -1.5 \cdot F_A$, or $F_N = -2 \cdot F_A$ is applied. Use the following values: $R = 2$ mm, $E^* = 10$ MPa, $\gamma^* = 0.05$ J/m^2, $\Phi \approx 10 \cdot \left(v / v_0\right)^{0.5}$, $v_0 = 1\ \mu m / s$.

Solution: The problem is solved with Equation (16.35), which we write in the following form:

---

[4] For the transition to a three-dimensional system, δ must be replaced by $4\,\overline{\eta}$: $\mu = \frac{1}{3}\left(\frac{2F_N}{\overline{\eta} v R}\right)^{1/2}$.

For a more detailed explanation see Chapter 19.

$$D-\gamma^{*}=10\gamma^{*}\left(v/v_0\right)^{0.5}.$$

With the denotations for adhesive force and equilibrium radius as

$$F_A=\frac{3}{2}\pi\gamma^{*}R \text{ (in our case} = 0.47\cdot10^{-3}\text{ N)}$$

and

$$a_0=\left(9\frac{\gamma^{*}\pi R^2}{2E^{*}}\right)^{1/3} \text{ (in our case} = 6.56\cdot10^{-5}\text{ m)},$$

respectively, the line load D can be presented in the following form:

$$D=\gamma^{*}\left[\frac{1}{4}\frac{F_N}{F_A}\left(\frac{a_0}{a}\right)^{3/2}-\left(\frac{a}{a_0}\right)^{3/2}\right]^2.$$

Before time $t=0$ there is an equilibrium condition without loading and a contact radius of a_0. At any time after $t=0$, the following equation is valid:

$$\gamma^{*}\left[\frac{1}{4}\frac{F_N}{F_A}\left(\frac{a_0}{a}\right)^{3/2}-\left(\frac{a}{a_0}\right)^{3/2}\right]^2-\gamma^{*}=10\gamma^{*}\left(\frac{v}{v_0}\right)^{0.5}.$$

For velocity, it follows that

$$v=-\frac{da}{dt}=\frac{v_0}{100}\left(\left[\frac{1}{4}\frac{F_N}{F_A}\left(\frac{a_0}{a}\right)^{3/2}-\left(\frac{a}{a_0}\right)^{3/2}\right]^2-1\right)^2.$$

Using the dimensionless variables $\tilde{a}=a/a_0$ and $\tilde{t}=tv_0/100a_0$, we obtain the equation

$$-\frac{d\tilde{a}}{d\tilde{t}}=\left(\left[\frac{1}{4}\frac{F_N}{F_A}\tilde{a}^{-3/2}-\tilde{a}^{3/2}\right]^2-1\right)^2$$

with the initial condition $\tilde{a}=1$ for $\tilde{t}=0$. Results of a numerical integration of this equation for three different ratios of F_N/F_A are presented in Fig. 16.10.

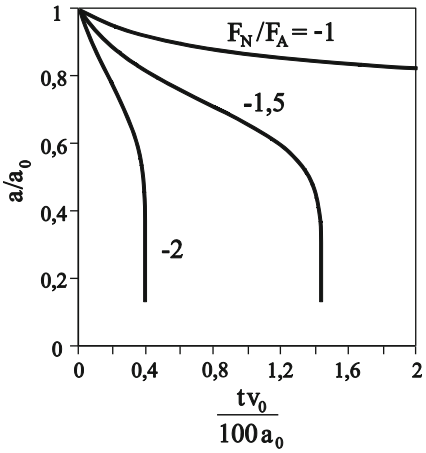

Fig. 16.10 Dependence of the contact radius on the time for various normal forces.

For $F_N = -F_A$, the system approaches equilibrium as $t \to \infty$. The normal force $F_N = -1.5 \cdot F_A$ corresponds to the over-critical separation force. The sphere separates at time $\sim 1.4 \cdot 100 a_0 / v_0 \approx 9 \cdot 10^3$ s.

17 Wear

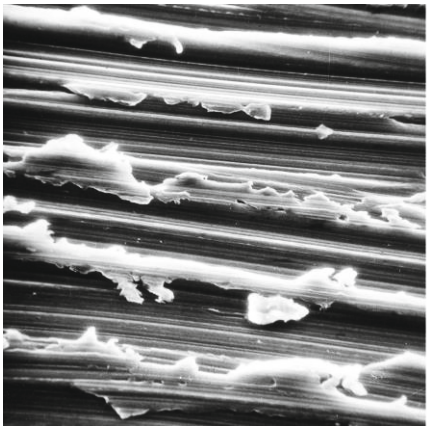

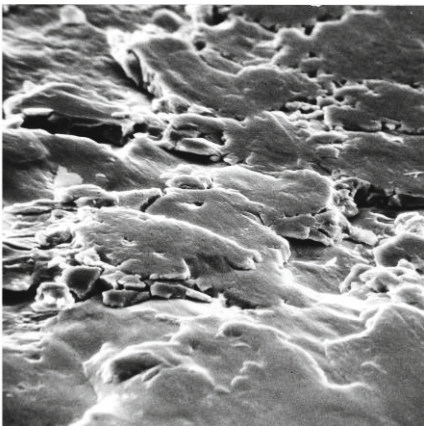

17.1 Introduction

Wear is one of the main causes for component damage and subsequent failure of machines and devices. Its mitigation by appropriate material choice, coating, surface design, or lubrication is, therefore, of high economic importance.

Even though friction and wear always appear together, in practice, they are qualitatively different phenomena. One can already see this in the fact that one can imagine friction without wear, at least in a model. For example, there is friction, but no wear in the Prandtl-Tomlinson model. Even wear without friction can be envisioned: wear can already be caused by a normal contact without tangential movement.

The often different physical mechanisms for friction and wear make themselves visible in the fact that the wear rate for various friction pairs (at otherwise identical conditions) can vary by several orders of magnitude. At the same time, it can be noted that in specific situations, the processes that lead to friction also cause wear to occur at the same time, for example, the plastic deformation of microcontacts. In these cases, friction and wear can have a close correlation.

In most cases, friction is considered an unwanted phenomenon. Wear can, however, also be the basis for various technological processes, such as grinding, polishing, or sandblasting.

It is common to differentiate the following fundamental types of wear according to their physical mechanisms:

- Abrasive wear occurs, if two bodies with distinctively different hardnesses are in contact or the third-body contains hard particles.
- Adhesive wear occurs even in contacts between bodies with the same or similar hardnesses.

V.L. Popov, *Contact Mechanics and Friction*,
DOI 10.1007/978-3-662-53081-8_17

- Corrosive wear is associated with chemical modifications of the surface and finally erosion of the surface layer.
- Surface fatigue is caused by repeated loading of the surface either by sliding or rolling, where in every single loading cycle, no noticeable changes in the surface appear.

17.2 Abrasive Wear

During abrasive wear the asperities of the harder material penetrate and cut the softer material. The gouges that run in the sliding direction are, therefore, a sign of abrasive wear. In order to estimate the wear rate for abrasive wear, we consider a simple model in which all micro-contacts on the hard surface are cone-shaped. First, we look at a single micro-contact with the normal load ΔF_N.

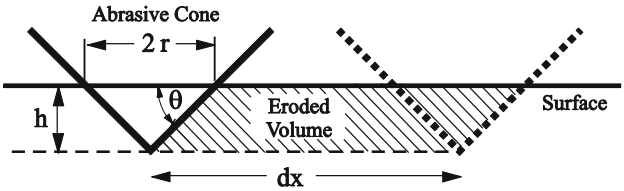

Fig. 17.1 Gouging of a material by a rigid cone.

Under the influence of this normal force, the cone penetrates into the softer material. According to the definition of hardness σ_0 (of the softer material)

$$\Delta F_N = \sigma_0 \cdot \pi r^2 . \tag{17.1}$$

The area of the projection of the cone on the vertical plane is equal to rh. For a displacement of dx, the cone would cut out a volume dV, which is given by the following equation:

$$dV = rh \cdot dx = r^2 \tan\theta \cdot dx = \frac{\Delta F_N \tan\theta \cdot dx}{\pi\sigma_0} . \tag{17.2}$$

As a rough estimate, we relate this volume to that of the volume of wear debris of the material. The wear rate – defined as the volume of wear debris divided by the sliding length – is, therefore, equal to

$$\frac{dV}{dx} = \frac{\Delta F_N \tan\theta}{\pi\sigma_0} . \tag{17.3}$$

The summation of all of the micro-roughnesses results in a volume of wear debris of

$$V = \frac{F_N \overline{\tan\theta}}{\pi\sigma_0} x, \tag{17.4}$$

where $\overline{\tan\theta}$ is a weighted average of $\tan\theta$ of all of the micro-contacts. This equation is usually written as the *Archard wear equation*:

$$V = \frac{k_{abr} F_N}{\sigma_0} x. \tag{17.5}$$

The volume of wear debris is proportional to the normal force, the sliding length, and inversely proportional to the hardness of the material. The wear coefficient k_{abr} represents the specific geometry of the abrasive surface.

The wear between a soft material and an abrasive body in which hard particle are solidly embedded is called *two-body wear*. A special form of abrasive wear is the wear of bodies between which hard, abrasive particles are present. This case is called *three-body wear*.

As can be seen in Table 17.1, the wear coefficients for two-body wear lie between $6 \cdot 10^{-2}$ and $6 \cdot 10^{-3}$, while for three body wear, they are approximately one order of magnitude smaller.

Table 17.1 Abrasive Wear Coefficients. Source: E. Rabinowicz: Friction and wear of materials. Second Edition. John Wiley & Sons, inc., 1995.

Authors	Wear Type	Asperity Size (μ)	Material	$k\left(\text{x}10^{-3}\right)$
Spurr et al. (1975)	2-Body	--	Many	60
Spurr et al. (1975)	2-Body	110	Many	50
Avient et al. (1960)	2-Body	40-150	Many	40
Lopa (1956)	2-Body	260	Steel	27
Kruschov and Babichev (1958)	2-Body	80	Many	8
Samuels (1956)	2-Body	70	Brass	5
Toporov (1958)	2-Body	150	Steel	2
Rabinowicz et al. (1961a)	2-Body	80	Steel	1.7
Rabinowicz et al. (1961a)	2-Body	40	Many	0.7

From the wear equation in (17.5), it follows that the volume of wear debris is proportional to the sliding length. This is only valid as long as the roughnesses of the harder material are not “filled” by the softer material. When this occurs, the wear rate decreases with time (Fig. 17.2).

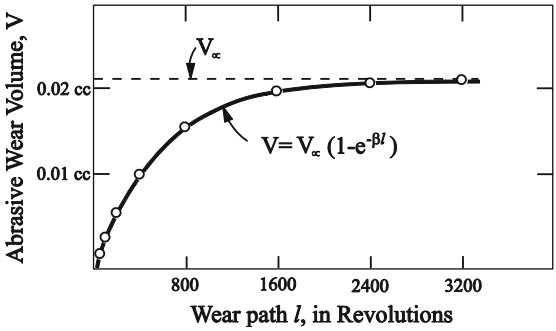

Fig. 17.2 Change in the wear coefficient with time. Data from Mulhearn, T.O., and Samuels L.E., The abrasion of metals: A model of the process, Wear, 1962, v. 5, 478-498.

As long as the surface properties of the partners are not changed (this can be achieved by regular cleaning the surfaces of debris particles), the volume of wear debris is proportional to the sliding path. Equation (17.5) indicates that the wear rate is inversely proportional to the hardness σ_0 of the softer material. The reciprocal value $\in = dx / dV$, called the *wear resistance*, is proportional to its hardness. This dependence was confirmed in many experiments (Fig. 17.3). The hardness of the abrasive, on the other hand, influences the wear rate only marginally.

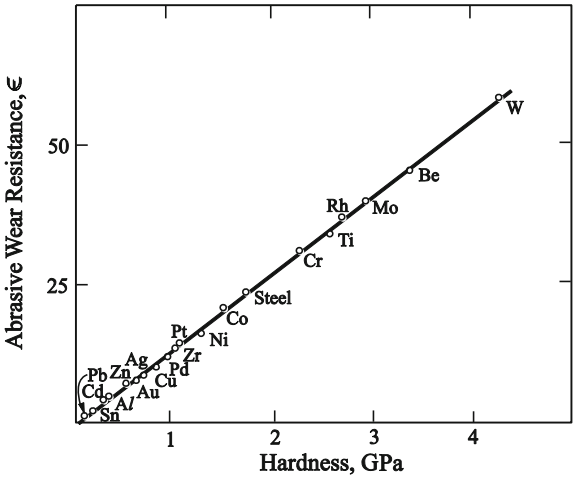

Fig. 17.3 The abrasive wear resistance of metallic materials is proportional to the hardness with a high accuracy. Experimental data from Хрущев М. М., Бабичев М. А., Исследования изнашивания металлов (Investigations on the wear of metals), Moscow, 1960.

By the choice of abrasive materials, not only must the hardness be taken into account, but also its ability to form sharp cutting edges. From this, it follows that brittle materials with higher hardnesses are preferred.

Equation (17.4) can also be interpreted in another way. Because the coefficient of friction μ caused by the gouging process is equal to $\overline{\tan\theta}$, (17.4) can also be presented in the following form

$$V = \tilde{k}\frac{F_N \mu x}{\sigma_0} = \tilde{k}\frac{W}{\sigma_0}, \tag{17.6}$$

where W is the frictional work. According to this, the volume of wear debris is proportional to the dissipated energy divided by the hardness of the material. The proportionality of the volume of wear debris to the energy contribution is also valid for adhesive wear (see next section) and erosive wear (see Problem 1 in this chapter) and is often applied as a general "law of wear" for even more types of wear.

17.3 Adhesive Wear

If the frictional partners have comparable hardnesses, then another type of wear begins to play a primary role: adhesive wear. Adhesive wear is the most important type of wear in tribological applications in which the wear should be minimized and, therefore, the conditions at which abrasive wear occurs should be avoided. The mechanism of adhesive wear can be imagined as the welding together of micro-roughnesses followed by the volume elements (wear particles) close to the surface being torn away. We investigate the conditions for the welding and tearing away of a particle according to this mechanism.

The fundamental property of metallic materials is that they deform plastically after a critical stress is exceeded. If the material is, thereby, loaded in tension, then after some critical deformation, failure occurs. In contrast, if the elastic limit is exceeded under pressure, then the two partners are welded together. Even if this effect is not macroscopically noticeable (similar to the case of adhesion), it is valid for individual micro-contacts.

Now, we consider an asperity, which comes into contact with another asperity during the relative movement between contact partners and forms a junction with diameter D and afterwards breaks away (Fig. 17.4).

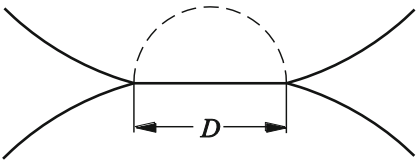

Fig. 17.4 A "cold-weld" junction between two asperities.

In the typical strength hardened state for the surface layer, all three critical stresses, namely yield strength, ultimate strength, and "welding stress," are of the same order of magnitude. The stress in the micro-contact reaches the order of magnitude of the penetration hardness σ_0 of the material as the asperities come together. Thereby, the asperities weld together. If they then separate, nearly the same stress σ_0 is again reached just before failure, only with a different sign. The elastic potential energy directly before failure has the order of magnitude $U_{el} \approx \frac{\sigma_0^2}{2G} D^3$. It is only sufficient to dislodge a particle when it is larger than the adhesive energy, $U_{adh} \approx \gamma_{eff} D^2$, which is required in order to create two free surfaces. Here, γ_{eff} is the *effective surface tension* of the inner interface in the material (also called the fracture toughness). The dislodging of a particle is, therefore, only possible if $U_{el} > U_{adh}$ and thus:

$$D > \frac{2G\gamma_{eff}}{\sigma_0^2}. \tag{17.7}$$

For many simple crystals $\sigma_0 \propto G$. Then, (17.7) assumes the form

$$D_c = const \frac{\gamma_{eff}}{\sigma_0}. \tag{17.8}$$

This equation gives the order of magnitude of the diameter of the wear particle as a function of the hardness and the effective surface energy. The experimental value for the constant in (17.8) is around 60000[1].

Since the dislodging of a particle leads to the creation of a cavity of about the same depth as the diameter of the dislodged particle, it is safe to assume that the roughness created by wearing is on the same order of magnitude as (17.8).

In many applications, it is required that the clearance between two moving parts is as small as possible. Experience shows, however, that the clearance should also not be too small. Otherwise, gradually increasing damage to the surface begins to take place, which is called "galling." It is obvious that the required minimum clearance has the same order of magnitude as the characteristic diameter of the wear particle. An empirical equation for the minimum clearance $h_{\min}$ is

$$h_{\min} = 180{,}000 \frac{\gamma_{eff}}{\sigma_0}. \tag{17.9}$$

In order to estimate the wear rate for adhesive wear, we consider two rough surfaces in contact (Fig. 17.5).

[1] For this, see the book by E. Rabinowicz, Friction and wear of materials. Second Edition, John Wiley & Sons, inc., 1995.

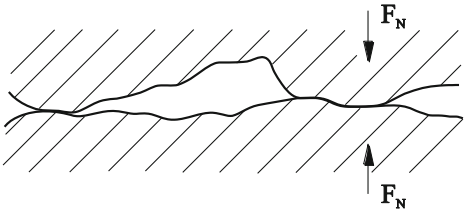

Fig. 17.5 Two rough surfaces in contact.

The normal force F_N is related to the contact area and the hardness of the contacting bodies:

$$F_N = \sigma_0 A\,. \tag{17.10}$$

We denote the average diameter of a contact with D and the number of micro-contacts with n. It is then obvious that $A \approx \frac{\pi D^2}{4} \cdot n$. From this, it follows that

$$n = \frac{4A}{\pi D^2} = \frac{4F_N}{\pi D^2 \sigma_0}\,. \tag{17.11}$$

The "existence length" of a micro-contact has the same order of magnitude as the diameter D of the contact. This is the length over which a contact is formed and again destroyed. The total number of contacts which have been formed along the path x is equal to

$$N \approx n\frac{x}{D} \approx \frac{4F_N x}{\pi\sigma_0 D^3}\,. \tag{17.12}$$

If we assume that not every formation and destruction of a micro-contact leads to the dislodging of a wear particle, rather the wear particles form with a probability k^*, then the total volume of generated wear particles is equal to

$$V = \frac{1}{2}\cdot\frac{4}{3}\cdot\frac{\pi D^3}{8}\cdot k^* N = \frac{\pi D^3}{12}\cdot k^* \cdot \frac{4F_N x}{\pi\sigma_0 D^3} = \frac{k^*}{3}\cdot\frac{F_N x}{\sigma_0}\,. \tag{17.13}$$

By defining $k^*/3$ as the coefficient k_{adh}, we obtain the law for adhesive wear:

$$V = k_{adh}\frac{F_N x}{\sigma_0}\,. \tag{17.14}$$

Also for adhesive wear, the volume of wear debris is proportional to the normal force, the sliding length, and inversely proportional to hardness. This equation is often called the *Holm-Archard Equation*.

Due to the "probability of the generation of a wear particle," which now comes into play and can be dependent, for example, on the contamination of the surface, the adhesive wear coefficients may vary by a few orders of magnitude. The typical value of the wear coefficient for a non-lubricated contact between two alloy-forming metals is approximately $k_{adh} \sim 10^{-3}$, but can be three or four orders of magnitude smaller in the presence of a very good lubricant or for two non-compatible metals.

17.4 Conditions for Low-Wear Friction

The conditions for low-wear sliding are dependent on many parameters and it is difficult to formulate simple rules to deal with it. Different situations present themselves in lubricated and non-lubricated systems. Roughnesses serve as a reservoir for lubricants in lubricated systems and in this way, can minimize wear, while in dry operating systems, it is usually desired to create as smooth a surface as possible. If the yield stress of the material is not reached in the micro-contact, then only purely elastic deformation of the surfaces takes place – assuming that no chemical reactions occur between the two surfaces[2]. Since the average stress in the micro-roughnesses has the order of magnitude $\frac{1}{2}E^*\nabla z$, according to (7.16), and the maximum stress that occurs in the individual micro-contacts can reach approximately $E^*\nabla z$, the condition $E^*\nabla z < \sigma_0$ must be met, or

$$\nabla z < \frac{\sigma_0}{E^*} . \tag{17.15}$$

For many metallic materials, the hardness correlates with the modulus of elasticity and the following is valid[3]:

$$\frac{\sigma_0}{E} \approx 0.01 . \tag{17.16}$$

In order for the frictional partners to deform only elastically, the surfaces must be extremely smooth: the average gradient of the surfaces cannot exceed the value 0.01. Additionally, it is desirable to keep the wave length of the roughness as small as possible, so that the diameter of the micro-contacts remains below that found in (17.8) and the condition for adhesive wear is not fulfilled. If the average gradient is larger than that in (17.15), then the softer material in the contact area

[2] A simple criterion for this is that the contacting materials form no alloys.

[3] For related statistical data, see: E. Rabinowicz, Friction and Wear of Materials. Second Edition, John Wiley & Sons, inc., 1995.

plastically deforms. The consequences that plastic deformation has on wear are significantly dependent on the properties of the uppermost surface layers.

The description of adhesive wear in the previous section assumes that the formation of cold-weld junctions and their subsequent destruction takes place at different places in the material. If the material forms a layer of oxides or is lubricated, then it is possible that the destruction of the contacts occurs at the same interface as their formation. The relation between the strength of the surface interface and the volume strength of the material, therefore, plays a very large role in adhesive wear, even if they are not explicitly represented in Equation (17.14). This motivated Kragelski[4] to introduce the "*principal of positive hardness gradient*" as the essential principal for formulating conditions for low-wear friction. According to this principal, the strength of the uppermost surface layers of the material should increase with the depth. This can be achieved by lubrication, chemical modification of the surface layers, by material softening using local temperature increases, as well as by designing surface layers with low surface energies. For low-wear contacts, it is beneficial if the contacting materials do not form alloys, or at least an alloy for which the strength is smaller than that of both of the base materials. If the hardness gradient is negative for whatever reason, then the wear rate increases abruptly. Therefore, the processes of oxidation and interactions with molecular layers of the lubricating film are very relevant to wear, but until now, have not been able to be brought into the framework of a simple contact mechanical model.

17.5 Wear as the Transportation of Material from the Friction Zone

In order to analyze wear, it is not sufficient to establish the conditions for the dislodgment of wear particles. As long as the wear particles remain in the friction zone, they continue to be exposed to intensive tribological loading and are repeatedly reintegrated into the surfaces of the frictional partners. The wear first becomes noticeable when the material has left the friction zone. Therefore, the wear is in a broader sense, not only a problem of strength, but also a problem of material transport out of the friction zone.

According to Kragelski, in order for a material to be wear resistant, it is beneficial for the surface to have a lower yield strength than the inner material. We will investigate the wear resistance of a material with such a soft surface layer with a shear strength of τ_c and thickness h. Let the diameter of the friction zone be L.

The wear rate can be estimated using the following qualitative considerations. Assuming that the layer exhibits ideal plastic behavior, the tangential stress in the layer remains constant, independent from the sliding velocity, and equal to τ_c.

[4] I.V. Kragelski, Friction and Wear. Butter Worth, London, 1965, 346 pp.

One can formally introduce an effective viscosity of the layer η_{eff} so that the shear stress in the layer can be calculated using the same rule as with a viscous fluid:

$$\tau_c = \eta_{eff} \frac{v}{h} . \tag{17.17}$$

From this, it follows that

$$\eta_{eff} = \frac{h\tau_c}{v} . \tag{17.18}$$

A surface layer that is already in a state of plastic yielding has no yield strength with respect to other stress components (e.g. normal stress) and behaves, in a first order approximation, like a liquid with the effective viscosity (17.18). Thus, it is squeezed with a velocity that can be estimated using Equation (14.27):

$$\left|\dot{h}\right| \approx \frac{2h^3}{3\pi\eta_{eff}R^4} F_N \approx \frac{2h^2 v}{3\pi R^4 \tau_c} F_N . \tag{17.19}$$

The volume that is squeezed out of the friction zone (material that is worn away) divided by the sliding path is, therefore, equal to $\frac{dV}{dx} = \frac{\left|\dot{h}\right|\pi R^2}{v} \approx \frac{8}{3}\frac{F_N}{\tau_c}\left(\frac{h}{2R}\right)^2$. Numerical simulations confirm that this equation is accurate up to a proportionality factor. Therefore, the wear equation can be written in the following form[5]:

$$V \approx \frac{F_N}{\sigma_0}\left(\frac{h}{L}\right)^2 x . \tag{17.20}$$

Here, we introduced the hardness of the material σ_0. This relationship has the same form as that of the wear equation (17.14), but with a geometric factor $(h/L)^2$, which accounts for extremely low wear rates for small values of h and large values of L.

17.6 Wear of Elastomers

The wear of elastomers is a very complicated process that is not completely understood even today. We can apply the wear equation (17.14) for a rough estimate of adhesive wear, where the hardness σ_0 must be replaced by the average stress (16.10) in the micro-contacts:

[5] V.L. Popov, I.Yu. Smolin, A. Gervé and B. Kehrwald, Simulation of wear in combustion engines. Computational Materials Science, 2000, v. 19, No.1-4, pp. 285-291.

$$V = k_{adh} \frac{\kappa F_N x}{4\left|\hat{G}(vk)\right|\nabla z} \tag{17.21}$$

with $\kappa \approx 2$ and k being the characteristic wave number of the roughness.

In order to characterize the wear of rubber, one often uses the so-called *abradability* γ as the ratio of the volume of wear debris to the energy loss[6]. For this, we have the approximation

$$\gamma = \frac{V}{\mu F_N x} = \frac{\kappa k_{adh}}{\mu 4\left|\hat{G}(vk)\right|\nabla z} = \frac{\kappa k_{adh}}{4\nabla z^2 \mathrm{Im}(\hat{G}(vk))}. \tag{17.22}$$

The abradability is inversely proportional to the imaginary part of the complex modulus and exhibits a minimum in the middle velocity domain (Fig. 17.6). The abradability curve determined by experiments is presented in Fig. 17.7 as a function of velocity.

In addition to viscoelastic properties, rubber also exhibits plastic properties. These properties can be characterized by defining a critical stress σ_c, the "yield stress," whereby, this critical stress is even more loosely defined as it is in metals. We assume that the penetration hardness of rubber is three times this value: $\sigma_0 \approx 3\sigma_c$. According to (16.10), the characteristic stress in the micro-contacts has an order of magnitude of

$$\sigma \approx 4\kappa^{-1}\left|\hat{G}(vk)\right|\nabla z\,. \tag{17.23}$$

If this stress reaches the hardness of the material, then the rubber deforms plastically and the wear increases rapidly. The critical velocity at which this occurs is calculated using the condition

$$\sigma_0 \approx 2\left|\hat{G}(v_c k)\right|\nabla z\,. \tag{17.24}$$

A more exact consideration of frictional and wear processes should also take into account changes in temperature in the micro-contacts, because the complex modulus is temperature dependent.

For large coefficients of friction, an instability develops in the frictional contact for which a part of the contact surface is in a sticking state. Further movement of the body is then only possible by the propagation of detachment waves, the so-called *Schallamach waves*. In this regime, another wear mechanism is characteristic, the formation of rubber rolls.

[6] Abradability γ should not be confused for the surface tension, for which we use the same letter.

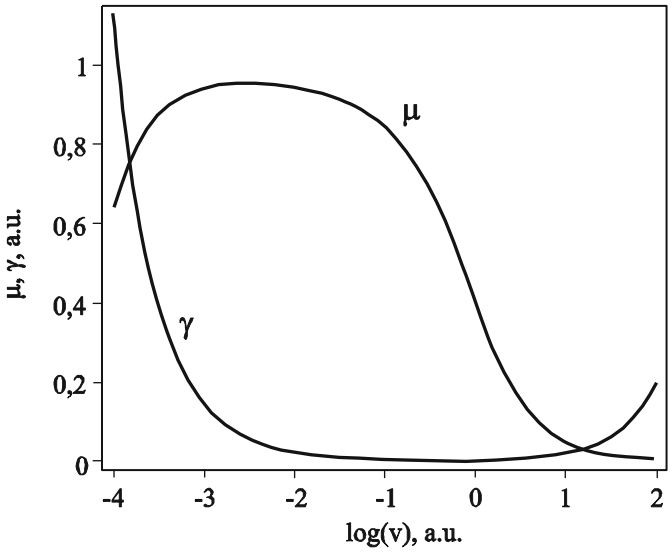

Fig. 17.6 Velocity dependence of the coefficient of friction and the abradability, according to Equation (17.22), for the rheological model (15.51) with $G_0 = 1$, $G_1 = 1000$, $\tau_1 = 10^{-2}$, $\tau_2 = 10^2$, and $g(\tau) = \tau_1 \tau^{-2}$.

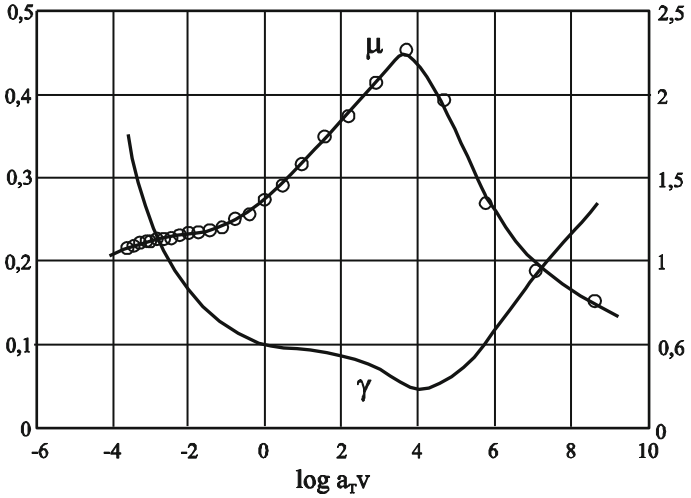

Fig. 17.7 Experimental velocity dependence of the coefficient of friction μ and the abradability γ for a rubber. Data from: K.A. Grosch, The rolling resistance, wear and traction properties of tread compounds. Rubber Chemistry and Technology, 1996, v. 69, pp. 495-568.

Problems

Problem 1: Erosive wear at low velocities. A hard, round particle with the radius R and a velocity v_0 impacts a surface (hardness σ_0) perpendicularly. Determine the penetration depth, the diameter of the penetration, and the volume expelled by the impact.

Solution: The time-dependent penetration depth $d(t)$ is related with the time-dependent contact radius $a(t)$ according to $a(t) \approx \sqrt{2Rd(t)}$. The contact surface is calculated as

$$A(t) \approx 2\pi R d(t) .$$

Let the average stress in the contact area be constant at every point and equal to the hardness of the material. The contact force acting on the spherical particle is, therefore, equal to $-\sigma_0 2\pi R d(t)$. The equation of motion yields

$$m\frac{\partial^2 d(t)}{\partial t^2} = -2\pi\sigma_0 R d(t) .$$

Its solution with the initial conditions $d(0) = 0$, $\dot{d}(0) = v_0$ is given by

$$d(t) = \frac{v_0}{\omega}\sin \omega t$$

with $\omega = \sqrt{\frac{2\pi\sigma_0 R}{m}}$. The maximum penetration depth is equal to

$$d_{\max} = \frac{v_0}{\omega} = v_0\sqrt{\frac{m}{2\pi\sigma_0 R}} .$$

By expressing the mass of the particle using the density: $m = \frac{4}{3}\pi R^3 \rho$, we obtain

$$d_{\max} = R\sqrt{\frac{2}{3}\frac{\rho v_0^2}{\sigma_0}} .$$

The "penetrated" volume ΔV is equal to

$$\Delta V \approx \pi R d_{\max}^2 = \frac{4}{3}\pi R^3 \frac{\rho v_0^2}{2\sigma_0} = V\frac{\rho v_0^2}{2\sigma_0} = \frac{m v_0^2}{2\sigma_0} .$$

The penetrated volume for the impact of the particle is equal to the kinetic energy of the particle divided by the hardness of the material.

The wear volume is dependent not only on the penetrated volume, but also from the mechanism of the removal of the displaced material. As a rule, however, the wear volume is proportional to the penetrated volume.

Problem 2: Fretting wear. An axially-symmetrical profile $z = f_0(r)$ is pressed into an elastic half-space with the indentation depth d, and then oscillates in the tangential direction with a given amplitude $u_x^{(0)}$. For small amplitudes, wear will take place only in the annular slip area at the border of the contact area. Determine the limiting shape of the worn profile $z = f_\infty(r)$ after very large numbers of oscillation cycles. It is assumed that the Coulomb's law of friction is valid and that only the indenter profile is worn.

Solution[7]: According to the simplest form of the Coulomb's law of friction, the maximum static frictional stress $\tau_{\max}$ is equal to the sliding tangential stress τ_{slip} and this is equal to the normal pressure p multiplied with a constant coefficient of friction μ: $\tau_{\max} = \mu p$, $\tau_{\text{slip}} = \mu p$. The no-slip condition is $\tau \le \mu p$. For the wear law, we make the very general assumption that wear takes place only in the areas where both pressure *and* relative displacement between the surfaces are not zero. Therefore, no wear takes place in the areas where either the pressure or the relative displacement is zero: this corresponds to the areas without contact (no pressure) and the stick area (no relative displacement). Due to wear outside of the sticking region with the radius c, the local pressure in the worn area will decrease with the number of vibration cycles and increase in the sticking region. This is why the original stick-area will remain in the stick state and is not worn. In the slip region of the contact area, the progressive wear process will take place until the pressure in the sliding region vanishes. Thereby, a state will be reached in which no further wear can take place. From the above it can be concluded that this limiting shape does not depend on the exact form of the wear law. This limiting profile can be determined using the procedure of the method of dimensionality reduction (MDR) described in Chapters 5 and 8.

In the framework of the MDR, an elastic foundation is defined according to (5.56) and (8.41) and an MDR-modified profile $g(x)$ according to (5.52). In the following, this profile is analyzed in the framework of the MDR model instead of the original three-dimensional profile $f(r)$. If the profile is moved tangentially by $u_x^{(0)}$, the springs will be stressed both in the normal and tangential direction. The radius of the stick region will be given by the condition that the tangential force is equal to the coefficient of friction μ multiplied with the normal force:

$$G^* u_x^{(0)} = \mu E^* \left(d - g(c) \right).$$

[7] This solution follows the paper: V.L. Popov, Analytic solution for the limiting shape of profiles due to fretting wear, Sci. Rep., 2014, v. 4, 3749.

According to the rules of the MDR, the pressure distribution in the contact area is calculated using Eq. (5.59), which we will repeat here again for the sake of convenience

$$p(r) = -\frac{1}{\pi}\int_r^\infty \frac{q_z'(x)}{\sqrt{x^2 - r^2}}\,\mathrm{d}x = \frac{E^*}{\pi}\int_r^\infty \frac{g'(x)}{\sqrt{x^2 - r^2}}\,\mathrm{d}x\,.$$

In the limiting state, the pressure outside of the stick area is zero: $p(r) = 0$ for $r > c$. From the pressure equation, it follows that in this area

$$g'(x) = 0 \;\text{ and } g(x) = const\,,\; \text{for } \; c < x < a\,.$$

The shape of the equivalent one-dimensional profile in the final state is thus given by the following equations (Fig. 17.8):

$$g_\infty(x) = \begin{cases} g_0(x), & \text{for } 0 < x < c \\ d, & \text{for } c < x < a \end{cases}.$$

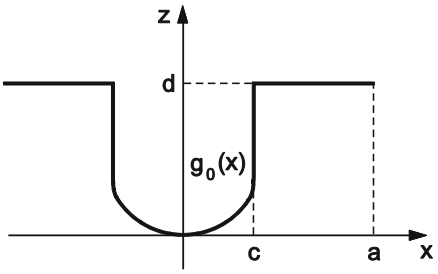

Fig. 17.8 One-dimensional MDR-transformed profile in the final state.

The corresponding three-dimensional profile is determined by the reverse transformation (5.53)

$$f_\infty(r) = \begin{cases} f_0(r), & \text{for } 0 < r < c \\ \dfrac{2}{\pi}\displaystyle\int_0^c \frac{g_0(x)}{\sqrt{r^2 - x^2}}\,\mathrm{d}x + \frac{2}{\pi}d\int_c^r \frac{1}{\sqrt{r^2 - x^2}}\,\mathrm{d}x, & \text{for } c < r < a \end{cases}.$$

We consider an example with a parabolic profile $f_0(r) = r^2/(2R)$. The corresponding MDR-transformed profile is $g_0(x) = x^2/R$ (see Problem 7 of Chapter 5). The radius of the stick-region is obtained by the equation $G^* u_x^{(0)} = \mu E^* \left(d - c^2 / R\right)$. It follows that

$$c = \sqrt{R\left(d - \frac{G^*}{E^*}\frac{u_x^{(0)}}{\mu}\right)}\,.$$

The worn shape in the final state is calculated as

$$f_\infty(r)=\begin{cases}\dfrac{r^2}{2R}, & \text{for } 0<r<c\\ d-\dfrac{2}{\pi}\left(d-\dfrac{r^2}{2R}\right)\arcsin\dfrac{c}{r}-\dfrac{r^2}{\pi R}\left(\dfrac{c}{r}\right)\sqrt{1-\left(\dfrac{c}{r}\right)^2}, & \text{for } c<r<a\end{cases}.$$

In the dimensionless variables (vertical coordinates normalized by the indentation depth and horizontal coordinates normalized by the initial contact radius $a_0=\sqrt{Rd}$):

$$\tilde f=f/d,\quad \tilde d=d/d=1$$
$$\tilde r=r/a_0,\quad \tilde x=x/a_0,\quad \tilde c=c/a_0,\quad \tilde a=a/a_0,$$

this profile can be written in the form

$$\tilde f_\infty(\tilde r)=\begin{cases}\dfrac{\tilde r^2}{2}, & \text{for } 0<\tilde r<\tilde c\\ 1-\dfrac{2}{\pi}\left(1-\dfrac{\tilde r^2}{2}\right)\arcsin\dfrac{\tilde c}{\tilde r}-\dfrac{\tilde r\tilde c}{\pi}\sqrt{1-\left(\dfrac{\tilde c}{\tilde r}\right)^2}, & \text{for } \tilde c<\tilde r<\tilde a\end{cases}$$

This function is illustrated in Fig. 17.9 for different values of the dimensionless radius of the stick area.

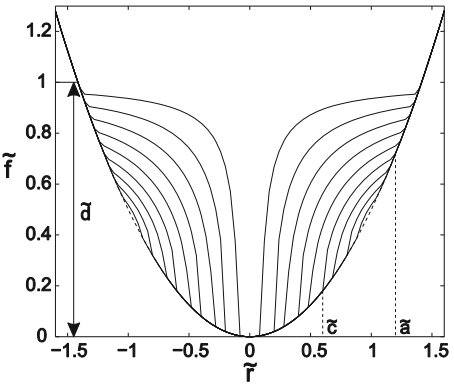

Fig. 17.9 Worn 3D-profiles in the final state for 9 linearly increasing values of the parameter $\tilde c$ from 0.1 to 0.9.

The contact radius and, thus, also the outer radius of the worn area is given by the condition $\tilde f_\infty(\tilde a)=\tilde f_0(\tilde a)$:

$$1-\frac{2}{\pi}\left(1-\frac{\tilde{a}^2}{2}\right)\arcsin\frac{\tilde{c}}{\tilde{a}}-\frac{\tilde{a}\tilde{c}}{\pi}\sqrt{1-\left(\frac{\tilde{c}}{\tilde{a}}\right)^2}=\frac{\tilde{a}^2}{2}.$$

The normal force is calculated as

$$F_N=2\int_0^a E^*\left(d-g(x)\right)\mathrm{d}x=2\int_0^c E^*\left(d-x^2/R\right)\mathrm{d}x=2E^*\left(dc-\frac{c^3}{3R}\right)$$

or considering the equation for the radius of the stick region:

$$F_N=\frac{4}{3}E^*R^{1/2}\left(d-\frac{G^*}{E^*}\frac{u_x^{(0)}}{\mu}\right)^{1/2}\left(d+\frac{G^*}{2E^*}\frac{u_x^{(0)}}{\mu}\right).$$

In the paper[8], it was shown that the above limiting shape is universal and will appear also under conditions of multi-mode fretting (e.g. superposition of normal, tangential and torsional oscillations.)

[8] A.I. Dmitriev, L.B. Voll, S.G. Psakhie, V.L. Popov, Universal limiting shape of worn profile under multiple-mode fretting conditions: theory and experimental evidence, Sci. Rep., 2016, v. 6, 23231.

18 Friction Under the Influence of Ultrasonic Vibrations

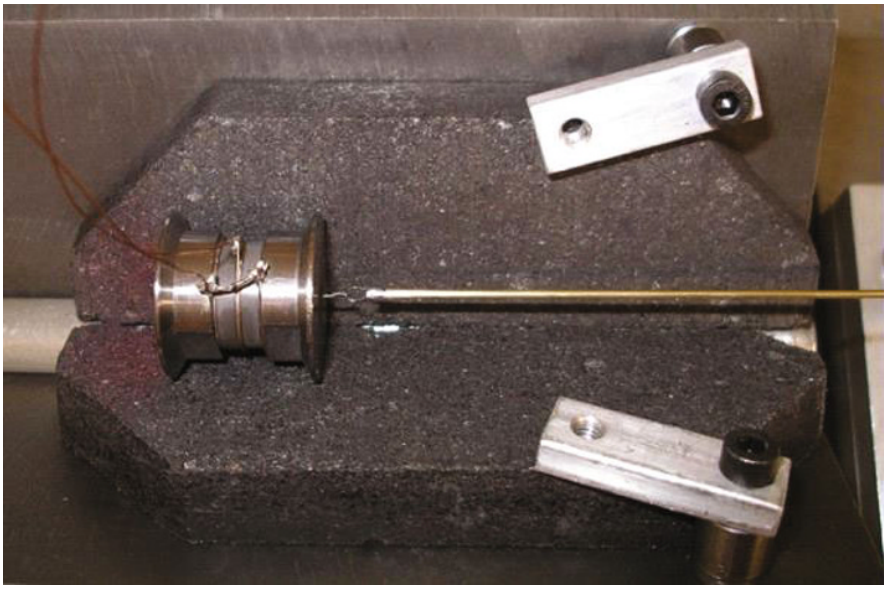

Vibrations of various frequencies and amplitudes are used in many technical fields to influence frictional forces. The most known low frequency applications are vibration compactors and plates. High frequency oscillations are utilized to influence friction forces in metal working, assembly, wire drawing, and cutting. They are also used to combat contact instabilities in nanotribological instruments (e.g. in atomic force microscopy). There are several methods to induce directional motion based on exploiting the interactions between vibrations and friction. For example, methods of transportation and separation of mixtures using vibration belong to this category. The principle of operation of traveling-wave motors, which are used in cameras and objectives, is based on ultrasonic oscillations. Oscillations usually lead to a decrease in frictional force. Under certain conditions, they can also give rise to an increase in friction or to the welding of the contact partners. Ultrasonic welding and ultrasonic bonding in microchip technology are based on this principle. Finally, oscillations can be used to explore the mechanisms of friction.

V.L. Popov, *Contact Mechanics and Friction*,
DOI 10.1007/978-3-662-53081-8_18

18.1 Influence of Ultrasonic Vibrations on Friction from a Macroscopic Point of View

I. Influence of vibration on static friction

We investigate a body that is supported on a base at two points (Fig. 18.1). Let the coefficient of friction between the base and the specimen be μ. As a first order approximation, the specimen can be considered to be a rigid body whose length can be varied periodically by means of a built-in piezoelectric element.

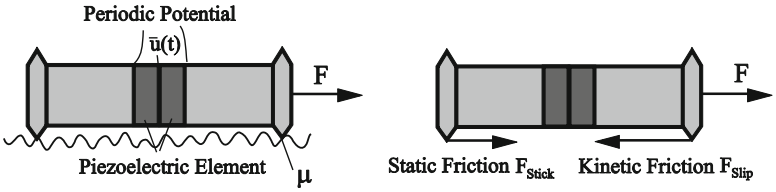

Fig. 18.1 (a) An oscillating specimen in the sliding direction. (b) The forces acting on the specimen in the horizontal direction.

In the absence of vibrations, a critical force of $F_s = \mu F_N$ must be applied to the specimen in order to set it into motion, where F_N is the normal force and, in our case, is equal to the weight of the specimen. Contrarily, if the length of the specimen is changed so that a relative motion between the contact points and the base is generated, then the specimen is already set into motion by an arbitrary small force F. The free-body diagram of a specimen whose length increases with time is shown in Fig. 18.1 b. For slow length changes, the process is quasi-static and all forces must be in equilibrium at every point in time. Since the magnitude of the kinetic frictional force is constant in every point of contact:

$$F_{slip} = \tfrac{1}{2}\mu F_N , \tag{18.1}$$

the frictional forces can only remain in equilibrium with external forces if the one end of the specimen slides and the other sticks. In the phase where the specimen contracts, the rear contact slides and the forward contact sticks. In this way, the specimen exhibits a worm-like movement and moves with the period Δl, where Δl is the amplitude of the change in length. This means, *assuming that the Coulomb's law of friction is valid*, that an arbitrarily small oscillation amplitude and an arbitrarily small external force are sufficient to set the specimen into macroscopic motion: the force of static friction vanishes. Experiments show, however, that this conclusion is only valid for large enough oscillation amplitudes (see the experimental measurements of the force of static friction as a function of oscillation amplitude below).

II. The influence of vibration on kinetic friction

Next, we will investigate the influence of vibration on the force of kinetic friction. The oscillation frequency should be high enough so that the oscillations are not influenced by the steady movement of the specimen. This means that the movement of the specimen can be assumed to be the superposition of a movement with a constant velocity v_0 and an oscillating velocity.

(1) Oscillation in the sliding direction

If the specimen oscillates according to the harmonic relation

$$l = l_0 + \Delta l \sin \omega t \,, \tag{18.2}$$

then the coordinates of the contact points can be defined as

$$x_1 = v_0 t + \tfrac{1}{2} l_0 + \tfrac{1}{2} \Delta l \sin \omega t \,, \quad x_2 = v_0 t - \tfrac{1}{2} l_0 - \tfrac{1}{2} \Delta l \sin \omega t \,. \tag{18.3}$$

Their velocities relative to the base are

$$\dot{x}_1 = v_0 + \tfrac{1}{2} \Delta l \omega \cos \omega t \,, \quad \dot{x}_2 = v_0 - \tfrac{1}{2} \Delta l \omega \cos \omega t \tag{18.4}$$

or

$$\dot{x}_1 = v_0 + \hat{v} \cos \omega t \,, \quad \dot{x}_2 = v_0 - \hat{v} \cos \omega t \,, \tag{18.5}$$

with $\hat{v} = \tfrac{1}{2} \Delta l \omega$. For simplification, we assume that the normal force is evenly distributed between both contact points, each with $F_N / 2$ and it does not change with time. Under this assumption, we obtain a total frictional force acting on the specimen of

$$F_R = \frac{\mu F_N}{2} \left[\operatorname{sgn}\left(v_0 + \hat{v} \cos \omega t \right) + \operatorname{sgn}\left(v_0 - \hat{v} \cos \omega t \right) \right]. \tag{18.6}$$

We obtain the macroscopic frictional force by averaging this force over the oscillation period:

$$\left\langle F_R \right\rangle = \frac{1}{T} \int_0^T F_R(t) \mathrm{d}t = \frac{1}{2\pi} \frac{\mu F_N}{2} \int_0^{2\pi} \left[\operatorname{sgn}\left(v_0 + \hat{v} \cos \xi \right) + \operatorname{sgn}\left(v_0 - \hat{v} \cos \xi \right) \right] \mathrm{d}\xi \,. \tag{18.7}$$

By averaging over the period, the contributions of both terms in the integral are the same so that it is sufficient to integrate one of them and then multiply by 2:

$$\left\langle F_R \right\rangle = \frac{\mu F_N}{2\pi} \int_0^{2\pi} \operatorname{sgn}\left(v_0 - \hat{v} \cos \xi \right) \mathrm{d}\xi \,. \tag{18.8}$$

We consider the two cases:

(a) $v_0 > \hat{v}$. In this case, the velocity always remains positive and the frictional force is constant in both magnitude and direction. The average frictional force is, in this case, equal to $\langle F_R \rangle = \mu F_N$.

(b) $v_0 < \hat{v}$. Here, the velocity is positive in one part of the period and negative in the other (these time periods are shown in Fig. 18.2 and denoted with +1 and -1, respectively). The frictional force in the positive domain is μF_N and $-\mu F_N$ in the negative domain. The instant of the change in the sign of the velocity is determined from the condition $v_0 - \hat{v}\cos\xi^* = 0$. From this, it follows that

$$\xi^* = \arccos\left(v_0 / \hat{v}\right). \tag{18.9}$$

With help from Fig. 18.2, it is easy to see that the integral (18.8) is calculated to

$$\langle F_R \rangle = \mu \frac{F_N}{2\pi}\left(\left(2\pi - 2\xi^*\right) - 2\xi^*\right) = \mu \frac{2F_N}{\pi}\left(\frac{\pi}{2} - \xi^*\right) = \mu \frac{2F_N}{\pi}\left(\frac{\pi}{2} - \arccos\left(\frac{v_0}{\hat{v}}\right)\right)$$

or

$$\langle F_R \rangle = \begin{cases} \dfrac{2\mu F_N}{\pi} \arcsin\left(\dfrac{v_0}{\hat{v}}\right), & \text{for} \quad v_0 < \hat{v} \\ \mu F_N, & \text{for} \quad v_0 > \hat{v} \end{cases}. \tag{18.10}$$

This dependence is presented in Fig. 18.3 in comparison with experimental data.

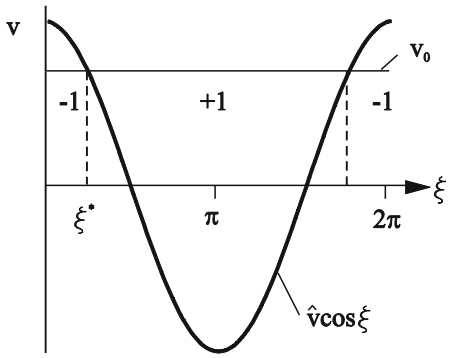

Fig. 18.2 Explanation for the calculation of the integral in (18.8).

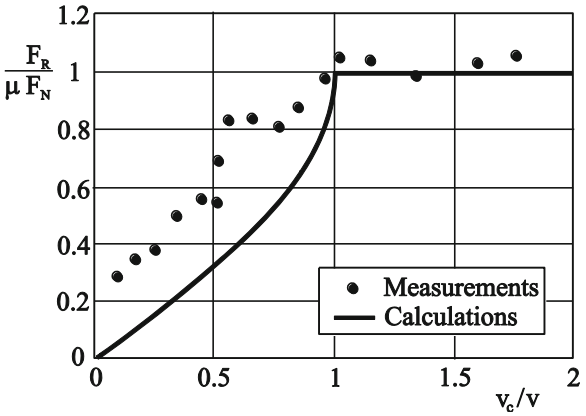

Fig. 18.3 Theoretically and experimentally obtained friction reduction using vibrations parallel to the direction of motion. Data from: Storck H., Littmann W., Wallaschek J., Mracek M.: The effect of friction reduction in presence of ultrasonic vibrations and its relevance to traveling wave ultrasonic motors. Ultrasonics, 2002, Vol. 40, p. 379-383.

(2) Vibration perpendicular to sliding direction.

In this case, the oscillation velocity

$$v_1 = \hat{v}\cos\omega t \tag{18.11}$$

is always directed perpendicular to the sliding direction (Fig. 18.4 b). The instantaneous value of the frictional force can be calculated with the help of the force diagram (Fig. 18.4 c) as

$$F_R = \mu F_N \cos\varphi\,. \tag{18.12}$$

Taking into account the relation $\tan\varphi = \hat{v}/v_0$, the frictional force is

$$F_R = \frac{\mu F_N}{\sqrt{1+\left(\frac{\hat{v}}{v_0}\cos\omega t\right)^2}}\,. \tag{18.13}$$

The macroscopic frictional force, as the average of the microscopic horizontal force, is calculated as

$$\langle F_R \rangle = \frac{\mu F_N}{2\pi}\int_0^{2\pi}\frac{\mathrm{d}\xi}{\sqrt{1+\left(\frac{\hat{v}}{v_0}\cos\xi\right)^2}}\,. \tag{18.14}$$

This dependence, together with experimental data for comparison, is presented in Fig. 18.5. Contrary to the case of vibrations parallel to the sliding direction, the

coefficient of friction always remains smaller than without ultrasonic vibrations in this case.

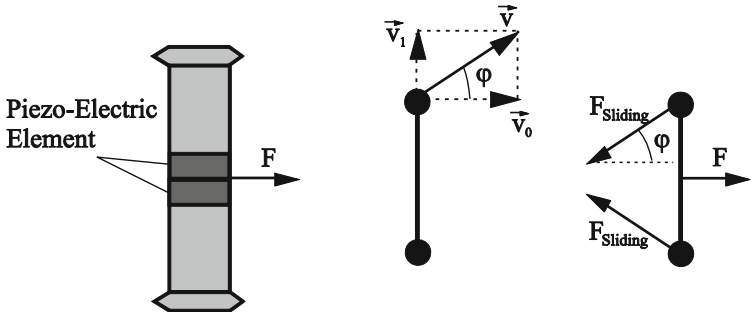

Fig. 18.4 Oscillations perpendicular to the sliding direction (top view): (a) Schematic presentation of experiments, (b) Velocity diagram, (c) Force diagram.

A significant difference between theoretical and experimental results is that the experimentally obtained coefficient of friction does not approach zero at very low sliding velocities as predicted by theory. This is a sign that the macroscopic law of friction by Coulomb is no longer valid for small oscillation amplitudes.

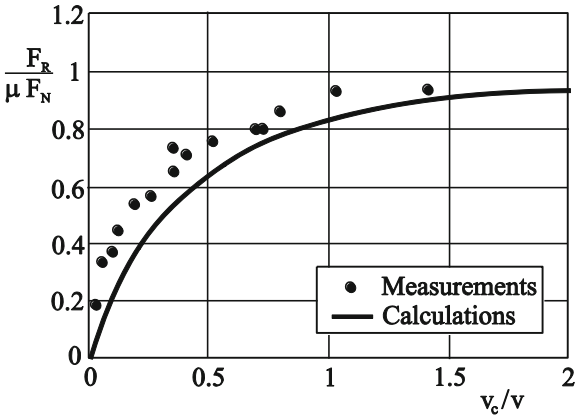

Fig. 18.5 Theoretically and experimentally obtained reduction in frictional force by vibrations perpendicular to the direction of motion. Data from: Storck H., Littmann W., Wallaschek J., Mracek M.: The effect of friction reduction in presence of ultrasonic vibrations and its relevance to traveling wave ultrasonic motors. Ultrasonics, 2002, Vol. 40, p. 379-383.

18.2 Influence of Ultrasonic Vibrations on Friction from a Microscopic Point of View

The macroscopic frictional force is nothing other than the time-averaged value of the tangential force acting between the body and the substrate. The term "macroscopic frictional force" can, therefore, only be used in relation with a specified time interval over which it is averaged. On sufficiently small spatial and time scales, the macroscopic law of friction breaks down. Therefore, it cannot be applied to the investigation of the influence of vibrations on friction for arbitrarily small oscillation amplitudes.

We illustrate the fact that the macroscopic law of friction breaks down on small scales and must be modified, with the Prandtl-Tomlinson model (Chapter 11), which we adapt to the above two-contact system. We consider two point masses with a total mass m whose distance changes according to the expression

$$l(t) = l_0 + \Delta l \sin \omega t \,. \tag{18.15}$$

Both masses are found in a periodic potential. Equation (11.1) is modified to

$$m\ddot{x} = F - \eta\dot{x} - \frac{F_0}{2}\left[\sin k\left(x - l(t)/2\right) + \sin k\left(x + l(t)/2\right)\right]. \tag{18.16}$$

Without vibrations, the force

$$F_{s,0} = F_0 \left|\cos\left(\tfrac{1}{2} k l_0\right)\right| \tag{18.17}$$

must be applied to the system in order to set it in motion. Therefore, $F_{s,0}$ has the physical sense of the force of static friction without ultrasonic vibrations.

Now, we let the length l oscillate according to (18.15) and average Equation (18.16) over the period $T = 2\pi/\omega$; we denote the average over this time with the angled parentheses:

$$m\langle\ddot{x}\rangle = F - \eta\langle\dot{x}\rangle - \frac{F_0}{2}\left\langle \sin k\left(x - l(t)/2\right) + \sin k\left(x + l(t)/2\right)\right\rangle. \tag{18.18}$$

As long as there is no macroscopic motion of the system (i.e. it is macroscopically in a static state), the average values $\langle\ddot{x}\rangle$ and $\langle\dot{x}\rangle$ are equal to zero and the force of static friction is

$$\begin{aligned} F &= \frac{F_0}{2}\left\langle \sin k\left(x_0 - \left(l_0 + \Delta l \sin(\omega t)\right)/2\right) + \sin k\left(x_0 + \left(l_0 + \Delta l \sin(\omega t)\right)/2\right)\right\rangle \\ &= F_0 \sin k x_0 \cdot \left\langle \cos k\left(l_0 + \Delta l \sin(\omega t)\right)/2\right\rangle \\ &= F_0 \sin k x_0 \cdot \left(\cos\left(\tfrac{1}{2} k l_0\right)\left\langle \cos\left(\tfrac{1}{2} k \Delta l \sin \omega t\right)\right\rangle - \sin\left(\tfrac{1}{2} k l_0\right)\left\langle \sin\left(\tfrac{1}{2} k \Delta l \sin \omega t\right)\right\rangle\right). \end{aligned} \tag{18.19}$$

The average of the second term is equal to zero (because we are averaging an odd function). The average value of the first term can be calculated with help from the expansion[1]

$$\cos\left(\zeta \sin\varphi\right) = J_0\left(\zeta\right) + 2\sum_{n=1}^{\infty} J_{2n}\left(\zeta\right)\cos\left(2n\varphi\right), \tag{18.20}$$

where J_n is a Bessel function of n[th] order. Therefore, the frictional force is

$$F = F_0 \sin kx_0 \cos\left(\tfrac{1}{2}kl_0\right) J_0\left(\tfrac{1}{2}k\Delta l\right). \tag{18.21}$$

This force is a function of the coordinate x_0. Its maximum possible value,

$$F_s = F_0 \left|\cos\left(\tfrac{1}{2}kl_0\right) J_0\left(\tfrac{1}{2}k\Delta l\right)\right| = F_{s,0}\left|J_0\left(\tfrac{1}{2}k\Delta l\right)\right|, \tag{18.22}$$

is the force of static friction. According to this, the force of static friction is dependent on the oscillation amplitude. This dependence is presented in Fig. 18.6.

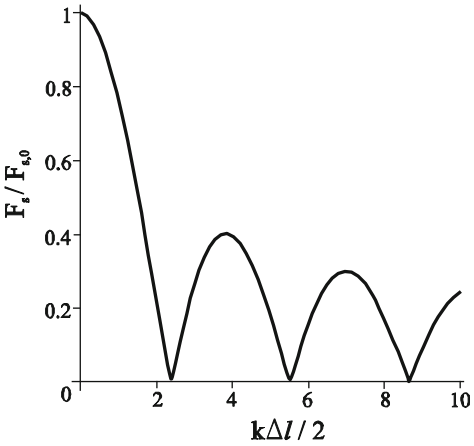

Fig. 18.6 Dependence of the force of static friction on the oscillation amplitude for a two body system in a spatially periodic potential.

The frictional force decreases with the amplitude and vanishes for $k\Delta l/2 = 2.4048$ (i.e. when $\Delta l \approx 0.77\Lambda$), where Λ is the wavelength of the potential. If the interaction potential contains several Fourier components, then the oscillations of the force of static friction become blurred and we obtain a continuously decreasing function. In this example, we can recognize the gradual transition from static friction without ultrasonic vibrations to the macroscopic result in the presence of ultrasonic vibrations ($F_s = 0$). We see that the oscillation amplitude at which we have a significant decrease in the force of static friction provides us in-

[1] O.J. Farrell, B. Ross, Solved Problems: Gamma and beta functions, Legendre Polynomials, Bessel functions. The Macmillan Company, 1963, 410 pp.

formation about the characteristic wavelength of the interaction potential. This fact is used in tribospectroscopy for the investigation of frictional mechanisms.

18.3 Experimental Investigations of the Force of Static Friction as a Function of the Oscillation Amplitude

The system shown in Fig. 18.1 was experimentally investigated and the force of static friction was measured as a function of oscillation amplitude[2]. Experiments were conducted at frequencies of about 60-70 kHz with oscillation amplitudes up to about 1 μm. The oscillation amplitude was measured with a laser vibrometer. Results are presented in Fig. 18.7 for pairings of various materials with a steel specimen.

For most pairings, the coefficient of friction decreases with the oscillation amplitude. The length at which the frictional force significantly decreases determines the characteristic spatial scale of the frictional process for the given friction pairing under the given conditions. The characteristic spatial scale for frictional processes is different for various materials. In Table 18.1, the results are summarized for 9 different investigated materials. Thereby, we distinguish between the first experiment and experiments after the system has been run in.

For most materials, the characteristic length scale after running-in is smaller than in the initial state. The exceptions are brass and glass. As can be seen in Table 18.1, the characteristic scales lie between about 10 and 100 nm for all materials investigated. For metals, it varies between 20 and 60 nm. The physical origin of this scale is not yet completely understood; possibly, it has something to do with the thickness of the boundary layer. At larger oscillation amplitudes, the specimen heats up and the boundary layer loses its effectiveness. Therefore, it is typical for the coefficient of friction to increase once again at large ultrasonic amplitudes. At even larger amplitudes, we would be dealing with strong metallic adhesion and *frictional welding*.

Rubber and aluminum exhibit a qualitatively different behavior (Fig. 18.8). With rubber, we are dealing with a case where the scale is principally not determined by interactions on the nanoscale. Aluminum is known for its differing tribological behavior compared to other metals, which is possibly due to ease with which the oxidation layer is broken through and the frictional process leaves the domain of boundary layer friction.

The coefficient of friction for teflon in Fig. 18.7 is not only small, but becomes *negative* with increasing oscillation amplitudes. This is possible when the surface

[2] A more detailed description can be found in: J. Starcevic, Tribospektroskopie als neue Methode zur Untersuchung von Reibungsmechanismen: Theoretische Grundlagen und Experiment, Dissertation, TU Berlin, 2008.

exhibits an asymmetric structure so that it forms a "ratchet[3]" and directional motion takes place even in the absence of external forces.

Investigations using tribospectroscopy show that under the conditions for boundary layer friction, the macroscopic law of friction is already applicable from oscillation amplitudes of about 100 nanometers. A rapid decrease in the coefficient of friction takes place at very small amplitudes on an order of magnitude 20-60 nanometers. Such amplitudes are sufficient to control the coefficient of friction.

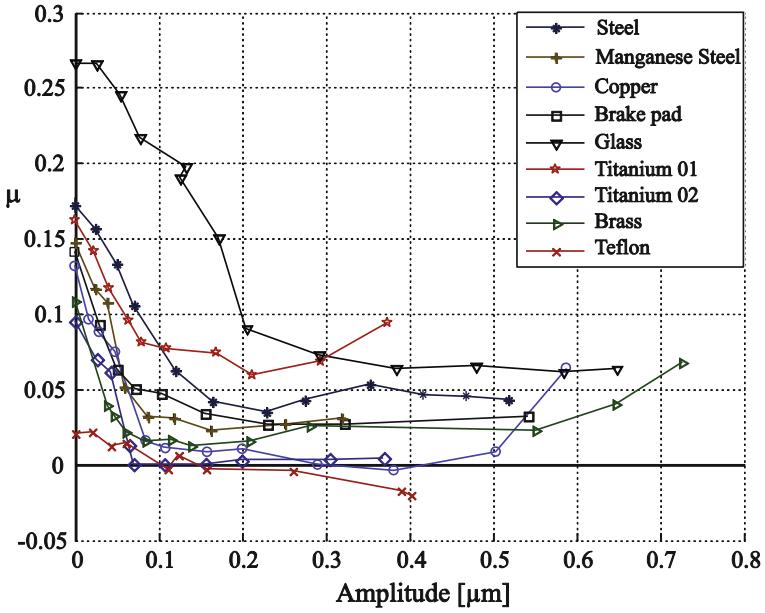

Fig. 18.7 Dependence of the coefficient of static friction on the oscillation amplitude for an array of materials on steel C45.

[3] For a more detailed commentary to ratchets, see Section 11.5.

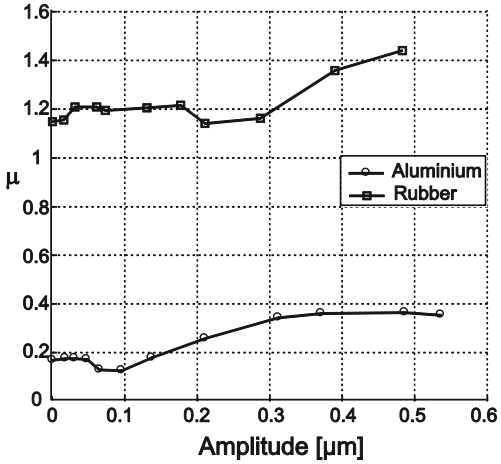

Fig. 18.8 Dependence of the coefficient of static friction on the oscillation amplitude for rubber and aluminum.

Table. 18.1 The characteristic frictional scale l_0 of various materials calculated for the first experiment and for the average of the experiments after running-in.

Material of Frictional Plate	l_0 [nm] 1st experiment	l_0 [nm] After running-in
Mild Steel C 45	61	41
Austermitic Mangenese Steel X120Mn12	39	24
Titanium TI01	34	27
Titanium TI02	25	22
Titanium TI03	50	--
Copper	42	37
Brass	17	29
Brake Pads	31	29
Glass	104	111

18.4 Experimental Investigations of Kinetic Friction as a Function of Oscillation Amplitude

For many applications of active control of frictional force, it is important to know how the force of *kinetic* friction is dependent on the oscillation amplitude. In this

section, the typical experimental results are presented that were obtained using an ultrasonic pin-on-disc tribometer[4] (schematically shown in Fig. 18.9 a).

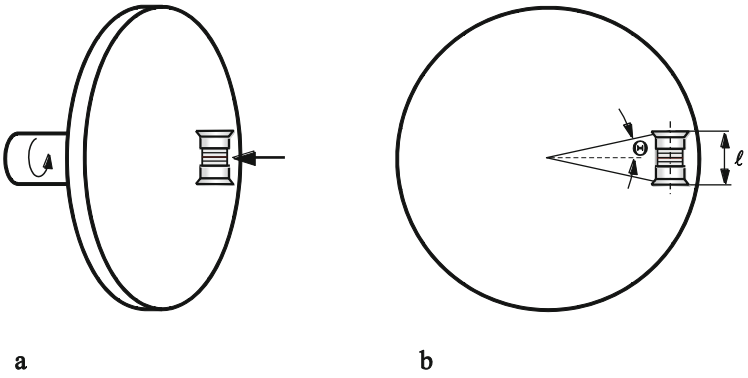

Fig. 18.9 (a) Schematic presentation of an ultrasonic pin-on-disc tribometer; (b) Geometry of sliding in an ultrasonic pin-on-disc tribometer.

The dependence of kinetic friction on the sliding velocity for various oscillation amplitudes is presented in Fig. 18.10 for a pairing of steel on steel .

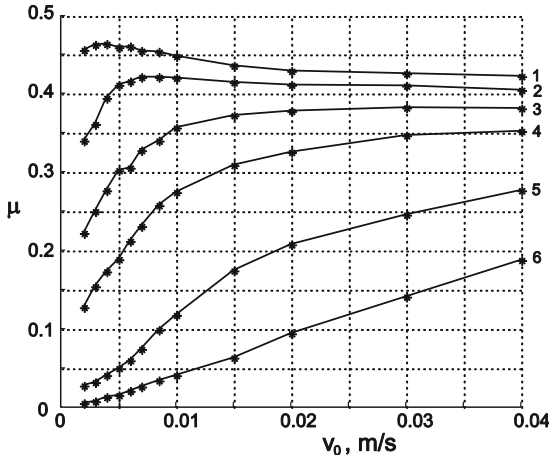

Fig. 18.10 Dependence of the coefficient of friction on the sliding velocity and the oscillation amplitude for a pairing of "steel on steel" for a frequency of 45 kHz, $\theta = 31.5°$ and the following oscillation amplitudes: (1) 0.023 μm , (2) 0.056 μm , (3) 0.095 μm , (4) 0.131 μm , (5) 0.211 μm , (6) 0.319 μm . Source: V.L. Popov, J. Starcevic, A.E. Filippov. Influence of ultrasonic in-plane oscillations on static and sliding friction and intrinsic length scale of dry friction. – Trib. Lett., 2010, v.39, pp.25-30.

[4] V.L. Popov, J. Starcevic, A.E. Filippov. Influence of ultrasonic in-plane oscillations on static and sliding friction and intrinsic length scale of dry friction. – Trib. Lett., 2010, v.39, pp.25-30.

Qualitatively similar dependences are also found for other tribological pairings. It is characteristic that the frictional force slightly decreases as velocity increases in the absence of vibration (Curve 1 in Fig. 18.10). This can lead to the development of an instability. If we excite the system using ultrasonic oscillations with an amplitude of about 0.1 μm, then the frictional force becomes a monotonically increasing function of the sliding velocity (Curve 3 in Fig. 18.10). This effect can be used to suppress frictionally induced instabilities.

Aluminum is an exception: In the pairing of steel on aluminum, the coefficient of friction is dependent on neither the sliding velocity nor the oscillation amplitude and exhibits only strong fluctuations about a constant value $\mu \approx 0.6 \pm 0.1$ (Fig. 18.11).

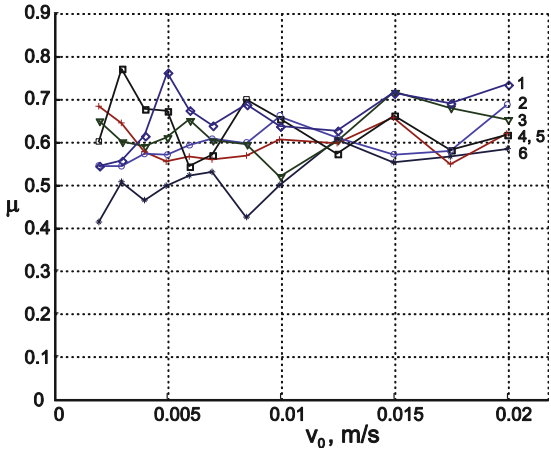

Fig. 18.11 Dependence of the coefficient of friction on a pairing of aluminum/steel for an oscillation frequency of 48 kHz and the following oscillation amplitudes: (1) 0.21 μm, (2) 0.081 μm, (3) 0.31 μm, (4) 0.14 μm, (5) 0.41 μm, (6) 0.035 μm. The coefficient of friction exhibits strong fluctuations about a value of 0.6, but shows no systematic dependence on the sliding velocity or the oscillation amplitude. Source: V.L. Popov, J. Starcevic, A.E. Filippov. Influence of ultrasonic in-plane oscillations on static and sliding friction and intrinsic length scale of dry friction. – Trib. Lett., 2010, v.39, pp.25-30.

Problems

Problem 1: Investigate the influence of oscillation of the normal force on the static and dynamic friction, in particular, the dependence of the mean frictional force on the mean sliding speed under the assumption of Coulomb's law of friction with a constant coefficient of friction μ.

Solution: We consider the simplest model of a tribological system consisting of a rigid block (mass m) in contact with a rigid plane (Fig. 18.12). The normal force is changed by the law

$$F_N(t) = F_{N,0} + \Delta F_N \cos \omega t \, .$$

If the minimum value $\mu\left(F_{N,0} - \Delta F_N\right)$ is larger than the static friction F, then the body remains at rest: the macroscopic value of static friction is, thus, equal to

$$F_s = \mu\left(F_{N,0} - \Delta F_N\right).$$

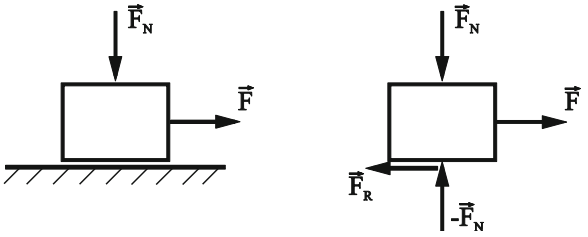

Fig. 18.12 A rigid block is pressed onto a plane with a time-dependent normal force F_N and dragged in the horizontal direction with a force F.

However, if the force F is larger than F_s, as shown in Fig. 18.13, there will be a moment in time at which the dragging force is larger than the static friction. At this moment, the body begins to move.

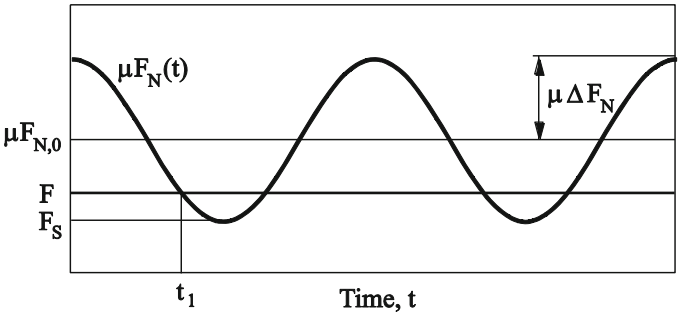

Fig. 18.13 Time-dependence of the normal force multiplied by the coefficient of friction. The minimum value of this function is the macroscopic force of static friction F_s.

The equation of motion during the sliding state is

$$m\ddot{x} = F - \mu(F_{N,0} + \Delta F_N \cos \omega t) \, .$$

It can be rewritten in the form

$$m\ddot{x} = \left[F - \mu\left(F_{N,0} - \Delta F_N\right)\right] - \mu\Delta F_N\left(1+\cos\omega t\right)$$

or after dividing by $\mu\Delta F_N$

$$\frac{m}{\mu\Delta F_N}\ddot{x} = \frac{\left[F - \mu\left(F_{N,0} - \Delta F_N\right)\right]}{\mu\Delta F_N} - \left(1+\cos\omega t\right)$$

By introducing the new variables $\tau = \omega t$ and $\xi = \frac{m\omega^2}{\mu\cdot\Delta F_N}x$, and the notations $f = \frac{\left[F - \mu\left(F_{N,0} - \Delta F_N\right)\right]}{\mu\Delta F_N}$ and $\xi'' = \partial^2\xi/\partial\tau^2$, it obtains the following dimensionless form:

$$\xi'' = f - \left(1+\cos\tau\right).$$

This equation contains a single parameter f. The body begins to move at the time τ_1 in which the equation $f - \left(1+\cos\tau\right) = 0$ is satisfied for the first time. It follows that

$$\tau_1 = \arccos\left(f-1\right).$$

Integration of the equation of motion twice with the initial conditions $\xi'(\tau_1) = 0$ and $\xi(0) = 0$ results in

$$\xi' = \left(f-1\right)\left(\tau - \tau_1\right) + \left(\sin\tau_1 - \sin\tau\right),$$

$$\xi = \frac{f-1}{2}\left(\tau^2 - 2\tau\tau_1\right) + \left(\tau\sin\tau_1 + \cos\tau\right) - 1.$$

At the time moment τ_2, the velocity will be zero again and the body comes to a halt, in which

$$\xi' = f\cdot\left(\tau_2 - \tau_1\right) - \left(\tau_2 - \tau_1\right) + \left(\sin\tau_1 - \sin\tau_2\right) = 0.$$

This moment in time differs from the time at the beginning of the movement by a full period 2π if $f = 1$: for larger values of the parameter f, the body will never come to a halt. The range of the parameter f in which we are interested is, therefore, $0 < f < 1$.

The average velocity of the body is calculated as

$$\left\langle\xi'\right\rangle = \frac{\xi(\tau_2) - \xi(\tau_1)}{2\pi} = \frac{f-1}{4\pi}\left(\tau_2 - \tau_1\right)^2 + \frac{1}{2\pi}\left(\left(\tau_2 - \tau_1\right)\sin\tau_1 + \cos\tau_2 - \cos\tau_1\right)$$

The average velocity, corresponding to the critical value $f = 1$, is

$$\langle \xi' \rangle_{crit} = \sin \tau_1 = \sqrt{1 - \cos^2 \tau_1} = \sqrt{1 - (f-1)^2} = 1 .$$

For small values of f, an analytical approximation can be found for the average velocity. It is easier to begin with the equation of motion and approximate the cosine function near the closest minimum as $\cos \tau \approx -1 + \frac{(\tau - \pi)^2}{2}$. The equation of motion is then $\xi'' = f - \frac{\hat{\tau}^2}{2}$ with $\hat{\tau} = (\tau - \pi)$. The movement starts at

$$\hat{\tau}_1 = -\sqrt{2f} .$$

The velocity and position during the sliding state are

$$\xi' = f \cdot (\hat{\tau} - \hat{\tau}_1) - \frac{\hat{\tau}^3 - \hat{\tau}_1^3}{6} ,$$

$$\xi = f \cdot \left(\frac{\hat{\tau}^2}{2} - \hat{\tau}_1 \hat{\tau} \right) - \frac{\hat{\tau}^4 - 4\hat{\tau}_1^3 \hat{\tau}}{24} .$$

The body comes to a standstill when

$$\xi'(\hat{\tau}_2) = f \cdot (\hat{\tau}_2 - \hat{\tau}_1) - \frac{\hat{\tau}_2^3 - \hat{\tau}_1^3}{6} = 0 .$$

This results in

$$\hat{\tau}_2 = -2\hat{\tau}_1 = 2\sqrt{2f} .$$

The average velocity is given by

$$\langle \xi' \rangle = \frac{\xi(\hat{\tau}_2) - \xi(\hat{\tau}_1)}{2\pi} = \frac{9f^2}{4\pi}$$

or solving for f:

$$f = \sqrt{\frac{4\pi}{9} \langle \xi' \rangle} .$$

Comparison with the numerical solution of the equation of motion shows that the exact solution in the entirety of the range of velocity in which we are interested $0 < \langle \xi' \rangle < 1$ can be very well approximated by the following equation:

$$f = \sqrt{\frac{4\pi}{9}\langle \xi' \rangle} + \left(1 - \sqrt{\frac{4\pi}{9}}\right)\langle \xi' \rangle^{1,2}.$$

With the original variables, it is

$$F = \mu\left(F_{N,0} - \Delta F_N\right) + \mu\Delta F_N \left[\sqrt{\frac{4\pi}{9}\frac{m\omega}{\mu\Delta F_N}\langle \dot{x} \rangle} + \left(1 - \sqrt{\frac{4\pi}{9}}\right)\left(\frac{m\omega}{\mu\Delta F_N}\langle \dot{x} \rangle\right)^{1,2}\right].$$

The domain of this function with dimensional variables is:

$$0 < \langle \dot{x} \rangle < \frac{\mu\Delta F_N}{m\omega};$$

At larger velocities, the frictional force remains constant and equals $F = \mu F_{N,0}$. The dependence of the frictional force on the sliding velocity for $\Delta F_N = F_N / 2$ is exemplarily shown in Fig. 18.14.

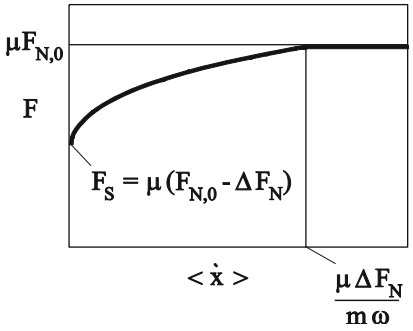

Fig. 18.14 Dependence of the mean frictional force of the mean sliding speed under oscillating normal force.

Note that the assumption of a constant horizontal force used in this problem corresponds to the case of a very soft measuring system: the system stiffness is considered here as equal to zero while the contact stiffness as infinitely large (a rigid body). The contrary case of a very stiff system and finite contact stiffness is cosidered in[5] and the general case of arbitrary relation of system and contact stiffness in[6].

Problem 2: A sample with variable length has two contact areas with the substrate, which are simply modeled as Hertzian contacts (Fig. 18.5). The length of

[5] M. Popov, V. L. Popov, N. V. Popov, Reduction of friction by normal oscillations. I. Influence of contact stiffness. - Friction, 2016, submitted.

[6] X. Mao, V.L. Popov J. Starcevic, M. Popov, Reduction of friction by normal oscillations. II. In-plane system dynamics. - Friction, 2016, submitted.

the sample oscillates according to the law $l(t) = l_0 + \Delta l \cdot \cos(\omega t)$. Determine the dependence of the macroscopically observable static friction coefficient on the oscillation amplitude under the assumption of a constant local coefficient of friction in the contact area.

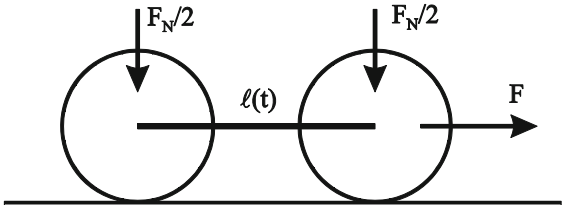

Fig. 18.15 Schematic representation of a sample with variable length. The contact points between the sample and the substrate are modeled as Hertzian contacts.

Solution: In the absence of external force F, the oscillation is symmetric and the maximum displacement of each body from the reference state is the same $\Delta l/2$. The relationship between the tangential force F_x and the tangential displacement u_x is determined by the equation (see Chapter 8)

$$F_x = \mu F_N \left(1 - \left(1 - \frac{u_x}{\mu\left(E^*/G^*\right)d}\right)^{3/2}\right) = \mu F_N \left(1 - \left(1 - \frac{\Delta l}{2\mu\left(E^*/G^*\right)d}\right)^{3/2}\right).$$

The difference between this force and the critical force μF_N is the macroscopically observable static friction force F_{static}:

$$F_{\text{static}} = \mu F_N \left(1 - \frac{\Delta l}{2\mu\left(E^*/G^*\right)d}\right)^{3/2}.$$

19 Numerical Simulation Methods in Friction Physics

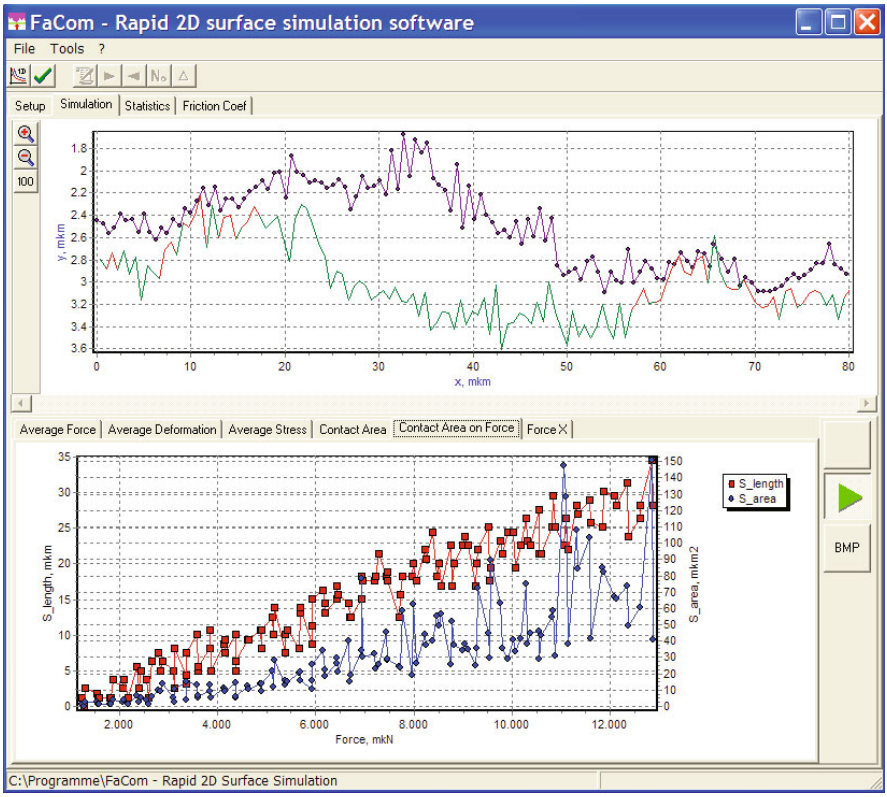

The contact and friction problems investigated in the previous chapters are based on simple model systems. Even when these models provide a general overview of complex tribological systems, a multitude of tribological problems, especially when they deal with the fine optimization of tribological systems, are not able to be calculated in analytical form. In these cases, researchers and engineers must fall back on numerical methods. At the same time, one must remember that the efficiency of numerical methods is dependent largely on the quality of the preceding analytical preparations.

In this chapter, we first present a short overview of the most important methods used in contact mechanics, describing them not in detail, but rather referring to existing literature.

V.L. Popov, *Contact Mechanics and Friction*,
DOI 10.1007/978-3-662-53081-8_19

19.1 Many-Body Systems

Computer simulations of many-body systems are indispensable for today's industrial development processes. With increasing demand on accuracy, the interest in reproducing contact and frictional phenomena as precise as possible is also increasing. A considerable part of research in this field is concentrated on finding methods for the implementation of simple contact conditions and Coulomb's law of friction. At the forefront, is the search for the most efficient algorithms possible (in terms of calculation time and implementation costs). Contact is typically seen as one-sided rigid constraint. For the laws of friction, there is assumed that there exists a maximum force of static friction and that the force of kinetic friction depends on sliding velocity. Frequently, the force of kinetic friction is assumed to be constant and equal to the maximum force of static friction.

The simplest method for integrating friction into many-body system programs is to approximate the law of friction using a continuous function of frictional force. The frictional force in treated as a given force for which the dependence on sliding velocity is known. Typically, a force in the following form is used (Fig. 19.1):

$$F_R = \frac{2}{\pi} \mu F_N \arctan\left(v / \hat{v}\right). \tag{19.1}$$

By using this form, one does not need to differentiate between static friction and kinetic friction. The characteristic velocity $\hat{v}$ must be chosen so that it is significantly smaller than the characteristic sliding velocity of the system to be simulated. In this case, the relation (19.1) expresses the behavior of the forces in both the stick and sliding domains[1].

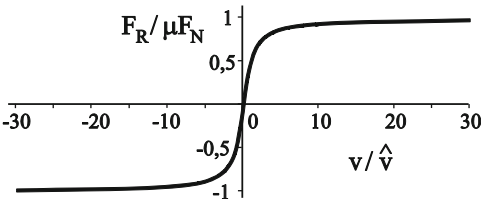

Fig. 19.1 Approximation of the law of friction by a continuous function of velocity.

[1] In this case, "sticking" is simply sliding at a very low velocity; the frictional force sets itself "automatically" equal to the correct force of static friction between $-\mu F_N$ and $+\mu F_N$. For many tribological applications, this "trick" corresponds even to the actual properties of the frictional force.

19.2 Finite Element Method

For many applications, the pressure distribution and the deformation of the contact interface are important. There are various simulation methods available for calculating elastic and plastic deformations, which give a principal possibility, to investigate adhesive contacts and frictional phenomena. Procedures based on discretizing the continuum equations are widely known, especially finite element methods (FEM) and boundary element methods.

Contact formulations in the framework of FEM were developed in the 1970's. Today, commercial FE-programs use the so-called *node-to-surface formulation*, which considers the nodes of the surface in relation to the elements of the other surface.

In many practical applications (seals, metal-forming processes, penetration tests), large deformations, non-linear behavior of materials, and large relative motion between the participating contact partners occur. In these cases, contact problems can be considerably more robustly and accurately simulated with *surface-to-surface formulation* (Mortar method)[2].

Rolling contact problems (wheel-rail, tire-street) are, likewise, investigated with the FE method. The *Arbitrary Lagrangian Eulerian* (ALE) method[3] is an effective method for calculating such contact problems. The spatially stationary discretization allows the resolution of the mesh for the contact areas to be refined. This is especially elegant in solving problems of steady state rolling, because the solution is time-independent in this case. However, taking inelastic material behaviors into account is difficult, because the mesh is not bound to the points of the material.

Advantages of a 3D-FE model are (1) the utilization of correct geometry (dimensions, surface topography, degrees of freedom) and (2) the ability to calculate stresses and deformations in the entire body. Due to the very fine mesh, however, 3D-FE models require high processing times for rough surfaces. This is an especially clear disadvantage when regarding extensive parameter studies and optimizations.

19.3 Boundary Element Method

The boundary element method is especially suited for calculating contacts, because only the discretization of the surface is necessary. Therefore, it is not neces-

---

[2] M.A. Puso und T. A. Laursen, A mortar segment-to-segment contact method for large deformation solid mechanics. Computer Methods in Applied Mechanics and Engineering, 2004, v. 193, pp. 601-629.

[3] U. Nackenhorst, The ALE-formulation of bodies in rolling contact: theoretical foundations and finite element approach. Computer Methods in Applied Mechanics and Engineering, 2004, v. 193, pp. 4299-4322.

sary to generate lattice points and include them in the calculation within the body. Because of the importance of this method for contact mechanics, we discuss it in some detail.

We consider the normal contact problem between an elastic half-space and a rigid body. The vertical displacement of a point on the surface of an elastic body being acted upon by a continuous pressure distribution is given by (5.7). We divide the parts of the domain to be investigated into $N \times N$ elements and assume the pressure $p_{\tilde{i}\tilde{j}}$ is constant in every individual square element. The vertical displacement at the center of element is notated as $u_{ij}^{(z)}$. The relationship between the pressure p_{ij} in a quadratic surface element and the vertical surface displacement $u_{ij}^{(z)}$ can be analytically calculated:[4]

$$u_{ij}^{(z)} = \sum_{\hat{i}=1}^{N} \sum_{\hat{j}=1}^{N} K_{ij\tilde{i}\tilde{j}}^{(z)} p_{\tilde{i}\tilde{j}} \,, \tag{19.2}$$

with

$$K_{ij\tilde{i}\tilde{j}}^{(z)} = \frac{\Delta}{\pi E^*} \left[a \ln \left(\frac{c + \sqrt{a^2 + c^2}}{d + \sqrt{a^2 + d^2}} \right) + b \ln \left(\frac{d + \sqrt{b^2 + d^2}}{c + \sqrt{b^2 + c^2}} \right) + c \ln \left(\frac{a + \sqrt{a^2 + c^2}}{b + \sqrt{c^2 + b^2}} \right) + d \ln \left(\frac{b + \sqrt{b^2 + d^2}}{a + \sqrt{a^2 + d^2}} \right) \right] \tag{19.3}$$

and

$$a = i - \hat{i} + \frac{1}{2} \,, \quad b = i - \hat{i} - \frac{1}{2} \,, \quad c = j - \hat{j} + \frac{1}{2} \,, \quad d = j - \hat{j} - \frac{1}{2} \tag{19.4}$$

Δ is the mesh spacing. Equation (19.2) can be written in matrix form as

$$\mathbf{u} = \mathbf{A}\mathbf{p} \,, \tag{19.5}$$

with a matrix $\mathbf{A}$ with dimensions $N^2 \times N^2$.

In contact problems, the size and location of the contact area is initially unknown. Therefore, contact problems must be solved iteratively. In the contact area, the separation between the surfaces is zero (i.e. in this area, the displacement

[4] A.E.H. Love, A Treatise on the Mathematical Theory of Elasticity. 4th edition., Cambridge, University Press. See also: K. L. Johnson, Contact mechanics. Cambridge University Press, 6th printing of the 1st edition, 2001, p. 54.

of the elastic surface is known). Outside of the contact area, the pressure is zero; the displacement, on the other hand, is generally not zero. To begin, a contact area is assumed. The variables are now partitioned into the variables $\mathbf{p}_i$ and $\mathbf{u}_i^{(z)}$ inside of the contact area and $\mathbf{p}_a$ and $\mathbf{u}_a^{(z)}$ outside of the contact area. $\mathbf{u}_i^{(z)}$ and $\mathbf{p}_a = 0$ are known. After rearranging according to (19.5), we obtain

$$\begin{bmatrix} \mathbf{A_1} & \mathbf{A_2} \\ \mathbf{A_3} & \mathbf{A_4} \end{bmatrix} \begin{Bmatrix} \mathbf{p_i} \\ \mathbf{0} \end{Bmatrix} = \begin{Bmatrix} \mathbf{u_i^{(z)}} \\ \mathbf{u_a^{(z)}} \end{Bmatrix} \tag{19.6}$$

and finally,

$$\mathbf{A_1 p_i} = \mathbf{u_i^{(z)}}, \tag{19.7}$$

$$\mathbf{A_3 p_i} = \mathbf{u_a^{(z)}}. \tag{19.8}$$

The solution to the system of equations in (19.7) yields a pressure $\mathbf{p_i}$ in the contact area. With these results, using (19.8), the displacement $\mathbf{u_a^{(z)}}$ in the domain outside of the contact can be calculated.

The first iteration step generally yields a negative pressure (tensile stress) in the contact area and a negative separation distance outside of the contact area. The new contact area is now chosen so that all of the points in tensile stress are removed from the contact area and all of the points with a negative separation difference are brought into it. With this new approximation of the contact area, the previously described calculation is repeated. The iteration continues until no more tensile stresses or negative separation distances exist (to a reasonable approximation).

19.4 Boundary Element Method: Tangential Contact

The tangential contact can be simulated using the boundary element method in almost the same way as the normal contact. Instead of (5.7) the relation of Cerruti (8.3) for a tangential contact should be used:

$$\begin{aligned} u^{(x)} &= \frac{1}{2\pi G} \int\int \left[\frac{1-\nu}{s} + \nu \frac{(x-x')^2}{s^3} \right] \tau(x', y') \, \mathrm{d}x' \mathrm{d}y' \\ s &= \sqrt{(x-x')^2 + (y-y')^2} \end{aligned} \tag{19.9}$$

In a discrete form, the tangential displacements are determined with an equation similar to (19.2) with

$$K_{ij\tilde{j}}^{(x)} = \frac{\Delta}{2\pi G}\left[(1-\nu)\left(a\cdot\ln\frac{c+\sqrt{a^2+c^2}}{d+\sqrt{a^2+d^2}} + b\cdot\ln\frac{d+\sqrt{b^2+d^2}}{c+\sqrt{b^2+c^2}}\right)\right. \\ \left. + \left(c\cdot\ln\frac{a+\sqrt{a^2+c^2}}{b+\sqrt{b^2+c^2}} + d\cdot\ln\frac{b+\sqrt{b^2+d^2}}{a+\sqrt{a^2+d^2}}\right)\right] . \quad (19.10)$$

Again, the equation for displacements can be represented in matrix-vector form similar to (19.5). If stick region (index "s" from “static”) and slip region (index "g" from “gliding”) should be differentiated from each other, the grid points must be partitioned. We assume that the corresponding normal contact problem has been solved and a fixed macroscopic tangential displacement $u_{\text{macro}}^{(x)}$ is given. For points in the slip region, the equation $\boldsymbol{\tau}_g = \mu \mathbf{p}_g$ is valid for tangential stress and the displacement is unknown. For the points where the surfaces stick, $u_{s,ij}^{(x)} = u_{\text{macro}}^{(x)}$ and tangential stress must satisfy the condition $\boldsymbol{\tau}_s < \mu \mathbf{p}_s$. Analogously to (19.6) we can write the following

$$\begin{bmatrix} \mathbf{A}_{11} & \mathbf{A}_{12} & \mathbf{A}_{13} \\ \mathbf{A}_{21} & \mathbf{A}_{22} & \mathbf{A}_{23} \\ \mathbf{A}_{31} & \mathbf{A}_{32} & \mathbf{A}_{33} \end{bmatrix} \begin{Bmatrix} \mu \mathbf{p}_g \\ \boldsymbol{\tau}_s \\ \mathbf{0} \end{Bmatrix} = \begin{Bmatrix} \mathbf{u}_g^{(x)} \\ \mathbf{u}_{\text{macro}}^{(x)} \\ \mathbf{u}_a^{(x)} \end{Bmatrix} . \quad (19.11)$$

Tangential stress $\boldsymbol{\tau}_g$ in the slip region is known and equal to $\boldsymbol{\tau}_g = \mu \mathbf{p}_g$ and the stress $\boldsymbol{\tau}_s$ in the stick region is calculated by solving equation $\mathbf{A}_{22}\boldsymbol{\tau}_s = \mathbf{u}_{\text{macro}}^{(x)} - \mu \mathbf{A}_{21}\mathbf{p}_g$. After this step, the displacement in the slip region $\mathbf{u}_g^{(x)}$ and outside the contact area $\mathbf{u}_a^{(x)}$ can be determined.

For all calculations (19.5) must be always multiplied or solved. In fact, the simulation speed and success depend critically on how this is achieved. Due to the convenient properties of $\mathbf{A}$ that are related to the underlying equations (5.9) or (8.3), the matrix-vector multiplication can be realized quickly using the fast Fourier transformation (FFT). Based on this, an iterative method, such as the conjugate gradient (CG), is used for the solution of the system of equations[5].

19.5 Boundary Element Method: Adhesive Contact

Under the assumption of a very small range of the adhesive forces, the adhesive contact can be described in the framework of the boundary element method as fol-

[5] R. Pohrt and Q. Li, Complete Boundary Element Formulation for Normal and Tangential Contact Problems, Physical Mesomechanics, 2014, v. 17, N.4, pp. 334-340.

lows[6]. We consider again an area which is divided into square elements with length Δ, each having a constant normal stress. During pulling up of the adhesive contact, these elements will bear not only compressive stresses but also some tensile stress. In order to determine the detachment condition of a boundary element, we use the principle of virtual work, which states that an element is located in the state of indifferent equilibrium if its energy does not change for a small change in the system configuration. Application to an adhesive contact means that the adhesive energy $U_{adh} = \Delta^2 \gamma_{12}$ for the separation of surfaces (the separation energy per unit area) is equal to the elastic energy which is released by the detachment of an element. This elastic energy is equal

$$U_{el} = \frac{1}{2} \int\int \sigma u \mathrm{d}A \,, \tag{19.12}$$

where u is the surface displacement associated with the stress σ. According to Boussinesq it is

$$u(x,y) = \frac{1}{\pi E^*} \int\int \frac{\sigma(\tilde{x},\tilde{y})}{\sqrt{(x-\tilde{x})^2 + (y-\tilde{y})^2}} \mathrm{d}\tilde{x}\mathrm{d}\tilde{y} \,, \tag{19.13}$$

In this case, we obtain the following expression for the energy of a single element:

$$U_{el}(\tau) = \frac{\sigma^2}{2\pi E^*} \int_0^{\Delta}\int_0^{\Delta}\int_0^{\Delta}\int_0^{\Delta} \frac{1}{\sqrt{(x-\tilde{x})^2 + (y-\tilde{y})^2}} \mathrm{d}\tilde{x}\mathrm{d}\tilde{y}\mathrm{d}x\mathrm{d}y = \frac{\sigma^2}{\pi E^*} \chi \tag{19.14}$$

with

$$\chi = \Delta^3 \frac{2}{3\pi} \left(1 - \sqrt{2} + \frac{3}{2} \log\left(\frac{\sqrt{2}+1}{\sqrt{2}-1} \right) \right) \approx 0.473201 \, \Delta^3 \,. \tag{19.15}$$

From the condition $U_{el} = U_{adh}$, the critical stress σ_c which is necessary for detachment of an element follows:

$$\sigma_c = -\sqrt{\frac{\pi E^* \gamma_{12}}{0.473201 \cdot \Delta}} \,. \tag{19.16}$$

In contrast to the non-adhesive contact, it must now be checked in each iteration that the tensile stress in any element on the edge of the contact exceeds the critical stress (19.16). Calculations of examples with the known analytical solutions (see Chapter 6) have shown that the method describes all these contact problems very accurately.

---

[6] R. Pohrt, V.L. Popov, Adhesive contact simulation of elastic solids using local mesh-dependent detachment criterion in boundary element method. – Facta Universitaties, series: Mechanical Engineering, 2015, v. 13, N. 1, pp. 3-10.

19.6 Particle Methods

Another approach to the simulation of contact and frictional problems is provided by particle methods, for which discrete particles are the focus of the calculations. These particles are not real (physical) objects, rather purely "units for calculation." The interactions between the particles must be chosen so that the elastic and plastic behavior of the material is correctly described. Thus, neither the macroscopic continuum equations nor the microscopic equations of molecular dynamics are solved, rather the microscopic equations of a suitable substitution system. The size of the particles can be adjusted to fit the problem. For example, for the investigation of earthquakes, the particle size can be on the order of meters.

The frictional force is determined by processes such as elastic and plastic deformation, fracture, and the dislodgement and reintegration of particles. These processes take place in micro-contacts. The *movable cellular automata* (MCA) method is a particle method with which the processes in micro-contacts are successfully simulated[7].

19.7 Method of Dimensionality Reduction

The method of dimensionality reduction (MDR) provides a further possibility for effective numerical calculation in contact mechanics. It has been discussed at several positions and illustrated with examples in this book. A detailed description of this method can be found in the book[8]. In this method, the original three-dimensional problem is represented by a contact with a series of independent elements (springs or generalized rheological elements). It is important to underline that this is not an approximation but an exact mapping. The method of dimensionality reduction simplifies contact problems in two ways: on the one hand, a system in which the degrees of freedom fill a three-dimensional space is replaced by a system in which the degrees of freedom fill only a one-dimensional space. On the other hand, the degrees of freedom after the MDR transformation are independent. These two features allow a massive reduction of the computation time (for typical problems in contact mechanics, depending on the exact problem, it is faster by 10^3 to 10^6 compared with optimized finite element or boundary element programs). This allows integrating the calculation of contact forces in simulations of system dynamics.

---

[7] V.L. Popov, S.G. Psakhie, Numerical simulation methods in tribology. Tribology International, 2007, v. 40(6), pp. 916-923.

[8] V.L. Popov, M. Heß, Method of Dimensionality Reduction in Contact Mechanics and Friction. Springer, 2015.

20 Earthquakes and Friction

Tectonic plate dynamics can also be seen as a part of tribology. The Earth's crust is composed of tectonic plates which slowly move relative to one another due to convection in the mantel. On a time scale of millions of years, these movements determine the structure of the Earth's surface. On a small time scale, they are responsible for earthquakes. Frictional models have applications for describing the dynamics of individual faults as well as describing the Earth's crust as a granular medium. Models for mechanisms of earthquakes are based on the fundamental observation that earthquakes do not arise as a result of a sudden formation and propagation of a new crack in the Earth's crust, rather they take place as a result of a sudden sliding along an already existing faults. In addition to other evidence, this is confirmed by the fact that the decrease in stress resulting from an earthquake (a few MPa) is much smaller than the strength of rock. Therefore, earthquakes are more a phenomenon of frictional physics than of fracture mechanics. Since the work of Brace und Byerlee[1], at the latest, earthquakes were understood to be a type of stick-slip instability[2].

[1] W.F. Brace and J.D. Byerlee, Stick slip as a mechanism for earthquakes. Science, 1966, v. 153, pp. 990-992.

[2] This is valid only for earthquakes initiating in the upper part of the Earth's crust.

V.L. Popov, *Contact Mechanics and Friction*,
DOI 10.1007/978-3-662-53081-8_20

20.1 Introduction

Due to the slow movement of tectonic plates, stresses build up in friction areas in the faults, which lead to quick, jerky movements when some critical value is exceeded. We perceive these movements as earthquakes. Similar instabilities appear even in the simplest of tribological laboratory systems, for example, a body that is slowly pulled by means of a soft spring. A few general properties of earthquakes can already be illustrated by mean of such a simple model. In the simplest model of a stick-slip instability (Problem 1 in Chapter 12), it was assumed that sliding begins when the ratio of the shear stress to the normal stress in the contact area exceeds the coefficient of static friction μ_s. If the body is put into motion, then the coefficient of friction falls to a smaller value μ_k, which leads to a stick-slip type of frictional instability. In Chapter 12 (Problem 1), we saw that the displacement u during the stick-slip phase is given by

$$u = 2\frac{F_s - F_k}{c}, \tag{20.1}$$

where c is the spring stiffness, $F_s = \mu_s F_N$ is the static friction force, $F_k = \mu_k F_N$ is the kinetic friction force and F_N the normal force. The energy dissipated during the slip phase is equal to

$$E = F_k u = 2\frac{F_k\left(F_s - F_k\right)}{c}. \tag{20.2}$$

In a real fault, we have no individual masses and no discrete spring elements. Instead, the equations of elasticity theory must be solved taking into account the law of friction. Here, we limit ourselves to a simple estimation. We assume that a contact area has a linear dimension L smaller than the thickness D of the brittle part of the Earth's crust (schizosphere)[3]. A correlated movement in this contact area leads to significant displacements and deformations in a volume with dimensions $L\times L\times L$. The stiffness of a cube with such dimensions is on the order of magnitude $c \approx G\cdot L$. From Equations (20.1) and (20.2), the following estimations for the displacement during a slip event and the dissipated energy result:

$$u \approx 2F_N\frac{\mu_s - \mu_k}{GL} \approx \frac{2\sigma_N L}{G}\left(\mu_s - \mu_k\right), \tag{20.3}$$

$$E \approx \mu_k F_N u \approx 2\sigma_N^2\frac{\mu_k\left(\mu_s - \mu_k\right)}{G}L^3, \tag{20.4}$$

where $\sigma_N = F_N / L^2$ is the normal stress.

[3] We call such earthquakes "weak earthquakes."

For a strong earthquake (with a sliding length larger than the thickness D of the schizosphere), the stiffness in the rupture zone with the length L can be estimated as $c \approx GD$. The displacement during a slip event can be estimated identically and the dissipated energy as

$$E \approx \sigma_N^2 \frac{\mu_k \left(\mu_s - \mu_k\right)}{G} DL^2 . \tag{20.5}$$

Therefore, the dissipated energy is proportional to the sliding length cubed for weak earthquakes and to the sliding length squared for strong earthquakes.

The duration of an earthquake can be estimated in this model as

$$T \approx \frac{4L}{c_{sound}}, \tag{20.6}$$

where c_{sound} is the velocity of the shear waves in the Earth's crust. For large earthquakes with $L \approx 100$ km, it is about a minute.

20.2 Quantification of Earthquakes

The *seismic moment*, M, is used as a measurement for the strength of an earthquake:

$$M = GAu , \tag{20.7}$$

where G is the shear modulus of rock (typically on the order 30 GPa), A is the area of the fracture, and u is the average displacement along the fracture surface. The seismic moment is the foundation of the *moment magnitude scale*. The moment magnitude M_w is defined as

$$M_w = \frac{2}{3}\left(\log_{10} M - 9.1\right) . \tag{20.8}$$

In the simple frictional model described above, we obtain the following estimations for the seismic moment:

$$M \approx 2\sigma_N \left(\mu_s - \mu_k\right) L^3, \text{ for weak earthquakes } (L < D) \tag{20.9}$$

$$M \approx 2\sigma_N \left(\mu_s - \mu_k\right) DL^2, \text{ for strong earthquakes } (L > D) \tag{20.10}$$

The seismic moment is, therefore, proportional to the normal stress in the fault, as well as proportional to the length of the sliding zone cubed for weak earthquakes and the length of the sliding zone squared for strong earthquakes.

20.2.1 Gutenberg-Richter Law

We consider a frictional contact between two elastic bodies with the apparent contact area $\tilde{A}$. The bodies are displaced relative to one another in the tangential direction by the length $\tilde{L}$, which should be much larger than the slip length u (20.3) during an instability event. If only earthquakes with the characteristic length L of the sliding zone were possible, then there would be a number $\tilde{A}/L^2$ of sliding domains in the contact area. According to this, a number of earthquakes,

$$N \approx \frac{\tilde{A}}{L^2}\frac{\tilde{L}}{u} \approx \frac{G\tilde{A}\tilde{L}}{2\sigma_N\left(\mu_s - \mu_k\right)L^3}, \tag{20.11}$$

must take place over the entire length $\tilde{L}$. Thus, the frequency of an earthquake with a given order of magnitude of the slip length is inversely proportional to the slip length cubed or, according to (20.9), inversely proportional to the seismic moment of the earthquake:

$$N \propto M^{-1}. \tag{20.12}$$

Since the system has no characteristic length in reality, one can assume that displacements of different lengths L can take place with the same probability. In this case, (20.12) is also valid for the distribution of earthquakes. Then, using the denotation $\phi(M)$ for the probability density of an earthquake, we can also write the estimation (20.12) in the form

$$N \propto \phi(M)\cdot M \propto M^{-1}. \tag{20.13}$$

From this, it follows that

$$\phi(M) \propto M^{-2}. \tag{20.14}$$

The probability $\Phi(M)$ of an earthquake with the seismic moment larger than M is equal to

$$\Phi(M) = \int_M^\infty \phi(M)\mathrm{d}M \propto \int_M^\infty M^{-2}\mathrm{d}M = M^{-1}. \tag{20.15}$$

This law was proposed in 1954 by Gutenberg and Richter based on empirical investigations and is called the *Gutenberg-Richter law*[4].

The scaling given by the Gutenberg-Richter law is valid for both weak and strong earthquakes. Fig. 1 illustrates the Gutenberg-Richter law using data taken from an earthquake catalog in California 1984-2000.

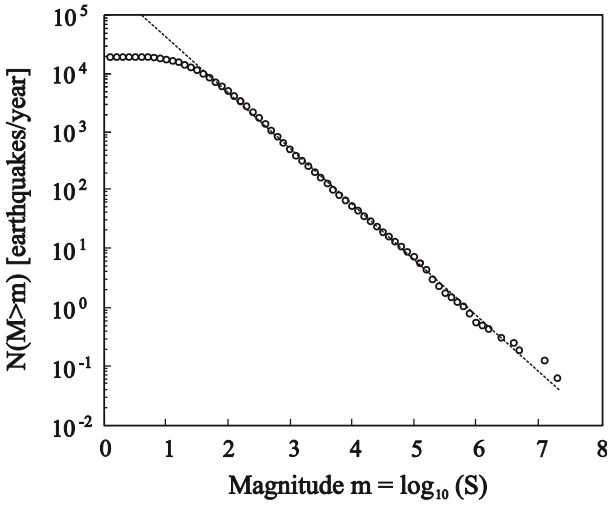

Fig. 20.1 The number of earthquakes $N(M > m)$ with a magnitude larger than m per year (circles). The line represents the Gutenberg-Richter law, $\log_{10} N(M > m) \propto -bm$, with $b = 0.95$. Data taken from an earthquake catalog in California 1984-2000 (335076 earthquakes, around 150 earthquakes/day). Source: P. Bak et.al. Phys. Rev. Lett. (2002), v.88, No. 17, 178501 (4 pp).

20.3 Laws of Friction for Rocks

The assumed law of friction (Fig. 12.11) in the estimation (20.1) is overly simplified. After the work of Brace and Byerlee, the laws of friction for rocks were intensively investigated, which led to a significant change in the "standard model" of dry friction. In particular, the differentiation between "static friction" and "kinetic friction" proved to be relative and was replaced with the concept of rate- and state-dependent friction[5]. The new concept for the generalized law of friction has

[4] B. Gutenberg and C.F. Richter, Seismicity of the Earth and Associated Phenomena. 2nd ed., Princeton, N.J.: Princeton University Press, 1954, pages 17-19 ("Frequency and energy of earthquakes").

[5] We have already discussed a simple example model for state-dependent friction in Section 12.6 in connection with the investigation of frictionally induced vibrations.

turned out to be very successful at describing such aspects as seismogenesis, seismic coupling, pre- and post-sliding, as well as the insensitivity to relatively high frequency stress oscillations (such as Earth tides). Therefore, we will extensively discuss the laws of friction for rock in the following.

Coulomb already knew that the coefficient of static friction increases slowly with time and that the coefficient of kinetic friction is velocity dependent. Experimental investigations by Dieterich[6], which were summarized in the theory of Ruina[7] to a rate- and a state-dependent law of friction, have shown that there is a close relation between these effects. In the law of friction from Dieterich-Ruina, the coefficient of friction is dependent on the instantaneous velocity v as well as the state variable θ:

$$\mu = \mu_0 - a \ln\left(\frac{v^*}{|v|} + 1\right) + b \ln\left(\frac{v^* \theta}{D_c} + 1\right) \tag{20.16}$$

where the following kinetic equation is valid for the state variable:

$$\dot{\theta} = 1 - \left(\frac{|v|\theta}{D_c}\right). \tag{20.17}$$

The constants a and b in Equation (20.16) are both positive and have an order of magnitude from 10^{-2} to 10^{-3}, D_c has an order of magnitude of 10 μm in laboratory conditions, its scaling for larger systems has not yet been clarified; typical values of v^* are on the order of 0.2 m/s. This law of friction proves to be very general and is applicable not only to rock, but also materials of various natures such as polymers, glass, paper, wood, and some metals.

In the static case, $\theta = t$ is valid. The state variable θ can, therefore, be interpreted as the average age of the micro-contacts beginning from the moment they were formed. In the case of motion at a constant velocity v and the initial condition $\theta(0) = \theta_0$, the solution to Equation (20.17) is

$$\theta(t) = \frac{D_c}{|v|} + \left(\theta_0 - \frac{D_c}{|v|}\right) \exp\left(-\frac{|v|t}{D_c}\right). \tag{20.18}$$

The state variable θ relaxes to its new equilibrium value at the sliding length D_c. According to this, the value D_c can be interpreted as the critical sliding length along which all of the existing micro-contacts are destroyed and replaced by new

---

[6] J.H. Dieterich, Modelling of rock friction: 1. Experimental results and constitutive equations. 1979, J. Geophys. Res., v. 84, pp. 2161-2168.

[7] A.I. Ruina, Slip instability and state variable friction laws. J. Geophys. Res., 1983, v. 88, 10359-10370.

ones. After the transition process $\theta(\infty) = \frac{D_c}{v}$ is valid, which is also compatible with the interpretation of the state variable θ as an age variable: in this case, the stationary value of θ is equal to the average contact time of the micro-contacts.

For steady sliding, the coefficient of friction is

$$\mu = \mu_0 - (a-b)\ln\left(\frac{v^*}{|v|}+1\right). \tag{20.19}$$

For small velocities, $|v| \ll v^*$, the law of friction (20.16) can be written in the form

$$\mu \approx \mu_0 - a\ln\left(\frac{v^*}{|v|}\right) + b\ln\left(\frac{v^*\theta}{D_c}\right). \tag{20.20}$$

We will quickly investigate its most important properties. The law of friction from Dieterich-Ruina describes not only the steady frictional processes well, but also unsteady transition processes. We consider a frictional process with the sliding velocity v_1. Thereby, the steady coefficient of friction is, according to (20.19), equal to

$$\mu^{(1)} \approx \mu_0 + (a-b)\ln\left(\frac{v_1}{v^*}\right). \tag{20.21}$$

If the sliding velocity changes abruptly from v_1 to v_2, then only the second term in (20.20) changes in the first moment and the coefficient of friction increases by $\Delta\mu_1 = a\ln\left(\frac{v_2}{v_1}\right)$ to the value

$$\mu^{(2)} = \mu_0 + a\ln\left(\frac{v_2}{v^*}\right) - b\ln\left(\frac{v_1}{v^*}\right). \tag{20.22}$$

After the transition, it assumes the value

$$\mu^{(3)} = \mu_0 + (a-b)\ln\left(\frac{v_2}{v^*}\right) \tag{20.23}$$

and, therefore, changes by $\Delta\mu_2 = -b\ln\left(\frac{v_2}{v_1}\right)$. This behavior is illustrated in Fig. 20.2 using experimental data from C. Marone[8]. For the system shown in Fig.

[8] C. Marone, Laboratory-derived friction laws and their application to seismic faulting. Ann. Rev. Earth Planet. Sci., 1998, v. 26, pp. 643-696.

20.2, $v_2 / v_1 = 10$, $\Delta\mu_1 \approx 0.01$, $\Delta\mu_2 \approx -0.014$. The constants a and b are $a \approx 0.004$, $b \approx 0.006$.

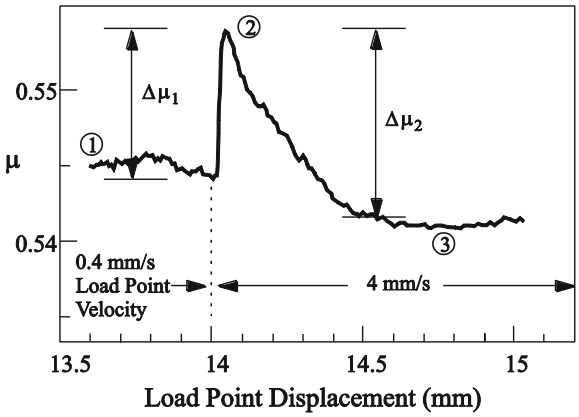

Fig. 20.2 Variation of the coefficient of friction for a sudden change in the velocity: the frictional force initially increases abruptly and afterwards relaxes to a new stationary value. From: Marone, C, 1998. Laboratory-derived friction laws and their application to seismic faulting. Annu. Rev. Earth Planet. Sci., v. 26, pp. 643-696.

Until now, we have discussed the law of friction for constant normal stress. It is easy to understand that this formulation is not complete. By increasing the normal stress, new asperities come into contact; for them, the "contact time" begins at this point. A sudden increase in the normal stress, therefore, leads to the renewal of contacts and the decrease in average contact time, even without tangential motion. Since the real contact area between the rough surfaces is proportional to the normal stress $A \propto \sigma_N$, in a first order approximation, a jump in the normal stress of $\mathrm{d}\sigma_N$ leads to a jump in the contact area $\mathrm{d}A \propto \mathrm{d}\sigma_N$. If we continue to interpret the state variable as the average contact time, then it changes as a result of the jump according to $\mathrm{d}\theta / \theta = -\mathrm{dA/A} = -\mathrm{d}\sigma_N / \sigma_N$ (because the age of the newly produced contact surface is zero). The kinetic equation (20.17) for θ must, therefore, be amended by addition of the term $-\dfrac{\theta\dot{\sigma}_N}{\sigma_N}$. An amendment of this form is consistent with experimental data from Linker and Dieterich[9], but with a phenomenological coefficient ζ:

$$\dot{\theta} = 1 - \left(\frac{|v|\theta}{D_c}\right) - \zeta\frac{\theta}{\sigma_N}\dot{\sigma}_N . \tag{20.24}$$

[9] M.F. Linker and J.H. Dieterich, Effects of variable normal stress on rock friction: observations and constitutive equations. J. Geophys. Res., 1992, v. 97, pp. 4923-4940.

20.4 Stability during Sliding with Rate- and State-Dependent Friction

We consider again the model shown in Fig. 12.1, which is described by the equation of motion

$$m\ddot{x} + F(\dot{x},\theta) + cx = cv_0 t\,, \tag{20.25}$$

where the frictional force, $F(\dot{x},\theta) = F_N \mu(\dot{x},\theta)$, is now defined by the Equations (20.20) and (20.17). The steady-state solution is given by

$$x = v_0 t - \frac{F(v_0,\theta)}{c}\,, \quad \theta_0 = \frac{D_c}{v_0}\,. \tag{20.26}$$

By considering the steady state solution with a small perturbation,

$$x = x_0 + v_0 t + \delta x\,, \qquad \theta = \theta_0 + \delta\theta\,, \tag{20.27}$$

we obtain the linearized equation in the form

$$m\delta\ddot{x} + F_{,v}\delta\dot{x} + c\delta x + F_{,\theta}\delta\theta = 0\,, \quad \delta\dot{\theta} = -\frac{1}{v_0}\delta\dot{x} - \frac{v_0}{D_c}\delta\theta \tag{20.28}$$

with

$$F_{,v} = \left.\frac{\partial F}{\partial \dot{x}}\right|_{\dot{x}=v_0} = F_N \frac{a}{v_0}\,, \qquad F_{,\theta} = \left.\frac{\partial F}{\partial \theta}\right|_{\theta=\theta_0} = F_N \frac{bv_0}{D_c}\,. \tag{20.29}$$

Substituting

$$\delta x = Ae^{\lambda t}\,, \qquad \delta\theta = Be^{\lambda t} \tag{20.30}$$

provides us with the characteristic equation

$$\lambda^3 + \lambda^2 \underbrace{\left(\frac{F_N a}{mv_0} + \frac{v_0}{D_c}\right)}_{P} + \lambda \underbrace{\left(\frac{c}{m} + \frac{F_N(a-b)}{mD_c}\right)}_{Q} + \underbrace{\frac{cv_0}{mD_c}}_{R} = 0\,. \tag{20.31}$$

The stability criterion demands that $R = PQ$ (See §12.7) or

$$\frac{cv_0}{mD_c} = \left(\frac{F_N a}{mv_0} + \frac{v_0}{D_c}\right)\left(\frac{c}{m} + \frac{F_N(a-b)}{mD_c}\right). \tag{20.32}$$

The critical stiffness follows as

$$c = \frac{(b-a)}{D_c}\left(F_N + \frac{mv_0^2}{aD_c}\right). \tag{20.33}$$

If $a > b$, then the sliding is always stable. In the opposite case, $a < b$, it is only stable for stiffnesses larger that the critical stiffness (20.33). For very small velocities, the stability criterion (20.33) simplifies to

$$c > \frac{(b-a)}{D_c} F_N . \tag{20.34}$$

This result can also be interpreted another way: sliding is only stable when

$$F_N < \frac{cD_c}{b-a}, \tag{20.35}$$

i.e. for sufficiently small normal forces. For a continuum, we use the relation $c \approx GL$; the sliding is only stable when $F_N < \frac{GLD_c}{b-a}$ or

$$L\sigma_N < \frac{GD_c}{b-a}, \tag{20.36}$$

where we have inserted the normal stress $\sigma_N \approx F_N / L^2$. According to this, sufficiently small blocks will always exhibit stable sliding, while blocks with linear dimensions larger than

$$L_c = \frac{GD_c}{\sigma_N (b-a)} \tag{20.37}$$

exhibit unstable sliding.

The most important parameter that determines the stability criterion, $(b-a)$, is dependent on the material, temperature, and pressure. For granite, the representative mineral of the Earth's upper crust, it is positive at temperatures lower than $300°C$ and becomes negative at higher temperatures (Fig. 20.3). This means that we can expect no earthquakes in the continental crust at depths in which the temperature reaches more than $300°C$.

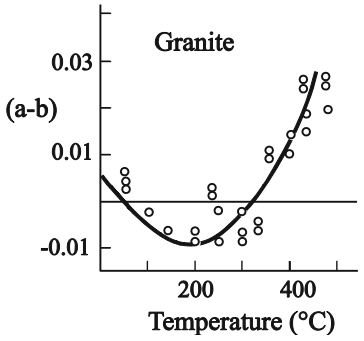

Fig. 20.3 Dependence of the parameter $(a-b)$ on the temperature for granite. Source: C.H. Earthquakes and Friction Laws., Nature, 1998, v. 391, pp. 37-42.

A more detailed, non-linear stability analysis shows that sliding using the law of friction in (20.20) for finite disturbances is described by a stability diagram which is qualitatively presented in Fig. 20.4.

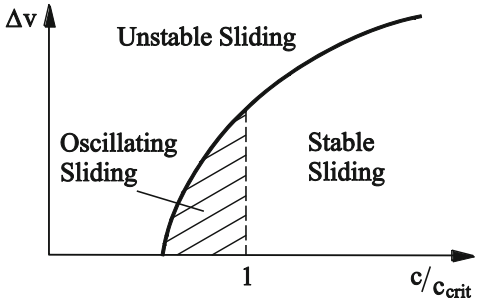

Fig. 20.4 Qualitative presentation of the stability diagram for a system (20.25) using the law of friction in (20.20), (20.17). Steady-state sliding is disturbed by a sudden change in the pulling velocity by Δv. The motion is stable for small disturbances and a spring stiffness larger than the critical stiffness. Sufficiently large disturbances, however, lead to the development of instabilities even for stiffnesses larger than the critical stiffness. For stiffnesses smaller than the critical stiffness, there is a domain in which the steady state sliding is stable, but the velocity is always finite and oscillates around a stationary value. In the domain of "unstable sliding" the sliding velocity (without taking inertia into account) becomes infinite in a finite amount of time.

The existence of three stability domains has the following implication for the dynamics of earthquakes: they can only nucleate in the areas of the crust in which the instability criterion is met. However, they can propagate into stable domains, as long as they produce a sufficiently large jump in velocity. Upon entering a stable domain, the propagation of the shearing is quickly braked.

20.5 Nucleation of Earthquakes and Post-Sliding

Even though people perceive earthquakes as sudden tremors that, as a rule, have no noticeable warning signs, they are preceded by slowly developing processes, which can be called nucleation. In this stage, they can be treated as quasi-static: the equilibrium conditions must be fulfilled for every point in time. In the simple "block model" with the simplified law of friction (20.20) from Dieterich and under the assumption that the spring is pulled with the constant velocity v_0, the equilibrium condition has the following form:

$$c\left(x_0 + v_0 t - x\right) = F_N\left(\mu_0 - a\ln\left(\frac{v^*}{|v|}\right) + b\ln\left(\frac{v^*\theta}{D_c}\right)\right). \tag{20.38}$$

This equation, together with the kinetic equation for the state variable,

$$\dot{\theta} = 1 - \left(\frac{|\dot{x}|\theta}{D_c}\right), \tag{20.39}$$

can be numerically solved. Directly before the slip, however, there is an accelerating creep and the sliding velocity $v = \dot{x}$ is then much larger that the velocity at steady creep: $v >> D_c / \theta_0 = v_0$. Thereby, Equation (20.39) reduces to

$$\frac{\mathrm{d}\theta}{\mathrm{d}x} = -\left(\frac{\theta}{D_c}\right), \quad \theta = \theta_0 e^{-x/D_c}. \tag{20.40}$$

Substitution into Equation (20.38) provides us

$$\frac{c}{F_N}\left(x_0 + v_0 t - x\right) = \left(\mu_0 + a\ln\frac{\dot{x}}{v^*} + b\ln\frac{\theta_0 v^*}{D_c}\right) - \frac{bx}{D_c}. \tag{20.41}$$

This equation can be explicitly integrated:

$$A\int_0^t \exp\left(\frac{cv_0}{aF_N}t\right)\mathrm{d}t = \int_0^x \exp\left(-\frac{Bx}{a}\right)\mathrm{d}x, \tag{20.42}$$

where

$$A = v^*\exp\left(-\frac{\mu_0}{a} - \frac{b}{a}\ln\frac{\theta_0 v^*}{D_c} + \frac{cx_0}{aF_N}\right) = \dot{x}_0, \tag{20.43}$$

is equal to the sliding velocity $\dot{x}_0$ at time $t = 0$ and

$$B = \left(\frac{b}{D_c} - \frac{c}{F_N}\right). \tag{20.44}$$

Equation (20.42) has the following solution:

$$x = -\frac{a}{B}\ln\left[1-\frac{\dot{x}_0 BF_N}{cv_0}\left(\exp\left(\frac{cv_0}{aF_N}t\right)-1\right)\right]. \tag{20.45}$$

A typical trend for creep, according to this equation, is shown in Fig. 20.5. The time until the appearance of the instability is calculated using the condition that the argument of the logarithm in (20.45) is zero:

$$t_c = \frac{aF_N}{cv_0}\ln\left(1+\frac{cv_0}{\dot{x}_0 BF_N}\right). \tag{20.46}$$

Near the instability, (20.45) can be approximated using the expression

$$x \approx -\frac{a}{B}\ln\left[\frac{\dot{x}_0 B}{a}\left(1+\frac{cv_0}{\dot{x}_0 BF_N}\right)(t_c - t)\right]. \tag{20.47}$$

The sliding velocity increases according to the relation

$$\dot{x} \approx \frac{a}{B}(t_c - t)^{-1}. \tag{20.48}$$

Accelerating creep before a slip event is also detected in simple tribological models in the laboratory (Fig. 20.6).

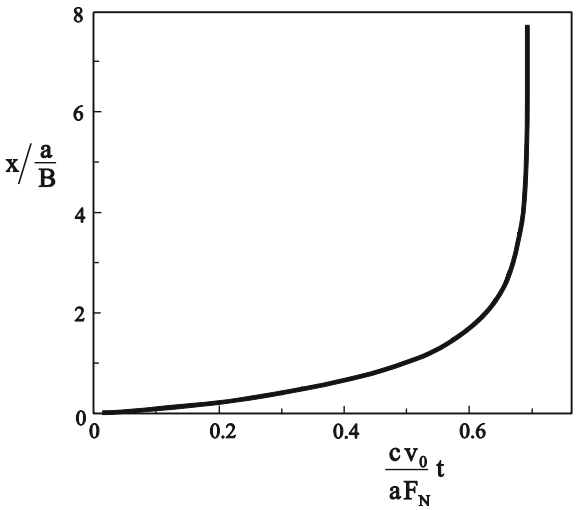

Fig. 20.5 Accelerating creep before slip according to the Equation (20.45) with $\frac{\dot{x}_0 BF_N}{cv_0} = 1$.

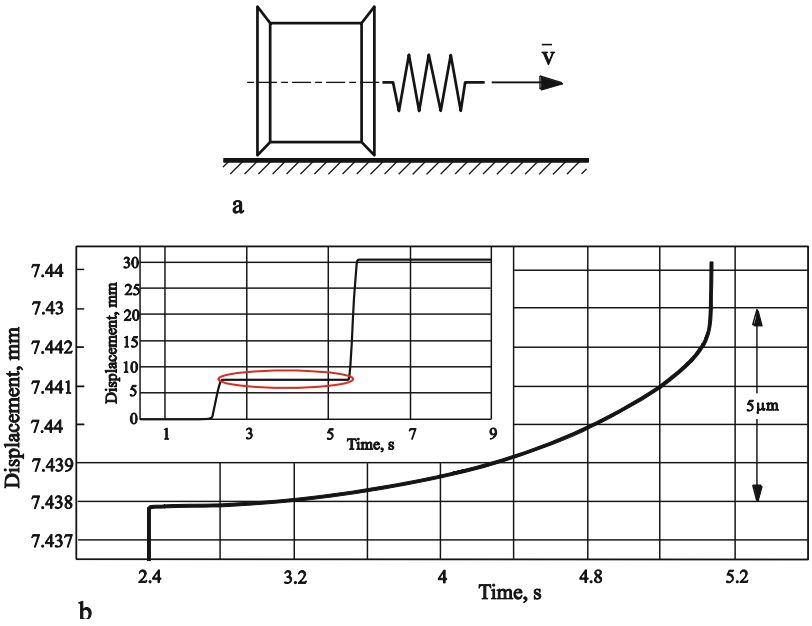

Fig. 20.6 (b) An experimental recording of the position of a sliding steel body on a steel substrate as a function of time for the experiment shown schematically in (a). The position is measured with a resolution of 8 nm. In the subplot, one can see two jumps one after the other of about 8 and 22 mm, respectively. The entire "stick" phase (circled in subplot) is shown in the main plot with a higher resolution. One can see that during the entire "stick" phase, there is a slow creeping motion which quickly accelerates near the "slip" phase. (Experiment: V.L. Popov and J. Starcevic, TU Berlin).

Also *after* a slip, there is generally a certain "post-sliding" which can be described using the same law of friction. Immediately after the slip, the variable θ becomes practically zero because of the large slip path (see Equation (20.40)). Thus, directly after the slip, it can be described by the equation

$$\dot{\theta} \approx 1, \quad \theta \approx t - t_c', \tag{20.49}$$

where t_c' is the time at which the slip ends. For small velocities v_0, the "spring force" F can be assumed to be constant. Equation (20.38) can then be written in the form

$$\frac{F}{F_N} = \left(\mu_0 + a \ln \frac{\dot{x}}{v^*} + b \ln \frac{v^* \left(t - t_c' \right)}{D_c} \right). \tag{20.50}$$

From this, it follows that

$$\dot{x} = v^* e^{\frac{1}{a}\left(\frac{F}{F_N} - \mu_0\right)} \cdot \left(v^* \frac{t - t_0'}{D_c} \right)^{-b/a} . \tag{20.51}$$

The exponent b/a always has an order of magnitude of 1. In the example shown in Fig. 20.2, it is equal to 1.5. The intensity of the post-sliding is different than that of pre-sliding in that it is very sensitive to residual stress (proportional to $\left(F/F_N - \mu_0'\right)$), which is dependent on the precise structure of a fracture site or the pairing of materials.

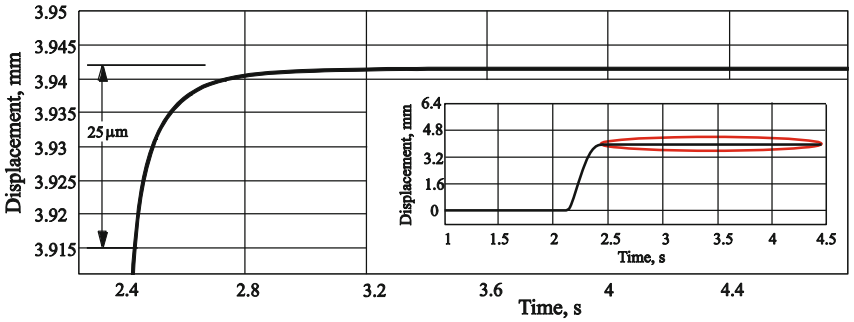

Fig. 20.7 An experimental record of the position of a sliding steel body on a glass substrate as a function of time for an experiment schematically shown in Fig. 20.6 (a). In the subplot, one can see a slip of about 4 mm. In the main plot, the "stick" phase after the slip (circled in the subplot) is shown with a higher resolution. One sees that there is a slowing creep motion during the "stick" phase (Post-sliding). (Experiment: V.L. Popov and J. Starcevic, TU Berlin).

20.6 Foreshocks and Aftershocks

If the creeping described by Equation (20.48) takes place in the form of a series of discrete slips (foreshocks) of the same length l, then the following equation describes the frequency $\dot{n}$ of the foreshocks:

$$\dot{n}_{foreshocks} \approx \frac{a}{Bl}\left(t_0 - t\right)^{-1} . \tag{20.52}$$

This is similarly valid for "post-sliding": If the post-sliding described by Equation (20.51) take place in the form of a series of discrete slips (*aftershocks*) with the same length l, then the following equation describes the frequency $\dot{n}$ of the aftershocks:

$$\dot{n}_{aftershocks} = \frac{v^*}{l} e^{\frac{1}{a}\left(\frac{F}{F_N} - \mu_0\right)} \cdot \left(v^* \frac{t - t_0'}{D_c} \right)^{-b/a} . \tag{20.53}$$

The power functions in the forms of (20.52) and (20.53) for foreshocks and aftershocks were empirically determined in 1894 by Fusakichi Omori and are known as the *Omori laws*.

Foreshocks are a part of the nucleation of earthquakes. In a more detailed, continuous representation, they take place near the epicenter of the "main shock." Conversely, the aftershocks provide a mechanism for the release of the stress that is produced by the main shock. As a rule, they are concentrated on the edge of sliding domain of the main shock.

20.7 Continuum Mechanics of Block Media and the Structure of Faults

In general, geomedia are granular media composed of individual fragments. The shear strength of such a medium is essentially determined by the frictional forces between the individual blocks. We consider a granular, porous medium being acted upon by a stress tensor with the principle stresses $\tilde{\sigma}_3 < \tilde{\sigma}_2 < \tilde{\sigma}_1$ and the pore pressure p, which is shown schematically in Fig. 20.8a. In the presented two-dimensional diagram, the middle stress $\tilde{\sigma}_2$, which acts in the direction perpendicular to the figure plane, plays no role.

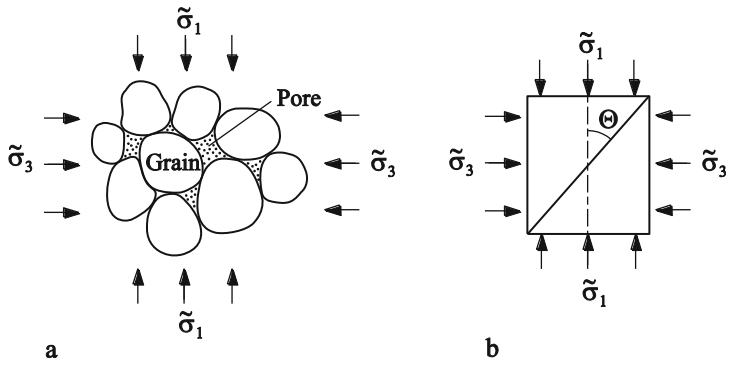

Fig. 20.8 Porous, granular medium being acted upon by the principal stresses σ_1 and σ_3, and with the pore pressure p.

The *effective stress tensor*, which determines the behavior of the material, is calculated by subtracting the hydrostatic pore pressure from the stress tensor:

$$\sigma_1 = \tilde{\sigma}_1 - p\,,\quad \sigma_2 = \tilde{\sigma}_2 - p\,,\quad \sigma_3 = \tilde{\sigma}_3 - p\,. \tag{20.54}$$

Normal and tangential stresses in a cross-section, which form the angle θ with the axis "1" (Fig. 20.8b), are calculated as

$$\sigma_N = \frac{(\sigma_1 + \sigma_3)}{2} - \frac{(\sigma_1 - \sigma_3)}{2}\cos 2\theta\,, \tag{20.55}$$

$$\tau = \frac{(\sigma_1 - \sigma_3)}{2}\sin 2\theta \tag{20.56}$$

or

$$\sigma_N = \frac{(\tilde{\sigma}_1 + \tilde{\sigma}_3)}{2} - \frac{(\tilde{\sigma}_1 - \tilde{\sigma}_3)}{2}\cos 2\theta - p\,, \tag{20.57}$$

$$\tau = \frac{(\tilde{\sigma}_1 - \tilde{\sigma}_3)}{2}\sin 2\theta\,. \tag{20.58}$$

According to this, the pore pressure leads to a decrease in normal stress in an arbitrary cross section, but has no influence on the shear stress.

Sliding begins in the cross-section only when the shear stress τ reaches the value $\mu\sigma_N$:

$$\tau = \mu\sigma_N\,, \tag{20.59}$$

or taking the adhesive contribution into account

$$\tau = \tau_0 + \mu\sigma_N\,. \tag{20.60}$$

Here, μ is the "internal coefficient of friction," which can, in principle, be determined from independent experiments. Fig. 20.9 illustrates this criterion using experimental data from various types of rock. The typical experimental value of the coefficient of friction is between $\mu \approx 0.6$ and $\mu = 0.85$ for rock.

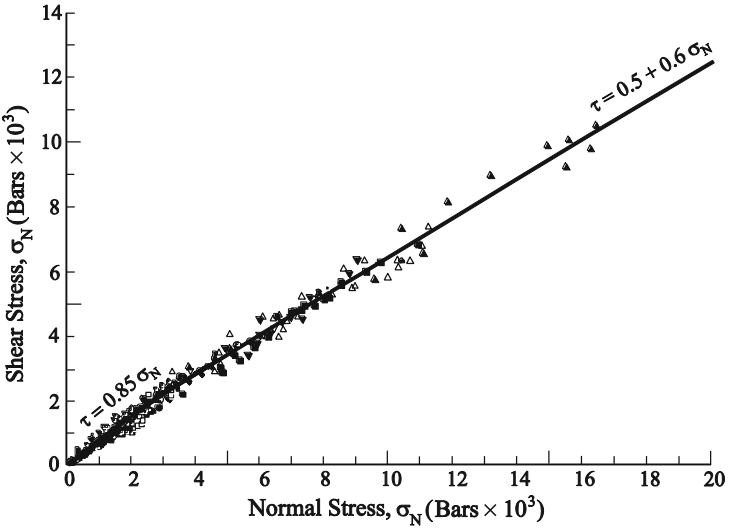

Fig. 20.9 "Frictional strength" for several types of rock as a function of the normal stress. Source: Byerlee, J.D. Friction of rocks. Pure. Appl. Geophys., 1978, v. 116, pp. 615-626.

This criterion is called the *Coulomb fracture criterion* for granular media. This dependence is presented graphically with a straight line in Fig. 20.10. The entirety of all of the normal and tangential stresses, (20.55) and (20.56), in cross-sections with an arbitrary θ form a circle on the plane (σ_N, τ), the so-called Mohr's circle. If the total circle lies under the line (20.60), as is shown in Fig. 20.10 a, then the fracture condition is not met in any cross-section. By increasing the principal stress σ_1, decreasing σ_3, or shifting the total stress circle to the left (for example, by increasing the pore pressure according to (20.57)), Mohr's circle would touch the line (20.60) (Fig. 20.10b). At this moment, the fracture criterion is met for the first time for a cross-section with the angle

$$\theta = \frac{\pi}{4} - \frac{\varphi}{2}, \tag{20.61}$$

where φ is the friction angle:

$$\tan\varphi = \mu\,. \tag{20.62}$$

For a coefficient of friction of $\mu = 0.6$, we obtain $\theta \approx 0.52$ (or $\approx 30°$) and for $\mu = 0.85$ $\theta \approx 0.43$ (or $\approx 25°$).

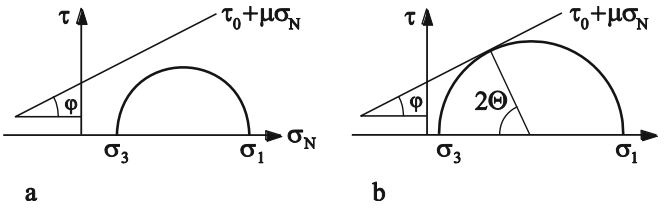

Fig. 20.10 Mohr's circle for plane stress and Coulomb's fracture criterion.

With the help of Fig. 20.10b, one can express the criterion (20.60) using the principal stresses:

$$\sigma_1\left(\sqrt{1+\mu^2}-\mu\right)-\sigma_3\left(\sqrt{1+\mu^2}+\mu\right)=2\tau_0\,. \tag{20.63}$$

Therefore, between the principal stresses in the fracture area, there exists a linear dependence. Stress measurements using deep drilling show that this condition is fulfilled at all depths. This means that the Earth's crust is found to be near the critical state at all depths. If the primary stress σ_3 is negative (in tension), then, as a rule, the following criterion is applied to the fracture:

$$\sigma_3=-\sigma_0\,. \tag{20.64}$$

Anderson[10] was the first to recognize that the fundamental types of faults can be easily explained using the properties of granular media. His classification is based on observations that the principal axes of the stress tensor in the upper crust often lie normal and parallel to the surface, respectively. There are three possibilities for the orientation of the axis of the largest principal stress (σ_1) and the axis of the smallest principal stress (σ_3) with respect to the Earth's surface, which are shown in Fig. 20.11a-c. The resulting fault types are *normal faults* (Fig. 20.11a), *thrust (reverse) faults* (Fig. 20.11b), and *strike-slip faults* (Fig. 20.11c). If the smallest primary stress is negative, then the surfaces separate in a plane perpendicular to the axis of the negative stress (*divergent faults*, Fig. 20.11d). The type of slip during an earthquake influences, in addition to its magnitude, the resulting destruction. Strike-slip faulting (c) leads to maximum tangential acceleration and normal faulting, to strong tsunamis (in the case that the earthquake takes place under the ocean).

[10] E.M. Anderson, The dynamics of faulting. Edinburgh, Oliver & Boyd, 1951.

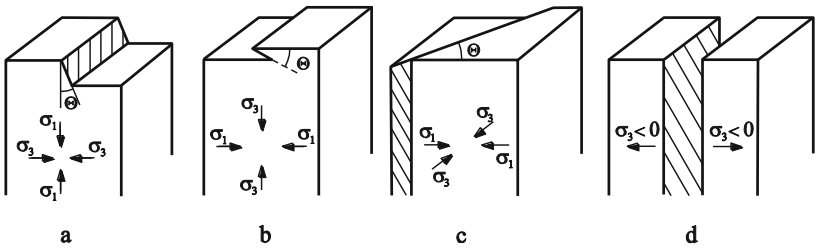

Fig. 20.11 Primary types of slips according to Anderson: (a) Normal fault, (b) Thrust (reverse) fault, (c) Strike-slip fault, (d) Divergent fault.

20.8 Is it Possible to Predict Earthquakes?

This question has been heavily discussed in the last decade. The two answers to this question each have their prominent supporters. Both points of view can be followed using even the simple earthquake model described above.

If an earthquake is considered a stick-slip instability and we use the simple law of friction with constant static and kinetic coefficients of friction, then there is no movement before the beginning of the slip event. Because of this, there would also be no indication of the approaching slip and, therefore, predicting the earthquake would be impossible. An extension of this to continuums does not fundamentally change anything regardless of how complicated the system becomes. A distributed system exhibits complicated behavior, which is mirrored by the known statistical properties of earthquakes (Gutenberg-Richter and Omori laws). These properties, however, have a purely statistical character. Therefore, they can serve as *a posteriori* analysis, but not as a prediction at a given place and time.

This conclusion, however, is based on a concept that is not completely correct. Laboratory experiments (see Section 20.5) as well as seismic measurements show that an earthquake is always preceded by an accelerating creep, which is a warning sign for the fact that the local stresses are approaching the critical value. This fact is a reason for some optimism[11]. At the same time, the experimental data presented in Section 20.5 show where the problem lies: to effectively observe creep processes, it is necessary to conduct measurements of displacements in the Earth's crust with very high resolution. Since the frequency domain of up to date seismological measurements still does not allow for high resolution measurements of very slow

[11] A theoretical and experimental analysis of possibilities for predicting stick-slip instabilities can be found in: B. Grzemba, Predictability of Elementary Models for Earthquake Danymics, epubli GmbH, Berlin, 2014.

displacements, only the hope remains that better measurement methods and models in the future lead to a breakthrough in our ability to predict earthquakes[12].

Problems

Problem 1: We consider two elastic half-spaces. They are pressed together with the normal stress σ_N and then acted upon by an increasing tangential stress τ until a stick-slip instability develops. Under the assumption that Coulomb's law of friction is valid at the interface with a constant static and kinetic coefficients of friction (μ_s and μ_k, respectively), determine the relative sliding velocity and acceleration of the fracture surfaces.

Solution: Under the described conditions, only shear waves exist in the medium, which are described by the wave equation

$$\frac{\partial^2 u}{\partial t^2} = c_{sound}^2 \frac{\partial^2 u}{\partial z^2} \quad , \quad \text{with} \quad c_{sound}^2 = \frac{G}{\rho} .$$

The same equation is also valid for all time and spatial derivatives of u and according to this, also for the stress $\tau = G\partial u/\partial z$:

$$\frac{\partial^2 \tau}{\partial t^2} = c_{sound}^2 \frac{\partial^2 \tau}{\partial z^2} .$$

The stress directly before the instability is equal to $\tau_s = \mu_s \sigma_N$ and after the beginning of motion, to $\tau_k = \mu_k \sigma_N$. The solution of the wave equation with these boundary conditions is a step function with the height $\Delta\tau = \sigma_N \left(\mu_k - \mu_s\right)$, which propagates in the depth of the material with the velocity $c_{sound} = \sqrt{G/\rho}$. For an arbitrary solution of the wave equation in the form of a wave propagating from the surface $u(z - c_{sound} t)$, the following expressions are valid: $v = \frac{\partial u}{\partial t} = -c_{sound} \frac{\partial u}{\partial z} = -\frac{c_{sound}}{G}\tau$. Between the jump in the stress $\Delta\tau = \sigma_N \left(\mu_k - \mu_s\right)$ and the jump in the velocity Δv, the following relation exists:

[12] For a discussion on this theme based on experimental data from earthquakes in California see: C. Thurber and R. Sessions, Assessment of creep events as potential earthquake precursors: Application to the creeping section of the San Andreas fault. California, Pure appl. Geophys., 1998, v. 152, pp. 685-705.

$$\Delta v = -\frac{c_{sound}}{G}\Delta\tau = \frac{c_{sound}}{G}\sigma_N\left(\mu_s - \mu_k\right) = \frac{\sigma_N\left(\mu_s - \mu_k\right)}{\sqrt{G\rho}}.$$

The accompanying acceleration is zero everywhere except on the wavefront, where it is infinity.

Problem 2: As in Problem 1, we consider two elastic half-spaces in contact. It is assumed that the coefficient of static friction μ_s linearly decreases to that of the coefficient of kinetic friction μ_k over a length D_c (sliding length). Determine the maximum acceleration of the fracture surfaces in this case.

Solution: From the beginning of the relative sliding of the interface until a relative displacement of D_c, the frictional stress in the contact interface is

$$\tau = G\left.\frac{\partial u}{\partial z}\right|_{z=0,t} = \sigma_N\left(\mu_s - \frac{\mu_s - \mu_k}{D_c}u\big|_{z=0,t}\right).$$

The general solution to the wave equation in the form of a propagating surface wave has the form $u = \frac{\tau_0}{G}z + f(z - c_{sound}t)$, where $\tau_0 = \mu_s\sigma_N$ is the constant macroscopic stress far away from the fracture point. Therefore, we obtain the following equation for the displacement of the surface

$$\frac{\partial u}{\partial t} = \frac{\sigma_N c_{sound}}{G}\frac{\mu_s - \mu_k}{D_c}u.$$

If the motion begins with a disturbance u_0, then the displacement of the surface is

$$u = u_0\exp\left(\frac{\sigma_N c_{sound}}{G}\frac{\mu_s - \mu_k}{D_c}t\right).$$

The acceleration is equal to

$$\ddot{u} = \left(\frac{\sigma_N c_{sound}}{G}\frac{\mu_s - \mu_k}{D_c}\right)^2 u_0\exp\left(\frac{\sigma_N c_{sound}}{G}\frac{\mu_s - \mu_k}{D_c}t\right).$$

Therefore, between the displacement and the acceleration, the following relation exists: $\ddot{u} = \left(\frac{\sigma_N c_{sound}}{G}\frac{\mu_s - \mu_k}{D_c}\right)^2 u$. At the moment when the displacement reaches $u = D_c$, the acceleration Δv reaches a maximum value of

$$\ddot{u}_{\max} = \frac{\sigma_N^2 \left(\mu_s - \mu_k\right)^2}{G\rho D_c}.$$

According to this, the maximum value of the acceleration is inversely proportional to the sliding length D_c. The maximum value of the velocity is the same as in Problem 1.

Problem 3: As in Problem 1, we consider two elastic half-spaces in contact. It is now assumed that during a slip, the coefficient of friction exponentially decreases from its static value μ_s to its kinetic value μ_k, with a characteristic time t_0 (relaxation time)[13]. Determine the maximum velocity and acceleration of the fracture surfaces in this case.

Solution: From the beginning of the relative sliding of the interface, the frictional stress in the contact interface is

$$\tau = G\frac{\partial u}{\partial z}\bigg|_{z=0,t} = \sigma_N \left(\mu_s e^{-t/t_0} + \mu_k \left(1 - e^{-t/t_0}\right)\right).$$

The general solution to the wave equation in the form of a propagating surface wave is $u = \frac{\tau_0}{G} z + f(z - c_{sound} t)$, where $\tau_0 = \mu_s \sigma_N$ is the constant macroscopic stress far away from the fracture surface. Therefore, we obtain the following equation for the velocity of the surface

$$\frac{\partial u}{\partial t} = \frac{\sigma_N c_{sound}}{G}\left(\mu_s - \mu_k\right)\left(1 - e^{-t/t_0}\right) = \frac{\sigma_N \left(\mu_s - \mu_k\right)}{\sqrt{G\rho}}\left(1 - e^{-t/t_0}\right).$$

The acceleration is equal to

$$\frac{\partial^2 u}{\partial t^2} = \frac{\sigma_N \left(\mu_s - \mu_k\right)}{\sqrt{G\rho} t_0} e^{-t/t_0}.$$

The velocity reaches its maximum value of

$$\dot{u}_{\max} = \frac{\sigma_N \left(\mu_s - \mu_k\right)}{\sqrt{G\rho}}$$

at $t \gg t_0$ and the acceleration Δv reaches its maximum value of

---

[13] This assumption corresponds to a linear scaling of the sliding length D_c with velocity, which is typical for granular media. (See e.g. T. Hatano, Scaling of the critical slip distance in granular layers. Geophysical Research Letters, 2009, v. 36, L18304 doi: 10.1029/2009GL039665.)

$$\ddot{u}_{\max} = \frac{\sigma_N \left(\mu_s - \mu_k \right)}{\sqrt{G \rho} t_0}$$

at $t = 0$.

Appendix

Appendix A - Normal Displacement under the Effect of Selected Pressure Distributions

In this appendix, the displacements of the surface of an elastic half-space under several stress distributions are calculated, which are of interest in contact mechanics.

a. Normal stress in a circle with the radius a according to the expression

$$p = p_0\left(1-\frac{r^2}{a^2}\right)^{-1/2}, \quad r^2 = x^2 + y^2 . \tag{A.1}$$

Here, we limit ourselves to the calculation of normal displacements of the surface. They are given by Equation (5.7), which we repeat here:

$$u_z = \frac{1}{\pi E^*}\iint P_z(x',y')\frac{dx'dy'}{r}, \quad r = \sqrt{(x-x')^2+(y-y')^2}, \tag{A.2}$$

with

$$E^* = \frac{E}{\left(1-\nu^2\right)} . \tag{A.3}$$

The coordinate system used is shown in Fig. A.1a.

V.L. Popov, *Contact Mechanics and Friction*,
DOI 10.1007/978-3-662-53081-8

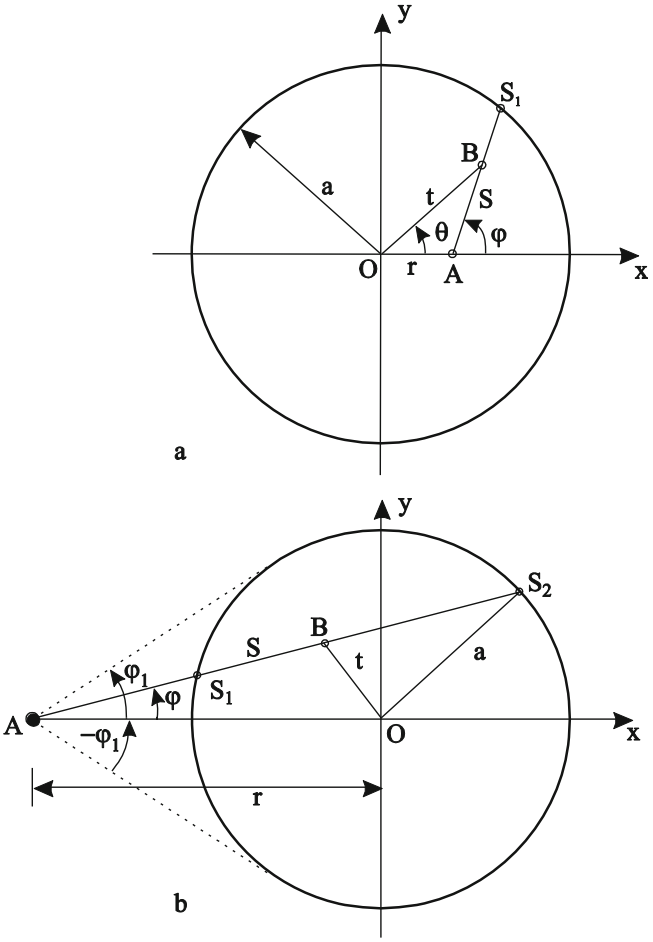

Fig. A.1 Calculation of the vertical displacements under a normal stress in a circular region: (a) at a point within the pressure area, (b) at a point outside the pressure area

Due to rotational symmetry of the stress distribution, the normal displacement at a point is dependent only on the distance *r* from the origin. Therefore, it is sufficient to determine only the displacements of the points on the x-axis. In the following, we calculate the normal displacement at point A. For this, the displacement at point A, caused by the stress in the "varying" point B, must be determined and, finally, integrated for all possible positions of point B in the area being acted upon by the stress. The stress in point B is dependent only on the distance t from the origin due to rotational symmetry. For this distance, we obtain $t^2 = r^2 + s^2 + 2rs\cos\varphi$. Therefore, the pressure distribution is

$$p(s,\varphi) = p_0\left(1-\frac{r^2+s^2+2rs\cos\varphi}{a^2}\right)^{-1/2} = p_0 a\left(a^2-r^2-s^2-2rs\cos\varphi\right)^{-1/2} = p_0 a\left(\alpha^2-2\beta s-s^2\right)^{-1/2}, \tag{A.4}$$

where we have introduced $\alpha^2 = a^2 - r^2$ and $\beta = r\cos\varphi$.

For the z-component of the displacement, we obtain

$$u_z = \frac{1}{\pi E^*} p_0 a \int_0^{2\pi}\left(\int_0^{s_1}\left(\alpha^2-2\beta s-s^2\right)^{-1/2} ds\right) d\varphi. \tag{A.5}$$

Here, s_1 is the positive root of the equation $\alpha^2 - 2\beta s - s^2 = 0$. The integral over ds is calculated to

$$\int_0^{s_1}\left(\alpha^2-2\beta s-s^2\right)^{-1/2} ds = \frac{\pi}{2} - \arctan\left(\beta/\alpha\right). \tag{A.6}$$

It is apparent that $\arctan\left(\beta(\varphi)/\alpha\right) = -\arctan\left(\beta(\varphi+\pi)/\alpha\right)$. Therefore, by integrating over φ, the term with "arctan" vanishes. Therefore,

$$u_z = \frac{1}{\pi E^*} p_0 a \int_0^{2\pi}\frac{\pi}{2} d\varphi = \frac{\pi p_0 a}{E^*} = d = const, \quad r \le a. \tag{A.7}$$

where the indentation depth d is introduced.

We now consider a point A outside of the contact area (Fig. A.1 b). In this case,

$$p(s,\varphi) = p_0 a\left(\alpha^2+2\beta s-s^2\right)^{-1/2}. \tag{A.8}$$

The displacement is then given by the equation

$$u_z = \frac{1}{\pi E^*} p_0 a \int_{-\varphi_1}^{\varphi_1}\left(\int_{s_1}^{s_2}\left(\alpha^2+2\beta s-s^2\right)^{-1/2} ds\right) d\varphi \tag{A.9}$$

where s_1 and s_2 are roots of the equation

$$\alpha^2 + 2\beta s - s^2 = 0 \tag{A.10}$$

Accordingly, it follows that

$$\int_{s_1}^{s_2}\left(\alpha^2+2\beta s-s^2\right)^{-1/2} ds = \pi. \tag{A.11}$$

The remaining integration in (A.9) now results trivially in $u_z = \frac{2}{E^*} p_0 a \varphi_1$, or taking into account the obvious geometric relation from Fig. A1b, $\varphi_1 = \arcsin(a/r)$

$$u_z = \frac{2}{E^*} p_0 a \cdot \arcsin\left(a/r\right), \qquad r > a \tag{A.12}$$

which with account of (A.7) can also be written as

$$u_z = \frac{2}{\pi} d \cdot \arcsin\left(a/r\right), \qquad r > a\,. \tag{A.13}$$

From the result (A.7), it follows directly how to generate the assumed pressure distribution: it is generated by an impression of a rigid cylindrical punch.
The total force acting on pressure area equals

$$F_N = \int_0^a p_0 \left(1 - \frac{r^2}{a^2}\right)^{-1/2} 2\pi r \mathrm{d}r = 2\pi p_0 a^2\,. \tag{A.14}$$

The contact stiffness is defined as the ratio of force to displacement:

$$k = 2aE^*\,. \tag{A.15}$$

The pressure distribution (A.1) can be also represented in the following form with the consideration of (A.7)

$$p(r) = \frac{1}{\pi} \frac{E^* u_z}{\sqrt{a^2 - r^2}} = \frac{1}{\pi} \frac{E^* d}{\sqrt{a^2 - r^2}}\,. \tag{A.16}$$

b. Hertzian Stress Distribution

$$p = p_0 \left(1 - \frac{r^2}{a^2}\right)^{1/2}\,. \tag{A.17}$$

We obtain a vertical displacement of

$$u_z = \frac{1}{\pi E^*} \frac{p_0}{a} \int_0^{2\pi} \left(\int_0^{s_1} \left(\alpha^2 - 2\beta s - s^2\right)^{1/2} ds \right) d\varphi\,. \tag{A.18}$$

The integral over *ds* in this expression is calculated as

$$\int_0^{s_1} \left(\alpha^2 - 2\beta s - s^2\right)^{1/2} ds = -\frac{1}{2}\alpha\beta + \frac{1}{2}\left(\alpha^2 + \beta^2\right) \cdot \left(\frac{\pi}{2} - \arctan\left(\beta/\alpha\right)\right). \tag{A.19}$$

By integrating over $d\varphi$, terms with $\alpha\beta$ and "arctan" vanish. The rest of the terms are

$$\begin{aligned} u_z &= \frac{1}{\pi E^*}\frac{p_0}{a}\int_0^{2\pi} d\varphi \frac{\pi}{4}\left(\alpha^2+\beta^2\right) \\ &= \frac{1}{4E^*}\frac{p_0}{a}\int_0^{2\pi}\left(a^2-r^2+r^2\cos^2\varphi\right)d\varphi \\ &= \frac{1}{E^*}\frac{\pi p_0}{4a}\left(2a^2-r^2\right). \end{aligned} \tag{A.20}$$

c. Uniform Stress Distribution in a Thin Circular Ring

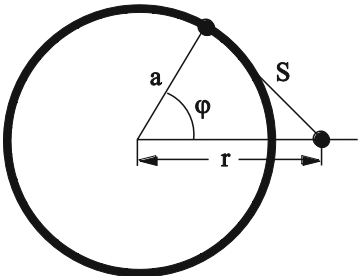

Fig. A.2 A sketch for the calculation of the vertical displacement at point r for a uniform pressure distribution in a thin circular ring.

The displacement at point r is calculated as

$$\begin{aligned} u_z &= \frac{1}{\pi E^*}\int_0^{2\pi}\frac{F_N}{2\pi}\frac{d\varphi}{s} \\ &= \frac{1}{\pi E^*}\int_0^{2\pi}\frac{F_N}{2\pi}\frac{d\varphi}{\sqrt{a^2+r^2-2ar\cos\varphi}} \\ &= \frac{F_N}{2aE^*}\frac{4}{\pi^2(1+r/a)}K\left(2\frac{\sqrt{r/a}}{1+r/a}\right), \end{aligned} \tag{A.21}$$

where F_N is the normal force and $K(\kappa)$ is the complete elliptic integral of the first kind:

$$K(\kappa)=\int_0^{\pi/2}\frac{d\varphi}{\sqrt{1-\kappa^2\sin^2\varphi}}. \tag{A.22}$$

This displacement is graphically presented in (Fig. A.3). For $r \approx a$, the displacement has a logarithmic singularity:

$$u_z = \frac{F_N}{2aE^*}\frac{2}{\pi^2}\ln\frac{8}{|r/a-1|}, \quad |r/a-1| \ll 1. \tag{A.23}$$

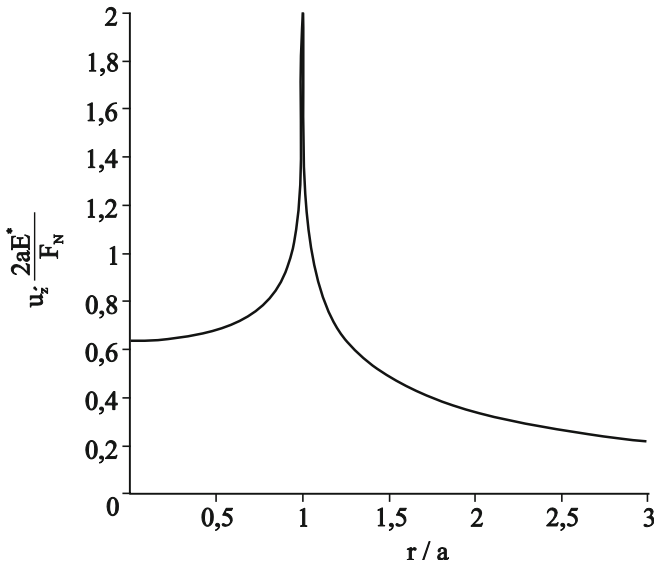

Fig. A.3 Displacement of the surface by pressure in a thin circular ring.

Appendix B - Normal Contact of Axially Symmetrical Profiles

In this appendix, the contact problem for axially-symmetrical profiles with a compact contact area will be solved in general terms, while solution of the contact problems for a rigid, flat, cylindrical indenter is assumed to be known (see Appendix A). As a side product, we will provide the rigorous proof for the basic equations of the Method of Dimensionality Reduction (MDR, see Section 5.6).

We consider a contact between a rigid indenter with shape $z = f(r)$ and an elastic half-space, which is characterized by the effective elastic coefficient E^*. The indentation depth under the effect of the normal force F_N is d and the contact radius a. For a given profile of the indenter, each of these three variables can be determined by the other two, especially the indentation depth is a unique function of the contact radius, which we denote by

$$d = g(a). \tag{A.24}$$

We consider the indentation process from the first contact to the final indentation depth and investigate the current values of the force, indentation depth and contact radius $\tilde{F}_N$, $\tilde{d}$ and $\tilde{a}$. The entire process consists of a change in indentation depth

from $\tilde{d}=0$ to $\tilde{d}=d$, where the contact radius changes from $\tilde{a}=0$ to $\tilde{a}=a$ and contact force from $\tilde{F}_N=0$ to $\tilde{F}_N=F_N$. The normal force at the end of the process can be written as follows

$$F_N=\int_0^{F_N}\mathrm{d}\tilde{F}_N=\int_0^a\frac{\mathrm{d}\tilde{F}_N}{\mathrm{d}\tilde{d}}\frac{\mathrm{d}\tilde{d}}{\mathrm{d}\tilde{a}}\mathrm{d}\tilde{a}\,. \tag{A.25}$$

Taking into account that the stiffness of contact area with radius $\tilde{a}$ is given by

$$\frac{\mathrm{d}\tilde{F}_N}{\mathrm{d}\tilde{d}}=2E^*\tilde{a} \tag{A.26}$$

(see (A.15)) and using relation (A.24), we obtain

$$F_N=2E^*\int_0^a\tilde{a}\frac{\mathrm{d}g(\tilde{a})}{\mathrm{d}\tilde{a}}\mathrm{d}\tilde{a}\,. \tag{A.27}$$

Partial integration now results in

$$F_N=2E^*\left[a\cdot g(a)-\int_0^a g(\tilde{a})\mathrm{d}\tilde{a}\right]=2E^*\left[\int_0^a\big(g(a)-g(\tilde{a})\big)\mathrm{d}\tilde{a}\right]. \tag{A.28}$$

Let us now turn to the calculation of the pressure distribution in the contact area. An infinitesimal indentation depth by $\mathrm{d}\tilde{d}$ of an area with radius $\tilde{a}$ produces the following contribution to the pressure distribution (see (A.16)):

$$\mathrm{d}p(r)=\frac{1}{\pi}\frac{E^*}{\sqrt{\tilde{a}^2-r^2}}\mathrm{d}\tilde{d},\quad\text{with}\quad r<\tilde{a}\,. \tag{A.29}$$

The pressure distribution at the end of the indentation process is equal to the sum of the incremental pressure distributions:

$$p(r)=\int_{d(r)}^{d}\frac{1}{\pi}\frac{E^*}{\sqrt{\tilde{a}^2-r^2}}\mathrm{d}\tilde{d}=\int_r^a\frac{1}{\pi}\frac{E^*}{\sqrt{\tilde{a}^2-r^2}}\frac{\mathrm{d}\tilde{d}}{\mathrm{d}\tilde{a}}\mathrm{d}\tilde{a} \tag{A.30}$$

or with consideration of notation (A.24)

$$p(r)=\frac{E^*}{\pi}\int_r^a\frac{1}{\sqrt{\tilde{a}^2-r^2}}\frac{\mathrm{d}g(\tilde{a})}{\mathrm{d}\tilde{a}}\mathrm{d}\tilde{a}\,. \tag{A.31}$$

The function $g(a)$, (A.24), thus, unambiguously determines both the normal force (A.28) and the pressure distribution (A.31). Therefore, the problem is reduced to simply determining the function $g(a)$, (A.24).

The function $d = g(a)$ can be determined as follows: The infinitesimal displacement of the surface at the point $r = a$ caused by an infinitesimal indentation depth $\mathrm{d}\tilde{d}$ of contact area with the radius $\tilde{a} < a$ is, according to (A.13), equal to

$$\mathrm{d}u_z(a) = \frac{2}{\pi}\arcsin\left(\frac{\tilde{a}}{a}\right)\mathrm{d}\tilde{d}\,. \tag{A.32}$$

The total sinking of the surface at the end of indentation process is, therefore, is equal to

$$u_z(a) = \frac{2}{\pi}\int_0^d \arcsin\left(\frac{\tilde{a}}{a}\right)\mathrm{d}\tilde{d} = \frac{2}{\pi}\int_0^a \arcsin\left(\frac{\tilde{a}}{a}\right)\frac{\mathrm{d}\tilde{d}}{\mathrm{d}\tilde{a}}\mathrm{d}\tilde{a} \tag{A.33}$$

or considering the notation (A.24)

$$u_z(a) = \frac{2}{\pi}\int_0^a \arcsin\left(\frac{\tilde{a}}{a}\right)\frac{\mathrm{d}g(\tilde{a})}{\mathrm{d}\tilde{a}}\mathrm{d}\tilde{a}\,. \tag{A.34}$$

This sinking, however, is obviously equal to $u_z(a) = d - f(a)$:

$$d - f(a) = \frac{2}{\pi}\int_0^a \arcsin\left(\frac{\tilde{a}}{a}\right)\frac{\mathrm{d}g(\tilde{a})}{\mathrm{d}\tilde{a}}\mathrm{d}\tilde{a}\,. \tag{A.35}$$

Partial integration and consideration of (A.24) lead to the equation

$$f(a) = \frac{2}{\pi}\int_0^a \frac{g(\tilde{a})}{\sqrt{a^2 - \tilde{a}^2}}\mathrm{d}\tilde{a}\,. \tag{A.36}$$

This is Abel's integral equation, which is solved with respect to $g(a)$ in the following:[1]:

$$g(a) = a\int_0^a \frac{f'(\tilde{a})}{\sqrt{a^2 - \tilde{a}^2}}\mathrm{d}\tilde{a}\,. \tag{A.37}$$

With the determination of the function $g(a)$ the contact problem is completely solved.

It is easy to see that the equations (A.37), (A.36), (A.24), (A.28) and (A.31) coincide exactly with the equations of the Method of Dimensionality Reduction (Chapter 5, equations (5.51), (5.52), (5.54), (5.56) and (5.58)), which proves the validity of the MDR.

[1] R. Bracewell, The Fourier Transform and Its Applications, McGraw-Hill Book Company, New York, 1965.

Appendix C - Adhesive Contact of Axially Symmetrical Profiles

The Method of Dimensionality Reduction described in the Appendix B for the solution of non-adhesive contact of rotationally-symmetric bodies can be easily generalized to adhesive contacts. The generalization is based on the basic idea of Johnson, Kendall and Roberts that the contact with adhesion can be determined from the contact without adhesion plus a translation of a rigid body. In other words, the configuration of the adhesive contact can be obtained when we firstly press the body without considering the adhesion to a certain contact radius (Fig. A.4 left) and then pull up the body by maintaining the contact area until a certain critical height $\Delta l_{\max}$ (Fig. A.4 right) is reached. Because both indentation of any rotationally-symmetric profile and the subsequent rigid body translation can be mapped correctly by the MDR, this is valid also for the superposition of these two movements.

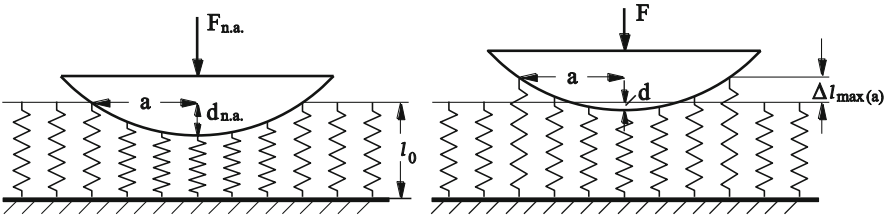

Fig. A.4 Qualitative representation of the pressing and pulling-up process of a one-dimensional indenter with an elastic foundation, which exactly represents the characteristics of the adhesive contact between a rigid spherical punch and an elastic half-space.

The still unknown critical length $\Delta l_{\max}$ can be determined by the principle of virtual work. According to this principle, the system is in equilibrium when the energy does not change for small variations of its generalized coordinates. Applied to the adhesive contact, it means that the change in the elastic energy for a small reduction of contact radius from a to $a-\Delta x$ is equal to the change in the surface energy $2\pi a\Delta x\cdot\gamma_{12}$, where γ_{12} is the separation work of the contacting surfaces per unit area. Since the MDR can map the dependence of force-displacement exactly, the elastic energy can be also reproduced exactly. The change in the elastic energy can, therefore, be calculated directly in the MDR model. Due to the detachment of two springs at the edge of the contact, the elastic energy is reduced by $2\frac{1}{2}E^*\Delta x\Delta l_{\max}^2$. Balance in the elastic and the adhesive energy results in

$$2\pi a\Delta x\cdot\gamma_{12}=E^*\Delta x\Delta l_{\max}^2 \quad . \tag{A.38}$$

From this, it follows that

$$\Delta l_{\max} = \sqrt{\frac{2\pi a \gamma_{12}}{E^*}} \,. \tag{A.39}$$

This criterion for the detachment of the border springs in the adhesive MDR-model was found by M. Heß and is known as the rule of Heß[2].

The application of the method for specific contact forms is described in Chapter 6.

Appendix D - Tangential Contact of Axially Symmetrical Profiles

There is a very close analogy between normal and tangential contact problems. The normal force and pressure distribution for an indentation depth d of a flat cylindrical indenter with radius a are given by the equations (see Appendix A)

$$F_N = 2E^* a d \,, \quad p(r) = \frac{1}{\pi} \frac{E^* d}{\sqrt{a^2 - r^2}} \,. \tag{A.40}$$

The tangential force and stress distribution for a tangential displacement $u_x^{(0)}$ is

$$F_x = 2G^* a u_x^{(0)} \,, \quad \tau(r) = \frac{1}{\pi} \frac{G^* u_x^{(0)}}{\sqrt{a^2 - r^2}} \,, \tag{A.41}$$

which differ from those for the normal contact only by the symbols. Now we consider the impression of an axially-symmetric profile in the normal and tangential directions at the same time and characterize these movements through the normal and tangential displacements as functions of the contact radius

$$d = g(a) \,, \quad u_x^{(0)} = h(a) \,. \tag{A.42}$$

The force and stress during the indentation starting at the initial contact are then

$$F_N = 2E^* \int_0^a \tilde{a} \frac{\mathrm{d}g(\tilde{a})}{\mathrm{d}\tilde{a}} \mathrm{d}\tilde{a} \,, \quad p(r) = \frac{E^*}{\pi} \int_r^a \frac{1}{\sqrt{\tilde{a}^2 - r^2}} \frac{\mathrm{d}g(\tilde{a})}{\mathrm{d}\tilde{a}} \mathrm{d}\tilde{a} \tag{A.43}$$

and

[2] M. Heß, Über die exakte Abbildung ausgewählter dreidimensionaler Kontakte auf Systeme mit niedrigerer räumlicher Dimension, Cuvillier-Verlag, Göttingen, 2011.

$$F_x = 2G^* \int_0^a \tilde{a} \frac{\mathrm{d}h(\tilde{a})}{\mathrm{d}\tilde{a}} \mathrm{d}\tilde{a} \ , \qquad \tau(r) = \frac{G^*}{\pi} \int_r^a \frac{1}{\sqrt{\tilde{a}^2 - r^2}} \frac{\mathrm{d}h(\tilde{a})}{\mathrm{d}\tilde{a}} \mathrm{d}\tilde{a} \ . \tag{A.44}$$

We consider the following two-step process now. Firstly, the indenter is pressed in a purely normal motion until the contact radius c is reached and then further pressed in such a way that it moves normally and tangentially simultaneously until contact radius a is reached and

$$\mathrm{d}h = \lambda \cdot \mathrm{d}g \ . \tag{A.45}$$

The normal force and the pressure distribution at the end of this process is still given by the equation (A.43), while the tangential force and stress distribution obviously result in

$$F_x = 2G^* \int_c^a \tilde{a} \frac{\mathrm{d}h(\tilde{a})}{\mathrm{d}\tilde{a}} \mathrm{d}\tilde{a} = 2G^* \lambda \int_c^a \tilde{a} \frac{\mathrm{d}g(\tilde{a})}{\mathrm{d}\tilde{a}} \mathrm{d}\tilde{a} \tag{A.46}$$

and

$$\tau(r) = \begin{cases} \dfrac{G^*}{\pi} \lambda \displaystyle\int_c^a \frac{1}{\sqrt{\tilde{a}^2 - r^2}} \frac{\mathrm{d}g(\tilde{a})}{\mathrm{d}\tilde{a}} \mathrm{d}\tilde{a}, & \text{for} \quad r < c \\ \dfrac{G^*}{\pi} \lambda \displaystyle\int_r^a \frac{1}{\sqrt{\tilde{a}^2 - r^2}} \frac{\mathrm{d}g(\tilde{a})}{\mathrm{d}\tilde{a}} \mathrm{d}\tilde{a}, & \text{for} \quad c < r < a \end{cases} \ . \tag{A.47}$$

In the area $c < r < a$, the normal and tangential stress distribution have the same form:

$$\tau(r) = \lambda \frac{G^*}{E^*} p(r) \ . \tag{A.48}$$

If we set

$$\lambda \frac{G^*}{E^*} = \mu \ , \tag{A.49}$$

then the contact has the following properties:

$$\begin{aligned} u_x(r) &= u_x^{(0)} = const, \quad \text{for} \quad r < c \\ \tau(r) &= \mu p(r), \qquad\quad \text{for} \quad c < r < a \end{aligned} \ . \tag{A.50}$$

These conditions correspond exactly to the stick and slip conditions in a tangential contact with the coefficient of friction μ (see (8.30) and (8.31) in Chapter 8). Therefore, the force (A.46) and the stress distribution (A.47) under consideration of (A.48) solve the tangential contact problem:

$$F_x = 2\mu E^* \int_c^a \tilde{a} \frac{\mathrm{d}g(\tilde{a})}{\mathrm{d}\tilde{a}} \mathrm{d}\tilde{a} \ , \tag{A.51}$$

$$\tau(r) = \begin{cases} \mu \dfrac{E^*}{\pi} \left(\displaystyle\int_r^a \frac{1}{\sqrt{\tilde{a}^2 - r^2}} \frac{\mathrm{d}g(\tilde{a})}{\mathrm{d}\tilde{a}} \mathrm{d}\tilde{a} - \int_r^c \frac{1}{\sqrt{\tilde{a}^2 - r^2}} \frac{\mathrm{d}g(\tilde{a})}{\mathrm{d}\tilde{a}} \mathrm{d}\tilde{a} \right), & \text{for } r < c \\ \mu \dfrac{E^*}{\pi} \displaystyle\int_r^a \frac{1}{\sqrt{\tilde{a}^2 - r^2}} \frac{\mathrm{d}g(\tilde{a})}{\mathrm{d}\tilde{a}} \mathrm{d}\tilde{a}, & \text{for } c < r < a \end{cases}$$

or

$$\tau(r) = \begin{cases} \mu \left(p_a(r) - p_c(r) \right), & \text{for } r < c \\ \mu p_a(r), & \text{for } c < r < a \end{cases} , \tag{A.52}$$

where we denoted the normal pressure distribution at contact radii a and c by $p_a(r)$ and $p_c(r)$ correspondingly. The tangential displacement in the contact is obtained by integration of (A.45)

$$u_x^{(0)} = \mu \frac{E^*}{G^*} \left(g(a) - g(c) \right). \tag{A.53}$$

It is easy to see that the equations (A.51) and (A.53) coincide with equations (8.52) and (8.49) verifying the validity of the method of dimensionality reduction for tangential contacts.

Further Reading

This list of literature is in no way complete and serves only as a guide for further study or reference.

Chapter 1

D. Dowson, History of Tribology. Longman Group Limited, London, 1979, 678 pp.

E. Rabinowicz, Friction and wear of materials. Second Edition, John Wiley & Sons, inc., 1995.

F.P. Bowden, D. Tabor, The Friction and Lubrication of Solids. Clarendon Press, Oxford, 2001.

B.N.J. Persson, Sliding Friction. Physical Principles and Applications. Springer, 2002.

D.F. Moore, The friction and lubrication of elastomers. Pergamon Press, Oxford, 1972, 288 pp.

I.L. Singer and H.M. Pollock (Eds), Fundamentals of Friction: Macroscopic and Microscopic Processes. (Proceedings of the NATO Advanced Study Institute), Kluwer Academic Publishers, 1992.

B.N.J. Persson, E. Tosatti (Eds), Physics of Sliding friction. Kluwer, Dordrecht 1996.

G. Vogelpohl, Geschichte der Reibung, VDI-Verl., 1981, 87 S.

H. Czichos, K.-H- Habig, Tribologie-Handbuch: Reibung und Verschleiß. 2., überarb. und erw. Aufl., Wiesbaden, Vieweg, 2003. - IX, 666 S.

K.V. Frolov (Ed.), Modern Tribology: Results and Perspectives (in Russian). Moscow, 2008, 480 S.

E. Popova, V. L. Popov, The research works of Coulomb and Amontons and generalized laws of friction, Friction, 2015, v. 3, N.2, pp. 183-190.

E. Popova, V.L. Popov, On the history of elastohydrodynamics: The dramatic destiny of Alexander Mohrenstein-Ertel and his contribution to the theory and practice of lubrication. ZAMM: Z. Angew. Math. Mech., 2015, v. 96, N. 7, pp. 652-883.

Chapter 2

E. Rabinowicz, Friction and wear of materials. Second Edition. John Wiley & Sons, inc., 1995.

Chapter 3

J. Israelachvili, Intermolecular and Surface Forces. Academic Press (1985-2004).

A.J. Kinloch, Adhesion and Adhesives: Science and Technology, Chapman and Hall, London, 1987, p. 441.

B.V. Deryagin, N.A. Krotova and V.P. Smilga, Adhesion of solids. New York, Consultants Bureau, 1978, p. 457.

K. Kendall, Molecular Adhesion and its Applications, Kluwer Academic, 2001.

V.L. Popov, *Contact Mechanics and Friction*,
DOI 10.1007/978-3-662-53081-8

I.E. Dzyaloshinskii, E.M. Lifshitz und L.P. Pitaevskii, General Theory of van der Waals' Forces. Sov. Phys. Usp., 1961, v. 4 153-176.
D. Maugis, Contact, adhesion, and rupture of elastic solids. Springer-Verlag Berlin, Heidelberg, 2000.

Chapter 4

F.M. Fowkes (Ed.), Contact Angle, Wettability and Adhesion. American Chemical Society, 1964.
D. Maugis, Contact, adhesion, and rupture of elastic solids. Springer-Verlag Berlin, Heidelberg, 2000.

Chapter 5

H. Hertz, Ueber die Berührung fester elastischer Körper, Journal für die reine und angewandte Mathematik, 1882, v. 1882, No. 92, 156-171.
K.L. Johnson, Contact mechanics. Cambridge University Press, Ninth printing 2003.
L.D. Landau, E.M. Lifschitz, Theory of elasticity (Theoretical Physics, Vol. 7), 3rd edition, 1999, Butterworth-Heinemann, Oxford, §§ 8,9.
I.N. Sneddon, The Relation between Load and Penetration in the Axisymmetric Boussinesq Problem for a Punch of Arbitrary Profile. Int. J. Eng. Sci.,1965, v. 3, pp. 47–57.
V.L. Popov, M. Heß, Method of Dimensionality Reduction in Contact Mechanics and Friction, Springer, 2015.

Chapter 6

K.L. Johnson, Contact mechanics. Cambridge University Press, Ninth printing 2003.
B. V. Deryagin, N. A. Krotova and V. P. Smilga, Adhesion of solids. New York, Consultants Bureau, 1978. p. 457.
M.K. Chaudhury, T. Weaver, C.Y. Hui, E.J. Kramer, Adhesive contact of cylindrical lens and a flat sheet. J. Appl. Phys., 1996, v. 80, No. 1, pp. 30-37.
D. Maugis, Contact, adhesion, and rupture of elastic solids. Springer-Verlag Berlin, Heidelberg, 2000.
V.L. Popov, M. Heß, Method of Dimensionality Reduction in Contact Mechanics and Friction, Springer, 2015.

Chapter 7

S. Hyun, L. Pei, J.-F. Molinari, and M. O. Robbins, Finite-element analysis of contact between elastic self-affine surfaces. Phys. Rev. E, 2004, v. 70, 026117 (12 pp).
B.N.J. Persson, Contact mechanics for randomly rough surfaces. Surface Science Reports, 2006, v. 61, pp. 201-227.
R. Holm, Electric contacts : theory and application. 4th completely rewritten ed. Berlin, Springer, 1967. - XV, p. 482.

R. Pohrt, V.L. Popov, Contact stiffness of randomly rough surfaces. Sci. Rep., 2013, v. 3, 3293.

Chapter 8

K.L. Johnson, Contact mechanics. Cambridge University Press, Ninth printing 2003.
J. Jaeger, New Solutions in Contact Mechanics, WIT Press, 2005.
M. Paggi, R. Pohrt, V.L. Popov, Partial-slip frictional response of rough surfaces. Sci. Rep. 2014, v. 4, 5178.

Chapter 9

K.L. Johnson, Contact mechanics. Cambridge University Press, 6th printing of the 1st ed. 2001.
J.J. Kalker, Three-dimensional elastic bodies in rolling contact, 1990, Kluwer, Dordrecht, 314 S.
A. Böhmer, Auswirkung des Werkstoffverhaltens auf die rechnerisch ermittelte Belastbarkeit der Schiene. VDI-Verlag, Düsseldorf, 2004.

Chapter 10

F.P. Bowden, D. Tabor: The Friction and Lubrication of Solids. Clarendon Press, Oxford, 2001.
E. Rabinowicz, Friction and wear of materials. Second Edition. John Wiley & Sons, inc., 1995.
M. Köhler, Beitrag zur Bestimmung des Coulombschen Haftreibungskoeffizienten zwischen zwei metallischen Festkörpern. Cuvillier Verlag, Göttingen, 2005.
F. Heslot, T. Baumberger, B. Perrin, B. Caroli and C. Caroli, Creep, stick-slip, and dry-friction dynamics: Experiments and a heuristic model. Phys. Rev. E 1994, v. 49, pp. 4973 - 4988.
E. Popova, V. L. Popov, The research works of Coulomb and Amontons and generalized laws of friction, Friction, 2015, v. 3, N.2, pp. 183-190.

Chapter 11

E. Meyer, R.M. Overney, K. Dransfeld, T. Gyalog, Nanoscience: Friction and Rheology on the Nanometer Scale. Singapore: World Scientific, 1998, p. 373.
M.H. Müser, M. Urbakh, M.O. Robbins, Statistical mechanics of static and low-velocity kinetic friction. Advances in Chemical Physics, Ed. by I. Prigogine and S.A. Rice, 2003, v. 126, pp. 187-272.
A. E. Filippov and V. L. Popov, Fractal Tomlinson model for mesoscopic friction: From microscopic velocity-dependent damping to macroscopic Coulomb friction. Physical Review E, 2007, v. 75, Art. No. 027103.
P. Reimann, Brownian motors: noisy transport far from equilibrium. Physics reports, 2002, 361, 57-265.

V.L. Popov, Nanomachines: Methods of induce a directed motion at nanscale. Physical Review E, 2003, v. 68, Art. No. 026608.
V.L. Popov and J.A.T. Gray, Prandtl-Tomlinson Model: History and applications in friction, plasticity, and nanotechnologies.- ZAMM, Z. Angew. Math. Mech., 2012, v. 92, No. 9, pp. 683-708.
V.L. Popov, R. Wetter, Symmetry breaking as a general design principle of oscillation-based methods for fixation and manipulation of nano-objects, Advanced Biomaterials and Devices in Medicine, 2016, v. 3, No. 1, pp. 10-18.

Chapter 12

K. Magnus, K. Popp, Schwingungen: eine Einführung in physikalische Grundlagen und die theoretische Behandlung von Schwingungsproblemen. Stuttgart, Teubner, 2005, 400 S.
N.M. Kinkaid, O.M. O'Reilly, P. Papaclopoulos, Automotive disc brake squeal. Journal of sound and vibration, 2003, v. 267, Issue 1, pp. 105-166.
K. Werner, Auf Rad und Schiene: Millimeterstrukturen, Weiße Flecken, Riffeln und Risse, Furchen und Grübchen. Projekte Verlag 188, Halle, 2004, 147 S.
M. Schargott, V. Popov, Mechanismen von Stick-Slip- und Losbrech-Instabilitäten. Tribologie und Schmierungstechnik, 2004, Heft 5, S. 9-15.

Chapter 13

H. Blok, The flash temperature concept. Wear, 1963, v. 6, pp. 483-494.
J.C. Jaeger, Moving sources of heat and the temperature at sliding contacts. Proc. R. Soc., 1942, v. 56, pp. 203-224.
V.L. Popov, A. Fischersworring-Bunk, Thermisch-mechanische Instabilität in Reibkontakten. Tribologie und Schmierungstechnik, 2008, Bd. 55, Heft 5, S. 9-11.

Chapter 14

D.F. Moore, The friction and lubrication of elastomers. Pergamon Press, Oxford, 1972, 288 p.
N. Petrow, O. Reynolds, A. Sommerfeld, A.G.M. Michell, Theorie der hydrodynamischen Schmierung. Verlag Harri Deutsch, 2. Auflage, 2000, 227 S. (Reihe Ostwalds Klassiker, Bd. 218).
G. Vogelpohl, Betriebssichere Gleitlager: Berechnungsverfahren für Konstruktion und Betrieb. Springer-Verlag, Berlin, 1958, 315 S.
R. Gohar, Elastohydrodynamics, World Scientific Pub Co, 446 p., Second Edition, 2002.
M. Wisniewski, Elastohydrodynamische Schmierung. Grundlagen und Anwendungen. Renningen-Malmsheim: expert-Verlag, 2000 (Handbuch der Tribologie und Schmierungstechnik; Bd. 9).
E. Popova, V.L. Popov, On the history of elastohydrodynamics: The dramatic destiny of Alexander Mohrenstein-Ertel and his contribution to the theory and practice of lubrication. ZAMM: Z. Angew. Math. Mech., 2015, v. 96, N. 7, pp. 652-883.

Chapter 15
G. Saccomandi und R.W. Ogden, Mechanics and Thermomechanics of Rubberlike Solids (CISM International Centre for Mechanical Sciences Courses and Lectures). Springer, Wien 2004.
D. F. Moore, The friction and lubrication of elastomers. Pergamon Press, Oxford, 1972, 288 p.
A.S. Wineman and K.R. Rajagopal, Mechanical Response of Polymers. An Introduction. Cambridge University Press, 2000.

Chapter 16
K.A. Grosch, The Relation between the Friction and Visco-Elastic Properties of Rubber. Proceedings of the Royal Society of London, Series A, Mathematical and Physical Sciences, 1963, Vol. 274, No. 1356, pp. 21-39.
K.A. Grosch, The rolling resistance, wear and traction properties of tread compounds. Rubber Chemistry and technology, 1996, v. 69, pp. 495-568.

Chapter 17
E. Rabinowicz, Friction and wear of materials. Second Edition. John Wiley & Sons, inc., 1995.
I. Kleis, P. Kulu, Solid Particle Erosion. Springer-Verlag, London, 2008, 206 pp.
K.-H. zum Gahr, Microstructure and wear of materials, Elsevier, Amsterdam, 1987, 560 S.
M. Müller and G.P. Ostermeyer, Cellular automata method for macroscopic surface and friction dynamics in brake systems. Tribology International, 2007, v. 40, pp. 942-952.

Chapter 18
J. Starcevic, Tribospectroscopie als neue Methode zur Untersuchung von Reibungsmechanismen: Theoretische Grundlagen und Experiment. Dissertation an der Technischen Universität Berlin, 2008.
J. Wallaschek, Contact mechanics of piezoelectric ultrasonic motors. Smart Materials and Structures, 1998, v. 7, pp. 369-381.
T. Sashida, T. Kenio, An Introduction to Ultrasonic Motors. Oxford Science Publications, 1994.
E. Teidelt, Oscillating contacts: friction induced motion and control of friction, Technische Universität Berlin, 2015.

Chapter 19
P. Wriggers, Computational Contact Mechanics. Springer, 2006, 518 p.
P. Wriggers and U. Nackenhorst (Eds), Analysis and Simulation of Contact Problems: (Lecture Notes in Applied and Computational Mechanics). Springer, Berlin, 2006.

R. Pohrt, Q. Li, Complete Boundary Element Formulation for Normal and Tangential Contact Problems. Physical Mesomechanics, 2014, v. 17, No. 4, pp. 334-340.
R. Pohrt, V. L. Popov, Adhesive contact simulation of elastic solids using local mesh-dependent detachment criterion in boundary elements method. Facta Universitatis, Series: Mechanical Engineering, 2015, v. 13 (1), pp. 3-10.

Chapter 20

C.H. Scholz, The Mechanics of Earthquakes and Faulting. Cambridge University Press, 2002.
C.H. Scholz, Earthquakes and Friction Laws, Nature, 1998, v. 391, pp. 37-42.
J.H. Dieterich, Earthquake nucleation and faults with rate and state-dependent strength. Technophysics, 1992, v. 211, pp. 115-134.
M.D. Trifunac and A.G. Brady, On the correlation of seismic intensity scales with the peaks of recorded strong ground motion, Bull. Seism. Soc. Am., 1975, v. 65, No.1, pp. 139-162.
Y. Ben-Zion, Collective behavior of earthquakes and faults: Continuum-discrete transitions, progressive evolutionary changes, and different dynamic regimes, Rev. Geophys., 2008, v. 46, RG4006 (70 pp).
B. Grzemba, Predictability of Elementary Models for Earthquake Dynamics, epubli GmbH, Berlin, 2014.
V.L. Popov, B. Grzemba, J. Starcevic, M. Popov, Rate and state dependent friction laws and the prediction of earthquakes: What can we learn from laboratory models? Tectonophysics, 2012, v. 532-535, pp. 291-300.

Figure Reference

Chapter 1: Transportation of an Egyptian Colossus: from the gravestone of Tehuti-Hetep (ca. 1880 B.C.).

Chapter 2: Bearing of a bridge in Berlin Spandau (V. Popov, Institute for Mechanics, TU Berlin)
Chapter 3: Gecko on a stony wall (Zhengdong Dai, Institute for Bio-inspired Structure and Surface Engineering, Nanjing University of Aeronautics and Astronautics).
Chapter 4: Water drop on a garden plant (V. Popov, Institute for Mechanics, TU Berlin)
Chapter 5: Stress distribution in a contact between a photoelastic plate and a cylinder (J. Thaten, Institute for Mechanics, TU Berlin).
Chapter 6: Adhesive contact between a gelatinous body and a steel cylinder (J. Thaten, Institute for Mechanics, TU Berlin).
Chapter 7: Stress distribution in a contact between a photoelastic plate and a rough surface (J. Thaten, Institute for Mechanics, TU Berlin).
Chapter 8: Sliding zones and ring shaped wear (Fretting) in a contact between a plate and a sphere loaded at various angles with respect to the normal (with the friendly consent of K.L. Johnson and Cambridge University Press).
Chapter 9: Wheel-rail contact (J. Starcevic, Institute for Mechanics, TU Berlin).
Chapter 10: A pin on disc tribometer at the Institute for Mechanics at Berlin Institute of Technology (J. Thaten, Institute for Mechanics, TU Berlin).
Chapter 11: Tip of an atomic force microscope on an "atomically smooth" plane (schematic).
Chapter 12: An oscillation eigenmode of a disc brake measured with a scanning laser vibrometer (U. von Wagner, Institute for Mechanics, TU Berlin).
Chapter 13: A thermal image of a rolling tire at various slip angles (F. Böhm: SFB 181 Hochfrequenter Rollkontakt der Fahrzeugräder, Forschungsbericht 2. Halbjahr 1988-1. Halbjahr 1991, TU Berlin, S. A1-68).
Chapter 14: Creeping flow over a corrugated surface – experimentally measured flow lines and comparison to analytical calculation (with the friendly consent of M. Scholle, University of Bayreuth). Source: Scholle, M. Habilitation Treatise. See also: Scholle, M., Wierschem, A., Aksel, N.: Creeping films with vortices over strongly undulated bottoms, Acta Mech., 168, 167-193 (2004).
Chapter 15: Rubber (rubber eraser) (V. Popov, Institute for Mechanics, TU Berlin)
Chapter 16: Rubber tire (V. Popov, Institute for Mechanics, TU Berlin)
Chapter 17: Typical images of abrasive and adhesive wear. Left: abrasive wear of iron on aluminum, right: adhesively caused seizure, C45 hardened and tempered. Source: Bundesanstalt für Materialforschung und –prüfung, Berlin, Ms. Binkowski, provided by Dr. H. Kloß.
Chapter 18: Specimen in a tribo-spectrometer at the Institute for Mechanics at Berlin Institute of Technology (J. Starcevic, Institute for Mechanics, TU Berlin).
Chapter 19: A window in a user interface for a software used in the quick calculation of contact properties and friction between rough surfaces (FaCom – Fast

V.L. Popov, *Contact Mechanics and Friction*,
DOI 10.1007/978-3-662-53081-8

Computation of rough surfaces, V. Popov, T. Geike, S. Korostelev, A. Dimaki, Institute for Mechanics, TU Berlin).

Chapter 20: West Marin, 1906. Fissures in the Olema area were caused by the 1906 San Francisco earthquake. A photograph by G.K. Gilbert. (Photo courtesy of the Anne T. Kent California Room, Marin County Free Library).

Index

V.L. Popov, *Contact Mechanics and Friction*,
DOI 10.1007/978-3-662-53081-8